

N 7 3 - 2 1 5 6 1

NATIONAL AERONAUTICS AND SPACE ADMINISTRATION

Technical Memorandum 33-589

*Thermoelectric Outer Planets Spacecraft (TOPS)
Advanced Systems Technology Project
Final Report*

Prepared by the TOPS Project

**CASE FILE
COPY**

**JET PROPULSION LABORATORY
CALIFORNIA INSTITUTE OF TECHNOLOGY
PASADENA, CALIFORNIA**

April 1, 1973

NATIONAL AERONAUTICS AND SPACE ADMINISTRATION

Technical Memorandum 33-589

*Thermoelectric Outer Planets Spacecraft (TOPS)
Advanced Systems Technology Project
Final Report*

Prepared by the TOPS Project

**JET PROPULSION LABORATORY
CALIFORNIA INSTITUTE OF TECHNOLOGY
PASADENA, CALIFORNIA**

April 1, 1973

Prepared Under Contract No. NAS 7-100
National Aeronautics and Space Administration

PREFACE

The work described in this report was performed by the technical divisions of the Jet Propulsion Laboratory, under the cognizance of the Office of Research and Advanced Development and the Office of Flight Projects.

FOREWORD

The Thermoelectric Outer Planet Spacecraft (TOPS) Advanced Systems Technology Project, conducted at JPL between July 1968 and December 1971, investigated requirements and designs for outer planet spacecraft. The results of this effort were presented to industry in the TOPS Industry Briefing held September 21 to October 1, 1971. This final TOPS Project report has been developed from the transcript and visual aids of that briefing to provide a description of the TOPS project, system, and subsystems. The report covers the final status of TOPS as an integrated project effort, even though this document contains many references to continuing developments which were projected as elements of the ongoing JPL research and development programs. To provide this after the fact report at minimum cost, a number of economies such as direct use of presentation artwork have been involved. These economies are consistent with our intent to identify and describe the work and provide a path to further information through the cognizant engineering personnel. More detailed information on the TOPS design is available in the TOPS Functional Description which is available from Delta Microfilm.

CONTENTS

I.	Introduction	1
	A. Project Description	1
	B. TOPS Purpose and Objectives	3
	C. TOPS Programmatic History	3
	D. Conclusion	4
II.	The Opportunities	6
	A. Outer Planets Mission	6
	B. Science Objectives	15
	Bibliography	25
III.	Spacecraft Design	26
	A. Launch Vehicle Constraints	26
	B. Spacecraft Design Overview	28
	C. Requirements and Constraints	30
	D. Configuration	38
	E. Communications	39
	F. Data Handling	43
	G. Computation and Control	46
	H. Attitude Control	47
	I. Navigation and Guidance	49
	J. Power	50
	K. Temperature Control	54
	L. Structures and Mechanisms	56
	M. Mass	57
IV.	Environment and Radiation Constraints	61
	A. Environmental Requirements	61
	B. RTG Free-Field Radiation	70

CONTENTS (contd)

C.	RTG Simulation	74
D.	Spacecraft and RTM Radiation Mapping Test Model	82
E.	Radiation Test and Facilities	88
F.	Radiation Effects	93
	Bibliography	102
V.	Engineering Mechanics	103
A.	Spacecraft Configuration	103
B.	Mechanical Devices	106
C.	High-Gain Antenna	112
D.	Temperature Control	121
E.	Electronic Packaging and Cabling	132
	References	145
VI.	Reliability	146
A.	System Reliability	146
B.	Reliability Methodology and Failure Rates	149
C.	Reliability Status	153
D.	Custom-Metallized Multigate-Array	159
E.	CMMA Reliability	179
	References	187
VII.	Propulsion	188
A.	Trajectory Correction Propulsion Subsystem	188
B.	Attitude Propulsion System	200
C.	Long-Life Liquid Propulsion Technology	209
D.	Pyrotechnic Subsystem	215
E.	Pyrotechnic Devices	220
	References	226

CONTENTS (contd)

VIII.	Science Experiments	228
A.	Science Instrumentation	228
B.	Science Instrument and Interface Engineering	234
C.	Radiation Effects	237
D.	Imaging Subsystem	248
IX.	Spacecraft Data Acquisition	265
A.	Spacecraft Data Subsystem	265
B.	Measurement Processor Subsystem.	270
C.	Data Storage Subsystem.	282
D.	Command Decoder	287
E.	Control Computer	295
F.	Timing Synchronizer	304
X.	Telecommunications	309
A.	Telecommunications Subsystem Analysis	309
B.	Telecommunication Antenna Structure	315
C.	Radio Frequency Subsystem	321
D.	Transmitter Component Development	327
E.	Modulation/Demodulation Subsystem	329
XI.	Spacecraft Navigation	335
A.	Navigation Concept	335
B.	Approach Guidance Sensor	342
	References	352
XII.	Spacecraft Attitude Control	354
A.	Attitude and Articulation Control	354
B.	Attitude Control Analysis Studies	361
C.	Attitude Control Electronics	367

CONTENTS (contd)

D. Celestial Sensors 372

E. Inertial Devices 379

F. Single-Axis Simulator 383

G. Summary 386

Bibliography 389

XIII. Spacecraft Power 391

 A. Power Subsystem 391

 B. RTG Power Source 398

TABLES

1. Comparison of flight times, direct vs Grand Tour 7

2. Mission examples 12

3. Experiments and payload for fields and particles 24

4. Experiments and payload for planetology 25

5. Natural radiation restraints 31

6. Magnetic field restraints 35

7. Science constraints 36

8. Attitude Control Subsystem constraints 37

9. Antenna constraints 38

10. RTG power source characteristics 53

11. Power 54

12. Mass summary, JUN 1979 58

13. Comparison of Jupiter radiation belt design fluence 63

14. TOPS environmental design requirements magnetic field restraints 66

15. Asteroidal and micrometeoroid debris model and design requirements 67

CONTENTS (contd)

TABLES (contd)

16.	Planned radiation test levels for piece-parts	68
17.	Monte Carlo analysis of heterogeneous fuel capsule assembly	74
18.	Quantity of isotopes, mCi, for 2200 W (thermal) SR TG, 1.2 ppm ^{236}Pu	77
19.	Comparison of PUCK and HELIPAK designs	83
20.	TOPS configuration 12L geometric model	85
21.	HELIPAK/PUCK RTG radiation ratios	85
22.	Requirements for radiation test facilities	92
23.	Overall summary of test results	99
24.	Error budget	114
25.	Areas requiring power for temperature control	124
26.	Temperature control heater requirements	124
27.	Variation in equilibrium temperature	130
28.	Electronic part failure rates (failures/ 10^6 h)	152
29.	Summary of TOPS subsystem reliability	158
30.	CMMA standard gate performance characteristics	176
31.	CMMA driver gate performance characteristics	178
32.	Summary of radiation testing for CMMA output transistor	180
33.	TCPS functional requirements	188
34.	Monopropellant versus bipropellant system	189
35.	TCPS mass estimate	190
36.	Engine test duty cycle	196
37.	Compatibility rating of materials in contact with hydrazine	212
38.	Materials in contact with hydrazine	212

CONTENTS (contd)

TABLES (contd)

39.	Long-term storage specimens, purified hydrazine	214
40.	Ultraviolet photometry experiment performance goals	232
41.	Baseline payload instrumentation	238
42.	Maximum acceptable radiation levels	242
43.	Science instrument shield masses	247
44.	Baseline imaging system characteristics	256
45.	Baseline imaging system, estimated mass	257
46.	Weight and Power Constraints for Data Storage Subsystem.	283
47.	Comparison of STAR and TOPS Computer Character- istics.	299
48.	HCA link performance, X-band modulation model	312
49.	Link performance	313
50.	TOPS antenna particulars, constraints and require- ments.	316
51.	TOPS project receiver specifications.	326
52.	Comparison of characteristics of two-channel analog system and single-channel digital system	330
53.	Correction requirements	336
54.	Observation Modes	342
55.	Functional performance requirements	356
56.	General hardware constraints	357
57.	Selection criteria for single-degree-of-freedom	382
58.	MHW-RTG converter performance status.	405

FIGURES

1.	Mission possibilities.	11
2.	Possible flybys for JSP 1977 at Jupiter	11

CONTENTS (contd)

FIGURES (contd)

3.	Possible Jupiter flyby, JSP 1977, ecliptic plane projection	11
4.	Midcourse maneuver plan for JSP mission	14
5.	Radio navigation limiting accuracy	14
6.	Titan III D (7 seg)/Centaur D-IT/Burner II, 1043 kg	27
7.	Launch-vehicle performance estimates (courtesy Lewis Research Center, July 20, 1971)	27
8.	Location of RTG radiation levels	33
9.	Thermal design requirements	33
10.	Magnetometer boom requirements	34
11.	TOPS scan platform field of view	34
12.	TOPS configuration 12L	41
13.	Communication parameters vs data rate from Jupiter	41
14.	Baseline data rate capability	51
15.	Weight vs frequency	51
16.	Partial power profile and RTG output	59
17.	Spacecraft weight vs flight time	59
18.	Equatorial flyby electron fluences (shielded and unshielded)	62
19.	Equatorial flyby proton fluence (shielded and unshielded)	62
20.	Location of RTG radiation levels	65
21.	Magnetometer boom requirements	65
22.	General temperature design characteristics and restraints	71
23.	Total neutron yield from a 2.2-kW MHW PuO ₂ source	71
24.	Five- and 18-year-old gamma spectra from PMC fuel	71

CONTENTS (contd)

FIGURES (contd)

25.	Geometrical simulation of a 2200-W (thermal) RTG	73
26.	Power source isoflux distribution	76
27.	Simulated fuel capsule assembly	76
28.	Photograph of simulated fuel capsule assembly	78
29.	Simulated RTG	78
30.	Photograph of simulated RTG	79
31.	Simulated RTG assembly	80
32.	Models for analytic study	81
33.	Spectral comparisons of SRTG and RTG	81
34.	Total neutron yield from a 2.2-kW MHW PuO ₂ source	81
35.	TOPS RTG radiation environment	84
36.	Radiation test model	84
37.	Suspended RTM showing measurement boom	87
38.	Detector locations for RTM radiation map	95
39.	Comparison of high- and low-gain H _{FE} behavior at I _C = 10 μA for 2N930 NPN transistors	95
40.	TOPS science scan platform	107
41.	TOPS launch configuration	107
42.	RTG and science boom actuator-damper	109
43.	RTG deployment simulator	109
44.	Schematic drawing of 9.14-cm "astromast" boom	111
45.	Theoretical flow patterns of regenerative pump	111
46.	Long-life pump concept	113
47.	Performance of 6.35-cm-diam regenerative pump at 300 rpm	113
48.	Geometric error source	115

CONTENTS (contd)

FIGURES (contd)

49.	Geometric surface error	115
50.	Hinged radial rib antenna, 4.3 m in diameter	117
51.	Cross section of TOPS 4.3-m antenna	117
52.	Ring support	119
53.	Minimum temperature control power as a function of instrument temperature	127
54.	Series heat pipe assembly	127
55.	Thermal fluid loop	129
56.	Electronics compartment	129
57.	Thermal analysis of 41-W dissipation bay	133
58.	Specular ray trace	133
59.	Electronics compartment assembly	138
60.	Electronics assembly, module, and compartment interfaces	138
61.	Electronics assembly harness development	140
62.	Packaging functional densities for JPL spacecraft subsystems	140
63.	Composite module components	142
64.	Discrete multilayer module (digital circuit packaging)	142
65.	Module sizing flexibility	143
66.	Engineering spacecraft reliability block diagram	150
67.	Computer program example problem	150
68.	Power subsystem reliability block diagram	155
69.	Reliability for series-parallel array of 500 thermo- couples per RTG	155
70.	Spacecraft probability of success for 1979 JUN mission (2 launches, 30-day launch period)	162

CONTENTS (contd)

FIGURES (contd)

71.	CMMA die organization	162
72.	CMMA power distribution system	164
73.	Epitaxial base structure	164
74.	Aluminum oxide--aluminum interconnect system	166
75.	Schematic of standard gate cell	168
76.	Schematic of driver gate cell	168
77.	Schematic of extender gate cell	168
78.	Microphotograph of standard gate cell	170
79.	Microphotograph of driver gate cell	170
80.	Microphotograph of extender gate cell	170
81.	First-level interconnect pattern for CMMA	171
82.	Second-level interconnect pattern for four-bit adder/subtractor CMMA	171
83.	Dual 8-stage shift register	182
84.	Deposited SiO ₂ stripe crossing patterned aluminum	182
85.	Microsection of CMMA 2-level aluminum	183
86.	CMMA second-level aluminum over beveled first level	184
87.	TOPS baseline system	192
88.	Propulsion bay	192
89.	Propulsion model (configuration 12L/A)	193
90.	Normally closed squib valve after actuation	195
91.	TCPS propellant acquisition	199
92.	TCPS demonstration system	199
93.	Attitude propulsion subsystem	202
94.	Attitude propulsion subsystem schematic	202

CONTENTS (contd)

FIGURES (contd)

95.	Attitude propulsion subsystem, typical leg configuration	211
96.	Conical valve seating configuration	211
97.	Material compatibility, specimen capsule	211
98.	Hydrazine material compatibility, test specimen description	216
99.	Radiation test specimen	216
100.	Radiation-caused gas formation	216
101.	Two-step actuation of squibs	219
102.	Baseline squib firing circuit	219
103.	Alternate mechanizations of enable switch	219
104.	Typical pyrotechnic devices	221
105.	Approach to radiation problem	240
106.	Gamma and neutron design constraints and expected fluxes and fluences	240
107.	Jupiter radiation model	241
108.	Electronics, proton degradation	241
109.	Proton damage to science components	245
110.	Shielding from neutron damage with 5% borated polyethylene mass per shielded area	245
111.	Jupiter interference or damage radii, 1.1 R_J periapsis	250
112.	Brightness of the outer planet scene	250
113.	Estimated minimum weight of optics	250
114.	Estimated film shielding, primary proton radiation	253
115.	Image dissector camera, resolution/frame-time tradeoff	253
116.	Baseline imaging system, estimated exposure and signal-to-noise for narrow-angle camera	255

CONTENTS (contd)

FIGURES (contd)

117.	Baseline imaging system, estimated surface resolution of the narrow-angle camera	255
118.	Silicon target sensors, temperature/data rate tradeoff (no radiation damage)	263
119.	Principal requirements, approach guidance study	263
120.	Approach guidance camera design, 3.81-cm silicon intensifier target sensor	263
121.	Approach guidance camera design, 3.81-cm silicon vidicon	263
122.	Data system	266
123.	Functional block diagram measurement processor	274
124.	CCL functional block diagram for interfacing instrument with pulse data	280
125.	TV compressor block diagram	289
126.	Command decoder subsystem interface	289
127.	Command decoder subsystem, command formats	291
128.	Command decoder subsystem, functional block diagram	291
129.	Command decoder subsystem, mode control decoder	293
130.	Command decoder subsystem, command decoders--CDS and CDB	293
131.	Control computer block diagram	300
132.	TSS redundant oscillators, timing synchronizer	307
133.	Oscillator studied, timing synchronizer	307
134.	Functional diagram	310
135.	Circularly polarized S/X-band feed (side view)	317
136.	Measured results at 8448 MHz by waveguide method	319
137.	Main reflector axial defocusing effect	323
138.	Loss due to subreflector lateral displacement	323

CONTENTS (contd)

FIGURES (contd)

139.	Loss due to subreflector tilting	323
140.	Simplified RFS block diagram	323
141.	Multiplier phase shift temperature sensitivity vs first stage multiple	332
142.	Command flow diagram	332
143.	Command block diagram	333
144.	Telemetry modulator block diagram	333
145.	Mariner navigation concept	339
146.	Performance of improved Mariner Navigation System	339
147.	Accuracy of planet direction measurements	339
148.	Performance of combined Navigation System using satellite/star measurements	339
149.	Justification of improvements	345
150.	Sensitivity of command Navigation System to performance variations	345
151.	Typical approach guidance for Mariner 9 approach to Mars, November 11-13, 1971	345
152.	Required star magnitude and geometric accuracy vs field of view	347
153.	Satellite brightness during approach for a typical three-planet mission	347
154.	Attitude Control Subsystem	363
155.	Digital summing of position signals	363
156.	A digital suboptimal control scheme	364
157.	Suboptimal controller response	364
158.	Linear analysis using hybrid modes	366
159.	Yaw axis autopilot block diagram	366

CONTENTS (contd)

FIGURES (contd)

160.	TOPS yaw axis angular rate vs time (rigid body, $K_y = 2.2$)	368
161.	TOPS yaw axis angular rate vs time (flexible vehicle, $K_y = 2.2$)	368
162.	TOPS yaw axis angular rate vs time (flexible vehicle, $K_y = 1.0$)	368
163.	Autopilot stability in pitch and yaw	368
164.	HYPACE	371
165.	CSSL3 simulation showing recovery from a disturbance	371
166.	Digital star tracker	374
167.	Digital star tracker breadboard	376
168.	Image dissector	376
169.	Digital Sun sensor	378
170.	Digital Sun-sensor detector	378
171.	Inertial reference unit	385
172.	Reliability vs time and failure rate	385
173.	Single-axis simulator	385
174.	Single-axis table, pitch-axis simulation	387
175.	Single-axis simulator, pitch cruise data	387
176.	Power subsystem functional block diagram	392
177.	Spacecraft launch power profile	395
178.	Sequence shunt regulator thermal characteristics	399
179.	MHW-RTG	399
180.	Effect of gas conductivity on sealed MHW-RTG performance	404
181.	MHW-RTG reference heat source concept	404

ABSTRACT

A rare opportunity during the latter half of the 1970s to explore the planets beyond Mars prompted the Jet Propulsion Laboratory in 1968 to initiate research and advanced development work on a ballistic-mode, outer planet spacecraft using radioisotope thermoelectric generator (RTG) power. The resultant Thermoelectric Outer Planet Spacecraft (TOPS) Project was established to provide the advanced systems technology that would allow the realistic estimates of performance, cost, reliability, and scheduling that are required for an actual flight mission.

Such a mission would require long spacecraft life, emergency adaptability, and immunity from the environment, as well as compatibility between the RTG radiation environment and the spacecraft subsystems. Design, development, and testing provided the basis used to meet these objectives.

A system design of the complete RTG-powered outer planet spacecraft was made; major technical innovations of certain hardware elements were designed, developed, and tested; and reliability and quality assurance concepts were developed for long-life requirements.

At the conclusion of its active phase in December 1971, the TOPS Project reached its principal objectives: a development and experience base was established for project definition, and for estimating cost, performance, and reliability; an understanding of system and subsystem capabilities for successful outer planets missions was achieved. The system design answered long-life requirements with massive redundancy, controlled by on-board analysis of spacecraft performance data.

The Mariner Jupiter/Saturn 1977 Project continues to benefit from the understandings gained of the TOPS system and subsystem capabilities. It has been estimated that approximately one-half the technology developed during the TOPS Project will be used by the Mariner Jupiter/Saturn spacecraft and mission.

I. INTRODUCTION

A. Project Description

The planetary geometry of the solar system during the latter half of the 1970s makes possible the launch of missions to explore all of the outer planets beyond Mars, using gravity-assist, multiple-encounter trajectories and a minimal number of spacecraft. For equivalent launch energy, these conditions reduce flight times from 30 years for a direct mission to Neptune, to a maximum of about 12 years for a Jupiter-Saturn-Uranus-Neptune flyby.

Responding to National Aeronautics and Space Administration (NASA) and scientific community interest in this rare opportunity, the Jet Propulsion Laboratory (JPL) in 1968 focused part of its research on the definition and development of technology for these outer planet missions. The resulting Thermoelectric Outer Planet Spacecraft (TOPS) Project was organized to coordinate the effort as an "advanced systems technology" project.

Advanced systems technology projects integrate the research and advanced development work to demonstrate the ability to perform a specific set of missions and to gain an understanding of the required subsystems and their interfaces. Design and hardware experience from such an effort provides a basis for more realistic estimation of performance, cost, reliability, and scheduling for project definition and decision-making.

In a research and development R&D environment, an advanced systems technology project concentrates on the most demanding problems, investigating attractive but unproven concepts, and, most important, responding immediately to reflect development results. The TOPS Project developed the technology for a ballistic-mode outer planet spacecraft using radioisotope thermoelectric generator (RTG) power which incorporated early results from the Multi-Hundred Watt (MHW) RTG program of the Atomic Energy Commission (AEC).

The TOPS Project began in 1968 with the support of the NASA Office of Space Science and Applications (OSSA) and the Office of Advanced Research and Technology (OART). Initiation of the Project followed an investigation of missions by the Illinois Institute of Technology Research Institute and the beginning of a review of spacecraft requirements for outer planet missions by the Advanced Technical Studies Office at JPL.

The TOPS spacecraft development effort reflected requirements for the four-planet Jupiter-Saturn-Uranus-Neptune (JSUN) and the three-planet Jupiter-Saturn-Pluto (JSP) and Jupiter-Uranus-Neptune (JUN) mission opportunities during the latter half of the 1970s.

All of these missions require long spacecraft life, emergency adaptability, and environment immunity. The scientific experiments, similar for all of the missions, are demanding. In particular, imaging experiments must produce large quantities of data in order to study the dynamic characteristics of the outer planets. Techniques must be developed to assure compatibility between the RTG radiation environment and the spacecraft subsystems, including the radiation-detection science experiments. The spacecraft must be designed to operate in the intense but poorly defined Jovian radiation environment after hazardous transit of the asteroid belt between Mars and Jupiter.

As a result of these ambitious system requirements, each of the subsystems considered for TOPS reached beyond the then-current technology. However, the TOPS team projected that the required elements would be available early enough so that maturity could be achieved in advance of the multiplanet launch opportunities.

The TOPS spacecraft design was not considered as the ultimate configuration for outer planet missions. TOPS deliberately attacked the most difficult problems in order to broaden the options for later flight projects. TOPS represents a reliable, highly adaptive design that depends on an extrapolation of the existing technology. The outer planet flight project must then evaluate the maturity of this technology to establish firm mission and system design relevant to cost and schedule constraints.

B. TOPS Purpose and Objectives

The TOPS Project sought to gain an understanding of the system and subsystem capabilities required to perform missions to the outer planets. Design, development, and test experience were to provide a basis for estimating performance, reliability, cost, and schedule parameters for outer planet missions requiring advanced technology. In order to implement these objectives, the Project was to consist of

- (1) The system design of the complete RTG-powered outer planet spacecraft, leading to the establishment of functional requirements and interface parameters for all subsystems.
- (2) The design, fabrication, and test of certain hardware elements for subsystem capability demonstrations of major technical innovations representing significant departures from past practices.
- (3) The design, development, and fabrication of a feasibility model (FM) spacecraft incorporating those subsystems necessary to demonstrate required advanced technical capability.
- (4) A system test program to explore interactions between subsystems, including radiation environment, and demonstrate design concepts.
- (5) A reliability and quality assurance effort to facilitate achievement of Project purposes and objectives, particularly in reference to long-life requirements, and to provide a basis for planning future project assurance activities.

C. TOPS Programmatic History

In July 1968, the TOPS effort was initiated to study the RTG-powered outer planet ballistic spacecraft. A project team selected the Grand Tours as the missions to study and defined the content of the 3-year advanced systems technology project. At the completion of the TOPS Project Definition phase in December 1968, the research and advanced development (R&AD) funding required for this Project, as outlined above, was estimated at \$17.5 million, with the NASA OSSA Advanced Technical Development Program providing primary funding for demonstration hardware in Fiscal Years 1970 and 1971.

As the Project developed, it became evident that the funding originally requested for Fiscal Years 1970 and 1971 would not be allocated. Therefore, a less ambitious plan was selected, deleting the FM spacecraft and the associated system test and quality assurance efforts. The Project was subsequently extended into Fiscal 1972, permitting a number of design efforts to reach maturity within a constant funding rate. This extension brought the total Project funding to about \$21 million.

By the conclusion of its active phase in December 1971, the TOPS Project had generally accomplished its principal objectives: to establish a development experience basis for project definition and for estimating cost, performance, and reliability; and to understand the system and subsystem capabilities required for successful missions to the outer planets.

The information generated during the TOPS Project was utilized for estimating a number of possible outer planet flight missions. The project that was eventually selected by NASA--Mariner Jupiter/Saturn 1977 (MJS77)--continues to benefit from its general understanding of the TOPS system and subsystem capabilities. In addition, it has been estimated that approximately one-half of the technology developed during the TOPS Project will be utilized by the MJS spacecraft and mission. Many of the other developments will be used in other NASA programs.

D. Conclusion

The TOPS Project Management believes that the effort produced a design that meets the long-life, high-performance, and environmental challenges of the outer planet missions and is also consistent with the technology available for the late 1970s. The system design addressed long-life requirements with massive redundancy, controlled by onboard analysis of spacecraft performance data. At the time of the system design, TOPS represented a radical departure from the then current Mariner 1967 spacecraft, both in its organization and in its high-performance elements. Subsequently, many of the features that permitted the TOPS performance and organization, such as programmable telemetry, multiple data rates, single-channel digital commands, and S/X-band, have been introduced in the Mariner Venus Mercury 1973 (MVM73) and Viking Orbiter spacecraft. Other features, such as the power shunt regulator for the AEC-developed MHW RTGs, are being incorporated into MJS77.

Some designs, such as the fluid loop for temperature-control heat transfer and the digital sun sensor, are now considered poor choices from either a cost or reliability point of view. Some development work proved tortuous and inspired new approaches. The development of a single-axis digital attitude control subsystem for an air-bearing demonstration revealed the high complexity and large parts count associated with a digital mechanization of Mariner-type attitude control electronics and led to development of the hybrid processing attitude control electronics (HYPACE). This concept, which time-shared a single processor for three-axis attitude control, is being considered for MJS77.

A number of the subsystem designs, such as the self-test and repair (STAR) computer, the micromin radio, and the unfurlable antenna, are not now included on any active flight projects because R&D funding has not permitted development to a point where projects can accept the associated cost, schedule, reliability, and performance tradeoff. This comment also applies to aspects of the TOPS system organization.

As an advanced systems technology project, TOPS did provide an understanding of the requirements and hardware for outer planet missions. The broad application of the emerging digital spacecraft technology inherently provided system and subsystem flexibility that meets the requirements for a number of flyby, orbiter, and probe-carrying missions for the exploration of the inner as well as the outer planets. From this point of view, the TOPS effort initiated development of multi-mission designs which, through repetitive use, could potentially maintain high scientific performance at reduced mission cost. These multi-mission designs appear consistent with the technology available for the late 1970s.

II. THE OPPORTUNITIES

A. Outer Planets Missions

1. Opportunities in the 1970s. The alignment of the planets in the outer solar system in the late 1970s and early 1980s is such that a spacecraft can travel from one planet to the next (see Fig. 1). The planet mission opportunities that occur during this time, as shown in Fig. 1, are:

- (1) Jupiter-Saturn-Pluto (Pluto, with a 17-deg inclination to the ecliptic plane, is above the ecliptic.)
- (2) Jupiter-Saturn-Uranus-Neptune
- (3) Jupiter-Uranus-Neptune

The basic phenomenon involved in flying these multi-outer-planet missions is that the spacecraft, as it passes each intermediate planet, gains energy. Because the energy in the overall system is conserved, the kinetic energy of the planet is decreased slightly; and the kinetic energy of the spacecraft is increased enormously. The spacecraft, much less massive than the planet, does not significantly perturb the orbit of the planet. The gravitational attraction of the planet, however, does produce a significant perturbation of the spacecraft orbit. The spacecraft thus successively picks up energy in each planetary passage. When it passes the last planet, the spacecraft is in a hyperbolic orbit with respect to the Sun and escapes the solar system at about 3 AU per year. The Sun is moving through the galaxy in the direction of the Sun's apex as shown. An interface, or shock front, is thought to exist between the galactic-dominated region and the solar-dominated region. Speculations have placed the shock front from as close as around the orbit of Jupiter, to and beyond Neptune. Because the Grand Tour flights would penetrate this shock front, truly interstellar space can be viewed on these missions. The JSP missions travel in the direction of the Lyman-alpha activity, a recently discovered phenomenon. At each of the intermediate planets, the passage of the spacecraft is completely

constrained; e. g. , at Uranus, there is only one place that the spacecraft can pass to reach Neptune.

An obvious advantage of multi-outer-planet missions is that a single spacecraft can fly by several planets. A second advantage is the reduction in flight time, as shown in Table 1. Flight times for JSUN are variable, depending on whether the spacecraft goes beneath, outside, or through the rings of Saturn.

Table 1. Comparison of flight times, direct vs Grand Tour

Direct	Years	Grand Tour	Years
Jupiter	1.5		
Saturn	4.0	Saturn via Jupiter	3.0
Pluto	42.0	Pluto via Jupiter, Saturn	9.5
Uranus	8.5		
Neptune	17.0	Neptune via Jupiter, Uranus	9.5
		Neptune via Jupiter, Saturn (outside the rings), Uranus	11.0

2. Mission Characteristics

a. Mission-independent

- (1) Mission opportunities occur in 3 consecutive years, with the middle year considered the best because altitudes are usually moderate and flight times and energies are lower than during the other 2 years.
- (2) The flight times increase as the altitudes at the intermediate planets increase.
- (3) The flight times increase as the launch energy decreases.
- (4) Altitudes increase in later years.
- (5) The constrained flyby of Jupiter is near the equatorial plane.

- (6) Although the intermediate planet has a fixed flyby condition, the final planet flyby distance is selectable.
- (7) Uranus-approach is from the north pole. All other planets in the solar system rotate with their spin vector more or less perpendicular to the ecliptic plane; the Uranus spin vector is more or less in the ecliptic plane. When missions launched in the late 1970s arrive at Uranus, the spin vector is pointed almost at the Sun, so that the northern hemisphere of Uranus is continuously lit, an unusual characteristic.
- (8) Sun and Earth occultations occur at all the intermediate planets except at Saturn during JSP missions.

The relative positions of Uranus-Neptune favorable to JUN and JUS missions will not recur for 175 years after the decade of the 1970s. JSP missions occur at about 60-year intervals.

b. Mission-dependent

- (1) JSUN. The three JSUN opportunities occur in 1976, 1977, and 1978, with a marginal opportunity in 1979. The Saturn flyby may be either interior or exterior to the rings. The interior ring missions are considered high-risk because current ring models show a questionably high probability of spacecraft damage from attempts to fly between the visible rings and above the atmosphere. Launch energy is also high, especially in 1978 and 1979. The alternative is to fly outside the rings. Although the visible rings stop at an altitude of about 60,000 km, present models indicate an altitude of approximately 130,000 km for an acceptable probability of no spacecraft damage. To reach this altitude would require a flight time to Neptune of more than 12-1/2 years. To fly just above the rings would require 11-1/2 years. For JSUN, the flybys of Saturn are near the equatorial plane, and Uranus altitudes are on the order of 100,000 km. Jupiter altitudes increase with the succeeding years from 50,000 km in 1976 to 700,000 km in 1977, and 1,800,000 km in 1978. JSUN opportunities to fly by the satellites at Jupiter, Saturn, and Uranus are good.

- (2) JSP. Opportunities for JSP launches occur in 1976, 1977, and 1978. The JSUN ring problem does not occur at Saturn for JSP because the Saturn flybys incline 40 deg or more to the equatorial plane and pass through the ring plane far from Saturn. The highly inclined flyby at Saturn is necessary because Pluto is far enough out of the ecliptic that the spacecraft must go under Saturn and then come up out of the ecliptic to reach Pluto.

No Sun or Earth occultation occurs at Saturn. The Saturn flyby altitudes are high (>500,000 km). Satellite encounter opportunities at Jupiter are good, especially in 1976 and 1977, and there are some opportunities for satellite-encounter at Saturn. The Jupiter altitude is quite low in 1976--5000 km; this is not small on a terrestrial scale, but is less than a tenth of the radius of Saturn, which is 70,000 km.

- (3) JUN. The opportunities for JUN occur toward the end of the decade. Jupiter altitudes increase from 80,000 km in 1978 to 640,000 km in 1979, and to 1,900,000 km in 1980. Uranus altitudes also increase during these years. Satellite encounter opportunities at Jupiter in 1978 and 1979 are good, and some opportunities exist at Uranus.

3. Baseline Mission Set

a. Flights. The following missions were selected for detailed study:

- (1) JSP 1976, one launch
- (2) JSP 1977, one launch
- (3) JUN 1979, two launches

These four flights were chosen because at least two spacecraft could fly to all planets beyond Jupiter, and because they avoid the ring hazard and long flight time associated with JSUN.

b. Trajectories. After the basic flights were chosen, the specific trajectories for each were selected within the following constraints:

- (1) Planet impact or launch vehicle capability. All intermediate planets must have positive altitudes; i.e., the spacecraft must

pass above the surface of the planet. In some opportunities, the launch vehicle capability and the spacecraft weight limit the short flight-time end of the trajectory range. The maximum acceptable flight is the softer constraint.

- (2) Launch date and one of the following parameters:
 - (a) Energy
 - (b) Flight time to planet X
 - (c) Arrival date at planet X (possibly timed for favorable satellite encounters)
 - (d) Altitude of closest approach at planet X

Once one of these parameters is selected, the flybys of the intermediate planets are fixed; but there are still 2 degrees of freedom available for the final planet. The arrival date is fixed, but the flight path relative to that planet is not fixed. After the final planet is passed, the spacecraft leaves the solar system at about 3 AU per year.

The range of choice is illustrated by Fig. 2, which shows the possible flybys for JSP 1977 at Jupiter. At about 30 hours before Jupiter encounter, the spacecraft is approximately 2,000,000 km from the planet. The near-encounter phase is on the order of 2-1/2 days, much longer than the near-encounter phase for Mariners 6 and 7. Both of these trajectories are close to the equatorial plane, and they cross the orbits of the four Galilean satellites. By careful selection of an arrival date, it is possible to obtain a close satellite encounter in addition to the flyby. The distance of satellite encounters is limited by the fact that the plane of motion of the satellite and the plane of motion of the spacecraft are not coincident.

The possibility of flying by several of the satellites with a single trajectory is shown in Fig. 3.

4. Mission Examples. Table 2 gives sample missions for JSP 1976 and 1977, and JUN 1979.

5. Navigation. Mission feasibility depends upon successful navigation. Considering the distance from Earth and the size of the intermediate planets, this navigation task is more difficult than any previously undertaken. Navigation goals are twofold. The first goal is to accurately target the

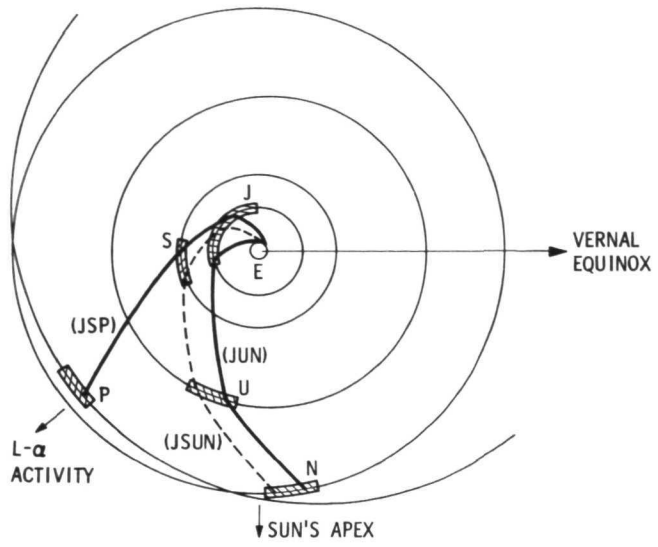


Fig. 1. Mission possibilities

Fig. 2. Possibly flybys for JSP 1977 at Jupiter

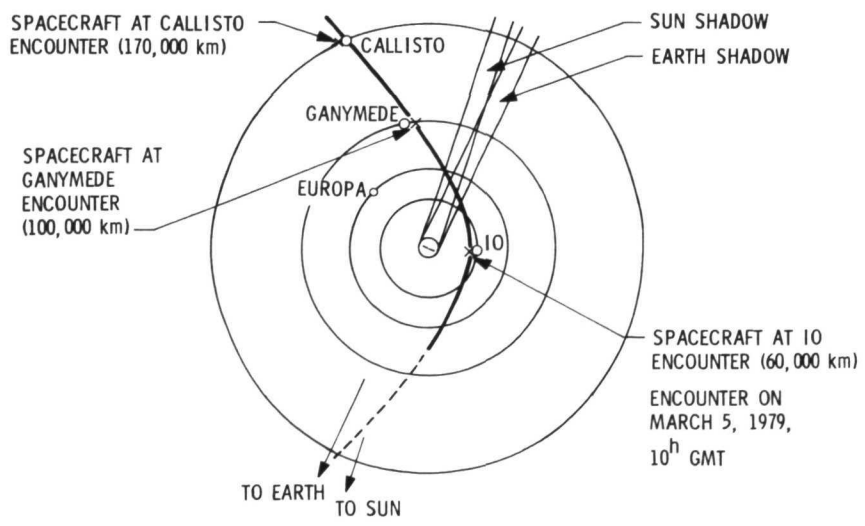
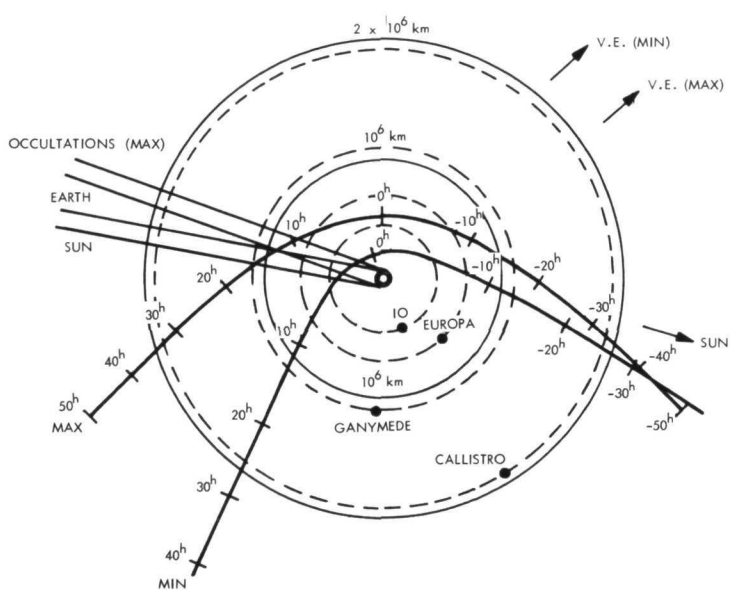


Fig. 3. Possible Jupiter flyby, JSP 1977, ecliptic plane projection

Table 2. Mission examples

JSP 1976	JSP 1977	JUN 1979
<p>Launch period, 7/22/76 to 8/6/76</p> <p>Jupiter encounter, 1/31/78 (fixed)</p> <p>Closest approach, 5000 km</p> <p>Inclination to Jupiter equator, 5 deg</p> <p>Encounters with Ganymede (190,000 km), Amalthea (32,000 km) Io (141,000 km), and Europa (151,000 km)</p> <p>Saturn encounter, 4/18/80 (varies)</p> <p>Closest approach, 479,000 km</p> <p>Inclination to Saturn equator, 36 deg</p> <p>Pluto encounter, 4/15/86</p> <p>Flyby chosen for 20,000-km altitude and Sun and Earth occultation</p>	<p>Launch period, 8/26/77 to 9/10/77</p> <p>Jupiter encounter, 3/3/79 (varies)</p> <p>Closest approach, 250,000 km</p> <p>Inclination to Jupiter equator, 6 deg</p> <p>Saturn encounter, 11/13/80 (fixed)</p> <p>Closest approach, 556,000 km</p> <p>Inclination to Saturn equator, 55 deg</p> <p>Encounters with Titan (428,000 km) Iapetus (46,000 km)</p> <p>Pluto encounter, 10/4/86</p> <p>Flyby chosen for 8000-km altitude and Sun and Earth occultation</p>	<p>Launch period, 10/28/79 to 11/17/79</p> <p>Jupiter encounter, 4/16/81 (fixed)</p> <p>Closest approach, 343,000 km</p> <p>Inclination to Jupiter equator, 2 deg</p> <p>Encounters with Europa (137,000 km), Io (19,200 km), and Ganymede (228,000 km)</p> <p>Uranus encounter, 5/19/85 (varies)</p> <p>Closest approach, 14,000 km</p> <p>Inclination to Uranus equator, 83 deg</p> <p>Neptune encounter, 7/23/88 (varies)</p> <p>Flyby chosen for closest approach, 285,000-km and 12,500-km encounter with Triton</p>

planets and satellites for scientific purposes. A navigation accuracy of 500 to 600 km (a $3\text{-}\sigma$ aiming zone) appears to be accurate enough for the expected planet and satellite science experiments. The second goal is to minimize trajectory-correction fuel requirements. Flight navigation errors are extremely sensitive. For example, it is necessary to fly by Uranus at one precise point to reach Neptune. If that point is missed by 1 km, the resulting uncorrected miss at Neptune will be 20,000 km. Misses at Uranus are expected to be on the order of 200 km and, without trajectory correction, the miss at Neptune would be on the order of several hundred thousand kilometers

Figure 4 shows eight trajectory-correction maneuvers planned for the JSP mission. Figure 5 illustrates the miss distance in the B-plane for various ephemeris errors of the outer planets. The Earth-relative angular positions of the outer planets are known from processing Earth-based optical observations taken over the centuries. The ephemeris error in arc seconds shown in the figure is actually the uncertainty in the angular position of the planet, as seen from Earth. The angular geocentric positions of all the outer planets are known to about $1/2$ arc-s (3σ). As seen in Fig. 4, the position error for the outer planets increases with distance. When Earth-based radio tracking is used to navigate a spacecraft, which has been past procedure, it is necessary to know the position of the spacecraft relative to the Earth. However, for these swingby or gravity-assisted trajectories, it is important to know the position of the spacecraft relative to the planet. To do that with radio navigation, it is necessary to know the position of the planet relative to the Earth, and of the spacecraft relative to the Earth. The limitation here is knowing where the planet is relative to the Earth, because the current ephemeris error is not accurate enough to obtain misses of only 500 to 600 km. It is anticipated that the ephemeris error will be reduced to between 0.15 and 0.3 arc-s by the time these missions are flown, but even at 0.15 arc-s, the errors, especially at Uranus, are excessive. It is necessary, then, to use some other technique, such as optical measurements on board the spacecraft, to determine the spacecraft/planet position more accurately.

One plan that has been developed is to observe the satellites of the outer planets against the star background during the approach and to infer the satellite orbits and the spacecraft trajectory from a 10- to 35-day measurement arc. With this information, a pre-encounter maneuver would be

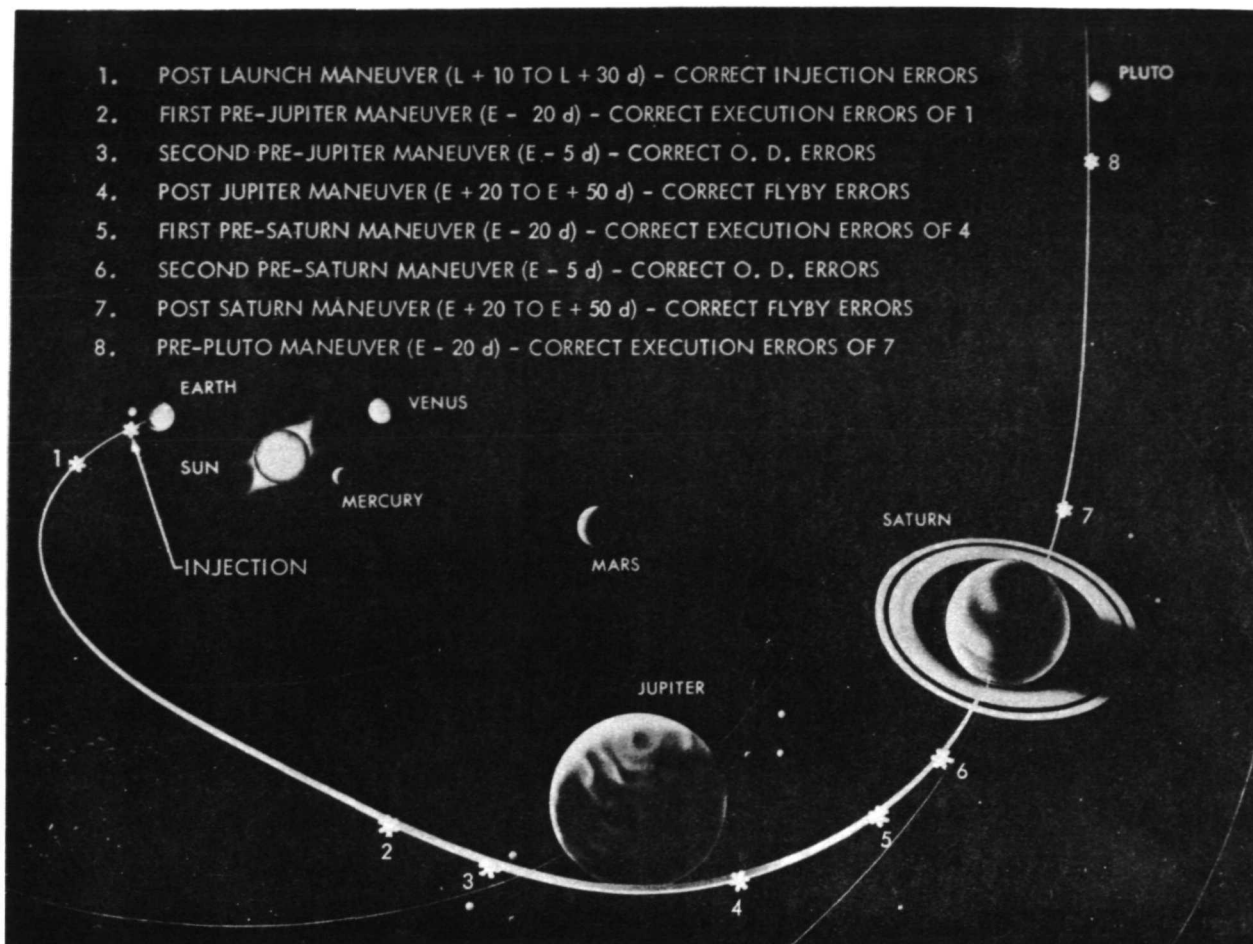


Fig. 4. Midcourse maneuver plan for JSP mission

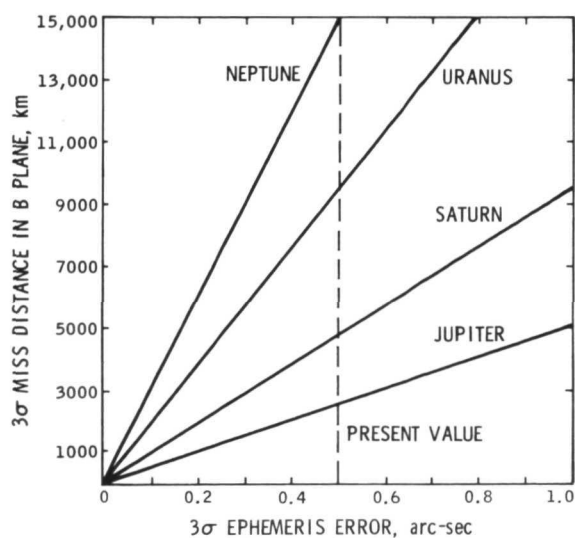


Fig. 5. Radio navigation limiting accuracy

performed approximately 5 days before encounter to refine the trajectory to an acceptable level for the flyby (see Section XI).

B. Science Objectives

1. Major Planets

a. Body structure and rotation. The major planets, sometimes called the giant or Jovian planets, are Jupiter, Saturn, Uranus, and Neptune. In contrast with the inner, or terrestrial, planets, these bodies are very large and have low density, optically thick atmospheres, and high rotation rates.

The low density of the major planets implies a large abundance of lighter elements, particularly hydrogen and helium. The mean density of these bodies is important because density is one of the major boundary conditions that must be applied to any model of the interior of these bodies.

The size and mass of Jupiter and Saturn are sufficiently well known that the mean density can be calculated with reasonable accuracy. This is not true, however, for Uranus and Neptune. The interiors of these planets are subject to temperatures and pressures not found in smaller bodies, and this may result in presently unknown properties of liquids and solids. In fact, it has not been determined whether Jupiter has a solid crust or is fluid throughout.

b. Energy balance. Evidence from Earth-based observations indicates that Jupiter and Saturn both radiate about two-and-a-half times as much thermal energy as they receive from the Sun. Similar data from Uranus and Neptune are not available because of their lower temperature and greater distance from Earth. Since Jupiter and Saturn are always seen at nearly full phase, there is no opportunity to measure thermal radiations at higher phase angles, including the night side. For an accurate determination of energy balance, the radiation from 4π steradians must be totaled.

Two significant improvements in these measurements can be made from a spacecraft: (1) the signal-to-noise ratio can be improved, and (2) the planets can be viewed with a large variety of phase angles. It should also be possible to achieve sufficient spatial resolution to determine whether the source of excess energy is planet-wide or localized (e.g., at

certain latitudes or areas), and whether or not it correlates with specific features such as the great red spot.

c. Atmospheres. The entire visible surface of the major planets is covered with dense clouds supported in the molecular atmosphere. A major scientific objective is to determine the chemical and isotopic composition of these atmospheres. It appears likely, particularly in the case of Jupiter, that the great mass of the planet and the relatively low temperature have made it possible for Jupiter to retain, in the same abundances, all of the elements that were present at its formation. This is in contrast with the terrestrial planets, where the atmosphere has been modified by loss of the lighter elements, by volcanic activity, and, more recently, by biologic activity.

The composition of these atmospheres, particularly the hydrogen-helium ratio, if known, could indicate the abundances present during the formation of the solar system. However, abundance measurements would have to be made at some depth in the atmosphere where it is thoroughly mixed by turbulence.

From Earth, it is clear that the atmospheres of Jupiter and Saturn, and probably Uranus and Neptune, are dynamic. The Jupiter atmosphere is characterized by several periods of rotation. One period applies to the clouds at most latitudes; another shorter period, known as the equatorial jet, applies near the equator in a band of ± 10 deg.

As determined by spectroscopy, the molecular atmosphere above the clouds appears to have a period different from the cloud features. To understand the driving mechanism for the dynamics of the atmosphere, it is important to acquire thermal maps of the atmosphere in three dimensions, with particular emphasis on features such as the red spot, and the bands and zones.

The need for comparative measurements applies particularly to atmospheres. Information about the atmosphere and the magnetic properties of the Earth, although plentiful, does not provide a rigorous test of the theories evolved to explain them. The atmosphere of the Earth is quite complicated because of the biological activity and the high water content. The dynamic atmospheres of these larger planets may be simpler and easier to model.

It is believed that a reducing, rather than an oxidizing, atmosphere is a favorable condition for the beginning of life and a reducing atmosphere is common to the major planets. We do not expect to find fully developed organisms floating in the atmosphere, but conditions may be favorable for the formation of organic molecules and photochemical products. The requirements for the beginning of life are there: the reducing atmosphere, the raw materials, and an energy source. Some suggestions for energy sources sufficient to initiate biologic activity are solar radiation, lightning, and even thunder in the atmosphere.

d. Magnetic fields. Information about magnetic fields can be obtained by studying the field itself, the resulting trapped particle population, and the resulting radio emissions from the trapped particle population.

The fields. To date, the only indication that the major planets have dynamo fields is the detection of nonthermal radiation from Jupiter. Jupiter is a very strong radio source at times, and it is believed that this is caused by synchrotron radiation of relativistic trapped electrons in its magnetosphere. The existence of these trapped electrons indicates a strong magnetic field. Similar indications from Saturn, surprisingly, are not observable. Uranus and Neptune are still unknown.

From Earth, the magnetic field is studied from radio signals. From a close enough flyby to the planet, the magnetosphere itself can be sampled, and both the strength and the dipole moment of the field can be measured. In fact, the magnetic field and the gravity potential are the only two direct measurements that can be made from a flyby and which apply to the interior of the planets.

Two interesting phenomena are associated with a magnetic field:

- (1) At Jupiter, the dipole moment and the spin axis are not co-linear; they differ by something on the order of 10 deg. This fact makes it possible to measure the period of the magnetic field, which may differ from the period of rotation for the planet.
- (2) From measurements of the radio emissions, it is known that those regular satellites which are either within the magnetosphere or which dip into it at times during orbit strongly modulate the radio emissions. A direct measurement from a flyby after the

passage of a satellite would determine whether or not the other satellites also modulate the magnetic field. Furthermore, the search for magnetic fields at other planets, in particular Saturn, can be made from a flyby.

Trapped particles. Evidence of trapped particles has been found only at Jupiter, and there the evidence is limited to the existence of electrons. It is suspected that the particle belts do not contain electrons exclusively. From a flyby, the total composition of the trapped particle population--electrons, protons, alphas, and larger atomic-weight nucleons--can be measured.

The pitch angle of the flux of the particles can be measured to determine any satellite modulation of the particle population. It is not known at what rate these particles are replaced in the field, and it may be possible to determine the mechanism of injection, and possibly the mechanism by which particles are lost to the lower atmosphere, from a measure of the pitch angle of the flux.

If a magnetic field experiment discloses that Saturn does possess a dynamo field, we must then address the trapped particle-radio emission problem.

Radio emissions. The vicinity of Jupiter is a very strong source of decimetric radiations. If this incoherent synchrotron radiation were measured at higher resolution, it could be correlated with the motion of the satellites. In addition to the decimetric radiations, a second type of radio source exists which has longer wavelengths than the decimetric. The source appears to be localized on the surface of Jupiter; i. e. , it recurs on the same central meridian. These longer-wavelength emissions have the character of a noise storm, and they are strongly modulated by the satellite Io. High-resolution measurements would determine the true source and whether or not it is on the disc, which would contribute to understanding the mechanism causing these long-wavelength radio storms.

The data from magnetic field, particle, and radio measurements should be examined to determine whether or not the solar plasma is a major contributor to the particle population and whether or not there is any correlation of planetary particle field activity with solar activity.

2. Satellites, Pluto, and Rings

a. Ephemerides and completeness. There are 29 known satellites of the outer planets, with 6 comparable in size to the Earth's Moon. One of them is larger than Mercury. If these bodies were at 1 AU, they would probably be called planets. It is believed that most satellites are without atmospheres and that the rest have only thin atmospheres. Their densities are undetermined because of the difficulty of making accurate size and mass measurements, and the few measurements now available indicate strange density fluctuations. The satellites have longer periods of rotation than their primary planets. Whereas the major planets rotate on the order of 10 to 15 h, the satellites appear to be in synchronous rotation; i.e., their day is the same as their orbital period. Pluto, by virtue of its size, mass, density, and atmosphere, belongs in the same category. In fact, it has been suggested that Pluto could be an escaped satellite of Neptune, and its orbital period of about 6 days is not unreasonable for that assumption.

Possibilities for discovering an unknown satellite are not particularly great, although an optical search should be made. Ground-based instruments can set a very low limit for the detection of satellites, but the ground-based instrument faces one problem not encountered from a flyby; i.e., that of adjacent bright bodies. It may be possible to look near the rings of Saturn with a lighting geometry which would reduce the interference from the bright rings, and thereby detect a previously unfound satellite near them.

b. Body structure and rotation. The size of the satellites is now very uncertain. Direct size measurements are difficult to make. Often, sizes are calculated from the magnitude of the brightness of the satellite and from assumptions about the reflecting properties of the surface. Because of the uncertainties in diameters, great unknowns in densities exist. The mass of Pluto is uncertain probably by a factor of nearly 2. From flybys, it should be possible to make substantially improved density measurements.

Trends in satellite density as a function of distance from the primary planet have previously been reported, but some of these data are in question. Determination of the density trend would give an indication of conditions at the time of the formation of that particular planetary system.

c. Surfaces. Almost nothing is known about satellite surfaces. In some cases, unusual brightness variations have been observed during

attempts to take photometric measurements of periods. The satellite Iapetus seems to have one hemisphere on the order of 6 times brighter than the other. The Galilean satellites, the 4 large satellites of Jupiter, seem to have very high albedos. It is difficult to propose a surface material which has both the required reflecting properties and stability in the thermal regime that are experienced by the satellites. At present, only basic measurements are available for such features as polar caps, continents and basins, vulcanism, linearments, impact features, and transient frosts, temperatures, and dielectric constants of these bodies.

d. Atmospheres. Titan is the only satellite for which there is any evidence of atmosphere. (The evidence is spectroscopic.) However, calculations of retentivity indicate that Triton of Neptune is also capable of retaining a thin atmosphere.

Until more is known about the mass and temperature of Pluto, it is reasonable to assume that it retains at best a thin atmosphere. Based on reported measurements of post-eclipse brightening at Io and very marginal measurements at Europa, this assumption may also be made for the Galilean satellites. When Io reappears after an eclipse behind Jupiter, its brightness is slightly greater than prior to the eclipse, and this increased brightness persists for about 15 min. It has been proposed that condensation occurs during the eclipse, which causes increased brightness and which revaporizes once the satellite has emerged. However, calculations of the retention capability of these bodies indicate that, if there is an atmosphere, there must be some mechanism for replenishment.

e. Magnetic fields. No evidence supports the existence of magnetic fields on the Galilean satellites, but they do modulate the magnetic field of Jupiter. Because of their size, comparable to that of our Moon, a search should be made for a magnetic field.

f. Rings. There are some very serious questions about the rings of Saturn. If the rings are really as old as the solar system, it is hard to imagine how the uncountable numbers of particles of which they are made have avoided colliding with each other and collapsing the ring system.

On the other hand, if the rings are a recent addition to Saturn, how were they formed? Recent measurements indicate that, perhaps, the rings are not cleanly separated from Saturn, but that there is material extending

all the way down to the surface. Another question is why the rings were formed at Saturn instead of Jupiter. To answer such questions, measurements should be made of the

- (1) Total mass of rings
- (2) Ring thickness
- (3) Distribution of particle size
- (4) Composition of particle surface
- (5) Ring density profile
- (6) Interaction with charged particles
- (7) Rings, if any, at planets other than Saturn

Photography of the planets should show whether or not there are tenuous ring systems at other planets.

As mentioned, no nonthermal radio emissions from Saturn have been detected. One possible explanation is that Saturn, in fact, has a strong dipole, a strong dynamo field, and access to charged particles, but that, by some mechanism, the rings of Saturn absorb the particles and sweep them out of what would otherwise be the particle belts. Discovery of that mechanism would be significant.

3. Interplanetary Medium

a. Solar wind. The interplanetary medium is a region dominated by the Sun and by the solar wind, which is a stream of protons, electrons, and, to a lesser extent, other particles constantly thrown off by the solar corona, with occasional bursts or boosts during peaks of solar activity. The wind is accompanied by a solar or interplanetary magnetic field. Models of the solar wind indicate that there should be a strong gradient with distance from the Sun.

Most knowledge of the solar wind is from data taken from within the orbit of Mars. It should now be possible to measure the interplanetary medium all the way to the boundary of the solar system. Interest in the solar wind is (1) intrinsic (i.e., the properties of the wind itself and how it interacts with planets), and (2) extrinsic (how the solar wind interferes with study of the interstellar medium). Although it is known that the solar wind supports outwardly propagating waves (the Alfvén waves), little is known

about how these waves are excited, and less about how they are damped. Instabilities and discontinuities also exist. The fate of the waves as they propagate outward is unknown.

b. Planet and satellite modulation. The planets and the satellites of the solar system are significant barriers to the outward propagation of the solar plasma, and at least three categories of interactions of the plasma and the planets and satellites have been identified:

- (1) The strong category, which is an interaction in which a planet with a magnetosphere retards the flow of the solar plasma, as do the Earth and, probably, Jupiter.
- (2) The intermediate category, which applies to planets with small magnetic fields, but with substantial ionospheres that interact with the solar wind; e.g., Venus.
- (3) The weak category, which applies to bodies that lack both substantial atmosphere and substantial magnetic field so that the interaction of the solar plasma is with the surface or, to a lesser extent, the interior, depending upon the conductivity of the material.

The first two categories are characterized by a bow-shock transition (i.e., the magnetic field or the ionosphere retards the outward flow of solar plasma), and there is a shock wave at the point where the plasma goes from super- to subsonic flow. All three of these interactions are characterized by some form of wake. If the solar plasma flows around the body in some manner, there must be a trailing wake background.

On close flyby missions, it should be possible to detect the bow-shock, if one exists, and many details of the interaction with the magnetosphere, ionosphere, and the wake. For more distant trajectories, it should be possible to fly at least through the bow-shock and the wake.

c. Boundary of heliosphere. Although it is clear that the region of dominance by the Sun is limited, the extent of the region from the Sun is unknown. A simple model of the region requires a terminal shock wave similar to the shock fronts at the planet. The solar plasma slows from supersonic to subsonic motion at this terminal shock, and beyond the shock front is a region of heated and compressed plasma called the heliosheath.

It is hoped that the outer planet missions will cross this bow-shock, which is the beginning of the end of the solar dominance. Beyond that point, there may be much structure at the boundary between the solar plasma and the galactic plasma. It is probable that the boundary is not spherically symmetrical because the solar system is moving through the galaxy, and some asymmetry should result.

d. Meteoroids. The composition and evolution of the particulate matter which either originates in or is passing through the solar system, and the character of any interaction of this matter with the forces found at planets and at the Sun, are as yet undetermined. It would be desirable to determine the distribution of the particles, which seem to form clouds, and the radial distribution with distance from the Sun.

e. Asteroids. The asteroid belt presents both problem and opportunity. Since there is a small number of large satellites with known orbits, the asteroid belt offers an opportunity to make really significant measurements on these bodies, if it is possible to get close enough without too high a risk.

f. Galactic fields and particles. The final science objective is to measure the galactic cosmic rays in a region essentially free from modulation by the Sun. The missions to the outer planets provide the first opportunity to take measurements beyond the boundary of the heliosphere. The cosmic rays, which are the dominant energy source in the interstellar medium, may strongly influence the motions of interstellar gas and even participate in the formation of stars. It is important, therefore, to be able to characterize the composition and energy spectra of galactic cosmic rays and some streaming anisotropies, and to measure their mean-free path and lifetimes. Emphasis would be on the lower-energy particles because these are prevented from reaching the Earth by the heliosphere.

4. Scientific Experiments

a. Fields and particles. Table 3 shows the experiments, the TOPS payload instruments, and the science steering group teams appointed by NASA for mission definition. The payload listed does not represent a selection but provides a means of defining what support is required from the other spacecraft subsystems. There is some overlap in the three instruments

carried for the energetic particles experiment, but they are not identical. The chief difference is the different energy ranges for measuring the trapped particles.

Table 3. Experiments and payload for fields and particles

Experiment	TOPS payload	Science Steering Group teams
Energetic particles	Trapped radiation detector Trapped radiation instrument Charged particle telescope	Energetic Particles X-Ray
Plasma	Plasma probe Radio frequency propagation	Plasma Radio Science Lyman Alpha
Plasma wave	Plasma wave detector	Plasma Wave
Magnetic fields	Vector helium magnetometer	Magnetic Fields
Meteoroid	Meteoroid detector Meteoroid asteroid detector	Meteoroid
Radio astronomy	Radio emission detector	Planetary Radio Astronomy

b. Planetology. Table 4 shows the experiments and payload for planetology. One objective of the imaging experiment is to make polarization measurements. To ensure that the measurements are sufficiently accurate, a separate instrument may be flown, a polarimeter device without much angular resolution but with good photometry. The infrared experiment will primarily measure thermal balance and make thermal maps of the atmosphere. The ultraviolet photometer will identify a wide range of chemical species. Radio science is grouped with celestial mechanics into a single experiment to take advantage of the radio-frequency telemetry system on the spacecraft, which is used to measure atmosphere profiles. The science instruments are discussed in Section VIII-A.

Table 4. Experiments and payload for planetology

Experiment	TOPS payload	Science Steering Group teams
Imaging	TV	Imaging Photopolarimetry
Infrared spectroscopy	Infrared multiple radiometer	IR Spectroscopy
Ultraviolet spectroscopy	Ultraviolet photometer	UV Spectroscopy Lyman Alpha
Radio Occultation	Radio Frequency Subsystem	Radio Science
Celestial mechanics	Radio Frequency Subsystem	Radio Science

BIBLIOGRAPHY

Bourke, R. D., et al., "Design of Grand Tour Missions," presented at the AIAA 9th Aerospace Sciences Meeting, New York, N. Y., Jan. 1971, Preprint 71-187.

Hamilton, T. W., and Jordan, J. F., "Coursing Accurately to the Giant Outer Planets and Their Moons," Astronautics and Aeronautics, Vol. 8, No. 5, May 1970, pp. 66-70.

Kingsland, L., Jr., "Trajectory Analysis for a Grand Tour Mission to the Outer Planets," J. Spacecraft Rockets, Vol. 6, No. 8, Aug. 1969, pp. 897-902.

Long, J. E., "To the Outer Planets," Astronautics and Aeronautics, Vol. 7, No. 6, June 1969, pp. 32-47.

Penzo, P. A., "Satellite Flyby Opportunities for the Multi-Outer-Planet Missions," JPL Quarterly Technical Review, Vol. 1, pp. 1-12, Jet Propulsion Laboratory, Pasadena, Calif., Apr. 1971.

Penzo, P. A., "The Outer Planets--What Should the Missions Be?" presented at the AAS 17th Annual Meeting, Seattle, Wash., June 1971, Preprint 71-137.

Penzo, P. A., "Satellite Encounter Opportunities of the Grand Tour Missions," presented at the AAS/AIAA Astrodynamics Specialists Conference, Ft. Lauderdale, Fla., Aug. 1971, Preprint 71-259.

III. SPACECRAFT DESIGN

A. Launch Vehicle Constraints

1. Performance. Missions to outer planets require high launch energy (C_3), in excess of $100 \text{ km}^2/\text{s}^2$. Because of this requirement and the anticipated spacecraft weight range, it became evident early in the TOPS study that the Titan class of launch vehicles, with an additional injection stage, would be required. A Burner II stage with a large motor containing 1043 kg (2300 lb) of propellant was recommended on the basis of performance and availability. This choice provides three different launch vehicle candidates:

- (1) The Titan III D (5 seg)/Centaur D-1T vehicle, currently being developed for the Viking project, with the Burner II stage added for TOPS.
- (2) The Titan III D (5 seg)/GT Centaur/Burner II, with the Centaur propellant capability increased by 50% to yield higher performance.
- (3) The Titan III D (7 seg)/Centaur D-1T/Burner II, yielding the highest performance of all.

There are two aerodynamic shroud options: (1) the 3.05-m (10-ft)-diam shroud, which has previously been used on the Orbiting Astronomical Observatory (OAO) and currently on International Telecommunications Satellite (INTELSAT) missions, and (2) the 4.3-m (14-ft)-diam Centaur standard shroud to be used for Viking.

Figure 6 is a line drawing of the five-stage launch vehicle (LV). This configuration supplies a useful payload envelope 3.8 m (12-1/2 ft) in diameter by 6.1 to 7.6 m (20 to 25 ft) in length.

Figure 7 gives the performance estimates for this family of launch vehicles. The Lewis Research Center, source of the information, has retained a 68-kg (150-lb) spacecraft weight contingency. These performance estimates do not include any launch-vehicle, mission-peculiar changes.

The launch energy supplied by this class of vehicles is sufficient for a spacecraft weight range of 454 to 907 kg (1000 to 2000 lb). The TOPS project worked within this constraint.

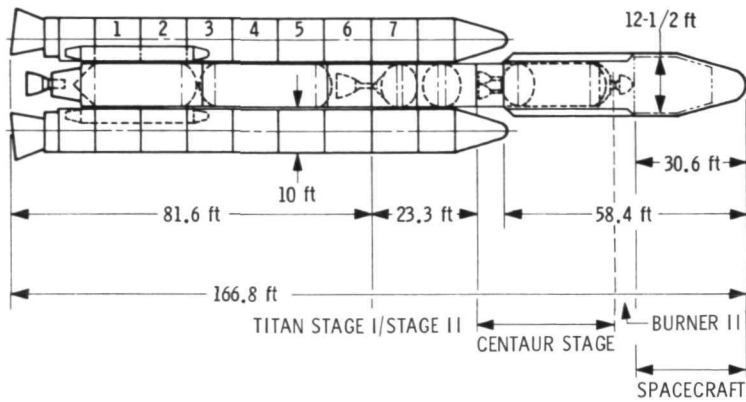


Fig. 6. Titan III D (7 seg)/Centaur D-IT/
Burner II, 1043 kg

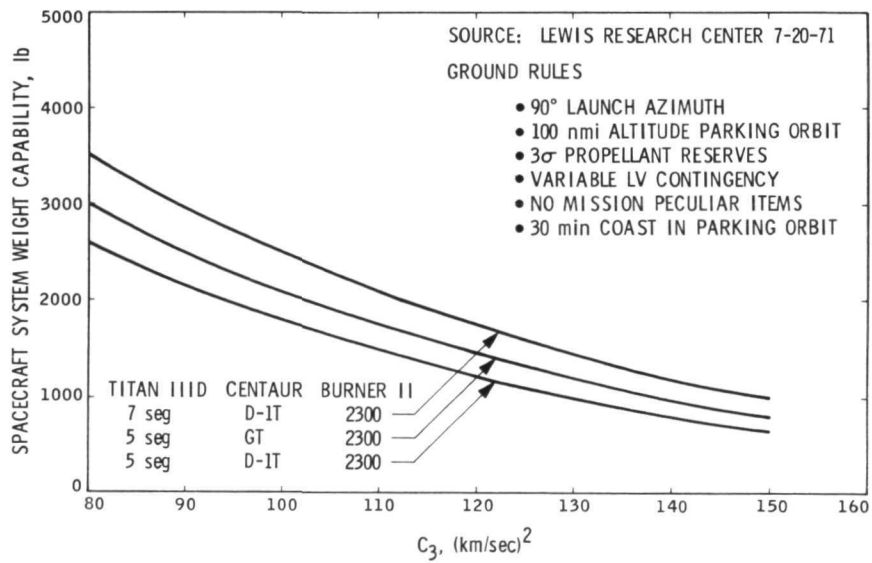


Fig. 7. Launch-vehicle performance estimates
(courtesy Lewis Research Center,
July 20, 1971)

2. Launch Operations. It is planned to launch the Titan/Centaur from pad 41 at the Air Force Eastern Test Range (AFETR). If there are two launches per opportunity, both spacecraft would be launched from the one pad, resulting in a launch period of 13 days minimum for one launch per opportunity and 26 days for two. Such a time constraint places a high premium on spacecraft design and operations to maximize the probability of launching in the first day or two and creates a need for a rapid turnaround for the spacecraft/shroud combination in the event of a spacecraft problem during countdown. The constraint becomes more critical if there is a need to recycle back to the explosive-safe area to decapsulate the spacecraft and to remove, replace, and test any equipment. If there are two launches from one pad, an extremely rapid turnaround is required to check out and launch the second spacecraft. An application of Viking Orbiter planning to TOPS indicates that a turnaround time of about 7 days is necessary for encapsulation. It is estimated that, if the first launch should not damage the pad and complications are minimal, the second vehicle can be launched in 11 days.

In the TOPS Project, it was planned to follow past JPL procedure by fully encapsulating the spacecraft in the explosive-safe facility. When early spacecraft used RTGs, which emit significant thermal energy and some nuclear radiation, an attempt was made to minimize resulting problems by installing the RTGs late on the pad. For TOPS, it was planned to mount the RTGs in the explosive-safe facility and then identify the problems which they introduce. Alternate solutions were developed along with an understanding and appreciation of AEC health physics and safety considerations, which are tantamount to RTG use on the spacecraft. The TOPS examination did not indicate any insurmountable difficulties. The exposure of spacecraft personnel to nuclear radiation would not excessively high if the RTGs were installed in the explosive-safe area. However, the personnel servicing the Burner II stage on the vehicle on the pad would be subjected to some radiation. For this reason, it is recommended that the flight project sponsor a more detailed study of this situation in conjunction with the launch vehicle center and the launch-vehicle-stage contractors.

B. Spacecraft Design Overview

1. Assumptions. The design discussed in this section is based upon a mission set of one JSP 1976, one JSP 1977, and two JUN launches in 1979;

the use of the Titan III D/Centaur D-1T/Burner II to provide the vehicle capability; a C_3 of $110 \text{ km}^2/\text{s}^2$; a 3.05-m-diam shroud, and a maximum spacecraft weight of 839.14 kg (1850 lb).

The Deep Space Network (DSN) 64-m-diam antennas and the 400-kW transmission from approved sites will be used for mission ground operations. To minimize the time required for DSN and mission operations, only one track per week during cruise is assumed. Planetary quarantine is obtained by biasing the trajectory rather than by sterilizing the spacecraft. The cut-off date for hardware state-of-the-art must be early in 1973 to meet the first launch in 1976. Tables 3 and 4 show the representative set of scientific instruments which perform cruise and encounter experiments.

2. Approach. Basic to the design approach was a projection of the future technology available to support a later flight project. In those areas where it was projected that the new technology required would be available, development work was undertaken to ensure that sufficient understanding of the new technology would be gained to allow its incorporation into the flight project with an acceptable level of risk.

A signal requires 8 h per round trip to travel to and from the spacecraft in the vicinity of the farthest planets during these missions. Even if corrective action is taken immediately upon receipt of the signal on Earth, the spacecraft could be affected seriously before the correction was received. For this reason, the self-test and repair concept was chosen so that the spacecraft could take care of itself.

Another design approach included the concept of providing enough system adaptability and flexibility to enable the spacecraft to gather additional information as dictated by knowledge gained by the experimenters during the flight itself. For example, as the spacecraft crosses the shock-front between galactic and solar systems, it could, through programs contained within the measurement processor and the computer, take higher quantities of the data considered most interesting.

3. Reliability. Reliability considerations and tradeoff studies were made to get the most reliable mechanization possible. Assembly-level, single-point failure modes were identified and either eliminated or justified on the basis that the risk associated with them was not great enough to

justify the installation of remedial hardware. Alternate modes can compensate for the loss of a primary function. A basic parts list has been compiled so that a number of well qualified parts could be used in designing the subsystems. An attempt is being made to decrease the electronic piece part types needed for the spacecraft to about 350 and then, through extensive qualification tests, verify that they have a lifetime capability of up to 12 years. Special components, such as the traveling wave tubes, tape recorders, and pumps, would be examined to ascertain how they should be handled to avoid problems occurring late in the project, thereby delaying the overall spacecraft schedule. In-flight calibration of certain instruments is necessary so that the degradation that takes place during flight can be understood.

C. Requirements and Constraints

1. Fundamental. Long life is a fundamental spacecraft requirement. Good scientific data can be gathered long after the spacecraft reaches the farthest planet in 9 to 12 years. It is desirable to get data back from out to 100 AU, which requires a 30-year lifetime. Other than part failure, the Sun sensors appear to be the limiting factor because of the diminishing intensity of the Sun, which will be down by a factor of 900 at 30 AU.

A solar-independent power source is needed. At this time, radio-isotope thermoelectric generators were the only practical way to achieve this goal.

Other fundamental spacecraft requirements are: structure to integrate the subsystems, attitude control, navigation, propulsion for multiple trajectory maneuvers, and environmental immunity.

2. Environmental. The following environmental requirements strongly influence spacecraft design:

a. Radiation. The extent of radiation received by the spacecraft on these missions is much greater than on the Mariners because of the RTGs and the Jovian radiation encountered.

Preliminary estimates of radiation were brought up to date in the 1971 summer workshop, and, as the levels are refined, further adjustments will be made (see Table 5). The electron environment of Jupiter has been inferred from measurements made from radio information and is fairly

well based in fact. The proton environment, however, is much more uncertain because it has to be inferred from the electrons.

Table 5. Natural radiation restraints

	Energy, MeV	Fluence, particles/cm ²	
		Pre-workshop	Workshop
Electrons	0.25 - 3	6.4×10^{10}	4.9×10^{10}
	3 - 10	5.1×10^{10}	1.1×10^{11}
	10 - 30	2.2×10^{11}	2.4×10^{11}
	30 - 100	3.2×10^{11}	2.0×10^{11}
	100 - 300	2.5×10^{10}	1.1×10^{10}
Protons	1 - 3	5.7×10^9	8.9×10^{11}
	3 - 10	1.7×10^{11}	1.7×10^{12}
	10 - 30	9.6×10^{11}	3.3×10^{12}
	30 - 100	3.9×10^{12}	6.9×10^{12}
	100 - 300	1.6×10^{12}	1.5×10^{13}
	300 - 1000	6.1×10^9	2.8×10^{13}
	1000 - 3000	4.7×10^8	2.0×10^{13}

Figure 8 shows the location of RTG radiation levels. (For a detailed discussion of RTG radiation, see Section IV.) Not only are the RTGs located opposite the sensitive electronics and the science instruments, but they are placed in series so that the front RTG effectively blocks out the radiation from the second RTG. The spacecraft electronics are to be designed to the 1.5-m (5-ft) level of RTG fluence. The radiation is lowest directly behind the electronics compartment, and a finger of radiation-depleted area goes toward the science area. Particularly sensitive science instruments could possibly be relocated there. In late 1971, the spacecraft carried shadow shielding to the level of 4.5 kg (10 lb) to shield the science instruments (see Section IV).

b. Thermal. Temperature control in the spacecraft presents a problem because of the fact that solar intensity decreases by a factor of 900. A fluid loop was designed to transport heat from the RTGs to the science instruments, where the heat was needed. However, as the science instruments became better defined, use of the fluid loop was replaced by use of both radioisotope and electrical heaters to provide the necessary heat. The thermal design requirements are shown in Fig. 9.

c. Magnetic cleanliness. The following guidelines were established at the first design stage to ensure magnetic control:

- (1) Avoid soft magnetic materials.
- (2) Use compensating magnet or degaussing loop.
- (3) Make piece-parts field measurement for qualification.
- (4) Employ good electrical wiring design practices.
- (5) Perform magnetic shielding tradeoff studies.
- (6) Perform magnetic mapping at all levels.

Magnetic field restraints are shown in Table 6. The piece-parts are shown at two levels to accommodate some parts that are more magnetic than others. For the close flybys included in the TOPS mission set (1976 JSP with $0.1 R_j$), the Jovian magnetic field of 30 G for a 2-h exposure was established as a maximum level on the basis of a nominal value at the planet surface of 12 G with a factor of 2 tolerance. The other outer planet sources do not appear to have any measurable magnetic field, and the interplanetary field is not stringent.

Figure 10 shows the relationship that determines the magnetometer boom requirements. Scientists would like the spacecraft-generated field at the end of the boom to be less than 0.01γ . A 9.14-m boom was selected as a basis to determine the ease or difficulty of providing attitude control stability. However, it now appears necessary to use a boom 15.24 m (50 ft) long to accommodate the dipole moment.

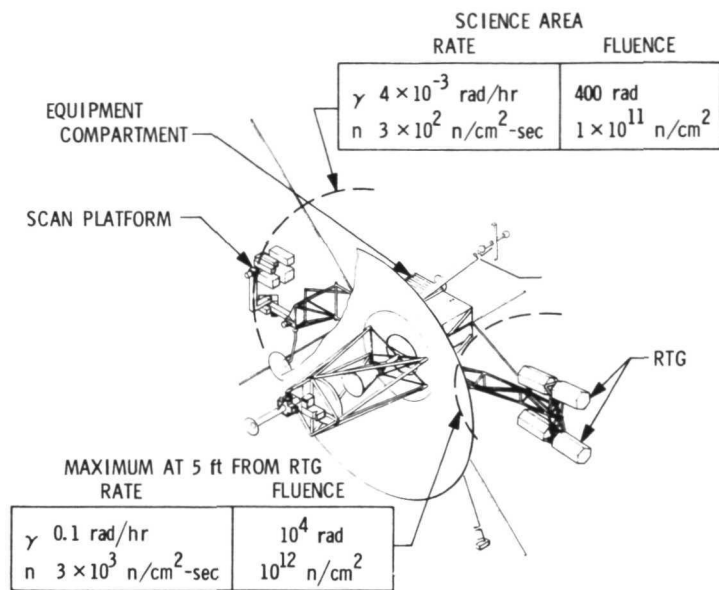


Fig. 8. Location of RTG radiation levels

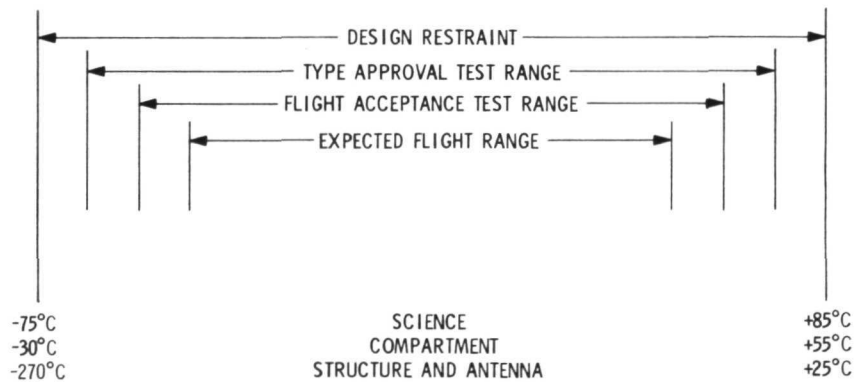


Fig. 9. Thermal design requirements

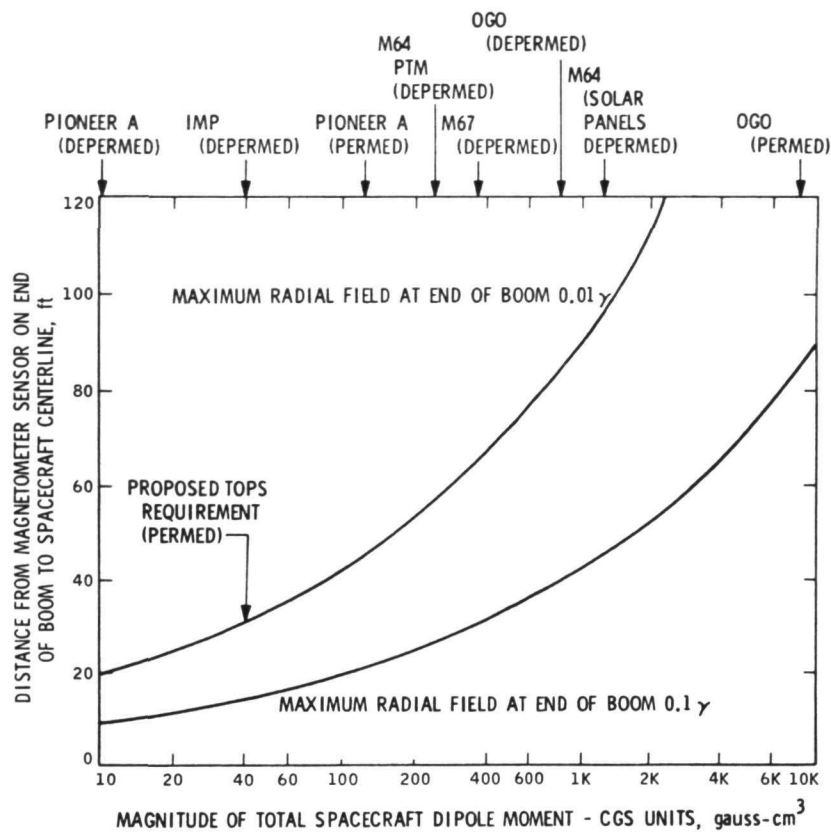


Fig. 10. Magnetometer boom requirements

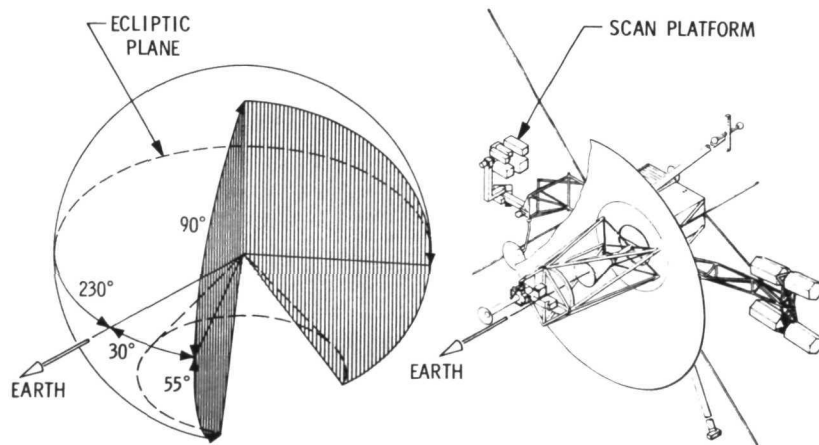


Fig. 11. TOPS scan platform field of view

Table 6. Magnetic field restraints

Static magnetic field and field stability	Sensor requirement 0.01 γ at 9.14 m (30 ft)
<p>Spacecraft hardware category</p> <p>Bay or assembly</p> <p>Subassembly</p> <p>Components</p> <p>Piece-parts</p>	<p>Maximum radial field (in γ) after exposure to 25 Oe</p> <p>5 γ at 0.91 m (3 ft)</p> <p>1 γ at 0.91 m</p> <p>2.5 γ at 30.48 cm (12 in.)</p> <p>20 γ at 15.24 cm (6 in.), 10 items/assembly</p> <p>1 γ at 15.24 cm, remainder/assembly</p>
<p>Natural magnetic fields: source</p> <p>Earth magnetic field</p> <p>Jupiter magnetic field</p> <p>Other outer planets</p> <p>Interplanetary magnetic field</p>	<p>Level</p> <p>0.5 G</p> <p>30 G; 2-h exposure</p> <p>Maximum represented by Jupiter</p> <p>10^{-3} G (maximum)</p>

d. Micrometeoroid protection. The meteoroid design constraint is that the probability will be about 0.99 that no failure of the spacecraft shall result from a meteoroid impact as severe as one by a particle of 2×10^3 g mass, 3.5 g/cm^3 density, and 20 km/s impact speed.

The design allocates 5.44 kg (12 lb) for a beta cloth shield located 2.54 cm (1 in.) in front of the structure. The particles initially hit the beta cloth and then are stopped by the structure surface. For the worst-case asteroid environmental model, the probability of survival moves down from 99 to 83%. Because Pioneers F and G fly through the same environment before TOPS, changes can be made, if necessary, late in the design.

3. Field of View

a. Science instrument. Table 7 gives the science constraints for the instrument field of view. The plasma probe actually articulates in both azimuth and elevation. The radio emission detector must be at least 1 m from the booms for the plasma wave detector and the vector helium magnetometer, which are both 9.14 m in length, to balance the spacecraft.

Table 7. Science constraints

Instrument	Half-cone-angle field of view	Location or look angle
Charged particle telescope (CPT)	32.5 deg	In plane of ecliptic Telescope 1, 45 deg from Earth line toward planet Telescope 2, 180 deg from telescope 1
Plasma probe (PP)	8 deg	Point nominally at Sun with motion of 15 deg in ecliptic plane and 8 deg out of ecliptic plane
Trapped radiation detector (TRD)	30 deg	45 deg from south ecliptic pole and 70 deg from Earth line
Radio emission detector (RED)	Crossed dipoles	Mounted orthogonal in plane normal to Earth line
Plasma wave detector (PWD)	Two mutually orthogonal sensors	Locate as far as possible from spacecraft electromagnetic interference (EMI) fields
Vector helium magnetometer (VHM)	Three mutually orthogonal axes	Locate remote from spacecraft for 0.01 γ background magnetic field Orientation to be known to 1 deg
UV photometer (UVP)	0.5 deg	Bore sighted with imaging
Infrared multiple radiometer (IMR)	0.5 deg	Bore sighted with imaging
Trapped radiation instrument (TRI)	22.5 deg 7.5 deg	In plane of ecliptic 0 deg from Earth line In plane of ecliptic 45 deg from Earth line
Micrometeoroid detector (MD)		Sensors mounted on 6.1 m ² of exposed spacecraft surface(s) perpendicular to ecliptic plane in general direction of travel
Meteoroid asteroid detector (MAD)	5.0 deg	In plane of ecliptic 45 deg from anti-Earth line
Science Imaging Subsystem (SIS)	0.5 deg 5.0 deg	Articulated to provide coverage of primary planets, satellites, and rings

b. Attitude control sensor. Table 8 lists the Attitude Control Subsystem constraints. The secondary Sun sensors are mounted on the forward side and on the back side of the spacecraft so that they can see the Sun from all 4π steradian.

Table 8. Attitude Control Subsystem constraints

Assembly	Half-cone-angle field of view	Location or look angle
Canopus tracker	12.5 × 35	0-deg clock angle
Primary Sun sensors	20 deg	0-deg cone angle
Secondary Sun sensors	Hemispherical coverage	0- and 180-deg cone angles
Approach guidance sensor	3 × 3 deg full field	Mount on science platform
Roll thrusters	45 deg	Normal to roll axis in clock-angle plane
Pitch thrusters	45 deg	Normal to pitch axis in yaw plane
Yaw thrusters	45 deg	Normal to yaw axis in pitch plane
Reaction wheels	- - -	Orient with wheel axes parallel to roll, pitch, and yaw axes, respectively

c. Antenna. The antenna constraints are shown in Table 9. The ± 10 -deg elevation angle of the medium-gain antenna compensates for the fact that the Canopus sensor allows the spacecraft yaw axis to move slightly as it goes through the trajectory. The antenna also serves as a downlink backup if the high-gain antenna (HGA) were not to deploy--an unlikely possibility.

Table 9. Antenna constraints

Antenna	Half-cone-angle field of view	Look angle and usage
High-gain antenna (X/S-band)	5 deg	0-deg cone-angle usage: Downlink except first 100 days and trajectory-correction maneuver Earth-pointing refinement
Medium-gain antenna (X-band)	10 deg	Azimuth angle: -10 to +200 deg Elevation angle: ± 10 deg Usage: Downlink for trajectory-correction maneuver Downlink backup
Forward low-gain antenna (S-band)	120 deg	0-deg cone-angle usage: Downlink for first 100 days Uplink
Aft low-gain antenna (S-band)	> 90 deg	180-deg cone-angle usage: Uplink during trajectory-correction maneuver Uplink during non-Earth pointing

d. Scan platform. Figure 11 shows the scan platform field of view. Although the science instruments usually look out from one side of the spacecraft at most of the planets during flyby, they must also point up as the spacecraft passes underneath Saturn. Because the spacecraft passes Pluto on the side opposite the Sun, the spacecraft must roll to bring the instruments into the proper field of view. Furthermore, as discussed in Section II A, satellites will be viewed at many points along the trajectory. For these reasons, the scan platform needs a full hemisphere of coverage at different times and in different locations. The spacecraft can be rolled, using either celestial or inertial references, such as a bright star without other stars around it, or the onboard gyros to point in other directions.

D. Configuration

Figure 12 shows configuration 12L of the TOPS spacecraft, with a representative payload. The high-gain antenna is stowed around the

subreflector during launch and then deployed, as shown for the rest of the flight. The propulsion compartment is designed for easy insertion at AFETR to avoid range safety problems. The electronics are packaged in six bays. The digital Sun sensors track the Sun as a primary source and are biased to point the spacecraft at the Earth so that communications can be maintained over the high-gain antenna. The medium-gain antenna is used for communications during trajectory corrections. The spacecraft is first rolled and then yawed; the antenna is counteryawed to maintain downlink communications.

E. Communications

1. Downlink. A large amount of data is generated during cruise and encounter, which must be played back within a reasonable amount of time. For design purposes, it was concluded that the maximum playback time from Neptune should be 30 days for two playbacks of the data.

Simultaneous S- and X-band is planned for tracking purposes to enhance radio navigation accuracy. X-band is used primarily to return the maximum amount of data to Earth. The S-band is used because it is continuous, is not affected by weather conditions at the site, and is the standard mode for all DSN stations. Two subcarrier channels are used: one with a programmable data format and one with a fixed data format. The highest data rate is 131,072 bits/s, which can be marginally handled by the DSN. Overseas stations need additional communication lines to relay information to the Mission Operations Center at JPL. Therefore, the fixed channel will be demodulated at the station to get the automatic gain control and static phase error information necessary for spacecraft communications. Late in the mission, when the data rate is low, the fixed subcarrier channel is turned off and serves as a backup to the programmable subcarrier channel. Similarly, variable data rate steps are used to comply with the data rate capability as the range changes and as the equipment aboard the spacecraft degrades.

The X-band transmitter power is variable; it is possible to transmit at 40 and at 20 W. The 40-W transmission is used when power is available; it increases performance by 3 dB. Early in the mission, power is available for all phases. Later in the mission, when less power is available, the 40 W can still be used during the playback phase.

Monopulse pointing was used to provide pitch and yaw error signals to the attitude control to maintain pointing within a narrow tolerance. Thus, during occultation, the uplink signal can be tracked to provide additional coverage through the refractive atmosphere to strengthen the RF occultation experiment at each of the planets.

The antenna size and transmitter power were selected after a power gain-vs-weight optimization study. An optimization, made at each of the data rates, disclosed an optimum in the classical U-shape. On one side, the dominant feature was the amount of power used to provide power to the transmitter, which is reflected back as RTG weight; on the other side, the weight due to increased size of the antenna and the science boom, which enables the science instruments to see around the antenna, is dominant. The results of the optimization study are summarized in Fig. 13. A data rate of 131 kbits/s was selected as reasonable, resulting in a transmitter power figure on the order of 18 W, which was rounded off to 20 W. An antenna diameter of 3.8 m was about optimum, and this was increased to 4.3 m for working purposes. The system weight includes a monopulse tracking capability which increases the weight slightly, but the increase is offset by the advantage of being able to track the uplink signal when entering occultation. Several different RTG weights were used because the watts-per-pound efficiency was uncertain at that time, varying from 1.2 to about 1.7 W. At present, 1.4 W is considered reasonable and possible to achieve with the MHW generator that the General Electric Company is building for the AEC.

The data rate capability is shown in Fig. 14. The 3-dB data-rate steps provide a good utilization of the communications capability. Performance shown does not include X-band degradation caused by bad weather or atmospheric moisture. For a period around Jupiter encounter, there is a slight loss in signal caused by radio noise emanating from the planet itself. This degradation is shown in Fig. 14. The data rate decreases from the 131 kbits/s at Jupiter down to about 2,000 bits/s at Neptune or Pluto. However, barring spacecraft failure, the data return capability continues to exist out to 100 AU. The data rate is adversely affected by a portion of the radiated power being moved from the subcarrier to the carrier to provide enough carrier power so that the carrier can be tracked.

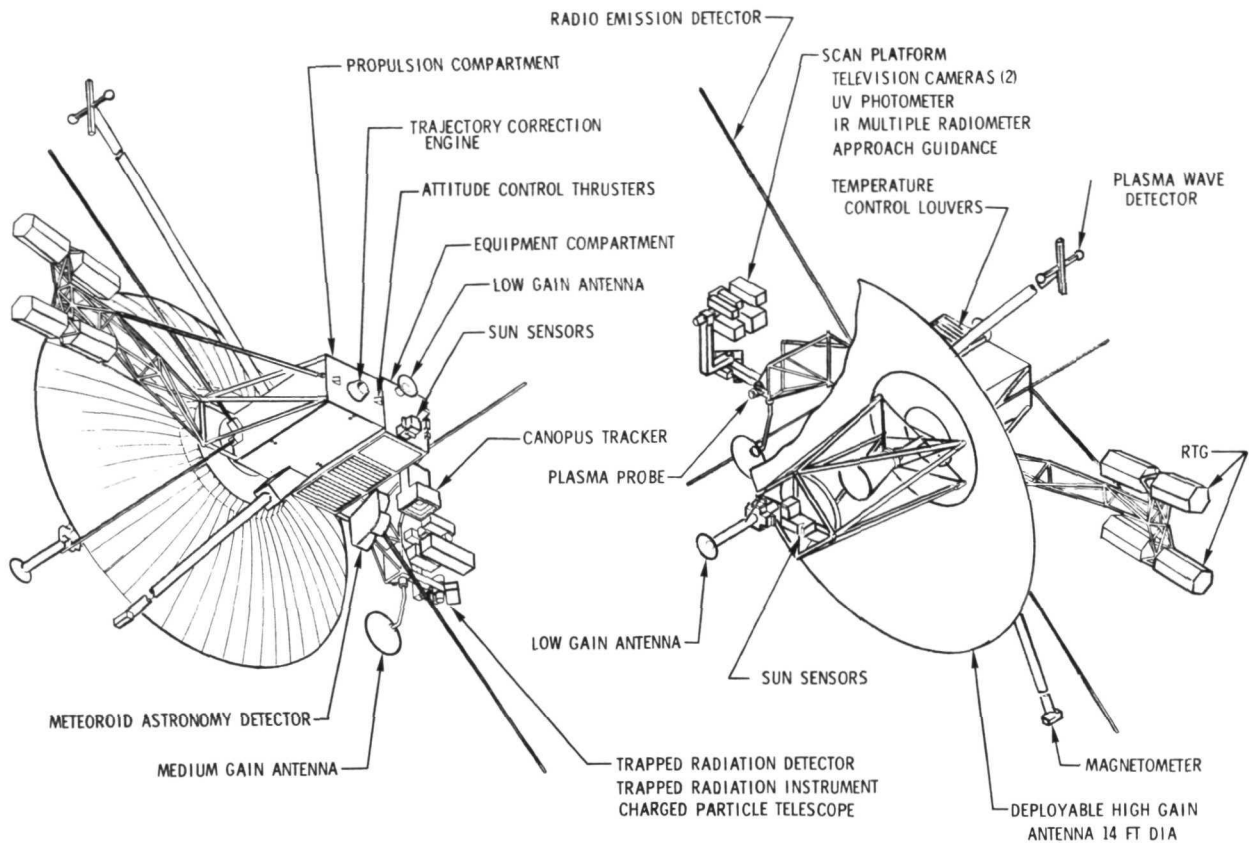


Fig. 12. TOPS configuration 12L

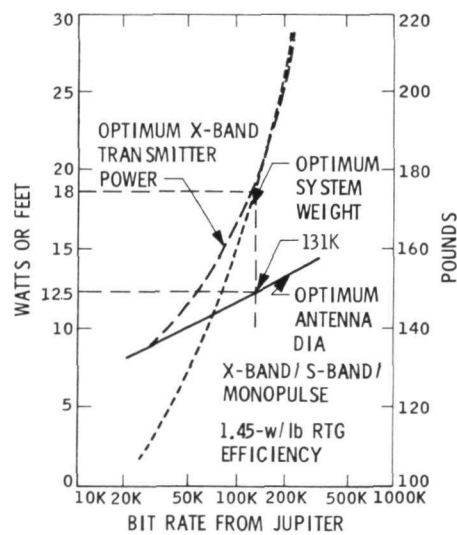


Fig. 13. Communication parameters vs data rate from Jupiter

2. Uplink. The communications uplink provides ground command capability out to 30 AU. In addition, a ranging capability is provided to assist in spacecraft navigation. It is desirable to have command capability beyond 30 AU. However, rather than impact the design by including an additional antenna to obtain 4π steradian coverage, partial coverage is provided in both the forward and aft hemisphere at 30 AU.

The design point was selected to include the use of separate command and ranging subcarriers modulated on an S-band carrier; two selectable bit rates for commands, 4 and 64 bits/s; and accommodation for an error rate of less than one bit error in 10^5 bits. Sixty-four bits/s over the high-gain antenna reprograms the entire computer in less than one station pass, and the 4 bits/s provides direct commands with reduced link performance.

3. Radio Frequency Subsystem. The Radio Frequency Subsystem (RFS) receives an S-band uplink carrier at 2.115 GHz and has a receiver sensitivity of -161 dBm at threshold. Antenna-pointing electronics provide pitch and yaw error signals. An S-band and/or X-band downlink carrier is provided with frequency coherency to the uplink by ratios of 240/221 and 880/221. An S-band solid-state amplifier transmits 20 W RF. A 20- and 40-W dual-mode traveling wave tube amplifier transmits the X-band carrier. Two-way ranging capability is provided over both S- and X-band.

4. Antenna Subsystem. The Antenna Subsystem includes

- (1) A high-gain, unfurlable, 4.3-m parabolic antenna. The main reflector is made of mesh supported by 48 ribs and has an allowable surface deviation of ≤ 0.089 cm (≤ 0.035 in.) RMS. A Cassegrain feed, circularly polarized, with a monopulse capability, transmits X- and S-band and receives S-band.
- (2) A medium-gain two-axis gimballed parabolic antenna, 0.76 m (2.5 ft) in diameter, which transmits at X-band. This provides communications during trajectory corrections. If the weather at the DSN site is bad, the trajectory correction may be delayed until acquisition at the next site.
- (3) The forward low-gain Mariner-class antenna, which transmits and receives at S-band. The backlobe of this antenna has to be cut down so that there is no interaction with the high-gain antenna. An aft low-gain antenna receives only.

5. Modulation/Demodulation Subsystem. The Modulation/Demodulation Subsystem generates the subcarriers and modulates them with data to provide a composite telemetry signal to the RFS. The high-rate channel is convolutionally coded. The demodulator includes a digital pulse-code-modulated correlation detector to provide command reception with a bit error probability of less than 10^{-5} .

F. Data Handling

The data-handling equipment was designed to (1) handle a broad spectrum of input data from 131 kbit/s down to infrequent engineering measurements, (2) provide in-flight adaptability for the solar system/galaxy interface and other interesting science phenomena, and for changes in the spacecraft engineering data, (3) maximize the information returned from the spacecraft, not necessarily maximize the raw data sent back to the Earth, and (4) provide continuous coverage for random interesting features or for anomalies occurring on the spacecraft. To fulfill these functions, the following design points were selected:

- (1) A special-purpose processor, which processes the data at the rate of more than 10,000 samples per second.
- (2) A control computer, which supports and backs up the special-purpose processor. The control computer in this backup mode can handle data rates comparable to the Mariner 1969 rates of 33-1/3 bits/s while performing its normal function.
- (3) Data compression to return information without having to return all of the data bits. Data compression techniques for zero-order and first-order compression are used on engineering as well as on science data. An information-preserving algorithm for imaging data, called the Rice machine, has been developed (see Section IX-B).
- (4) Central timing to ensure that all parts of the spacecraft are synchronized so that the functions of all subsystems are time-correlated.
- (5) Magnetic tape to provide bulk storage for the large quantities of data (1×10^9 bits).

- (6) A sample data rate sufficient for fault detection.
- (7) Control and conditioning logic to interface each of the science instruments with the special-purpose computer.

1. Measurement Processor Subsystem. The Measurement Processor Subsystem (MPS) is a special-purpose computer that provides two data channels to the radio: (1) the fixed format low-rate engineering channel, and (2) the in-flight-reprogrammable, high-rate channel. Data are sampled with a maximum rate of about 10,000 samples per second. There are 512 analog and digital measurements for science and engineering, excluding the science instrument data channels. The programmable output data rates range from 8 to 131,072 bits/s in 3-dB steps, a factor of 2. Data processing includes analog-to-digital (A/D) conversion, data formatting, and routing to the RFS directly or into data storage for later transmission.

The measurement processor can be programmed to determine whether or not any operation is out of tolerance; if such operation is detected, the processor alerts the control computer. The control computer then samples that measurement, as well as other measurements, to determine whether it is indeed a malfunction or a transient noise glitch. The measurement processor also adapts to changing sensor activity. For example, if a sensor failure causes an unrealistic amount of activity, the processor, by means of a stored program, can change the sample frequency and not send back useless information. Whenever its capabilities are exceeded, the measurement processor receives help from the control computer. The processor also controls and sequences the science payload through individual steps to gather data. The control computer has a state vector for controlling the measurement processor. The measurement processor, in turn, informs the science control and conditioning logic, which then has control over each of the science instruments.

2. Control and Conditioning Logic Subsystem. The Control and Conditioning Logic Subsystem (CCLS) is the flexible interface between each of the instruments and the measurement processor. It is an extension of the Measurement Processor Subsystem, and provides the special-purpose processing necessary to interface each instrument with the measurement processor. The CCLS also provides A/D conversion, pulse counting, and data editing and compression. It provides the instrument control necessary to

take measurements at prescribed times so that each measurement is correlated in time and can be reassembled on Earth. The Rice machine is located in one of these control-conditioning logic elements.

3. Data Storage Subsystem. The Data Storage Subsystem (DSS) has two 10^9 -bit magnetic tape recorders and 2×10^6 no-moving-part storage. Data are addressable by data blocks in the data storage in order to store and retrieve selected data without replaying the entire tape. The simultaneous store and playback capability on the spacecraft is such that, as the data out of one tape recorder are played back, data can be played into the other tape recorder, thus maintaining continuous coverage. A single-speed tape recorder with a rate buffer input and output makes it possible to remove much of the mechanical complexity associated with tape recorders, which reduces the problems associated with tape recorders during past flights. A fluid-filled system is used to reduce wear on the interfaces. There is no head-to-tape wear nor wear on the bearings in the tape recorders because of the fluid lubricant. A modular construction of plated wire or magnetic cores for the buffers is used. Thirty-five of these buffer modules provide a little more than 2.3×10^6 bits, which exceeds the overall requirement of 2×10^6 . Sixteen buffers are needed to operate each of the tape recorders, and there are three spares. Any one of these buffers can be configured into any one of the locations so that spacecraft degradation is gradual. There are 32 tracks for recording and three additional tracks: two for synchronization and one for the data selection capability.

4. Timing Synchronizer Subsystem. The TOPS spacecraft is a synchronous machine with all subsystems clocked from the Timing Synchronizer Subsystem (TSS). This is expected to reduce the inter-subsystem timing problems encountered in earlier projects. The present maximum frequency drift rate is $\leq 0.01\%$. Recent refinement of this drift rate indicates that one subsystem may require 0.001% , but it has not been verified that this is an absolute requirement. The timing synchronizer supplies the highest frequency to all subsystems except to the RFS, which has its own internal oscillator generating the frequencies for S- and X-bands. The RFS does use the timing synchronizer frequencies for command decoding, however.

G. Computation and Control

Computation and control are required to (1) control the sequencing of the state of the spacecraft; e. g., the transition from cruise into the encounter phase, then into occultation and into playback; (2) control spacecraft maneuvers; e. g., program the computer, turn the spacecraft, perform the burn, and then point the spacecraft back to Earth; (3) control fault detection, diagnosis, and repair; and (4) control ground command decoding and distribution.

1. Design Point Selection. The design point that was selected for this computation and control function is called the self-test and repair (STAR) computer, which has been in development at JPL since about 1961. A shared memory is provided so that the STAR computer has access to all of the measurements of the measurement processor to eliminate the necessity for an additional set of sensors and an additional set of cabling. There is a command bus to separately distribute the commands from the computer and from the command decoder, thus providing redundant paths. The computer is reprogrammable from the ground to change the status of the spacecraft as desired. The measurement processor provides interrupts to the computer to indicate that there is a fault which needs rectifying. The problem is verified and diagnosed before any corrective action is taken.

2. Control Computer Subsystem. The special-purpose digital computer of the Control Computer Subsystem (CCS) has roughly 100 instructions, a read-only memory at 4096 words, read/write memories at 8192 words, and a shared memory which is a 4096 words read/write memory. (The shared memory is defined as a read/write memory which is also interfacing with the measurement processor.) Each word is 32 bits in length (8 bytes and 4 bits each), and the last byte is used for error-correction purposes. The instructions and data words are coded for error detection, so that almost all errors that can occur in the computer are detected before they propagate into the rest of the spacecraft. Transient error detection and correction are accomplished by the roll-back process. A time allowance exists in the computation so that, if the computer does not agree with the result, it can then roll back and go through the operation again. If the error is a transient, the computer will proceed. If the failure is legitimate, the computer will

roll back again, provide a replacement unit, and then reprocess. Redundant processors are used for internal self-test and repair.

3. Command Decoder Subsystem. The Command Decoder Subsystem distributes ground commands with discrete switch closers by means of an independent command bus and remote decoder arrays in the user subsystems. This function is redundant to the CCS command decoding. By using CCS capability, fewer spare units have to be carried in the command decoder.

4. Pyrotechnic Subsystem. The Pyrotechnic Subsystem function provides the control needed to deploy the RTG boom, the science boom, the science scan platform, the magnetometer boom, the plasma wave detector boom, and the explosive devices to separate the spacecraft from the adapter connected to the Burner II stage.

The Pyrotechnic Subsystem accepts commands from the control computer or from the command decoder and sequences nonreversible functions (squib events) in the spacecraft. The system comprises redundant pyro-activated, electromechanical devices, and the squib firing assembly. Squib firing current comes directly off the power bus. Firing capacitors are no longer required because the power subsystem can handle this power load when it is needed.

H. Attitude Control

1. Attitude Control Subsystem. The Attitude Control Subsystem (ACS) provides the capability for science instrument pointing, antenna pointing, thrust vector pointing, and science maneuvers. Science maneuvers are a new concept in which the spacecraft is rolled every 1/2 AU to provide calibration for the following science instruments:

- (1) The UV photometer (The scan platform would be moved in 15-deg elevation angles to map the hemisphere.)
- (2) The magnetometers
- (3) The plasma wave detectors

The spacecraft is rotated ten revolutions in yaw for science calibration, as well as to provide other useful information every AU.

The design point selected is a three-axis stabilized system using celestial references during cruise, and inertial references during maneuvers. In addition, the inertial references can be used as backups to celestial references. Earth reference is used for high-accuracy antenna pointing. This high accuracy is provided by using the reaction wheel for control torque to minimize the amount of fuel mass that has to be used by the thrusters. Hot-gas thrusters are used to unload the wheels when they become saturated and to provide large torques. The initial Sun acquisition at spacecraft separation (the roll or yaw maneuvers) uses the thrusters to attain the proper rate. Commanded turns occur at 1 rev/h. However, the turns can occur at 3 rev/h without affecting the design appreciably.

The Attitude Control Subsystem includes

- (1) Gas-bearing gyros to provide long life.
- (2) Biased digital Sun sensors to point the spacecraft at the Earth while using the Sun as a reference.
- (3) Reaction wheels to reduce the number of gas jet firings and to decrease weight.
- (4) Programmable control law processing to provide limited cycle operation, thrust vector control, and science platform control.
- (5) A Canopus tracker to provide the roll reference.
- (6) Actuators for orienting the science platform so that the science instruments can see the planets and satellites of interest. The medium-gain antenna actuators point this antenna at the Earth during trajectory maneuver turns. A two-axis gimballed actuator system similar to that of MM71 was used for the trajectory-correction propulsion engine, but other approaches are under consideration. High-gain antenna focusing actuators are being used to compensate for temperature changes with solar constant. The latest design for refocusing used lead screws to move the subdish up and down to compensate for the defocusing.

2. Attitude Propulsion Subsystem. The Attitude Propulsion Subsystem (APS) provides the wheel unloading torques. The hydrazine fuel comes from the trajectory-correction propulsion subsystem and is used to fire the propulsion thrusters at 0.0225 N (0.1 lbf) for 0.1-s pulsewidth. Because of the nature of the blowdown pressurant system, the thrust reduces as the propellant is used during the flight.

Couples in roll are used to allow more flexibility in locating the roll thrusters to maintain control as the spacecraft center of gravity migrates. Moments in pitch and yaw provide the necessary torque about these axes. Solenoid latch valves and squib valves provide the capability to either (1) close off a leaking thruster with a latching valve, or (2) if a leak is above the latches, squib-isolate that entire half of the system and use the other half.

I. Navigation and Guidance

1. Navigation. Spacecraft navigation requires accurate aiming to the target planets with as little trajectory correction as possible to minimize the fuel requirements (see Section II-A). Furthermore, the spacecraft must be biased off the planet to meet planetary quarantine requirements, rather than be heat- or gas-sterilized.

The design point selections include:

- (1) One post- and two pre-encounter corrections at each of the planets except for the Earth and the last in the sequence.
- (2) The use of radio navigation and optical approach guidance.
- (3) Start of optical data acquisition 40 days before encounter at 12 to 24 pictures per day until trajectory correction.
- (4) A trajectory bias allocation of 40 m/s for the planetary quarantine.
- (5) An additional 15 m/s allocated for satellite encounter to compensate for the slight trajectory perturbation caused by the close satellite encounter.

2. Approach Guidance Sensor Subsystem. The Approach Guidance Sensor Subsystem (AGSS) must sense the position of the satellites against a star background. To do this, at least one satellite with a minimum of two

stars in the background must be detected to get the vectors necessary to determine where the barycenter of the satellite planet system is located. An imaging sensor, which is separate from the science instruments at present, provides this function. The sensor is articulated on the scan platform with the science instruments. The total sensor error is ≤ 15 arc-s (3σ), including ground data processing.

3. Trajectory-Correction Propulsion Subsystem. The Trajectory-Correction Propulsion Subsystem (TCPS) provides four trajectory-correction periods: post-Earth, and in the vicinity of each of the three planets. Squib valves are used to isolate the propulsion fuel from the nozzle during long cruise periods to eliminate leakage problems. At the beginning of a trajectory-correction period, a set of squibs is opened. Multiple trajectory burns, using solenoid valves in parallel series, provide as many maneuvers as required to hit the prescribed aiming points.

The subsystem has an 11.34-kg (25-lb), two-axis gimballed thrust engine with an $I_{sp} = 230$ s. The tanking is sized for 205 m/s to accommodate the JUN 1979 mission, and is fueled as required by the specific mission; e. g., 167 m/s for JSP 1976.

A surface tension propellant acquisition device is used instead of a bladder system to force the fuel from the tank to the trajectory-correction engine. An all-metal, welded-joint, blowdown system is used with nitrogen, rather than helium, as the pressurant because nitrogen is less likely to leak.

J. Power

1. Design Selection. RTGs were selected to fill the TOPS requirement for a solar-independent power source with long life. Power is distributed to all user subsystems by a 4800-Hz, AC distribution system, and by a 30-V regulated power system. There is no battery on the spacecraft; thus, reliability is increased.

2. Subsystem. The Power Subsystem uses four RTGs based on the multi-hundred-watt technology developed by the AEC. Indications are that the RTGs will supply 550 W at the beginning of launch and 462 W at 9 years.

A protected bus provides power for critical loads consisting of the measurement processor, the control computer, and the timing synchronizer—the three subsystems required to perform the onboard fault-detection

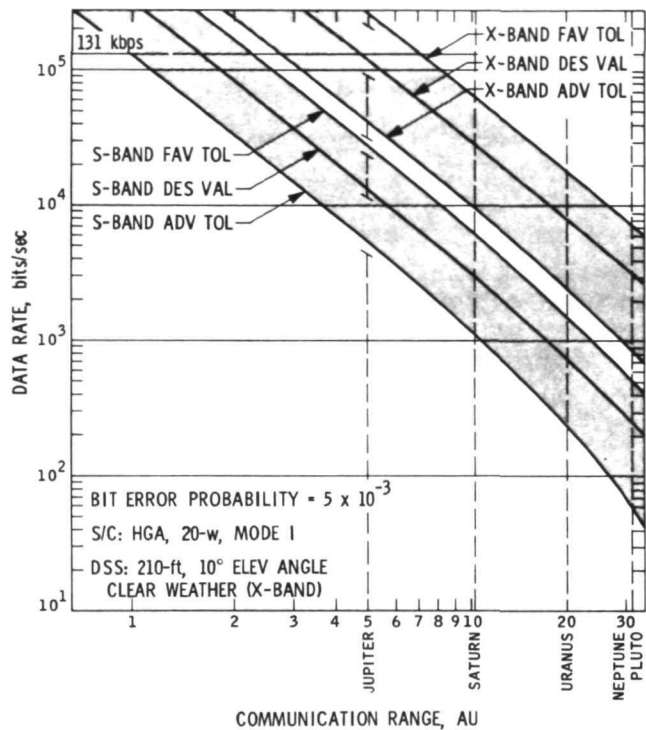


Fig. 14. Baseline data rate capability

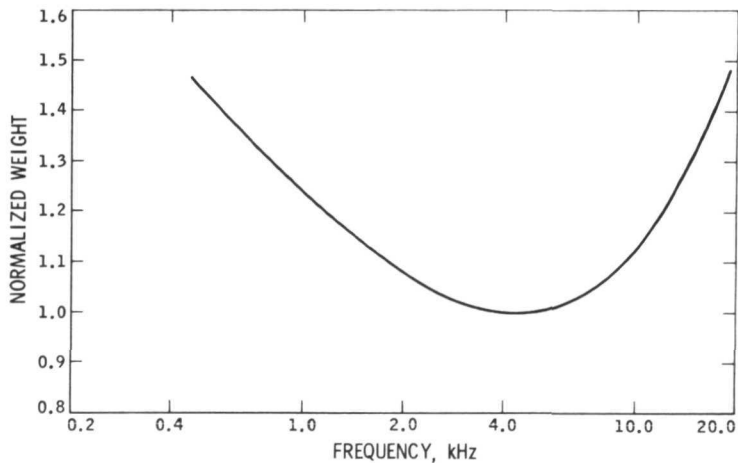


Fig. 15. Weight vs frequency

and-correction. These subsystems provide internally their own switching for small loads. The power is distributed as a 50-V rms square wave at 4.8 kHz from two inverters, one for the protected bus and one for the main bus. In some cases, 30-V DC regulated power is distributed to decrease the losses from inverter inefficiencies.

Table 10 shows the RTG power source characteristics. The hot-junction temperature (T_{HJ}) is 1000°C, and the outside of the RTG is 175°C, which complicates thermal handling. Electrical energy is provided by 312 thermocouples in series parallel combination, without redundancy for potential open or short failures.

Figure 15 is an optimization study of weight vs frequency. The near-optimal point is 4.8 kHz. However, scientists would prefer to operate closer to 10 kHz, or even higher frequencies, to reduce the interference problems with the plasma wave and radio emission detectors. Therefore, a higher frequency may be used.

Table 11 lists the power allocated to the subsystems for the encounter mode. The total power demand of 479 W is more than is available at the last planet, if degradation is as expected, partly because of the 120 W allocated to data storage. This large quantity of power is needed for simultaneous record and playback with both tape recorders and all buffers going simultaneously. However, at the last planet, it is possible to use the tape recorders sequentially because the data-gathering period is long enough to time-phase the recorders and buffers and to reduce the data storage requirement to 61 W. As a result, the maximum power required is below the quantity available.

The upper curve shown in Fig. 16 indicates an RTG operating perfectly with isotope decay only. The bottom curve is based on the assumption that the RTG gradually degrades as it continues to operate. A 25% overall degradation is depicted by the initial drop of the curve before it stays relatively parallel to the first curve. The spacecraft partial power profile, shown in the bottom curve, indicates that the power capability is exceeded only at Neptune encounter (the only encounter shown). Here the tape recorders are in record and playback, which, as previously explained, is not an absolute requirement at that time.

Table 10. RTG power source characteristics

Fuel material	Pure plutonium dioxide (^{238}Pu)
Thermoelectric material	Silicon-germanium
Performance per RTG	<p>Power (beginning of life) 147 W</p> <p>(end of mission at 12 yr) 110 W</p> <p>Voltage 30 V dc</p>
Fuel loading per RTG	2320 W (thermal)
Hot-junction temperature T_{HJ} (beginning of life)	1000°C
Geometry	<p>Diameter 34.3 cm (13.5 in.)</p> <p>Length 54.6 cm (21.5 in.)</p>

Table 11. Power

Subsystem	Encounter, W
Radio Frequency	77
Control Computer	40
Measurement Processor	14
Data Storage*	102
Attitude Control**	79
Power Telemetry	5
Timing Synchronizer	2
Temperature Control*	23
Attitude Propulsion thrusters**	18
Flight Command	8
Power conversion losses	30
Spacecraft subtotal	<u>398</u>
Science	
Control and conditioning logic	7
Cruise science instruments	35
Encounter science instruments	62
Power conversion losses	11
Science subtotal	<u>115</u>
Total power demand	479
*Time-share tape transport and record head drivers (36 W) with temperature control.	
**Time-share attitude propulsion thrusters with reaction wheels (11 W).	

K. Temperature Control

1. Requirements. Temperature control is required to maintain temperatures within acceptable limits as the solar constant decreases by a factor of 900 from Earth to the last planets in these missions.

Micrometeoroid protection must be incorporated in the outer layer of the thermal blanket. The following temperature ranges were selected as design points:

- (1) The outboard instruments, -40 to +40°C
- (2) The electronics compartment, +5 to +20°C
- (3) The propulsion module, +15 to +33°C

Passive temperature control techniques are used on the spacecraft whenever possible.

2. Temperature Control Subsystem. The Temperature Control Subsystem (TCS) comprises

- (1) Radioisotope heaters, located around the thrusters, which are not sensitive to radiation, to prevent freezing of the hydrazine. Radioisotope heaters are also used on the booms for the magnetometer and the plasma wave detector because those science instruments are not particularly sensitive to radiation. Further study may indicate that electrical heaters may be better on the booms than the radioisotope because electrical heaters are easy to install, but power and weight increases must be considered as part of the tradeoff.
- (2) Electrical heaters, used, in addition to the heat generated by the instrument or engineering function in the area, to compensate for heat loss.
- (3) Louvers, which provide a means to maintain equipment within temperature limits when changing the heat dissipated within a given area. They rid specific locations of excess heat. In particular, the radio, power, and storage bay heat loads vary and are hot when all the equipment is working.
- (4) Thermal shields are used as a passive technique wherever possible.
- (5) Thermal radiator surfaces dissipate heat to cool the IMR, which has to have a very cold temperature for one of its sensors, and also to cool the imaging sensor because the television (TV)

requires a temperature of at least -40°C to operate at 131 kbits/s.

L. Structures and Mechanisms

1. Requirements. Structures and mechanics requirements are to (1) integrate the subsystems physically, (2) align the components correctly, (3) provide ground handling capability for easy installation of equipment, (4) provide meteoroid protection additional to that supplied by the thermal shield, and (5) decrease spacecraft weight wherever practical.

2. Design. The structures and mechanisms design includes a centralized electronics compartment with deployable booms for the science platform, the RTGs, the magnetometer, and the plasma wave detectors. It is desirable for these devices to be self-supporting in the Earth field to minimize testing time and cost, and they are designed under the constraint that deploying them should be no more difficult than deploying the solar array on the Mariner spacecraft

High-density packaging is a requirement. Smaller cable connectors and smaller cabling bundles must be used so that the overall structures compartment can be made smaller. The standard module is 35.6×17.8 cm (14×7 in.) and as high as necessary to package the subsystem.

3. Structures Subsystem. Most of the major electronics are packaged in the electronics compartment. Some items (e. g., the reaction wheels) are packaged in the propulsion compartment; and some science electronics are packaged with the individual science instruments. Micro-meteoroid shielding and hoods are used to prevent the impact of particles on the optics of the TV and other sensors during the cruise period. The propulsion compartment is separable from the electronics compartment to facilitate parallel assembly and test. A high-gain antenna superstructure mates the high-gain antenna to the spacecraft. The Structures Subsystem also includes the structure for the science and RTG booms. An aluminum open-truss structure is employed throughout the subsystem except near the RTGs, where titanium is used because of the heat.

4. Mechanical Devices Subsystem. The Mechanical Devices Subsystem includes (1) the spacecraft separation mechanisms, such as the springs that push the spacecraft away from the Burner II stage and from the adapter;

(2) a boom mechanism for deployment and dampers to stop the deployment motion to avoid damage to the mechanism; (3) the science platform on which the encounter science is mounted; (4) the magnetometer and plasma wave detector booms, which deploy instruments 9.14 m from the spacecraft; (5) the high-gain antenna mechanisms, which pull the ribs into position to deploy the unfurlable portion of the antenna, and (6) the cable mechanism that holds the antenna in the launch configuration.

5. Cabling Subsystem. The Cabling Subsystem uses plug-in assemblies to minimize the total amount of cabling needed. Cabling lengths are shortened to reduce weight and improve circuitry. Small-gage wire, from 26-gage for system cabling to 30-gage for subsystem cabling, is used to reduce the weight. Fifty-mil node interconnections are used to ensure that the volume is primarily used for the electronic piece-parts themselves, with the cabling taking as little space as possible.

6. Packaging. In addition to high-density packaging and 50-mil node interconnections, plug-in assemblies with single side access are employed. A new packaging concept has been adopted for the microelectronics, and a new electronics package is being developed for the components themselves to reduce the magnetics problem associated with present packages and to increase reliability. Each electronic assembly has been functionally sized.

Parallel mechanical/electrical system operations have been a consideration in the packaging design. The redundant flight structure has been reduced by using jigs, etc., during buildup and test, when the structural integrity has been impaired by an incomplete assembly. With a complete spacecraft assembly, the jigs do not have to be flown. Precision tooling is used for this interface mechanical alignment.

M. Mass

Table 12 is a mass summary for the JUN 1979 spacecraft. As can be seen, there are several very heavy subsystems on this spacecraft, but the Power Subsystem is the heaviest. There is some uncertainty in the RTG weight number, which varies from the 34-kg (75-lb) figure given by the AEC, to 41.73 kg (92-lb) given for the first test unit by another project. At present, JPL is using 36.29 kg (80 lb) per RTG. Propulsion fuel requirement is dependent upon assumptions about ephemeris accuracy, the approach

guidance function, and the quarantine constraint. If the quarantine constraint can be mitigated, the 40-m/s velocity increment can be reduced. A 1-m/s velocity increment requires approximately 0.4 kg of propellant on the spacecraft when nonpropulsive elements are included.

Table 12. Mass summary, JUN 1979

Item	Mass	
	kg	lb
Structure	102.05	225
Radio	39.01	86
Modulation/demodulation	8.16	18
Command decoder	1.36	3
Power	180.53	398
Control computer	20.87	46
Measurement processor	6.35	14
Attitude control	45.81	101
Pyrotechnics	6.80	15
Cabling	25.40	56
Propulsion	106.14	234
Temperature control	17.69	39
Mechanical devices	33.11	73
Approach guidance	13.61	30
Attitude propulsion	14.06	31
Data storage	57.15	126
Antennas	30.39	67
Timing synchronizer	1.81	4
Science payload	106.60	235
Instruments (185)		
Control and conditioning logic (19)		
Redundancy (31)		
Science radiation shielding	4.54	10
Total	821.45	1811

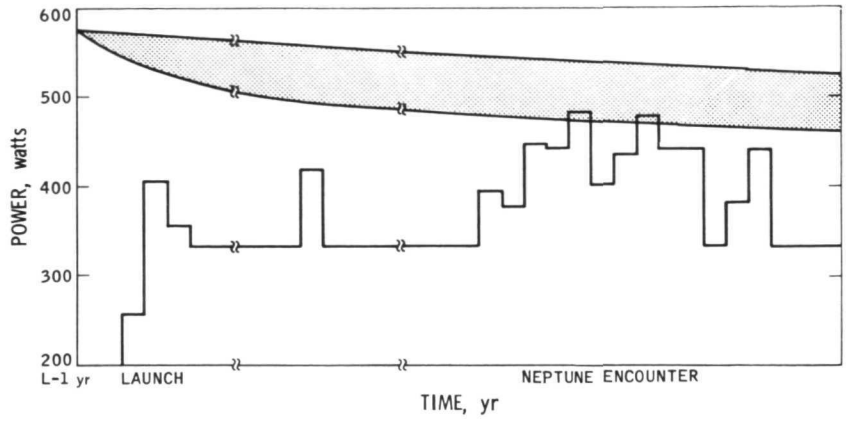


Fig. 16. Partial power profile and RTG output

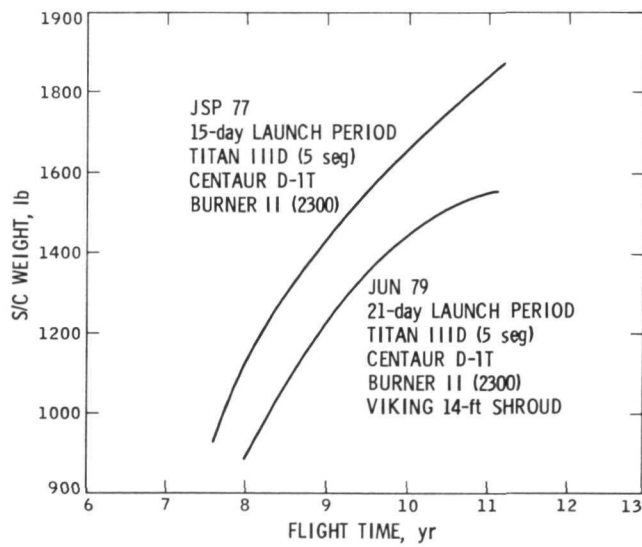


Fig. 17. Spacecraft weight vs flight time

Figure 17 shows spacecraft weight vs mission duration time. Weight has been reduced in some areas as much as possible without compromising mission requirements. However, further reductions must be made, difficult as this may be.

TOPS provides an approach to a versatile spacecraft design that can be adapted to mission requirements. The spacecraft has the capability to communicate large quantities of scientific information, and its flexibility makes it scientifically effective.

IV. ENVIRONMENT AND RADIATION CONSTRAINTS

A. Environmental Requirements

The objectives of the TOPS environmental studies were to develop engineering models of significant environments affecting a vehicle in outer space, and to provide related environmental design characteristics and restraints to the TOPS design team. Also, test requirements were established for the developmental testing of new piece-parts and existing radiation-sensitive parts, with the goal of standardization of radiation environmental test programs.

1. Jupiter Models. Jupiter radiation belt design and test requirements evolved from early maximum estimates of the trapped radiation belt that had been based on Earth analogy to estimates derived from studies of synchrotron emissions. The models presented are based on a NASA monograph, "The Planet Jupiter" (NASA-SP-8069, 1970), and results of the Jupiter Radiation Belt Workshop held at JPL in July 1971. The requirements derived from the latest models (Table 13) are maximum near-surface levels established for Jupiter flyby and without accounting for trajectory-dependency during flyby. The design levels in use at the close of the TOPS Project were for the proposed JSP 1976 mission. A comparison of two maximal near-surface models for the 1976 mission is provided in Figs. 18 and 19.

Electron and proton fluxes are shown in Figs. 18 and 19 as a function of altitude of closest approach. These are pre-workshop models which had a nominal model and an upper-limit model. The values used in the models show the influence of shielding on radiation and the influences of various distances of closest approach. The 150 mils of aluminum shielding constitutes that provided by the spacecraft itself and does not represent additional shielding allocated for protection.

2. RTG Radiation Requirements. During the roughly 3-year period of TOPS activity, RTG levels evolved from maximum estimates based on a bare fuel capsule to detailed estimates based on the Atomic Energy Commission's Multi-Hundred Watt RTG. In the early phases of TOPS design, spacecraft-afforded shielding was neglected and the levels were based on the maximum radiation conditions. However, as the spacecraft design

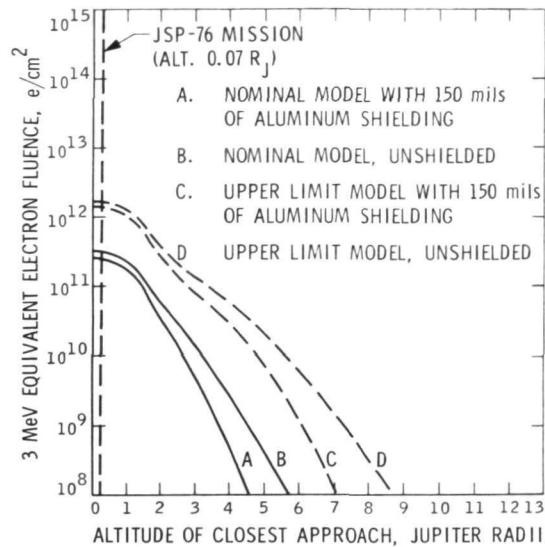


Fig. 18. Equatorial flyby electron fluences (shielded and unshielded)

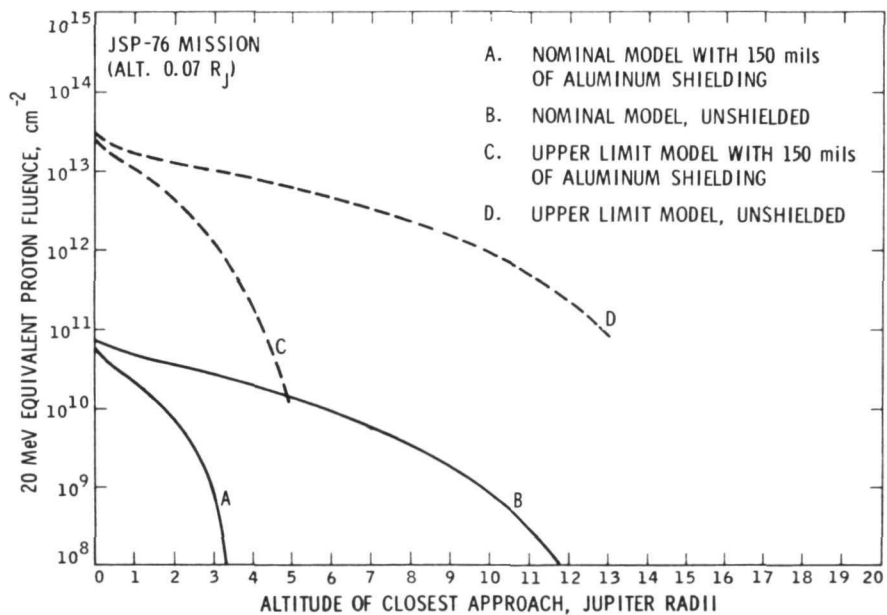


Fig. 19. Equatorial flyby proton fluence (shielded and unshielded)

Table 13. Comparison of Jupiter radiation belt design fluences

Electrons	Fluence (particles/cm ²)	
	Pre-workshop	Workshop
Energy, MeV		
0.25 - 3	6.4×10^{10}	4.9×10^{10}
3 - 10	5.1×10^{10}	1.1×10^{11}
10 - 30	2.2×10^{11}	2.4×10^{11}
30 - 100	3.2×10^{11}	2.0×10^{11}
100 - 300	2.5×10^{10}	1.1×10^{10}
Protons		
1 - 3	5.7×10^9	8.9×10^{11}
3 - 10	1.7×10^{11}	1.7×10^{12}
10 - 30	9.6×10^{11}	3.3×10^{12}
30 - 100	3.9×10^{12}	6.9×10^{12}
100 - 300	1.6×10^{12}	1.5×10^{13}
300 - 1000	6.1×10^9	2.8×10^{13}
1000 - 3000	4.7×10^8	2.0×10^{13}

evolved, separation distance from the RTG's and their orientation were considered, in addition to spacecraft-afforded shielding.

The location of the RTG's in the spacecraft configuration and their orientation to the electronics compartment and scan platform are illustrated in Fig. 20. Design restraints and piece-parts testing levels are also described in the illustration. These piece-parts test levels are independent of spacecraft design. At 10^5 rad and 1.5×10^{13} neutrons/cm², the piece-parts test levels are approximately 10 times higher than design restraint levels. This allows a sufficient safety margin; i. e., if the parts survive these higher levels, it is reasonable to expect that assemblies will satisfy the design restraint levels.

3. Other Environments. Magnetic constraints are applied to the TOPS spacecraft in order to avoid interference between the spacecraft field and the fields being measured. The magnetic fields also affect the spacecraft and its components. Magnetic levels, in turn, dictate the magnetometer boom requirements. The interference magnetic field experienced at the magnetometer sensor is derived from the magnetic moment of the spacecraft and the distance from the sensor to the spacecraft. A plot of the distance between the magnetometer sensor on the end of the boom and the spacecraft centerline as a function of the magnitude of total spacecraft dipole moment for a fixed field level is shown in Fig. 21. For TOPS, the requirement is 0.01 γ at the sensor. Examination of other spacecraft-produced magnetic fields led to an estimate that the 0.01 γ would correspond to a spacecraft dipole moment of about 40 gauss-cm³ and a boom requirement of approximately 9.14 m (30 ft).

The TOPS magnetic field requirements are also compared to those of other spacecraft in Table 14. For example, Pioneer A in a permed condition is higher than the TOPS dipole moment by a factor of nearly 3. Consequently, the TOPS designers were asked to design to a level about a factor of 3 more severe in the permed condition than the level used for Pioneer A. However, the magnetic field allocations for hardware on both spacecraft were about the same.

Allocations based on the 0.01- γ sensor requirement are given in Table 14. The allocations assessed for various compartments and subassemblies, components, and piece-parts assume that hardware will be exposed to 25 Oe (gauss). This appears to be the case both in the testing process (caused by vibrations and shaking) and in planetary encounters. These levels must be satisfied as testing is conducted for various categories ranging from piece-parts and component subassemblies to assembly.

The factor for TOPS was about 1/100 of the magnetic field levels that were satisfied for the Mariner spacecraft. However, Mariner missed satisfying its specified level by almost a factor of 10. Ultimately, the same fields existed for TOPS hardware as for the Mariner, but they must be satisfied, and satisfied in permed condition. This requirement is admittedly advanced, and might incur cost problems. Consequently, designers were required to avoid soft magnetic materials, employ compensating magnets

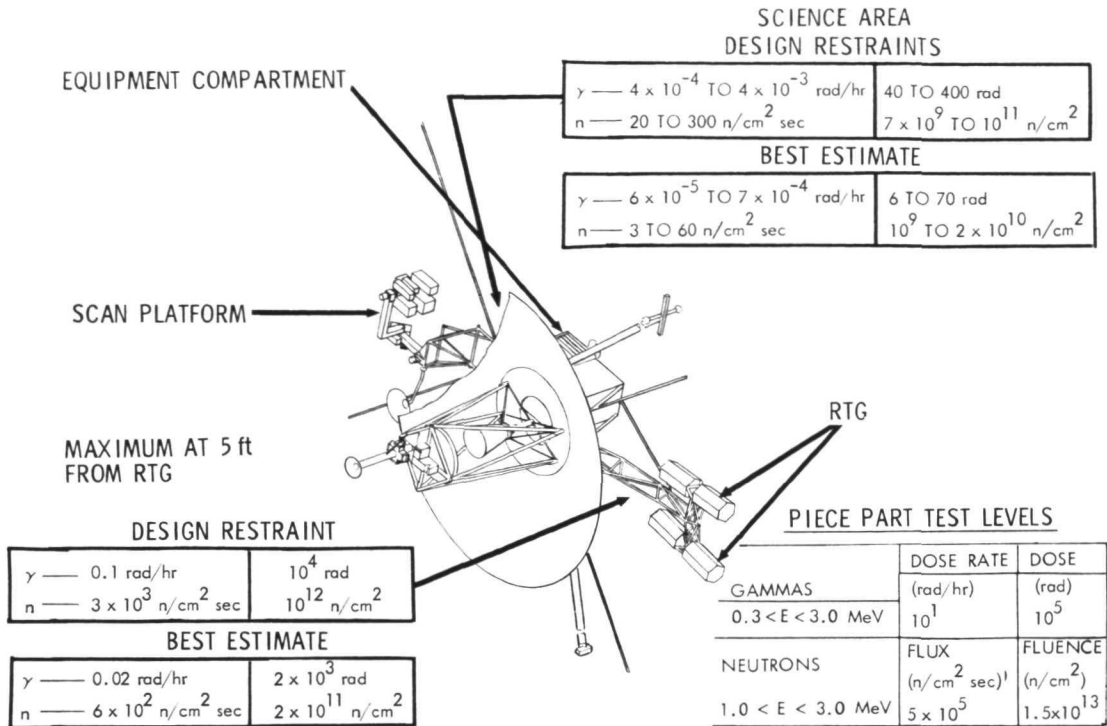


Fig. 20. Location of RTG radiation levels

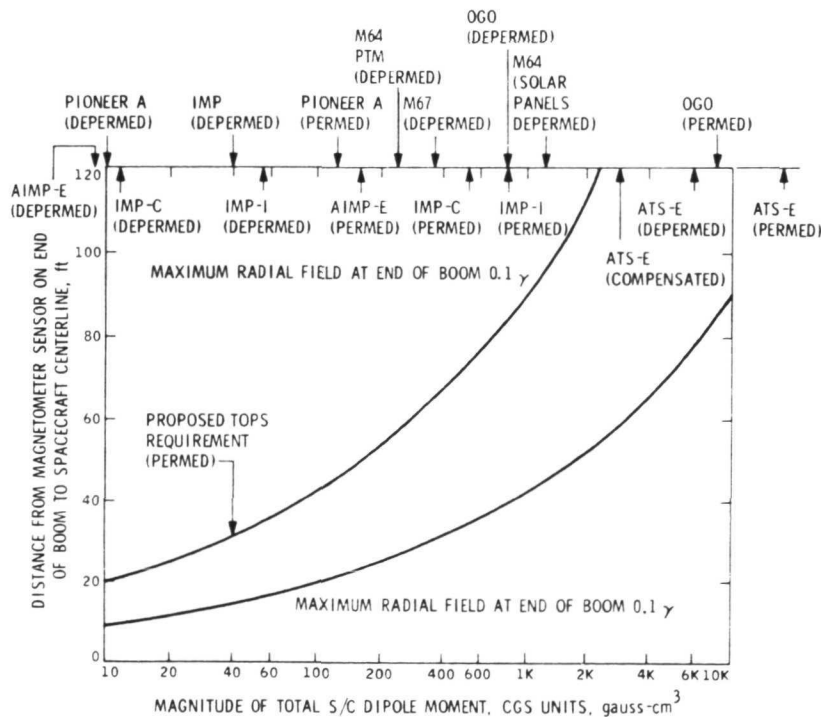


Fig. 21. Magnetometer boom requirements

Table 14. Tops environmental design requirements
magnetic field restraints

Static magnetic field and field stability	Sensor requirement $\leq 0.01 \text{ Y}$ at 9.14 m
Spacecraft hardware category	Maximum radial field after exposure to 25 Oe, γ^a
Bay or assembly	5 at 0.91 m
Subassembly	1 at 0.91 m
Components	2.5 at 30.48 cm
Piece-parts	20 at 15.24 cm - 10 items/assembly 1 at 15.24 cm - remainder/assembly
Natural magnetic fields	
Source	Level
Earth	0.5 G
Jupiter	30 G; 2-h exposure
Other outer planets	Maximum represented by Jupiter
Interplanetary	10^{-3} G (maximum)
^a Allowable level at the sensor is 1/100 of the level previously set on sensor of the Mariner spacecraft.	

with degaussing loops, and take piece-parts field measurements for qualification. They were also requested to employ efficient electrical wiring design practices, perform magnetic shielding tradeoffs, and conduct magnetic mappings at all levels of hardware.

4. Space Debris. The asteroid and micrometeoroid debris model was taken from the NASA monograph, "Space Vehicle Design Criteria for Interplanetary Meteoroid Environment Model" (NASA-SP-8038, 1970). Mass distributions for the expected number of impacts are presented in Table 15. The TOPS design point is to stop particles of mass $\leq 2 \times 10^{-3}$ g. If this could be accomplished, it would satisfy a design goal of 99% probability of

Table 15. Asteroidal and micrometeoroidal debris model and design requirements

Mass	Expected number of impacts /m ²
$2 \times 10^{-3} - 10^{-3}$	4.2×10^{-3}
$10^{-3} - 10^{-4}$	5.4×10^{-2}
$10^{-4} - 10^{-5}$	3.8×10^{-1}
$10^{-5} - 10^{-6}$	2.6×10^0
$10^{-6} - 10^{-7}$	1.8×10^1
$10^{-7} - 10^{-8}$	1.2×10^2
$10^{-8} - 10^{-9}$	8.6×10^2
Particle design mass	2×10^{-3} g
Particle impact velocity	20 km/s
Particle density	3.5 g/cm ³
Effective spacecraft exposure	2 m ²

no penetration into the spacecraft electronics. Some shielding would be required. Preliminary parametric studies show that the shielding requirement varies from, say, 9 to 90 kg (20 to 200 lb), depending on the penetration model and assumptions used. Weight and design of the shield were not determined.

A further requirement specified that no serious degradation of spacecraft subsystem functions with particle impacts occur at this level, and that smaller particles which could cause erosion also be stopped. Therefore, adequate protection is required for exposed critical areas, such as science optical equipment.

5. Temperature Considerations. The general temperature design characteristics and restraints are specified for the science scan platform, electronics compartment, spacecraft structure, and antenna. The levels described include margins over the operating range which are qualitatively identified (Fig. 22). Included are margins to the test range and an additional margin to the design range. The typical (JPL) margin of 25°C is added to

the temperature control range to obtain the test range, and an additional margin of 10°C is added to the test range to obtain the design range.

6. Piece-Parts Test Program. The piece-parts radiation test program produced significant information on test implementation, performance, and some basic results useful in parts selection. The basic objective of the testing was to produce radiation effects data on electronic devices (about 15 part types) to evaluate sensitive components and piece-parts.

In addition, the test results were used to develop radiation test requirements and procedures. Selected test levels are given in Table 16. The approach was to use available facilities and capabilities, test the selected parts, modify the test levels where necessary to expedite the operation, and characterize critical parameters, perform tests, and evaluate test results.

Table 16. Planned radiation test levels for piece-parts

Test	Energy, MeV	Flux or dose rate	Fluence or dose
Gamma damage	0.3< \bar{E} <3.0	<10 ⁵ rad/h	10 ⁵ rad
Electron damage	3.0	<10 ¹⁰ e/cm ² -s	4.5 × 10 ¹² e/cm ²
Neutron damage	1.0< \bar{E} <3.0	<10 ⁹ n/cm ² -s	1.5 × 10 ¹³ n/cm ²
Proton damage	3.0 - 4.0	<10 ¹⁰ p/cm ² -s	4.0 × 10 ¹² p/cm ²

In the electron test, 2 MeV was used as the test energy instead of 3 MeV as originally planned. The flux was near 10¹⁰ e/cm²-s, and total fluence was achieved. Gamma backgrounds were negligible.

In the neutron tests, a TRIGA reactor was used, with a modified fission spectrum having an average energy of about 1.5 MeV. Although the flux was somewhat high, no rate effects were expected. Because the reactor was used, a gamma background existed. However, the reactor gamma level was only 4% of the test level for gamma testing.

In the proton test, the requirements were also modified: 140-MeV protons were used instead of 4-MeV protons in order to make use of the Space Radiation Effects Laboratory. In either case, the test would have been

a spectrum equivalence test for either 140 or 3 to 4 MeV. The equivalent fluence was 9×10^{12} p/cm² of 140 MeV which is equivalent to 4×10^{12} p/cm² of 4-MeV protons. During the tests, neutron and gamma background radiation was present. The secondary gamma level was higher than anticipated: 5×10^4 rad. This constituted 50% of the test requirements for a gamma level, but only 8 or 9% of the proton test dose of 6×10^5 rad.

7. RTG Radiation Test Model Test. The radiation test model measurements helped to provide experimental verification of analytic methods. The analytic method is a Monte Carlo solution of the transport equations for both neutrons and gammas. In this test, only gamma measurements were obtained for correlation with the analytic solutions.

It was desirable also to determine experimental techniques for performing large system radiation testing, which includes RTGs aboard the spacecraft. In addition, use of the RTM was a first step toward verifying subsystem orientation and positioning, and toward identification of potential interference with sensitive scientific instruments. The important aspect of this type of testing is that it allows study of science instrumentation orientation.

The tests were performed in the JPL 3-m (10-ft) simulator building. The RTM simulated the structure, antenna, electronics compartment propellant and tankage, and the science scan platform. Gamma radiation (from the RTGs) was also simulated with radioisotopes, using a simulated RTG.

Analytic methods of unfolding detector radiation responses were used to interpret radiation measurements and to examine the free-field spectrum surrounding the spacecraft simulated configuration. These reduced measurements were compared with the computed fields for the RTM. The correlations were used to update current RTG radiation analytics and estimates.

The test development phase of the RTM study was completed during the TOPS Project. The second phase was in progress at the close of the Project, including in-air mappings, air-scattering measurements, and preliminary mappings for the RTM. The third-phase final mapping was not conducted.

In conclusion, radiation studies conducted at JPL showed that the piece-parts test levels may be moderately damaging to some parts. For the Jovian radiation belt within $2R_J$, electrons may be moderately damaging to some parts, while protons may be seriously damaging to many parts. On the other hand, in the Jovian radiation belt beyond 2 or $3 R_J$, the fluence decreases significantly and the energy decreases nominally. The advantage of both of these decreases is found in the provision of a large order of tradeoffs for mission design.

B. RTG Free-Field Radiation

In analyzing the RTG and its radiation implications to the spacecraft and the instruments, three topics were examined in detail: (1) the heat source, (2) the MHW thermoelectric generator, and (3) radiation free-field analysis.

1. Heat Source. The heat source involves two different areas: neutron characterization and gamma characterization.* The number of fuel spheres required for the HELIPAK heat source varies from 18 to 24, depending upon power requirements, but 24 spheres was assumed, with a net thermal power of 2200 W. Fresh fuel was assumed for neutron yield, and 18-year-old fuel was assumed for gamma radiation. Neutron emission from the fuel was assumed to be 40,000 neutrons/s-g ^{238}Pu , with a subcritical multiplication factor of 1.25. An assumption of 1.2 ppm ^{236}Pu was also made.

In neutron characterization, five areas were examined in detail: (1) characterization of spontaneous fission from plutonium; (2) examination of neutron yield from (α, n) reactions with impurities; (3) investigation of neutron yield from (α, n) reactions with oxygen, particularly ^{18}O ; (4) estimation of photo-neutron formation; and (5) determination of the subcritical neutron multiplication.

The overall neutron yield from a 2.2-kw MHW heat source in neutrons/g PuO_2 -s-MeV vs neutron energy in MeV is illustrated in Fig. 23. The spontaneous fission yield is very low. The neutron yield from the (α, n) reactions on impurities such as fluorine is larger, followed by the (α, n) reaction with ^{18}O . The topmost curve shows total yield.

*Plutonium molybdenum cermet fuel form was assumed throughout the analysis.

AFFECTED SPACECRAFT AREA	TEMPERATURE DESIGN RANGE, °C	
	LOW	HIGH
SCIENCE SCAN PLATFORM	-75	85
ELECTRONICS COMPARTMENT	-30	55
STRUCTURE AND ANTENNA	-255	125

Fig. 22. General temperature design characteristics and restraints

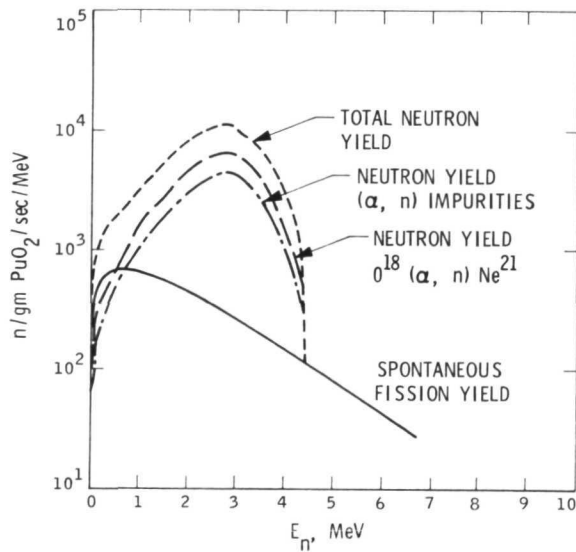


Fig. 23. Total neutron yield from a 2.2-kW MHW PuO₂ source

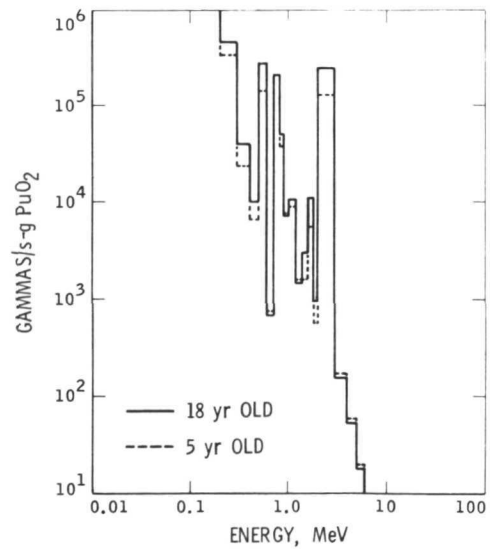


Fig. 24. Five- and 18-year-old gamma spectra from PMC fuel

Gamma characterization is difficult since gamma energies extend from 17 keV up to approximately 2.8 MeV. Considered are the various plutonium isotopes and the decay of ^{236}Pu . The $^{18}\text{O}(\alpha, n)^{21}\text{Ne}$ reaction gives rise to gamma energies from 350 keV to approximately 2.8 MeV. Again, spontaneous fission gammas contribute to the overall spectrum, as do the equilibrium fission product gammas.

Another problem is the decay chain of ^{236}Pu . Fresh fuel produces a relatively simple spectrum, but as the fuel ages, a spectral buildup occurs, particularly with respect to the 2.6 MeV line from ^{208}Tl . In view of this buildup, an 18-year-old fuel was assumed as the point of maximum buildup.

The overall gamma spectrum, which takes into account all of the isotopic contributions plus the ^{236}Pu decay, is shown in Fig. 24. An 18-year-old spectrum is shown in solid lines and a 5-year-old one in dashed lines. These spectra are cut off at about 150 keV somewhat arbitrarily. Photons below this energy will probably be captured in the heat source.

2. MHW Thermoelectric Generator. The second aspect of the three tasks includes the physical description of the MHW thermoelectric generator and its application in a free-field analysis.

The physical description consists of geometric simulation of the generator, including generation of surface sources. After comparing surface sources to actual MHW-RTG results, acceptable sources were applied to generate free fields for the TOPS spacecraft. A comparison between an actual RTG and the geometric simulation used in this Monte Carlo analysis is presented in Fig. 25.

The surface sources were developed and used as a method of approximation. The RTG surface was sectioned into 6 radial and two axial parts. Detector points used were at 1 m from the center of the RTG at 0, 45, and 90 deg from the longitudinal cylinder axis. The results of an actual Monte Carlo analysis of the heterogeneous fuel capsule assembly is shown in Table 17. At 90 deg, the results indicate a 50% overprediction, at 45 deg, they show a worst-case underprediction of 38%, and at 0 deg, the worst-case result is a factor of 3 overestimate. The neutron results are considerably better.

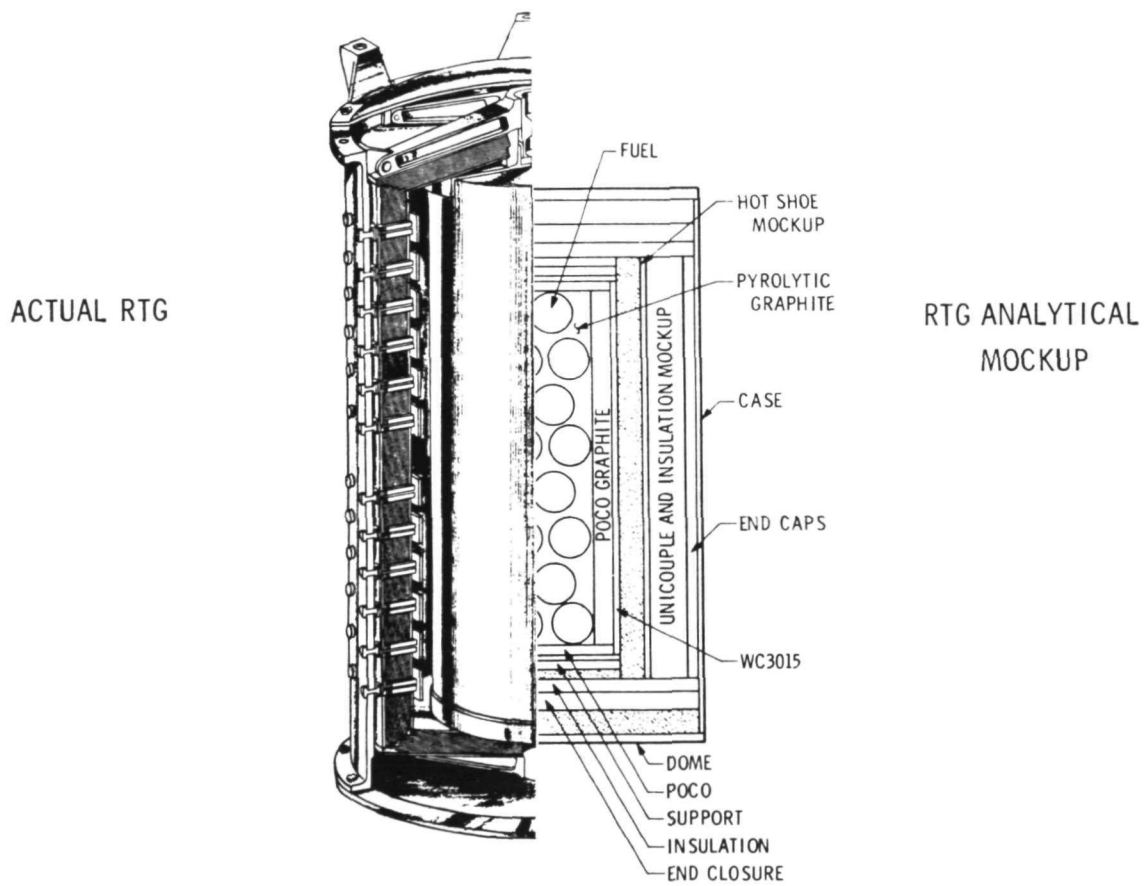


Fig. 25. Geometrical simulation of a 2200-W (thermal) RTG

Table 17. Monte Carlo analysis of heterogeneous fuel capsule assembly

Detector point	Number flux ratio	Energy flux ratio	Dose rate ratio
90 deg, 100 cm	1.47	1.57	1.56
45 deg, 100 cm	0.841	0.624	0.641
0 deg, 100 cm	2.32	3.03	2.92

3. Free-Field Analysis. The surface source terms were applied to a free-field analysis of the TOPS spacecraft. Figure 26 illustrates the isoflux lines for both neutrons and gammas resulting from leakage radiation from the four RTGs. The 500-cm point at 0 deg is very important because of sensitive science instruments in this area. The neutron flux at this point is 1000, and the gamma is 500, based upon the assumptions given.

4. Radiation Summary. The major tasks of the RTG radiation analysis was fuel source characterization, physical description of the MHW-RTG, and free-field analysis. Results will allow the scientific community to assess their experiments with regard to long-term neutron and gamma interference and/or damage on a TOPS-type mission.

C. RTG Simulation

A simulated radioisotope thermoelectric generator (SRTG) was developed as part of the TOPS Project to produce a low-cost, safe, and readily available device using small fuel inventory, that would simulate gamma ray and neutron spectra in both energy and intensity. In order to use the SRTG on a radiation test-model-type spacecraft, the device was configured as closely as possible to a real RTG.

The SRTG permitted radiation mapping on a spacecraft mockup. The energy spectrum and dose rate could be determined at any given location on the mockup or, on the other hand, could be applied to any location. Again, the SRTG enabled a determination of radiation interference with science instruments on the spacecraft. A special advantage of the SRTG over use of the RTG itself was cost-effectiveness: the RTG was priced at over \$1 million, the SRTG at a few thousand dollars. Other advantages were a very flexible simulation of fuel age and impurity concentration.

In developing the SRTG, primary consideration was given to the gamma-ray spectrum and the overall configuration; only minimal effort was devoted to neutron simulation. Two developmental approaches were considered: (1) simulation of the gamma-ray spectrum emitted by the RTG, and (2) simulation of the gamma-ray spectrum emitted by nuclei of the fuel material. The latter approach was chosen. Once a match was achieved between simulated and fuel material radiation, the self-attenuation of the fuel material was simulated, followed by simulation of the absorption and scattering of all other RTG material. Next, radiation transport methods were employed on an input fuel spectrum to calculate the gamma-ray spectrum external to the SRTG. The calculated spectrum derived was then compared with a calculated spectrum from the real RTG; if there was not acceptable agreement, the simulation was modified and reiterated until a satisfactory simulated spectrum was obtained. Thereafter, a simulated fuel capsule assembly was fabricated, and ultimately, the entire simulated RTG.

To simulate the gamma-ray spectrum emitted by the nuclei of the fuel material itself, the gamma-ray intensities from ^{238}Pu were lumped with impurities into broad energy groups. These groups were simulated, using gamma rays from radioisotopes where ^{133}Ba was used to mock up low-energy regions of the spectrum, ^{137}Cs medium-energy regions, and ^{60}Co high-energy regions. The decay chain for ^{236}Pu impurity concentration was mocked up using ^{228}Th . Of the four fuels used in the simulation, the ^{228}Th produces the greatest amount of radiation after a few years of fuel age, emitting 102 millicuries (mCi) at fuel age 18 years, compared to 2.05 mCi for ^{133}Ba , 23.10 mCi for ^{137}Cs , and 0.64 mCi for ^{60}Co (see Table 18). Mockup of the fuel age for simulation purposes was accomplished by varying the amount of ^{228}Th in the ^{236}Pu impurity concentration. Or, in terms of final fuel age, a variation of the amount of ^{228}Th produced different initial impurity concentrations of ^{236}Pu .

Distribution of radioisotopes in a simulated fuel capsule assembly (SFCA) is illustrated in Fig. 27. The isotopes are distributed evenly in several stainless steel rods inserted in a hollow cylinder of depleted uranium, which simulates fuel self-attenuation. This cylinder was placed in a second cylinder of graphite which mocks up the ablative graphite used in re-entry of the real RTG, and this second cylinder was inserted, in turn, in an aluminum can, the whole comprising the complete SFCA (Fig. 28).

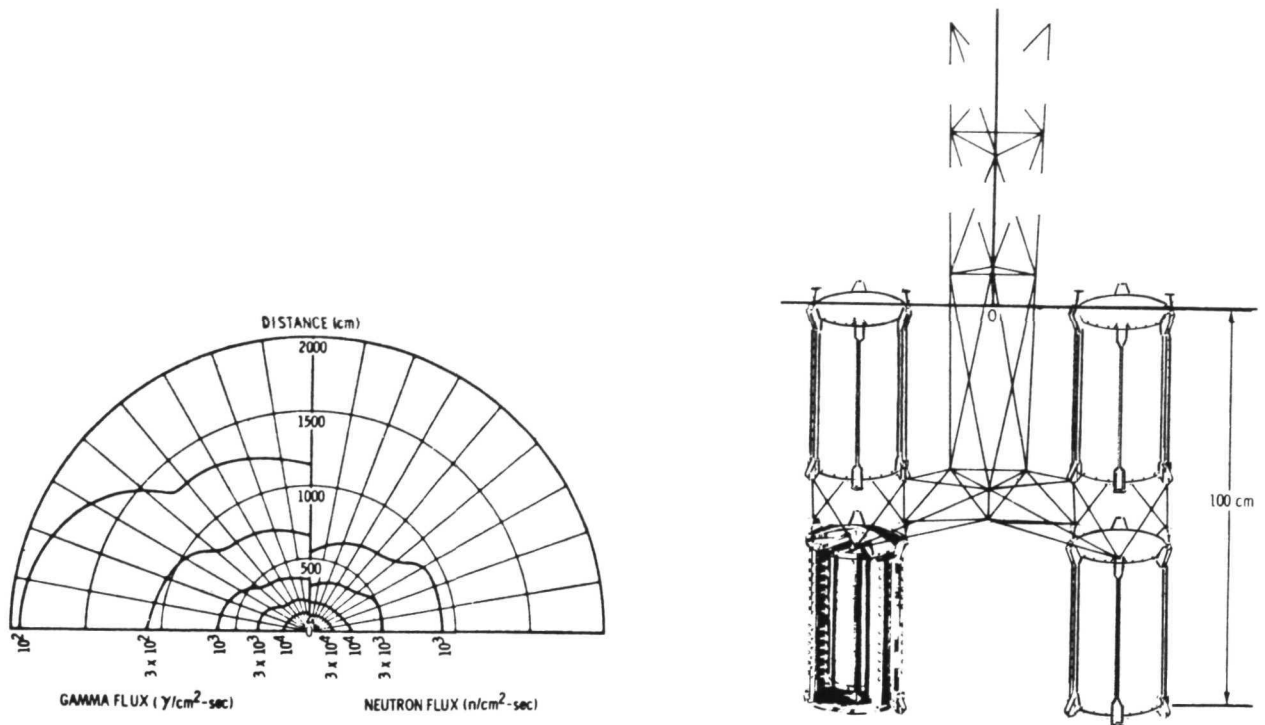


Fig. 26. Power source isoflux distribution

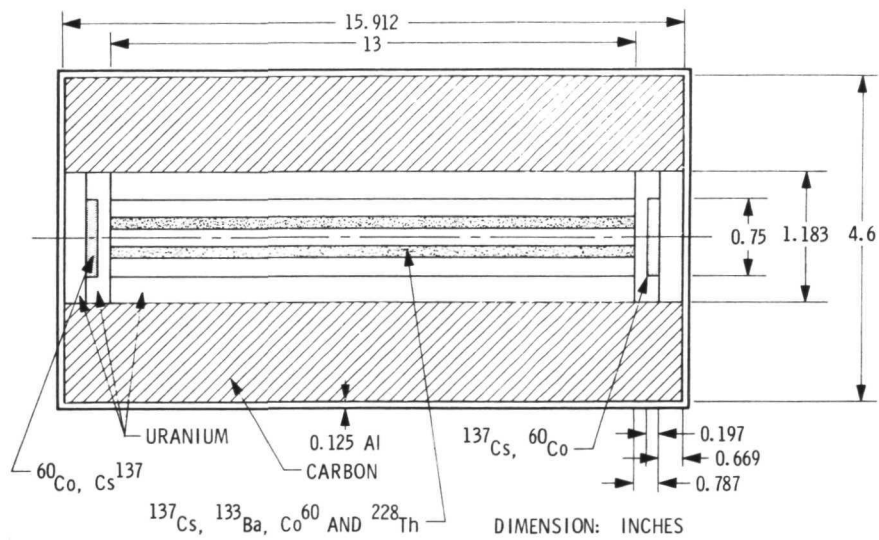


Fig. 27. Simulated fuel capsule assembly

Table 18. Quantity of isotopes, mCi, for 2200 W (thermal) SRTG, 1.2 ppm ^{236}Pu

Fuel age, years	^{133}Ba	^{137}Cs	^{60}Co	^{228}Th
0	1.30	26.00	0.75	0.00
1	1.37	25.90	0.75	4.24
5	1.58	25.30	0.73	49.90
10	1.79	24.60	0.70	88.10
18	2.05	23.10	0.64	102.00

To formulate the final SRTG (Figs. 29 and 30), the fuel capsule assembly was enclosed in an outer housing containing both a radial and an axial shield (Fig. 31), which mocked up the attenuation and scattering of gamma rays caused by thermoelectric elements, insulation material, and support structure of the real RTG. The overall dimensions of the SRTG closely approximate those of the real RTG. Thus, the device, when attached to a radiation test model spacecraft, will subtend the proper solid angle from any viewpoint on the spacecraft.

Mockup models used in analytical radiation studies are shown in Fig. 32. The upper half of the illustration depicts the real RTG analytic mockup, the lower half the simulated RTG, including the simulated fuel capsule assembly. From the models, radiation transport calculations were made to determine the spectrum at various angles from axial through the radial directions. The results of these calculations are illustrated in Fig. 33, where radial and axial radiation between a real RTG with 18-year-old fuel and the simulated RTG were compared. The relative gamma-ray intensity was plotted as a function of the gamma-ray energy, running from approximately 2.6 MeV down to about 400 kV. The simulation effort (i. e., the match) was considered successful.

Simulation of the neutron spectrum was more difficult than with gamma-radiation; however, neutron radiation poses a problem only to a small number of instruments. The primary concern arising from neutron radiation involves damage to instruments from a total dosage over a full mission

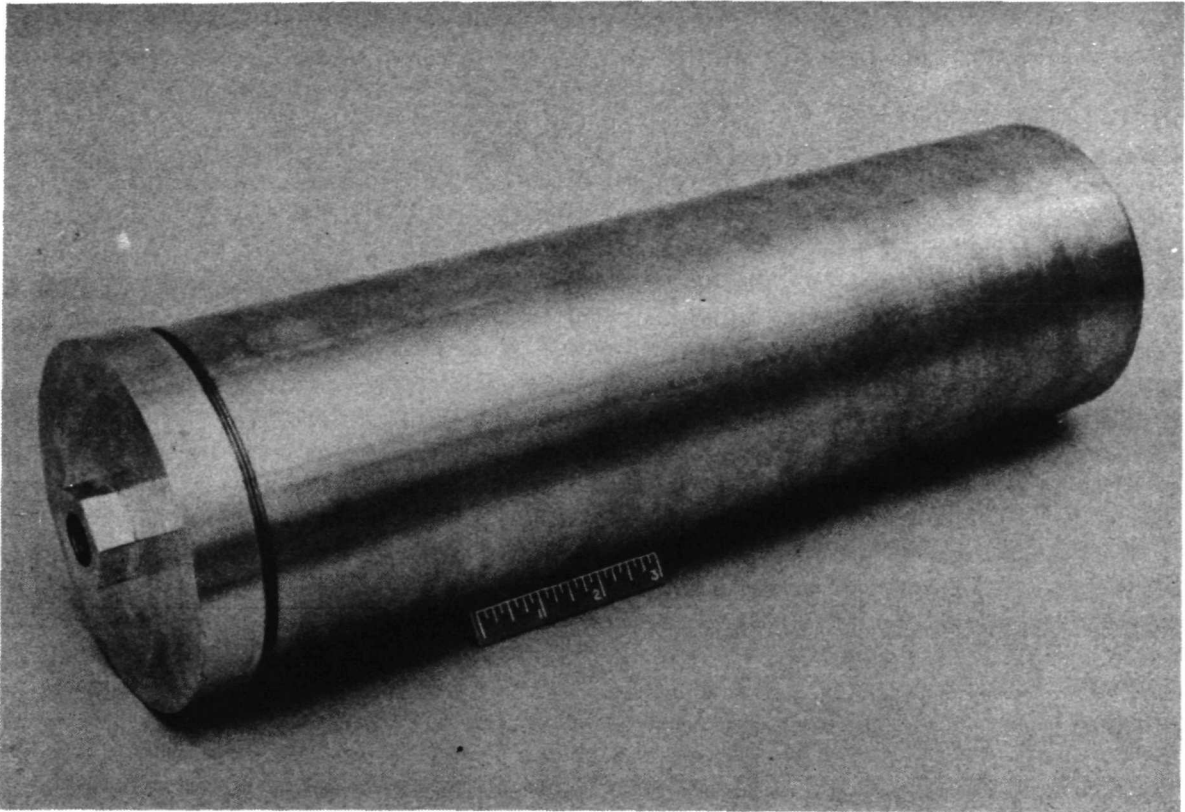


Fig. 28. Photograph of simulated fuel capsule assembly

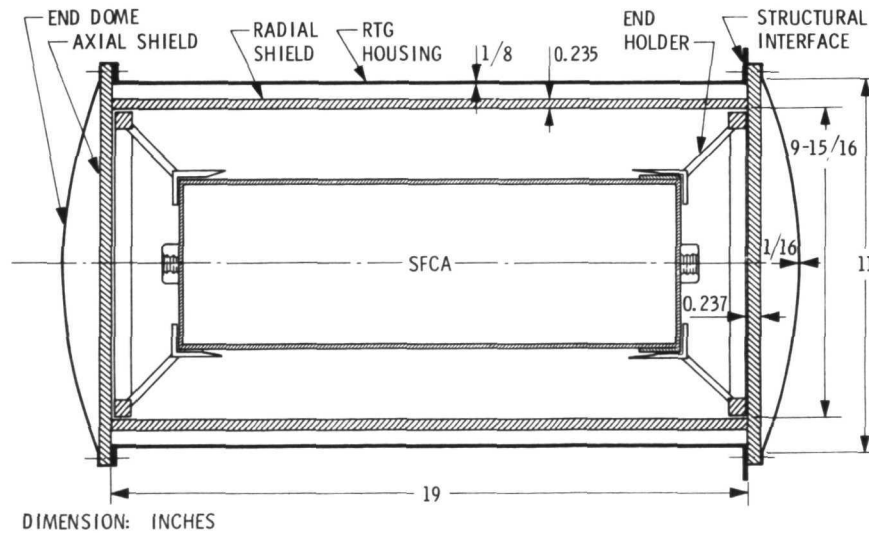


Fig. 29. Simulated RTG

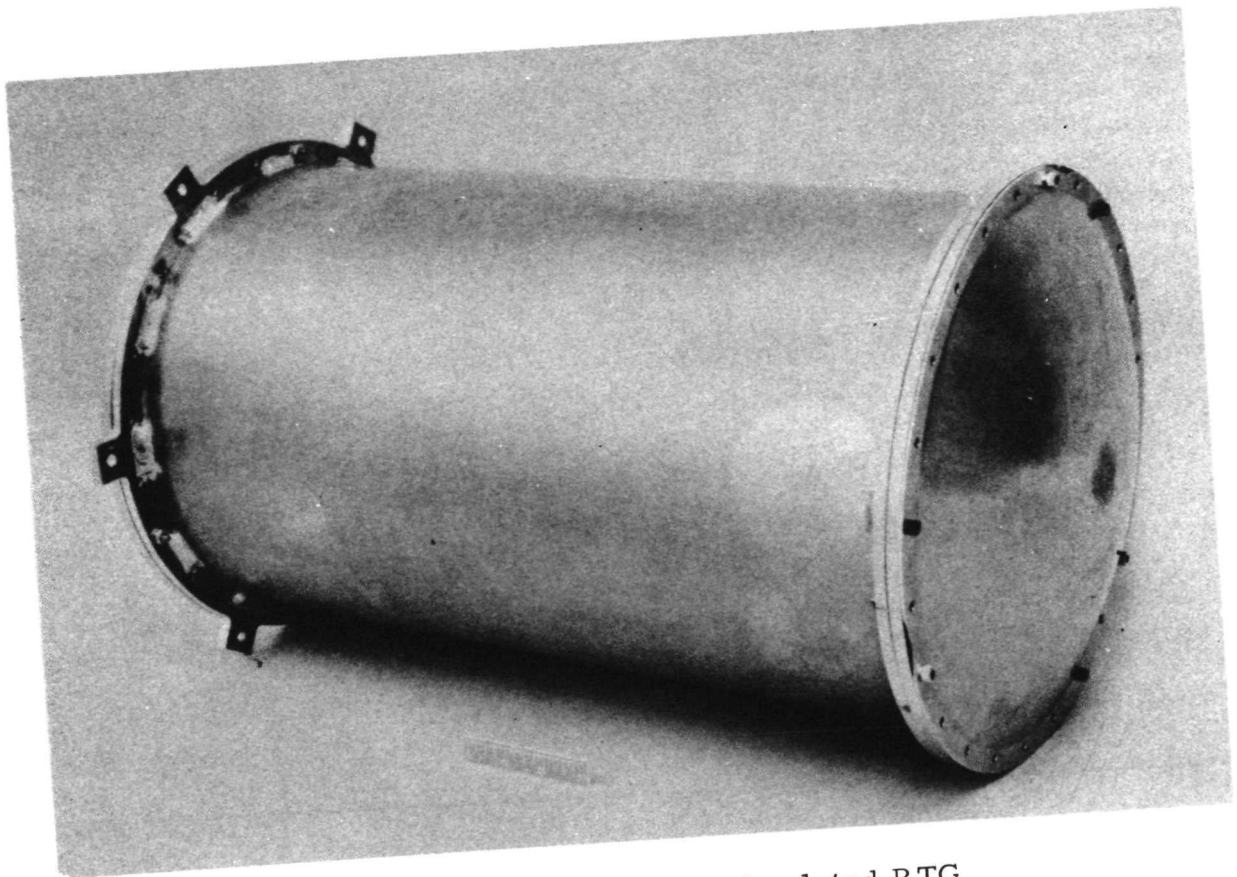


Fig. 30. Photograph of simulated RTG

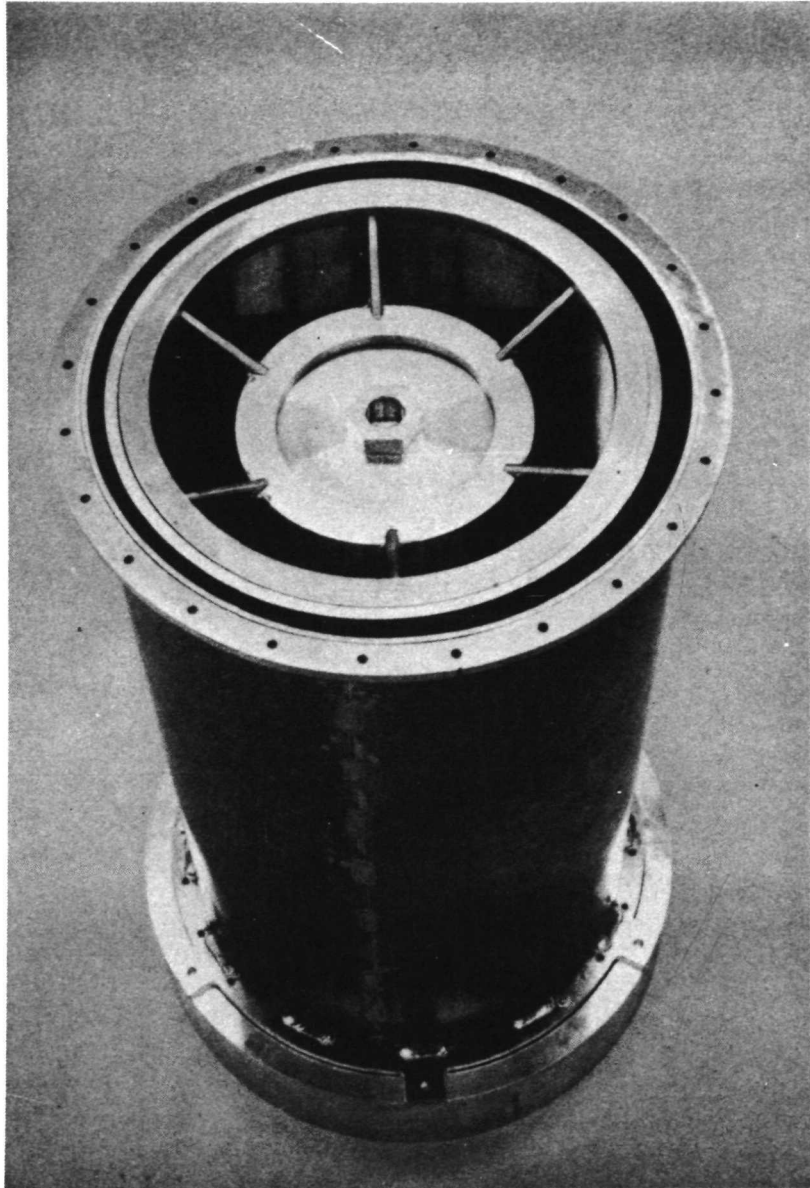


Fig. 31. Simulated RTG assembly

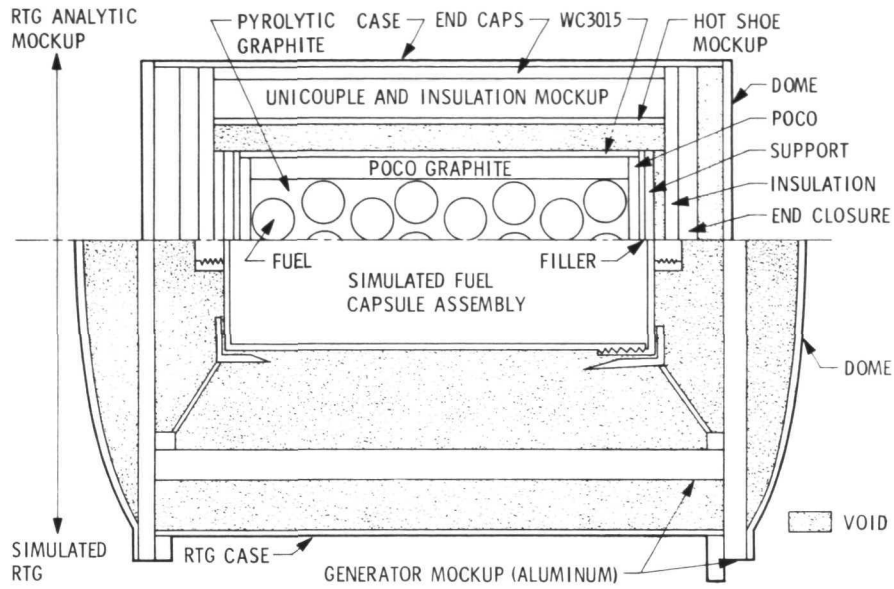


Fig. 32. Models for analytic study

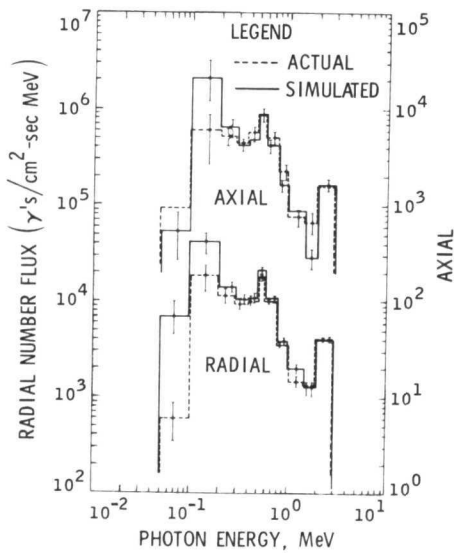


Fig. 33. Spectral comparisons of SRTG and RTG

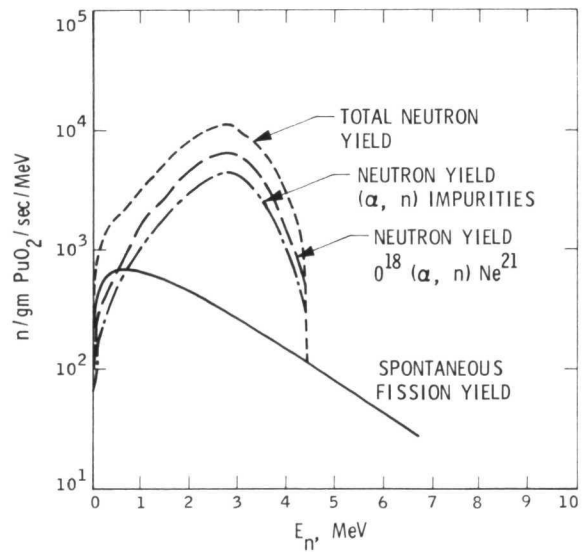


Fig. 34. Total neutron yield from a 2.2-kW MHW PuO₂ source

lifetime. The total neutron yield consists of those neutrons from the spontaneous fission plus various (α, n) reactions (Fig. 34). While the spontaneous fission yield was readily simulated, the high intensity of the total yield, reflecting (α, n) radiation, was not. The best solution was thought to be in the use of a ^{252}Cf spontaneous fission source, of sufficient mass to match the intensity of the total neutron yield. The resulting curve, however, would not match all areas of the true ^{238}Pu yield, and the resulting mockup would be considered, at best, a worst-case measurement. The selection of ^{252}Cf was not carried through to the point of bringing the material to the Laboratory.

To summarize, an adequate gamma-ray simulation for an RTG was developed that is economical, safe, and readily available, and which provided a representative profile of RTG radiation effects upon spacecraft instrumentation.

To support a complete test program, a neutron source should be included in the simulators. A neutron simulation concept has been analyzed, but this capability was not incorporated in the TOPS RTG simulators because of time and funding constraints.

D. Spacecraft and RTM Radiation Mapping Test Model

The primary purpose of radiation mapping is to estimate the radiation environment in the vicinity of the spacecraft, including the spacecraft attenuation and scattering. A second purpose is to provide spacecraft Engineering and Science Subsystem designers with appropriate radiation design data.

A Monte Carlo neutron and gamma radiation transport code was used to generate the radiation maps. Input to the transport code consists of a description of the radiation source and a model of the spacecraft geometry and materials. The source of TOPS gamma and neutron radiation is the RTG. Because TOPS has no simple symmetries, it was necessary to use a three-dimensional geometric model in order to provide proper simulation.

Radiation maps were generated for the PUCK RTG concept, consisting of solid solution cermet discs stacked in a refractory metal capsule. This old design is not the HELIPAK RTG, a later design for which maps were not generated. The two designs are compared in Table 19.

Table 19. Comparison of PUCK and HELIPAK designs

Parameter	PUCK	HELIPAK
Fuel loading, W (thermal)	2000	2200
Fuel age, years	5	18
Impurity concentration, ppm ^{236}Pu	1.2	1.2
Neutron emission rate	$2. \times 10^4$	$4. \times 10^4$
Neutron multiplication factor	1.3	1.25

1. Spacecraft Radiation Mapping. The geometric model of the spacecraft consisted of 70 material regions of homogeneous density and material composition. The total weight of 385.11 kg (849 lb) did not include the RTG and its boom, nor the science payload and its associated structure and boom (see Table 20).

The radiation map of the spacecraft is shown in Fig. 35. As can be seen, the science payload is not located in a region of minimum RTG radiation. Nevertheless, because of the attenuation of the spacecraft, both the gamma and neutron intensities at the science payload are approximately an order of magnitude less than the free-field intensities.

PUCK RTG free-field intensities are convertible to HELIPAK free-field intensities through multiplication of the appropriate quantities shown in Table 21. For example, to convert gamma number flux for the PUCK design to a gamma number flux for the HELIPAK, the gamma flux is multiplied by 5.9. This provides a simple, if crude, method of generating a new radiation map for TOPS for the HELIPAK RTG. A more accurate estimate would require a new Monte Carlo calculation.

2. RTM Radiation Mapping. The principal objectives of the TOPS radiation test model, shown in Fig. 36, are to provide experimental verification of the analytic model and to provide spacecraft designers with trade-offs for system design. The gamma-ray measurements planned with the RTM include dose rate, flux, spectral measurements, and directional measurements. Although the RTM housed four simulated RTGs, only one

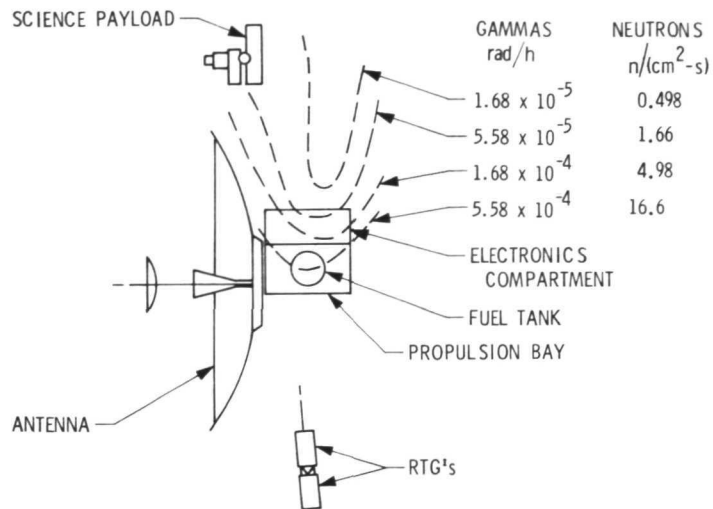


Fig. 35. TOPS RTG radiation environment

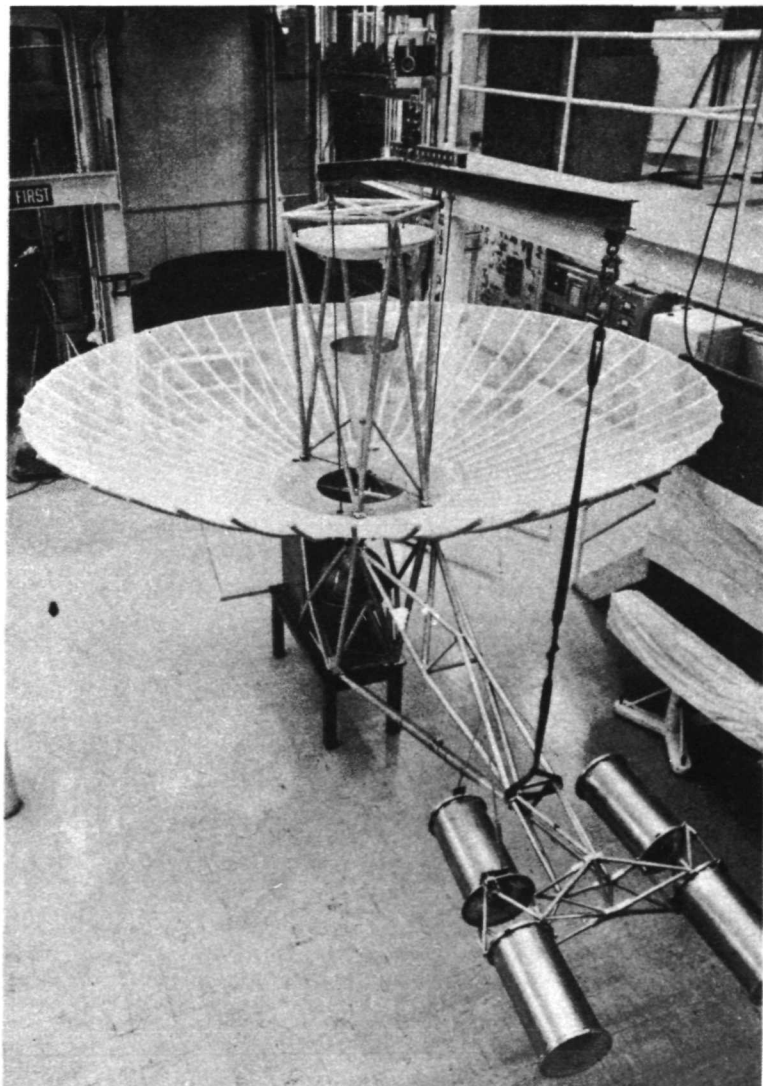


Fig. 36. Radiation test model

Table 20. TOPS configuration 12L geometric model

Region	Composition	Weight	
		kg	lb
Antenna			
Ribbs	Al	7.26	16
Mesh	Chromel-R	0.91	2
Hub	Al	9.53	21
Feed horn	Al	5.44	12
Sub dish	Al	0.91	2
Spacecraft bus			
Electronics chassis	Al	25.85	57
Electronics compartment	H		
	C		
	O	201.85	445
	Si		
	Cu		
	Al		
Fuel tank	Ti	10.43	23
Fuel (full tank)	N ₂ H ₄	56.25	124
Propulsion bay (other than Fuel tank and contents)	Al, Fe	66.68	147
		385.11	849

Table 21. HELIPAK/PUCK RTG radiation ratios

Radiation type	Number flux ratio	Dose rate ratio
Gamma	5.9	5.3
Neutron	3.4	3.8

contained a radiation source; the remaining three being dummies were used to simulate the scattering and attenuation properties of the real RTGs.

Physically, the RTM is 6.4 m (21 ft) long, including the measurement boom; 4.3 m (14 ft) wide (the antenna width); 3.7 m (12 ft) high; and weighs approximately 362.9 kg (800 lb). The radiation detectors are hung from the measurement boom, which is constructed of aluminum tubing (see Fig. 37).

Radiation test operations are conducted in a facility with a large open-bay area and a hoist. Storage facilities for SRTG sources are available, and the building has controlled access to ensure safety of personnel from inadvertent exposure to radiation. For total dose measurements, an ion chamber is used. Flux and energy spectrum measurements are made using a system which employs 4.44- to 5.08-cm (1 3/4- to 2-in.) sodium iodide crystals to input to four 256-channel pulse height analyzers. The purpose of using a four-input detector system is to expedite the mapping operation.

The following items are required for RTM radiation mapping: a complete RTM; operational SRTGs; complete free-field measurements; facility in readiness; safety approval obtained; test measurement equipment on hand; SRTGs mating to the RTM; SRTG storage pit and shield completed; measurement boom and fixtures constructed and secured; and the SRTG hoisting rig completed and tested.

Detector locations for radiation test model mapping are shown on the three-dimensional grid illustrated in Fig. 38. The detector locations are spaced about 0.61 m (2 ft) apart.

Analytical work remaining includes: calculating the influence of the TOPS spacecraft on HELIPAK RTG radiation; reducing RTM test data, including extensive spectral unfolding; correlating RTM test results with computer predictions; and performing a parametric RTG shielding study using HELIPAK RTG radiation and tungsten and lithium hydride slabs.

Experimental work remaining includes: completing a first radiation map using the ion chamber to determine total dosage; obtaining energy spectra and directionality measurements at specified locations on the RTM, using sodium iodide detectors; and determining the effects of spacecraft configuration changes, such as the variation between a full and an empty propellant tank.

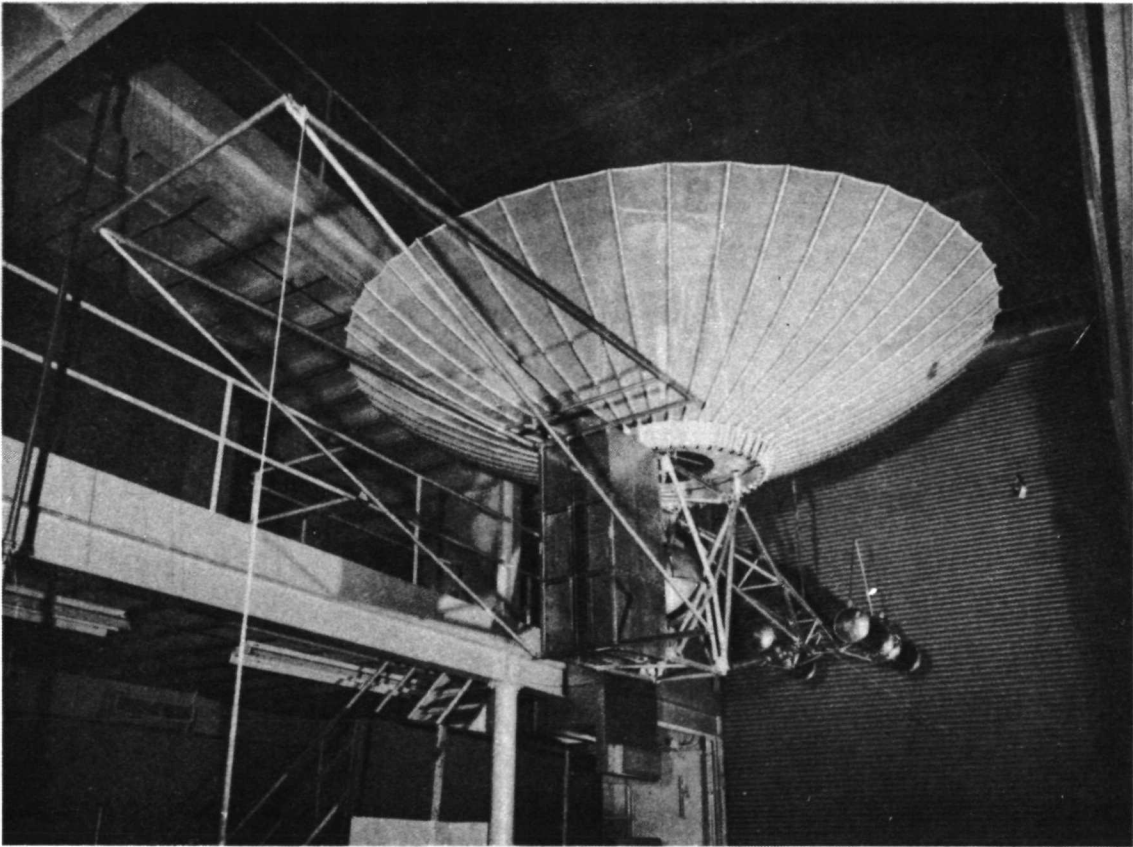


Fig. 37. Suspended RTM showing measurement boom

E. Radiation Test and Facilities

The TOPS radiation program was established to develop means of minimizing the effects of radiation on an outer planet spacecraft. This section deals with two aspects of that effort: (1) to determine the requirements for a radiation test facility, and (2) to develop a procedure for conducting tests efficiently in such facilities.

1. Radiation Test Facility Requirements. The test facilities to be used must generate an environment whose effects duplicate those of the real environment to be experienced by the spacecraft. The real environment is the superposition of two radiation fields of different origins. One of these is the radiation field generated by the onboard RTG and is characterized by chronic, low-level, ongoing gamma and neutron fluxes. The other field is of short duration (of the order of a day or so) during passage through the Jovian radiation belts, but gives very high flux rates of omnidirectional electron and proton impingements during that time, in addition to the RTG field.

The chronic, low-level, RTG-induced ongoing gamma and neutron fluxes can give rise to two types of effects on the spacecraft and its components. One is cumulative damage, which is a deterioration in the performance of a part or material that increases with the total duration of the exposure, until the part fails to perform satisfactorily. The other effect is interference with the electronic or optical performance of a science experiment sensor or component, manifested as increased background on a sensor, or decreased signal-to-noise ratio of a science experiment. It is proportional to the momentary intensity of the radiation field, but not to the cumulated dose.

The following useful generalizations can be made concerning the mechanism of cumulative damage of materials, and the mechanism of science experiment interference:

- (1) Cumulative damage caused by gamma traversal depends only on the ionization produced. There are no resonances at any particular energy within the gamma spectrum of the RTG. Testing for cumulative damage by gamma is spectrum-insensitive.

- (2) Cumulative damage caused by neutron traversal depends on displacement damage and nuclear interactions. Both of these are critically sensitive to the energy distribution of the neutrons, particularly in the epithermal range. Testing for cumulative damage by neutrons requires a close spectral match to the real RTG neutron spectrum.
- (3) Interference by gamma radiation generally manifests itself by producing background signals in radiation sensors, or light scintillations in optical sensors. Such sensors almost invariably have a response that varies widely with gamma-ray energy. Testing for interference by gamma rays requires a close spectral match to the real RTG gamma spectrum.
- (4) Interference by neutron interaction does not constitute a problem since radiation sensors and optical sensors are neutron-insensitive and do not respond to the anticipated neutron fluxes from the RTG. Testing for interference by neutron flux is not required.

Based on the above reasoning, we are now able to specify the radiation test facility requirements for each type of test:

- (1) Cumulative damage caused by gamma radiation. Since this is spectrum-insensitive, we can use conventional radioisotope irradiators. For cumulative damage studies for test levels of 10^5 rad, a ^{60}Co cavity irradiator with 5000-Ci loading can give gamma fluxes of 10^4 rad/min, or a test level acceleration of 5×10^5 . Such an irradiator accommodates samples in a 9.52×12.70 cm (3.75×5 inch) cavity, and has temperature control, provision for circulating gas, vacuum, and electrical connections for active testing. Larger samples are accommodated in a 150-Ci ^{60}Co beam irradiator housed in a test cell, capable of time acceleration from 100 times test level to 10^4 test level. A special-purpose test facility consists of an ultrahigh-vacuum chamber containing a 10-Ci ^{192}Ir source. A number of extreme environments, such as outer space temperatures in addition to radiation, may be applied to a test object in this chamber. It is capable of time acceleration from 50 to 500

times test level. A ^{137}Cs beam irradiator with 15-Ci loading housed in a test cell is available and in use, primarily for assessing the effects of time-accelerated gamma testing.

- (2) Cumulative damage caused by neutron radiation. It is presently most cost-effective to use a TRIGA pool reactor for these tests, modifying the energy spectrum of the fission neutrons by interposing large sheets of lead and boral as filters between the reactor core and the test objects. The degree of spectrum correction thus attainable is limited. Furthermore, in using a reactor as a test facility, neutron flux rates (and thus time accelerations) are very high. If it is determined that a very close match of the spectrum is needed for critical components, it will be necessary to construct a radioisotopic source containing both ^{252}Cf and $^{239}\text{Pu-De}$. The relative amounts will depend on the particular composition of the RTG ^{238}Pu fuel chosen. Calculations and first-draft designs have been made for all foreseeable ^{238}Pu fuels.
- (3) Interference caused by gamma radiation. The requirements for a close spectral match and a dose rate which should range from 1/10 to 10 times real rate are very well met by the use of the SRTG. An alternate source has also been used consisting of ^{226}Ra alone. This gives a fair spectral match, having a wide spread of gamma energies up to 1.7 MeV. It is a small source of only 2-mg content, so is useful only for small test fields. But it is convenient to carry to experimental setups when it is not feasible to bring the setup to the room containing the SRTG with its higher loading. Some optical experiments are being performed that involve extensive electronics, and it is practical and convenient to use a 2-mg source in the experimenter's facility rather than rebuild the experiment in the SRTG cell.
- (4) Interference caused by neutron radiation. Such testing is not required on any foreseeable components or experiments.

The second part of the real environment to be simulated consists of the electron and proton fluxes expected to be active. These are primarily due to the Jovian trapped radiation belts and cover a wide range of energies, with

varying intensities at each energy. It is not practical, of course, to use a machine for simulation which reproduces the wide energy ranges of real electron and proton spectra. Instead, we have determined from other experiments or considerations an equivalent fluence at a single accessible energy. Tests are then carried out under monoenergetic electron or proton beams at an equivalent exposure. The equivalent fluence at the predetermined, preselected energy may vary for different classes of test objects, so the test levels are set specifically for the type of test object to be studied.

The use of monoenergetic machine sources of electrons and protons requires special consideration to assure that the equivalent energy is high enough to allow the electrons and protons to penetrate to the container. If this requirement necessitates the use of pulsed sources, rate effects may enter because all of the tests typically take the same length of time as real exposures; they are not at times one acceleration because the dose is delivered in pulses.

Electron fluxes may be derived from the following sources: a dynamitron of 2 MeV gives a continuous output; an electron linear accelerator of 12 or 25 MeV gives pulsed outputs in a 0.0001 duty cycle; a ^{90}Sr - ^{90}Y beta source with $E_{av} = 0.8$ MeV of 500 Ci is in the developmental stage. An individual assessment must be made of each test to determine whether the penetrating power and the pulse nature are acceptable for the test.

Proton fluxes may be taken from either a Dynamitron or Synchrocyclotron. The Synchrocyclotron can operate at high enough energies (20 to 144 MeV) to assure adequate penetration, but it has pulsed outputs with typically a 0.001 duty cycle. The Dynamitron, which has a continuous output, has a maximum working energy of 3 MeV, which may not give penetration through components or covers on components. Again, an individual assessment must be made of each test to determine whether the penetrating power and the pulsed nature are acceptable for the test.

A summary of the criteria for test facilities for gamma, neutron, proton, and electron testing is presented in Table 22.

Table 22. Requirements for radiation test facilities

Test	Neutron source	Gamma source	Electron source	Proton source
Cumulative damage	Close spectral match	Spectrum-insensitive	Pulsed OK, need high enough energy for penetration	Pulsed OK
Science interference	Testing not required	Close spectral match	Rate effects may enter if pulsed	Rate effects may enter if pulsed

2. TOPS Radiation Tests. The test facilities described above were set up to enable a testing program to be carried out on the candidate materials, components, and piece-parts to determine their resistance to degradation by radiation, or, in some cases, to determine the effect on design level operation caused by the radiation environments. A diversity of tests has been made and a wide variety of components, materials, and piece-parts has been covered. Some novel physical arrangements have been found useful for the less familiar tests. The results and conclusions from these tests, as far as they have been evaluated, are given in Section F.

Testing has been done with gamma, neutron, electron, and proton radiation in several areas; e. g., electronics, optics, lenses, Canopus star tracker, gyroscope, magnetometer components, pyrotechnic devices, heat-transfer fluids for fluid loops, accelerated radiation effects. Components that were subjected primarily to interference testing include geiger tubes, photomultiplier, image intensifiers, channel multipliers, photo diodes, silicon detectors Si(Li), Canopus tracker, and magnetometer.

Since neutron tests involve the use of a reactor, the safety requirements are much more stringent than those needed for the gamma tests. For instance, tests on fluids require evaluation of the fluids before undertaking the neutron test to determine the presence of off-gasses and to prevent gaseous buildup in the fluid containers. Both neutron and proton exposure produces radioactivity in the test material or the container, or both. After

the test is completed, the material must be held for decay of induced radioactivity, or tests must be made under stringent safety precautions on the still-active material.

The two final points in testing procedures to be considered are dosimetry and beam purity. Dosimetry is well developed for gamma and neutron testing, there being adequate American Society of Testing Materials (ASTM) methods and experience. We have devoted much effort to proton and electron dosimetry because no corresponding standards are in use, and this represents a large part of the effort expended.

Beam purity is concerned with the fact that sources of neutrons, protons, and electrons invariably produce small amounts of gamma radiation during their operation. Furthermore, proton sources also produce small amounts of neutrons. These stray exposures must be evaluated and their effect on the primary experimental material taken into account as part of the test design.

F. Radiation Effects

The effects of radiation on the electronic parts of the TOPS spacecraft were determined by miscellaneous experimental testing over a 12-month period and by sequential testing of nine specific device types. The primary purpose of the tests was to obtain maximum information on radiation effects from limited available resources; there was no attempt to establish standards or to qualify parts. All devices tested were of commercial grade, from limited sample sizes. Detailed analysis was made only of radiation-sensitive parameters. The data obtained were the mean of the parts in groups subject to radiation; in addition, control groups, not irradiated, were measured at each measurement step. All percentage changes in evaluation were accumulated from initial measurements.

The first of five miscellaneous experimental tests was designed to evaluate nonbias vs back-bias, and high-gain vs low-gain devices. One device tested was the 2N2907A low-power PNP transistor. Ten each of these were operated with 50-V back-bias collector base during irradiation; another ten were operated without bias. A second device, the 2N930, an NPN low-power transistor, was segregated into a low-gain and a high-gain group, the low-gain having a mean H_{FE} of 112 at an I_C of 10 μA , and the high-gain

a mean of 219 at 10 μ A. Of the low-gain devices, ten each were operated with back bias, and ten without bias. Again, ten each of the high-gain transistors were operated with back bias, and ten without bias.

The gamma radiation environment was produced by ^{60}Co with a fluence of 10^4 and 10^5 rad at 5×10^4 rad/h and 10^6 rad at 6×10^5 rad/h.

The effect of this radiation on the 2N2907A PNP transistors was much greater on the back-biased than on the nonbiased group. For example, at a gamma dose of 10^6 rad -- an overstressed level -- degradation of the former group was 90%, compared to 50% for the latter. H_{FE} at 10 μ A (initially 140) decreased to 115 with 10^5 rad, the nominal TOPS parts-test level.

In testing the low-gain group of the 2N930 transistor at various exposures, the back-biased transistors again evidenced severe degradation in relation to the nonbiased devices. At 10^5 rad, degradation was approximately 30% for the nonbiased group and 90% for the back-biased group. Again as a function of current, an initial H_{FE} of 115 at 10 μ A fell to 20 under a gamma dose of 10^5 rad. The severe loss in gain at low currents is corrected at a higher current. For example, at 1 μ A and 10^5 rad, the gain is on the order of 100 -- a reasonable figure. This points to a pivotal tradeoff to be considered by circuitry design engineers: conservation of spacecraft power through low currents vs sacrifice in gain.

In the case of high-gain resistors, the back-biased and nonbiased ratios remained about the same as with the low-gain group; i. e., the back-biased devices experienced markedly greater degradation than did the non-biased transistors. Also, as with the other tests, the greatest degradation was experienced at the lower currents.

A comparison of the high-gain back-biased group and the low-gain back-biased group showed greater percentage degradation with the latter, particularly at a gamma radiation of about 10^4 rad. Interestingly enough, the variance disappeared at 10^6 rad. In actual H_{FE} lost, rather than percentages, the high-gain group dropped from 119 initially to about 128 at 10^4 rad and to 21 at 10^5 rad. The low-gain devices dropped from 118 initially to 85 at 10^4 rad (see Fig. 39). It is apparent that at the higher radiation rates, the advantage of the high-gain transistors has all but been negated.

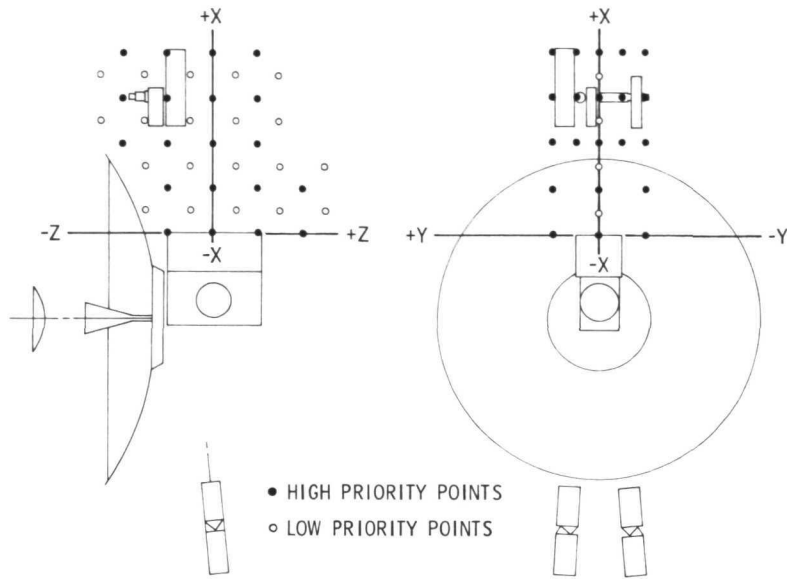


Fig. 38. Detector locations for RTM radiation map

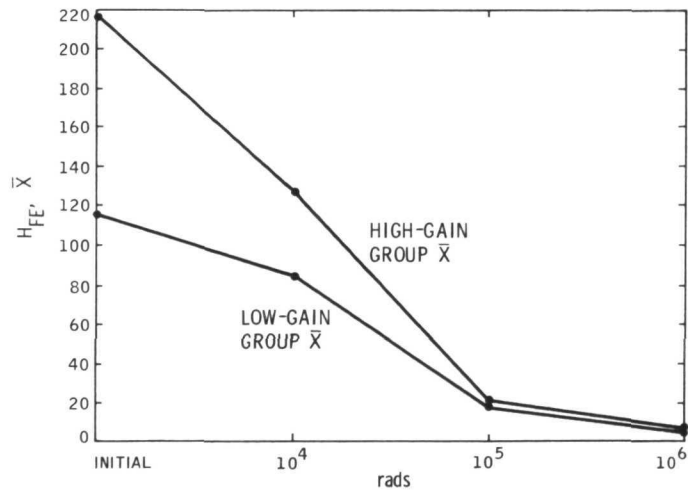


Fig. 39. Comparison of high- and low-gain H_{FE} behavior at $I_C = 10 \mu A$ for 2N930 NPN transistors

A second experimental test involved ^{60}Co irradiation of three transistors -- 2N2658, 2N2222A, and 2N2907A -- followed by high-temperature annealing. Four each of the 2N2658, 8 of the 2N2222A, and 8 of the 2N2907A were tested. The ^{60}Co environment consisted of 10^5 rad at 5×10^4 rad/h, 10^6 rad at 6×10^5 rad/h, and 10^7 rad at 6×10^5 rad/h. The devices were nonbiased, and were nonoperational during exposure.

Beginning with power transistor 2N2658 at 100 μA collector current, the percentage of H_{FE} degradation rose from an initial 0% to about 13% at 10^5 rad, 30% at 10^6 rad and 50% at 10^7 rad. With 1.0 μA , the degradation was 42% at 10^5 rad, 75% at 10^6 rad, and 87% at 10^7 rad. As was true of the 2N930 transistor already documented, degradation was more pronounced at the lower collector currents. At 10^7 rad, the 2N2658 transistors were subject to heating, and an annealing process commenced, followed by a reversal in the H_{FE} degradation factor. In an environment of 200°C , annealing occurred at some period during the first 16 h, thereafter, although heating continued for an additional 8 h, there was no further annealing. The degradation factor improved from a high of 87% downward to 44% during this 16-h period for the 1.0 μA collector current, and from 50% to 28% for the 100 - μA current. At these lower levels, degradation ceased to improve, and remained firm for the remaining 8 h of the test.

The results of tests on the 2N2222A NPN low-power transistor and the 2N2907A PNP low-power transistor were essentially the same as those for the 2N2658 NPN power transistors. Degradation was greatest for the low collector currents, and annealing was completed after 16 h at 200°C .

A third experimental test stressed the effects on electronic parts from neutron radiation. Devices were exposed, nonoperational, in a TRIGA reactor environment of 1.6×10^{13} neutrons/cm² with a gamma background of 4×10^3 rad.

The first device tested was SE 480Q, a quad 2 input NAND gate. The parameter of interest was V_{output} low. During exposure, voltage through the gate increased from an initial 0.166 to 0.177 V, an increase of only 6.5% and well within spec limits of 0.3 V.

A second device, 2N4352, a P-channel MOSFET, was tested to determine radiation effects on the instrument's threshold voltage. Voltage increased an insignificant 1.7% from 3.42 to 3.48 V.

The parameter of interest for another device, a 2N2907A PNP low-power transistor, was degradation of H_{FE} measured at 1- μ A collector current. An initial gain of 101 dropped to 31 -- a severe degradation of -69%

Another transistor, the 2N2222A, suffered an H_{FE} degradation under the neutron radiation of -65%, from an initial gain of 123 to 42.

A fifth device examined in this third experimental test was a high-power NPN transistor, 965V108. Parameters of interest were H_{FE} gain and V_{CE} saturation. The device was measured at 30 A. From an initial gain of 45, that factor dropped to 12.5 -- a 73% degradation. The V_{CE} saturation increased from 0.39 to 1.9 V. The V_{CE} increase was of concern, since a device designed for 0.5 V would have thermal runaway by the time saturation was achieved at almost 2 V.

The fourth of the miscellaneous experimental test was a relatively modest operation that subjected 10 each of 2N2222A NPN low-power transistors, biased at 50 V, to ^{60}Co , 5×10^4 rad, and 5×10^5 rad, per hour. The test was designed to measure H_{FE} gain as a function of collector current at various levels of radiation. Initial H_{FE} rose from 170 at 1 μ A to about 238 at 10 μ A, where it leveled off. Degradation commenced at about 80 μ A; H_{FE} measured 224 at 100 μ A and 208 at about 150 μ A. At 5×10^4 rad, H_{FE} rose from 110 at 1 μ A to 195 at 100 μ A, then degraded to 200 at about 150 μ A. Emphasizing the severe degradation of gain in a high-radiation environment and at low current, H_{FE} was 50 at 5×10^5 rad and 1 μ A; it rose to 128 at 10 μ A and 180 at 100 μ A, then degraded sharply to 170 at 150 μ A.

The fifth experimental test measured the performance of NAND gates in an electron radiation environment. Six SE480Q quad two input devices -- totaling 24 gates -- were subject to 1.5 MeV in a Van de Graaff generator. The fluence varied from 1×10^{11} e/cm²/s to 3×10^{15} , the latter constituting severe radiation. Three of the devices were operated with V_{out} low, and three with V_{out} high during irradiation. The parameter of interest for a digital device is V_{out} low. Under test conditions, greater degradation was experienced at V_{out} high than V_{out} low operating conditions. Although degradation commenced for both the high and low logic states at 1×10^{13} e/cm², such degradation was not of serious nature anywhere within the

radiation spectrum likely to be encountered in outer space. For example, V_{out} low was 0.197 at 1×10^{14} e/cm², well below the specification limit of 0.3 V, and yet within the reasonable upper range of anticipated radiation.

The second part of the TOPS radiation testing involved exposure of nine specific semiconductor device types to a radiation environment. Fifteen devices of each type were tested: ten were irradiated; five devices, not irradiated, were used as controls. In contrast to the previous tests, radiation in these exercises was in no instance overstressed. Devices were screened, and data obtained were the mean of each type tested. All experiments were conducted at room temperature.

The nine semiconductors and their functions are listed below:

<u>Device</u>	<u>Function</u>
SN54L00T	Quad 2 -- input NAND gate
RSN54L00T	Quad 2 -- input NAND gate
2N2658	Transistor NPN power
2N2907A	Transistor PNP low-power
2N2222A	Transistor NPN low-power
EA 1204	256-bit shift register
TIXL 102	Photocoupled isolator
MSX 194	Transistor S-band
MSC 3005	Transistor RF-power

The devices were exposed to gamma rays, electrons, neutrons, and protons in that order, with measurements taken following each exposure. Devices 2N2658, 2N2907A, 2N2222A, TIXL 102, MSX 194, and MSC 3005 were not subjected to gamma radiation; and both the EA 1204 and TIXL 102 devices failed before they reached the proton environment.

A summary of test results for the nine devices is found in Table 23. Of the ten SN54L00T devices tested, two experienced catastrophic failure during electron radiation. Subsequent failure analysis revealed extensive metallic damage, and it was inferred that failure was not radiation-caused. The 20% degradation was well within spec, as were all other parameters. Two catastrophic failures occurred in the RSN54L00T device type during electron radiation. One, revealing metallic damage in analysis, was not

Table 23. Overall summary of test results^a

Device	Number tested	Number of failures ^b	Parameters	Initial measurements	Total environment		Remarks
					After	$\Delta\%$	
SN54L00T	10	2	V_{OL} , V	0.165	0.199	+20.0	V_{OL} = gate output low state, 0.3 V is spec limit
RSN54L00T	10	2	V_{OL} , V	0.172	0.189	+10.0	Same as above
2N2658	10	0	H_{FE}	63	30	-53	At I_C of 1.0 A, 40-min limit
			H_{FE}	73	11	-86	At I_C of 100 mA
			H_{FE}	68	5.5	-92	At I_C of 10 mA
			$V_{CE(SAT)}$, V	0.25	1.5	+500	Max limit = 0.5 V
2N2907A	10	0	H_{FE}	162	83	-48	At I_C of 150 mA, 100-min limit
			H_{FE}	202	42	-79	At I_C of 1.0 mA, 100-min limit
2N2222A	10	0	H_{FE}	219	90	-60	At I_C of 150 mA, 100-min limit
			H_{FE}	128	35	-73	At I_C of 1.0 mA
EA1204	5	5	NA ^c	NA	NA	NA	All devices ceased operating after 6×10^{12} e/cm ²
TIXL102	10	10	NA	NA	NA	NA	All devices experienced catastrophic failures after neutron exposure

^aAll data are mean of specified parameter.

^bCatastrophic

^cNot applicable.

attributed to radiation; the second was termed a random failure. After exposure to the total environment, the $V_{CE}(\text{SAT})$ parameter of the 2N2658 devices increased 500%, revealing a thermal problem and calling for a design tradeoff.

Of five EA 1204 shift registers tested, all had suffered catastrophic failure by 6×10^{12} e/cm², although they exhibited no degradation under gamma radiation. Again, all ten of the TIXL 102 photocoupled isolators failed catastrophically; in this instance, under neutron radiation of 1.6×10^{13} n/cm². The input diode of the isolators had no control over the output transistor.

An interesting aspect of the tests concerned the 2N2658 NPN power transistor. Measuring the device at three different current ($I_c = 1.0$ A, 100 mA, and 10 mA) severe degradation was experienced under neutron radiation (1.6×10^{13} n/cm²) but little or no degradation under proton bombardment (9.0×10^{12} p/cm²). Degradation was 50% at 10 mA under the neutron radiation, and 40% in the electron environment, but only on the order of 1% under the proton radiation. The reason for this is unknown.

Degradation in $V_{CE}(\text{SAT})$ for the 2N2658 device was nonexistent under electron radiation, but was severe under both neutron and proton exposure. Saturation was 1.2 V at 1.6×10^{13} n/cm² (maximum spec limit: 0.5 V) and almost 1.5 V at 9.0×10^{12} p/cm².

The 2N2907A PNP low-power transistor was operated at $I_c = 150$ mA and 1.0 mA in electron, neutron, and proton environments. As customary, degradation was more severe at the lower power. In the latter state, degradation was 32% under 1.4×10^{13} e/cm², and 42% in a 1.6×10^{13} n/cm² environment. However, surprisingly, very little degradation (1%) was experienced under a proton exposure of 9.0×10^{12} p/cm², particularly at the lower collector current. Again, the lack of degradation in the proton environment was unexpected and remains unexplained.

The ten 2N2222A NPN low-power transistors were tested at $I_c = 150$ mA and 1.0 mA. In the low-power mode, degradation was severe under electron radiation (52% at 1.4×10^{13} e/cm²) but tended to level out in a neutron environment, and exhibited almost no degradation in a proton field of 9.0×10^{12} p/cm². At the higher collector current ($I_c = 150$ mA), however, degradation was almost the same for each of the three environments, averaging 20%.

The MSX 194 S-band transistors experienced negligible degradation from electron or neutron radiation, but underwent an acceptable 18% degradation in gain when exposed to a proton environment (9×10^{12} p/cm²).

The last of the nine devices to be tested in Part 2 -- the MSC 3005 RF power transistor -- evidenced no measurable degradation in power gain or efficiency due to radiation environments.

To summarize the test results of devices examined in Part 2; all measured parameters for the digital integrated circuits remained within specification limits; leakage current and saturation voltage increased but remained within specification limits for the low-power transistors; dc gain was a problem with all transistors tested, particularly in low-collector-current operations, and would necessitate certain circuitry design tradeoffs; and finally, the EA 1204 shift register and the TIXL 102 photocoupled isolator failed to survive the radiation environments.

In conclusion, three recommendations evolved from the test activity. (1) Each radiation-sensitive device type should be qualification-tested for the radiation environments; drawing broad conclusions from tests of a few devices is not sufficient. (2) A practical method of screening for radiation-sensitive devices should be provided so that behavioral characteristics identified in qualification tests will be assured in later devices implanted in the spacecraft. (3) Post-irradiation device parameter characterization must be provided to circuit designers to assure understanding of such factors as saturation voltage, fanout, and gain degradation.

BIBLIOGRAPHY

Anno, G. H., and Wolf, F., "TOPS RTG Nuclear Radiation Environment Analysis," Transactions of the American Nuclear Society, Vol. 13, 1970.

Davis, H. S., and Koprowski, E. F., "Nuclear Radiation Environment Analysis for Thermoelectric Outer Planet Spacecraft," Proceedings, National Symposium on Natural and Manmade Radiation in Space, Las Vegas, Nev., March 1971.

Jordan, T., RAMPART, A Time-Dependent Generalized-Geometry Monte Carlo Program for the Transport of Neutrons, Protons and Electrons, ART-49, ART Research Corporation, Los Angeles, Calif., 1970.

Wolf, F., "Nuclear Radiation Mapping of Thermoelectric Outer Planet Spacecraft," in Supporting Research and Advanced Development, Space Programs Summary 37-64, Vol III, p. 88, Jet Propulsion Laboratory, Pasadena, Calif., Aug. 31, 1970.

V. ENGINEERING MECHANICS

A. Spacecraft Configuration

The TOPS outer planet spacecraft structure evolved through several iterations to reflect changes occurring in the design process. The spacecraft design was dominated by two elements: (1) the RTG power source, which required physical separation and shielding, and (2) the large high-gain antenna, with its unique effect on instrument viewing capabilities.

The TOPS mechanical configuration design was constrained by the following requirements:

- (1) Satisfy viewing requirements for attitude control sensors, antennas, and science payload.
- (2) Separate and shield radiation-sensitive equipment from RTGs.
- (3) Ensure compatibility with launch vehicle mechanical requirements.
- (4) Provide center-of-gravity alignment with thrust vectors in both launch and maneuver configuration.
- (5) Align principal spacecraft axes with attitude control axes.
- (6) Provide stiffness to spacecraft structure to meet attitude control requirements.
- (7) Prevent impingement of propulsion system exhaust plume on critical spacecraft surfaces.
- (8) Provide equipment accessibility for spacecraft test and operations.
- (9) Group and locate spacecraft assemblies for ease of temperature control.
- (10) Minimize weight and cost.

No significant configuration studies were made in the following areas:

- (1) Launch vehicle integration. This includes the field joint-mechanical requirements, environmental considerations between the launch vehicle and the spacecraft (including radiation, contamination control, temperature control), and structural loads analysis.
- (2) The flow of the spacecraft through the electronic and environmental test facilities (e. g., the system test complex, vibration test facilities, and space simulators). Spacecraft preparation for launch at ETR, particularly hazardous operations in the explosive-safe facilities, were not investigated in depth.
- (3) Future payload changes. The TOPS baseline configuration is based on a representative science payload, and no provision has been made for future payload changes either prior to or during a flight project.

1. Cruise Configuration. The basic spacecraft comprises five major building blocks: (1) the propulsion module or propulsion compartment, (2) the electronics compartment, (3) the 4.3-m (14-ft) deployable high-gain antenna, (4) the four RTGs on the boom, and (5) the science payload both on the platform and the fixed cruise science (see Fig. 12).

The basic structural frame ties together the propulsion compartment and the electronics compartment. The high-gain antenna is attached to this basic structure on the forward, or Sun, side at three points, two of which are located on the propulsion module, and the third on the electronics compartment. The high-gain antenna consists of a central support ring, which houses the mechanisms for deploying the spokes and damping their deploying motion. The reflector surface of the dish consists of 48 radial spokes, to which is attached the reflective mesh surface. At the forward end of the antenna, the subdish is supported by a fiberglass tubular truss, which attaches to the support ring at four points.

The forward low-gain antenna, the forward acquisition Sun sensors, and the cruise Sun sensors are located on the subdish backup structure. Cabling from this forward equipment is routed along the superstructure through the dish and into the electronics compartment. The four identical

RTG assemblies are mounted to a deployable boom and separated from the sensitive science platform by about 4.57 m (15 ft). A thermal isolation blanket will probably be required to isolate the RTGs from the high-gain antenna reflector so that thermally induced distortions of the reflector surface will be minimized.

The propulsion compartment houses the trajectory-correction propulsion subsystem and the attitude control thrusters. The roll and pitch thrusters are located on the sides of the compartment and the yaw thrusters on the aft end. The attitude control momentum wheels are enclosed within the compartment. The vector helium magnetometer and the plasma wave booms, and one-half of the antenna system for the radio emission detector are attached to the compartment. The compartment itself is enclosed on all sides by thermal insulation and micrometeoroid protection, with the exception of the interface between it and the electronics compartment.

The electronics compartment consists of a rectangular box housing six electronics assemblies, three on each side. The external faces of these electronics bays are enclosed by a structural shear-plate member with louvers for regulating the rate at which thermal radiation leaves the compartment. These prime radiating surfaces are located out of the direct view of the warm RTGs to decrease the amount of thermal coupling between the two. The aft end of the electronics compartment contains (1) the aft low-gain antenna, which provides hemispherical coverage on the anti-solar/anti-Earth direction in normal cruise, (2) the aft acquisition Sun sensors, and (3) the separation-initiated mechanisms, which interface with the spacecraft adapter. In addition, there are pads on the basic structure that interface with the mechanisms which provide the impulse for spacecraft separation from the launch vehicle after insertion into the heliocentric trajectory.

2. Scan Platform. The science equipment, including cruise science on the boom and the planet viewing science outboard of the two gimbals, is located on a deployable boom. The science scan platform is shown in Fig. 40. The basic equipment supported by the boom, the plasma probe, the medium-gain antenna, the charged particle telescope, the trapped radiation detector, and the trapped radiation instrument, are all inboard of the scan platform gimbals. The platform-mounted equipment consists of the narrow-angle TV, approach guidance sensor, IR multiple radiometer, UV photometer,

and wide-angle TV. The yaw or azimuth axis has a rotational freedom of about 250 deg, and the elevation axis +90 to -55 deg, which provides a large sector for planet viewing. The major point of this particular platform arrangement was to derive a design where the gimbal axes intersected at the estimated center of mass for the outboard equipment. The purpose was to reduce the rotational inertia of the platform and thereby minimize the coupling during slewing operations with the attitude control system. The goal was 13.56 kg-m^2 (10 slug-ft^2) maximum, and estimates of this arrangement run between 6.78 and 8.13 kg-m^2 (5 and 6 slug-ft^2).

3. Launch. Figure 41 shows the spacecraft configuration as it would appear when enclosed within the 3.05-m (10-ft) aerodynamic fairing of the Orbiting Astronomical Observatory. The basic structure of the spacecraft attaches to the Burner II at four points through a very short truss arrangement. Enclosed within this truss is the pad for actuating separation-initiated devices and the springs to provide the separation impulse. The high-gain antenna, the deployable vector helium magnetometer, the plasma wave, and the radiation-emission detector booms are shown in their stowed configurations. The RTG boom, shown folded, attaches to the side of the Burner II, probably by a pyrotechnically released latch mechanism. The science platform, also shown folded, latches to the side of the electronic compartment. The center of gravity of the composite spacecraft during launch is essentially on the thrust axis of the Burner II and, after the booms are deployed during cruise flight, along the thrust axis of the propulsion engine.

B. Mechanical Devices

1. RTG and Science Boom Actuator-Damper. The RTG boom moment of inertia, 340 kg-m^2 (250 slug-ft^2), is larger than any previously used in Mariner spacecraft. Furthermore, the boom must deploy about 70 deg without perturbing the spacecraft during deployment. To accomplish this, it is necessary to use a continuously damped deployment system.

Several approaches to the deployment damper and actuator were investigated; it was decided that, by integrating the device into the structure as part of the basic hinge, weight and cost could be kept to a minimum. A prototype unit to replace the compression member on the hinge was built and tested.

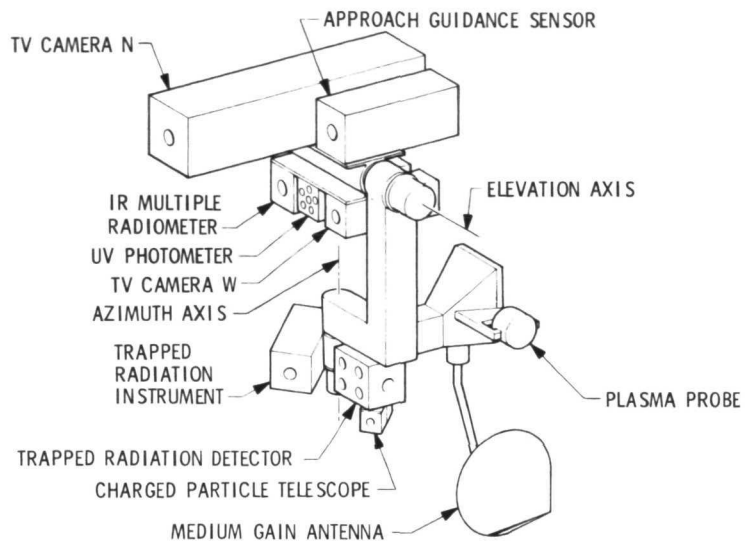


Fig. 40. TOPS science scan platform

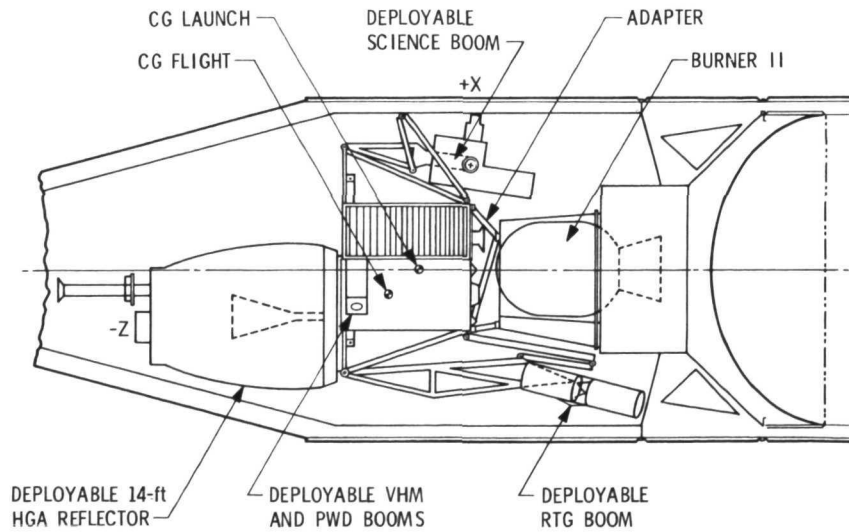


Fig. 41. TOPS launch configuration

Figure 42 is a somewhat foreshortened view of the RTG and science boom actuator-damper. The basic concept uses a torsion bar for the actuating force, and two concentric tubes with a damping fluid located between them.

The actuator was tested in Earth gravity by using an air-bearing support system to minimize the hinge bearing loads. The test program consisted of varying the masses. As shown in Fig. 43, with a critically damped system, the device became insensitive to mass changes.

References 1 and 2 describe in detail the air bearing used to support the mass and the instrumentation and various techniques used to accomplish the task.

2. Magnetometer and Plasma Wave Boom Survey. The requirements for the magnetometer and plasma wave booms are quite similar. As a result, it was possible to determine the following requirements and constraints for both:

- (1) Length, 9.15 m (30 ft)
- (2) End mass, 0.9 kg (2 lb)
- (3) Pointing accuracy, ± 3 deg
- (4) Capability to withstand 0.1 g extended
- (5) Small thermal distortions
- (6) Light weight
- (7) Magnetic cleanliness, $< 0.01 \gamma$
- (8) Ten-year life in the space environment

The two types of booms considered for TOPS application are the preformed, tubular metal foil and the triangular metal truss. The preformed, tubular metal foil boom has two advantages: it protects the electrical wires, which is important in view of the 10-year life requirement, and it is already developed. However, the torsional rigidity is poor, a fault of all tubular booms. It is heavy and not magnetically clean. Furthermore, the thermal distortion is high. This effect can be diminished by some techniques, such as putting holes in the tube, but this exposes the electrical wires to the environment. The triangular metal truss boom, although presently made of

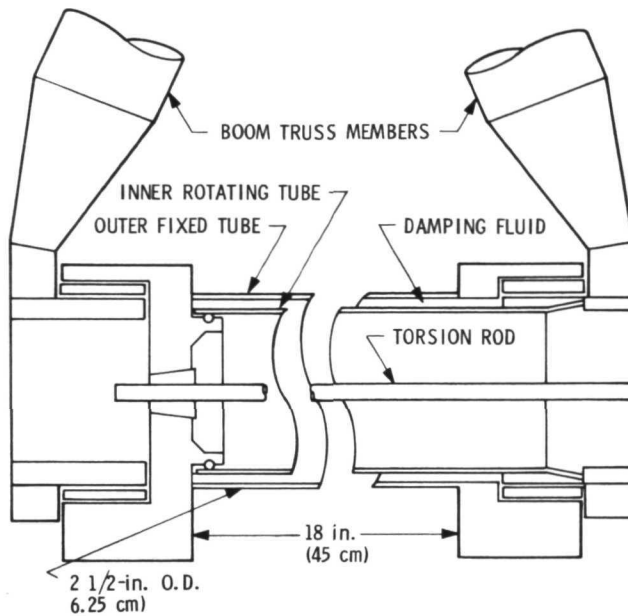


Fig. 42. RTG and science boom actuator-damper

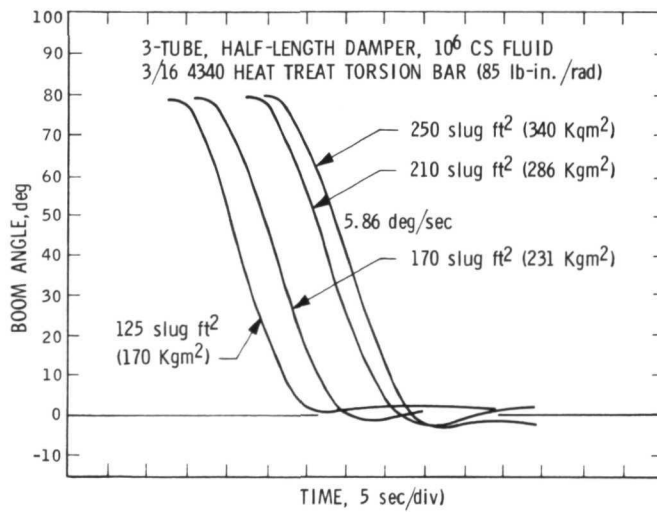


Fig. 43. RTG deployment simulator

material not suitable for this application, has light weight and good torsional rigidity with no thermal distortion, and more nearly fits TOPS requirements (see Fig. 44). References 2 and 3 describe the boom study in detail.

3. Fluid Loop Pump. The fluid loop pump must have a flow rate of 1.2 ml/s (9 lb/h) a head of 6.9 kN/m² (1 psi), and a lifetime of more than 100,000 h. The pump must be magnetically clean and use a minimum of power. A number of devices were examined for the specified flow rate. Magneto-hydrodynamic and ferrofluidic devices were ruled out early in the study because of their large magnetic fields and power requirements. A thermo-mechanical pump based on the Rankine vapor cycle was conceived, which would be driven by the waste heat from the RTG (Ref. 4). Development was abandoned after the first prototype because the seal friction made the unit marginal and the movement of contacting parts indicated a short lifetime.

The regenerative, or peripheral, pump was examined next. This pump works like a multistage centrifugal pump. As the fluid flows from cavity to cavity, it is put into a spiral motion around the periphery of the motor, with each vane acting as a pressure stage. A slight pressure increase is built up by each successive bucket. Although this pump is not new, no data could be found for the head and for the flowrate required. However, the pump was considered further because of its low speed (300 rpm) and its long-life characteristics. Figure 45 shows a section of the main rotor of the pump.

Use of a hydrodynamic bearing for the pump was considered to provide the required pump life. Early in the pump development, a 7.64-cm (3-in.) single rotor, mounted with conventional bearings, was built. This rotor has 76 vanes, a speed of 300 rpm, and a flow range of 0.5 to 1.2 ml/s. Efficiency was 1.4%, good for a small pump.

Next, a 6.35-cm (2.5-in.) diam dual rotor was developed, having 48 vanes, a speed of 300 rpm, and a flow range of 1.2 ml/s. The bearings are hydrodynamic, and the multipole, synchronous hysteresis motor will be integrated into the design. This pump is shown in Fig. 46. The subrotors create the pressure necessary to feed the hydrodynamic bearing. The main flow travels up the spiral annulus to the outer tips of the rotor, where the fluid is accelerated and picked up in a header. The rotor is completely suspended in the fluid to eliminate all metal-to-metal contact. A pump was constructed and tests proved the effectiveness of the axial-inlet peripheral pump in the

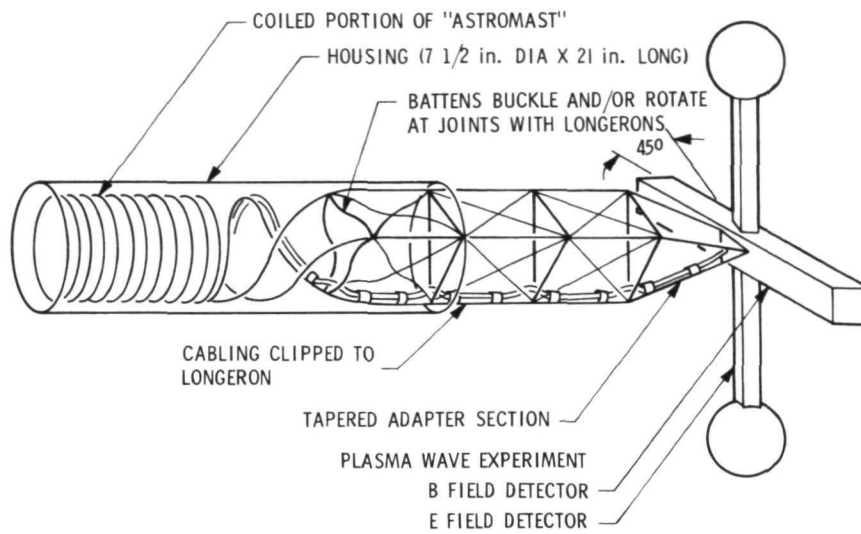


Fig. 44. Schematic drawing of 9.14-cm "astromast" boom

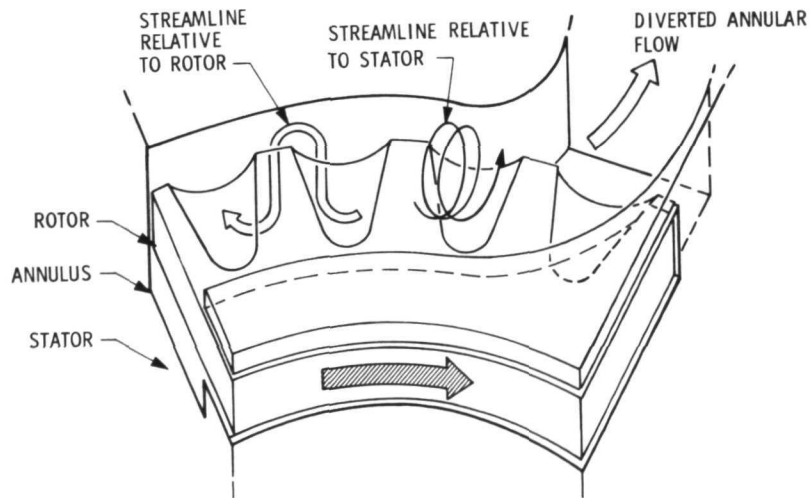


Fig. 45. Theoretical flow patterns of regenerative pump

TOPS fluid loop flow and pressure regime. However, considerable additional engineering evaluation, including tests, would have to be performed to adequately characterize this pump and its components.

The single rotor was developed and tested before it was built into the integral motor and the two-rotor combination. Figure 47 shows the performance of the 6.35-cm pump for various rotor configurations that were tried to determine which parameters were important. The design point was higher than actual performance. The operating point of a centrifugal pump of a given size and rpm was calculated as a measure of the efficiency under the same operating conditions. It was concluded that the laminar flow characteristic of the peripheral regenerative pump is more efficient.

C. High-Gain Antenna

The purpose of the high-gain antenna development was to gain experience with folding antennas, to develop evaluation tools, and to provide an antenna for TOPS. When this work began about 1969, the only folding antennas developed beyond the theoretical stage were used on classified projects, and information on these was limited.

1. Constraints and Requirements. The high-gain antenna has hinged radial ribs around the circumference of the solid central dish. The constraints and requirements placed upon the antenna development are:

- (1) A weight restriction of 16.78 kg (37 lb) for the reflector.*
- (2) A deployed diameter of 4.3 m (14 ft), and a stowed diameter of 1.37 m (4.5 ft).
- (3) A folded height of 1.98 m (6.5 ft), primarily based on the clearances of the 3.05-m (10-ft) shroud.
- (4) A 0.61-m (2-ft) feed access in the center of the main reflector.
- (5) A surface accuracy with an error of 0.9 mm (0.035 in.) rms from all sources, (e.g., the geometric approximation, manufacturing tolerances, deployment repeatability, thermal distortions, and the zero-g effect).

*The actual weight was 24.84 kg (54.75 lb), which included 4.67 kg (10.3 lb) due to intentional overdesign of the hub and damping system.

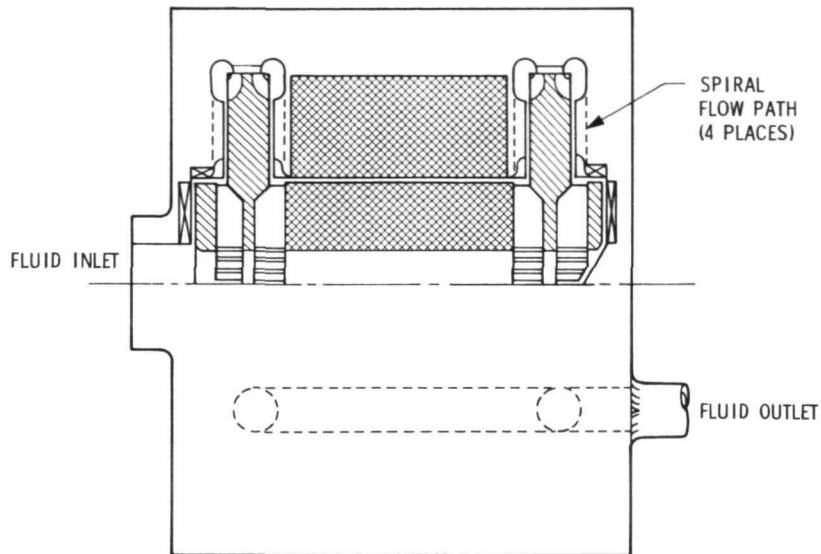


Fig. 46. Long-life pump concept

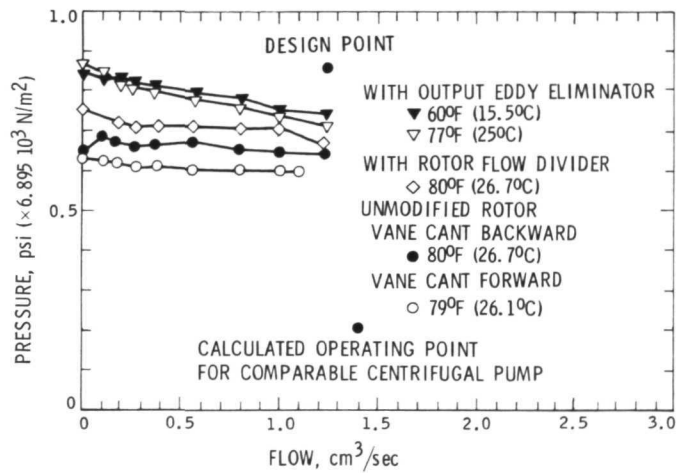


Fig. 47. Performance of 6.35-cm-diam regenerative pump at 300 rpm

- (6) The capability to withstand a temperature range of +93.3°C (+200°F) at near-Earth to as low as -240°C (-400°F) at Neptune.
- (7) A focal length-to-diameter ratio of 0.42. This ratio was chosen as a tradeoff between the feed, subdish, and main reflector elements to fit them into the overall size.
- (8) A minimum natural frequency of 8 Hz in the lateral and 3 Hz in the torsional directions.

To determine the source of the 0.9-mm surface error, a computer program which determines the surface of the antenna from a geometric standpoint was developed. As can be seen in Table 24, the geometric surface is the source of the largest error (0.05 cm rms). Figure 48 shows the source of the geometric error. When a mesh is stretched over the ribs, the mesh bows inward like the gores of an umbrella, which is the opposite of the desired parabolic surface. A computer was programmed at JPL to stretch the mesh across the parabolic rib, predict what the surface might be, and move the ribs backward until an average bowed-in mesh that bisects the desired parabolic shape was obtained. Thus, the geometric error is limited to 0.05 cm. The error can be reduced even further by increasing the number of ribs, but this increases the weight.

Figure 49 shows the results of the computer program, which was based on the 4.3-m diameter, the 1.37-m ring support height, the

Table 24. Error budget

	mm	in.
Geometric approximation	0.51 rms	0.020 rms
Manufacturing tolerances	0.25	0.010
Deployment repeatability	0.25	0.010
Thermal distortions	0.13	0.005
Total rms error ^a	0.89	0.035
^a $0.05 + \sqrt{0.025^2 + 0.025^2 + 0.013^2} = 0.89 \text{ mm}$		

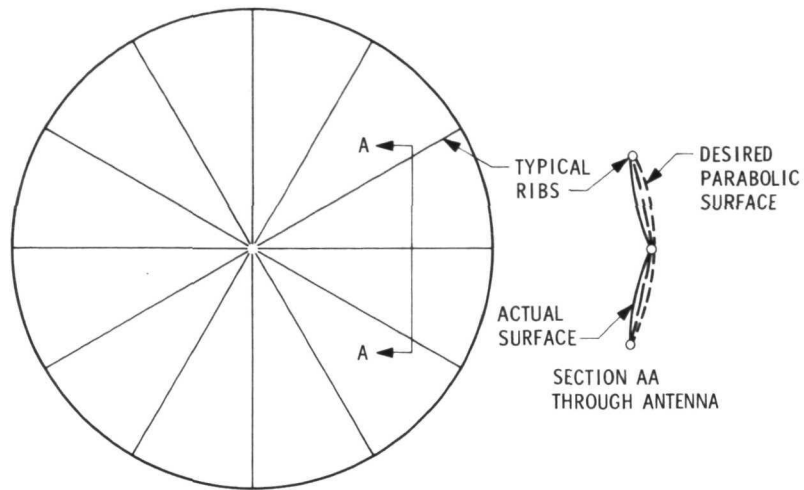


Fig. 48. Geometric error source

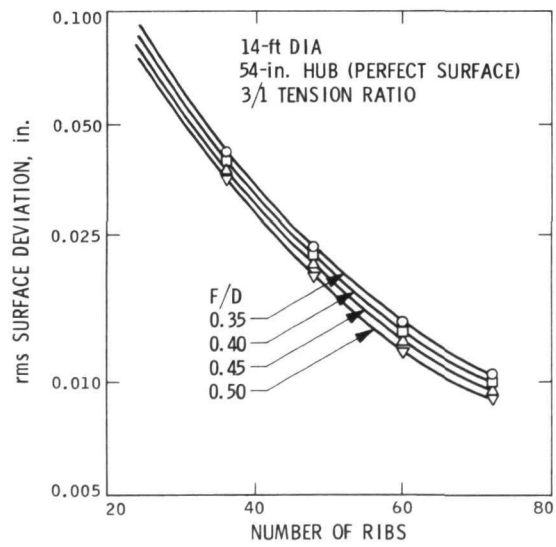


Fig. 49. Geometric surface error

assumption that the surface is perfect, and a 3-to-1 mesh tension ratio. From this information, it is possible to choose the number of ribs for the various focus-to-diameter ratios and to determine the rms error.

To confirm the information from the computer, two parabolic elements were set up, with a rubber membrane stretched at various tension ratios. The surface of this membrane was measured, and the computer then calculated what the surface should be. After a number of iterations, the two matched precisely for any particular tension ratio up to 6:1.

2. Configuration. Figure 50 is an artist's concept of the antenna. The ribs are covered with a Chromel R gold-plated mesh, and the center hub is solid.

a. Deployment. For deployment, a pair of constant-force springs are used for each rib deployment mechanism. One of each pair is redundant; one spring can deploy the rib against gravity and hold it against the stops. When the antenna is face up and the pairs of springs are assisted by gravity, the springs deploy the ribs too rapidly and overstress them as they hit the stops. To remedy this, a damping system is placed on every fourth rib.

Before the spring system was selected to actuate deployment, both electric motors and pneumatic systems were considered. Neither of these systems was chosen because electric motors use too much power, and pneumatic systems are subject to leaking.

Other alternatives are (1) torsional springs around the hinge axis (but a spring large enough to work and to provide the necessary redundancy leaves no space in the hinge area); (2) lever systems (but these protrude into the inner face of the dish); and (3) a cable system (but this system requires 48 cables running around a drum in the center). In the stowed position, a simple lanyard holds the ribs against a nesting ring which is notched for each individual rib.

Figure 51 shows a cross section of the antenna. In addition to the nesting ring and lanyard, the superstructure supports the electronic equipment above it. A thermal blanket is used behind to isolate the RTGs so that thermal distortions are kept to a minimum. The adjustment points are at the hinge point of each rib for adjustment of the rotational stop.

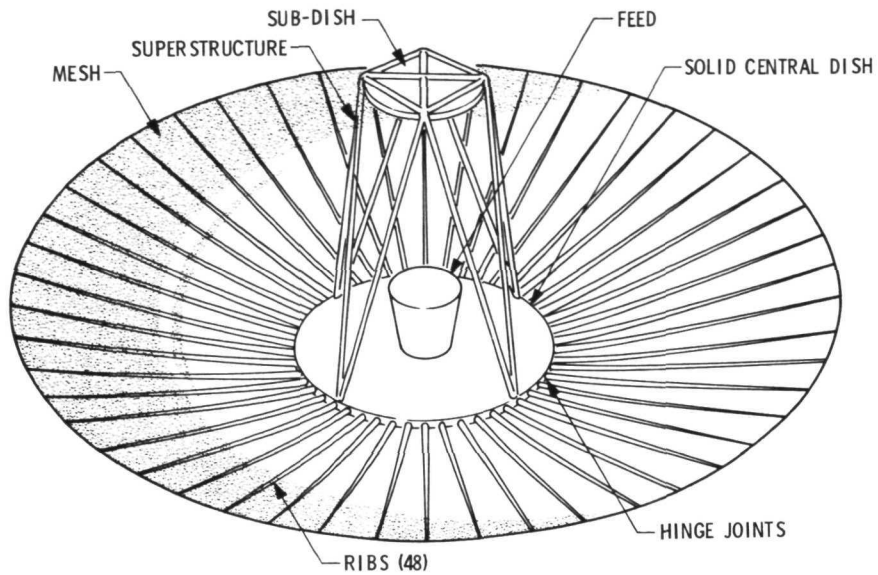


Fig. 50. Hinged radial rib antenna, 4.3 m in diameter

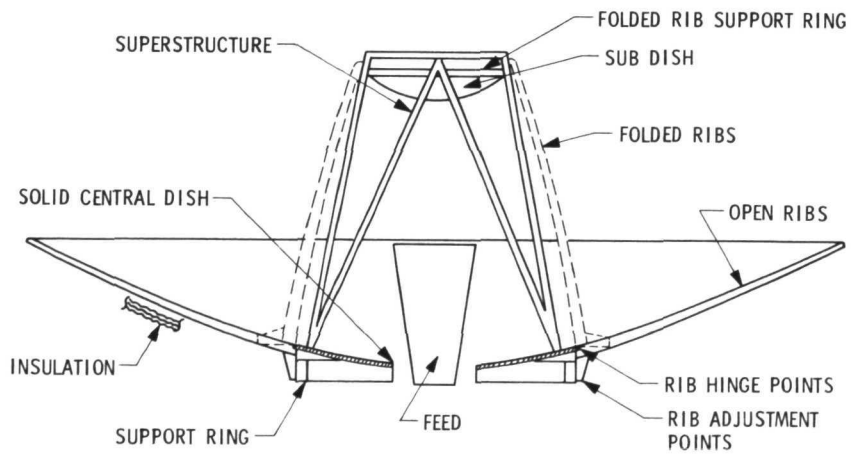


Fig. 51. Cross section of TOPS 4.3-m antenna

b. Support ring. To meet the stringent surface error requirement, it was decided to make the support ring as large as possible within the shroud constraint, thus limiting the deployable area and providing space around the circumference of the ring for the assembly of the hinges and the pins, etc., that make up the rotational mechanism. A diameter of 1.37 m was chosen as optimum. Stiffener sections, which incorporate the hinge and the rib stop, are connected together with flat shear plates. The flat plate stiffener design, as opposed to a curved plate, is analyzed easily; the analysis results appear to be satisfactory for all given loads; and it is reasonably easy to fabricate. Bonding agents and rivets are used for assembly.

Because it would have been costly, however, to make the stiffeners as light as desirable, the size of the stiffeners, the sheets, the rivets, and the entire structural assembly was increased by a factor of 1.5. This increased the weight from 6.35 kg (14 lb) to 9.98 kg (22 lb), and significantly lowered costs.

The support ring assembly was completed and the deployment system installed. The damping system was tested and is ready for installation.

Figure 52 shows the ring support after fabrication was complete. The stiffeners with the hinge mechanism are inside the ring, with the rib stops and the hinge points exposed.

An aluminum honeycomb structure for the central dish was found to cost almost as much as all the other antenna components combined. Although the honeycomb structure is preferable, it was replaced with fiberglass coated with aluminum for RF reflectance. Thermal tests may indicate that this thin fiberglass structure needs to be reanalyzed.

c. Ribs. The circular cross section was chosen for the ribs because it has the best thermal distribution or gradient across the rib from the top to the bottom, and it is structurally sound. The rib is a tube which tapers from 2.8 cm (1.1 in.) in diameter down to a diameter of 0.952 cm (0.375 in.). The wall is also tapered from 0.051 cm (0.020 in.) down to 0.038 cm (0.015 in.) at the tip. It was structurally optimized to reduce weight. The ribs were made as close to a flight antenna as possible

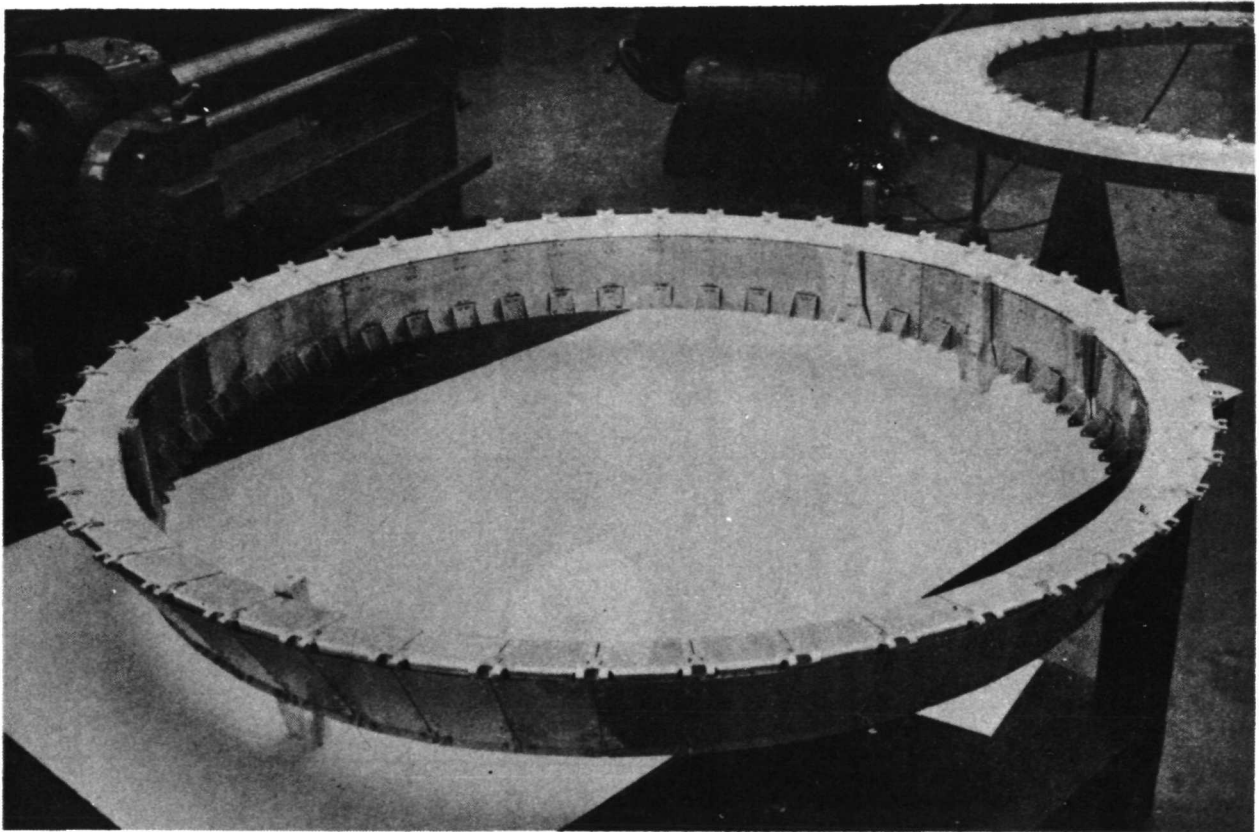


Fig. 52. Ring support

for evaluation purposes. After the ribs were tapered, they were bent into a parabolic contour, and a trim rib was placed on the concave side. The contour of any particular rib can be held within 0.015 cm (0.006 in.) of the desired parabolic surface.

d. Dampers. Existing dampers, such as linear, centrifugal brakes and escapement dampers, were either too large or too small or had some other problems. A decision was made to use a multivane, rotary damper with a silicon oil having a kinematic viscosity of 176,000 centistoke. This damper worked as predicted to prevent deformation of the ribs.

e. Mesh. The base material of the antenna mesh is Chromel R. A primary advantage of this material is its availability. It is commonly knitted into a tricot. To keep the RF losses down to 0.07 to 0.09 dB, the mesh must be gold-plated. Chromel R is unique in that it is passive; nothing sticks to it, including gold. The gold forms a tube around each individual strand of Chromel R so that, if it cracks, it has nothing to adhere to and thus flakes off. The electrolytic process results in a somewhat more ductile gold-plating. However, flaking is still a problem. Both plating methods produce a gold-plating which is brittle. As the mesh is worked, it cracks and, as observed with the scanning electron microscope, tends to come off.

Once the patterns between the ribs were determined by the JPL computer program (see Section V-C2), the gores were cut and sewn with a metallic thread. Most of the threads tested tended to fray or break. This problem was solved by wrapping the metallic thread with a teflon material, which kept the strands from tangling in the needle eye.

Materials other than Chromel R were investigated. One of these was Paliney 7; an alloy of platinum, palladium, and other rare metals. It has an RF loss of 0.11 to 0.28 dB, depending on the orientation. Paliney 20, a silver-based material, was also examined. Paliney 20 has not been tested yet, but its resistance indicates that its RF loss should be close to that of Chromel R. A mesh woven of beryllium copper also has a low resistance and looks promising. (See Refs. 5 and 6 for additional information.)

f. Superstructure. At first, it was planned to use a three-point support truss. However, a four-point truss was selected because the monopulse feed system would operate more easily and would provide better data with a symmetrical truss. The blockage from the four-point truss is slightly higher than from the three-point. The weight difference is small because it is necessary to use larger tubes for the three-point truss. An aperture cover was placed over the end of the feed to eliminate a feed-heating problem. The use of fiberglass tubes with very thin walls (about 0.051 cm) and a large diameter kept the RF blockage to about 30% of the optical blockage. The weight difference between this superstructure and the competitive trusses is small. The only constraint is that the load the tubes are able to carry is limited. An aluminum truss and composite materials were examined as alternatives. The aluminum truss was too heavy, and cost-limited the in-depth examination of composite materials. A thin, fiberglass frustum offered good thermal control, but its load capability was limited. When enough stiffeners were added to carry the load, the blockage increased and offset the advantages.

Additional information about the high-gain antenna may be found in Refs. 7 and 8.

D. Temperature Control

1. Requirements and Constraints. The basic requirement of the thermal control subsystem is to maintain temperatures within acceptable limits throughout the mission. The subsystem is constrained by the fact that

- (1) During encounter, when demand is at its peak, only a limited amount of electrical power is available for heating.
- (2) Gamma and neutron radiation from isotope heaters limits their use.
- (3) Solar intensity decreases by approximately 3 orders of magnitude during the mission.
- (4) Heat losses from warm instruments are maximum at the end of the mission, while the electrical output from the RTG is at a minimum.

There are three areas with more stringent temperature control requirements than those of Mariner 1971:

- (1) The electronic compartment shear plates are a typical temperature control surface and must be maintained in the range of 4.4 to 21.1°C (40 to 70°F).
- (2) The propulsion and attitude control fuel requires a lower temperature than that of Mariner -- 15.6 to 32.2°C (60 to 90°F) -- and the maximum temperature after motor firing, 48.9°C (120°F), is approximately 16.7°C (30°F) less than for Mariner.
- (3) The low-, medium-, and high-gain antennas require a much wider range of temperature than the Mariner antenna -- 93.3 to -240°C (+200 to -400°F).

The temperature requirements for science vary from none for the radio emission detector to -40°C (-40°F) for the vidicon target affecting the wide-angle, narrow-angle, and approach guidance cameras, a requirement difficult to achieve. A design solution for cooling the infrared multiple radiometer, with the Channel 3 bolometer requirement of -255°C (-424°F) at Neptune and Pluto was not developed in TOPS. All other science instruments have typical temperature requirements.

2. Philosophy. For the TOPS mission, it is believed that heat losses must be minimized. Warm electronics must be isolated from the variable solar heat load. Where large variations in power dissipation exist, such as the electronic compartment, the heat losses must be designed to pass through controllable surfaces (louvers). For small-powered instruments, one mode of heat transfer should be dominant. High conductance attachments to a surface whose temperature will greatly decrease must be avoided; e. g., the antenna attachment to the spacecraft compartment. Electrical heaters should be used for fine temperature control, and isotope heaters where boundary conditions permit. The antenna must be isolated from the RTG.

3. Baseline Subsystem Description. The subsystem weight, including six bays of louvers, is 17 kg (37 lb). The louver design is a combination of exposed white shear plates and louvered shear plate area. This arrangement maintains a 4 to 21°C environment on the shear plate as power

dissipation within the compartment varies from 280 W during the cruise phase to 400 W during encounter.

The temperature of the electronics compartment is higher than that of the propulsion bay, which operates at 21.1°C. The interface area between the two is large enough to transfer the extra heat from the electronics compartment to the propulsion bay to make up for the energy lost through the thermal blanket covering the propulsion bay. Thermal blankets are used on the nonlouvered external surfaces of the compartment to minimize losses and ensure that most of the power dissipation transfers through the controllable surfaces.

In each pair of roll, pitch, and yaw jets, there are small, 1-W radioisotope heaters to prevent freezing of the fuel behind the valve in the nozzle.

Thermal blankets and small strip heaters are used to keep the science scan platform at -17.8°C (0°F) to eliminate large conductance losses caused by attachments and cabling from the instruments to a cold structure. Temperature control losses are based upon the electronics and optics within the instruments, which are at -17.8°C. If the instruments were at 21.1°C, the losses would be double. The vector helium magnetometer and the plasma wave detector could possibly be warmed by isotope heaters; however, for the thermal control analysis, electrical heaters were assumed.

In all, the temperature control subsystem consists of thermal blankets, louvers, electrical and radioisotope heaters. The thermal blanket area, excluding the antenna, is approximately 10.50 m² (113 ft²). Around the outside layer of the thermal blankets is a white beta-cloth, which maintains a temperature of about 21.1°C under one-Sun conditions, thus preventing instrument heating near Earth.

Table 25 shows the areas requiring power for temperature control, and Table 26 gives the heater requirements.

Table 25. Areas requiring power for temperature control

Areas	Heat losses during cruise phase, W
Science and flight instruments	62
Propulsion module (blankets)	14
Main motor nozzle	3
Attitude control jets	8
Total	87

Table 26. Temperature control heater requirements

Heater	Requirements, W
Electrical	
At encounter	23.1
During cruise	36.65
Radioisotope	11.0

4. Subsystem Status

- a. Louvers. The louver technology is current, and no development is required. The louvers are individually actuated and highly reliable.
- b. Thermal blankets. The thermal blankets are state-of-the-art. The beta-cloth outer layer provides micrometeoroid protection.
- c. Electrical heaters. Also state-of-the-art, the electrical heaters are highly reliable.
- d. Radioisotope heaters. One-watt radioisotope heaters have already been developed. The decrease in heat from beginning of life to end of life is acceptable within the required temperature range.

e. Camera vidicon target. The passive design to provide a temperature of -40°C appears possible but extremely difficult to achieve because of the power dissipation within the cameras when they are on. Further component development is needed to support the baseline design.

f. IMR sensor. The passive design to achieve a sensor temperature of -255°C appears impractical because of the environment.

g. Fluid loop. In October 1968, it was determined that 14.5 W were dissipated when all the instruments were on during encounter and cruise. During cruise, when the encounter instruments were off, 7 W were dissipated. The current estimated power dissipation by a set of instruments similar to the payload assumed for TOPS in 1968 is 50 W.

Figure 53 illustrates why a fluid loop was developed. Before a favorable scan platform was designed (configuration 12L, Fig. 12), the instruments were mounted to a tubular structure, which could not be adequately blanketed for thermal control. Consequently, it was assumed that the instruments would be mounted to a cold structure, the losses calculated, and a heat-delivery system built to overcome the losses. At -17.8°C , there was a loss of about 120 W. With 7 W of power dissipated and approximately 25 W of power allocated, the temperature would be about -129°C (-200°F). A fluid loop delivering from 75 to 100 W maintains a temperature in the optimum range.

Some approaches that were taken to supply that amount of thermal energy were to

- (1) Use isotope heaters in each instrument. A thorough analysis disclosed that the weight of the shielding prohibited their use.
- (2) Develop low-temperature electronics to avoid the need for such a large amount of power. Typical electronic piece-parts were tested from -60 to -150°C . Results indicated that, although some parts were well qualified to -150°C , other parts, such as shift registers, failed at -60°C . The idea was dropped because not all the parts functioned within design limits.
- (3) Use an inflatable radiation pipe to transport RTG heat to science. This design was not developed because the pipe would have to be about 30 cm (12 in.) in diameter, and there were interface

branching and articulation problems, particularly in view of the fact that the scan platform must articulate in azimuth at an angle of about 250 deg and in elevation from +90 to -55 deg.

- (4) Increase RTG size to permit use of all-electrical heaters. At \$12,000 per watt, this idea is not practical.
- (5) Design a series heat pipe which uses RTG waste heat. A breadboard unit was built and tested, and performance was verified analytically. One section of an inflexible, copper, water heat pipe 2.13 m (7 ft) in length was built with a joint. Test results show that 110 W were absorbed from a source lower in temperature than the RTG, and 100 W were rejected to a sink at 110°C (230°F). There was a 21.1°C drop across this section. The large temperature drop occurred at the slip joint. By the time one more joint is crossed and two more 2.13-m sections are added, the rejector temperature is about 21.1°C. The heat pipe is self-pumping.

Figure 54 is a schematic of the series heat pipe as it interfaces into the spacecraft. After the pipe mates with the RTG, it passes through the articulated joint and branches to the cruise and encounter science. Louvers dissipate the heat as these instruments switch on and also regulate the surges that might occur in the system.

- (6) Develop a thermal fluid loop which uses RTG waste heat. Design of the thermal fluid loop paralleled that of the heat pipe, and the loop also was built, tested, and verified. Coolanol 45, absorbing 175 W from a source cooler than the RTG, was able to reject 75 W to a sink, which had a temperature much higher than the -17.8°C required by the science instruments. The flow energy needed to circulate this fluid was 0.01 W, so that an overall pump and motor efficiency of 1% uses less than 1 W of electrical power to deliver 75 W of thermal power by the fluid loop. In view of the difficulty of insulating a 0.63-cm (0.25-in.) line when the fluid leaves the RTG at a temperature of nearly 121°C (250°F), an allowance of 100 W was made for loss in the lines.

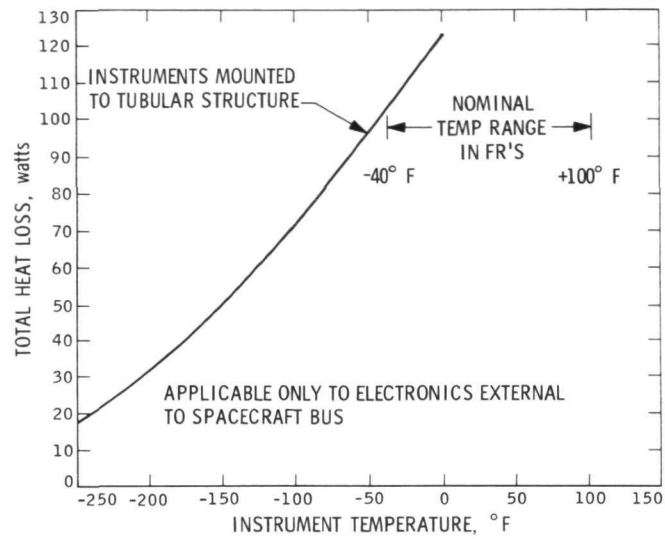


Fig. 53. Minimum temperature control power as a function of instrument temperature

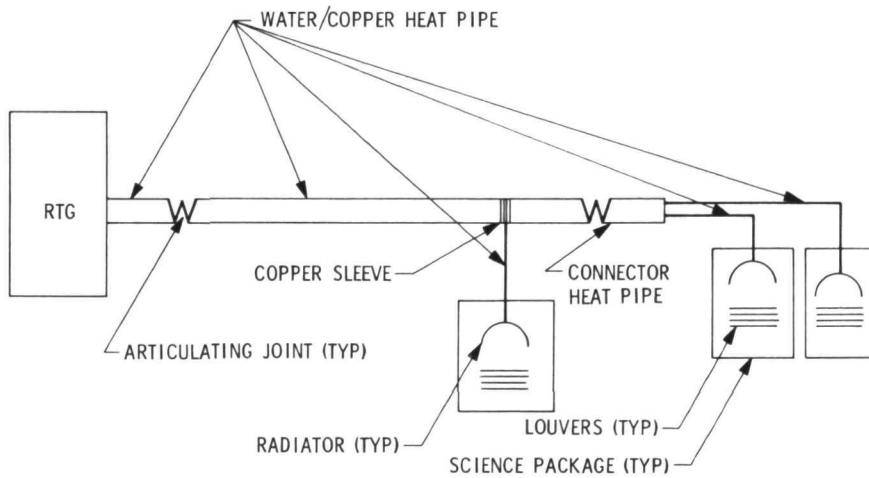


Fig. 54. Series heat pipe assembly

Figure 55 is a schematic of a thermal fluid loop. A resistance-heated plate at 185°C and with no radioactivity simulated the RTG used with the unit built. Three heat exchangers borrowed from the Apollo program were used at the cruise, encounter, and approach guidance instruments. A single inexpensive pump was used and, to get the desired flow rate without pressure surges, a needle valve had to be installed downstream.

The fluid loop was selected for the baseline Temperature Control Subsystem because it was a technique proven on the Gemini and Apollo programs, required less development, and was much easier to integrate into the spacecraft configuration than the heat pipe.

However, the fluid loop was later dropped from the baseline because (1) a new scan platform design made it possible to reduce heat losses, and (2) science operating power increased. Furthermore, the new low-temperature requirements on the wide-angle, narrow-angle, and approach guidance cameras were not compatible with a large heat-delivery system.

h. Electronics compartment. The electronics compartment is composed of six major equipment bays. Figure 56 illustrates changes in requirements for radiating heat vs temperature of the shear plates for TOPS and previous spacecraft. For TOPS, more power is to be rejected at lower shear-plate temperatures. Because this is a radiation heat-transfer problem, the heat is rejected at the fourth power of the temperature. If temperature control is to work within this envelope, the heat delivered to the shear plate must have a uniform flux density. All components are assumed to be thermally connected and to have high conductivity. Encounter power occurs at the midpoint of the temperature control louver range. With this design, as many as 33% of all louver blades can fail to open before the 21.1°C shear-plate temperature is exceeded. On the other hand, with encounter power, as many as 40% of all louver blades can fail to close before the lower 4.44°C temperature is exceeded because, when the louvers are open, their emittance is six times greater than when they are closed.

A thermal analysis of the electronics compartment was made because a new packaging concept was adopted. The results of the study show that temperature gradients are higher than the gradients for Mariner. The maximum gradient from the shear plate inward is 22.2°C (40°F).

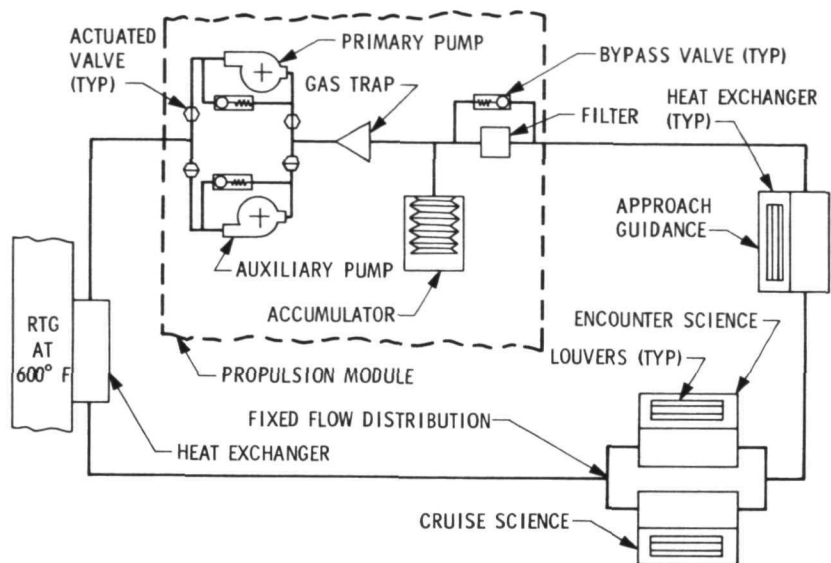


Fig. 55. Thermal fluid loop

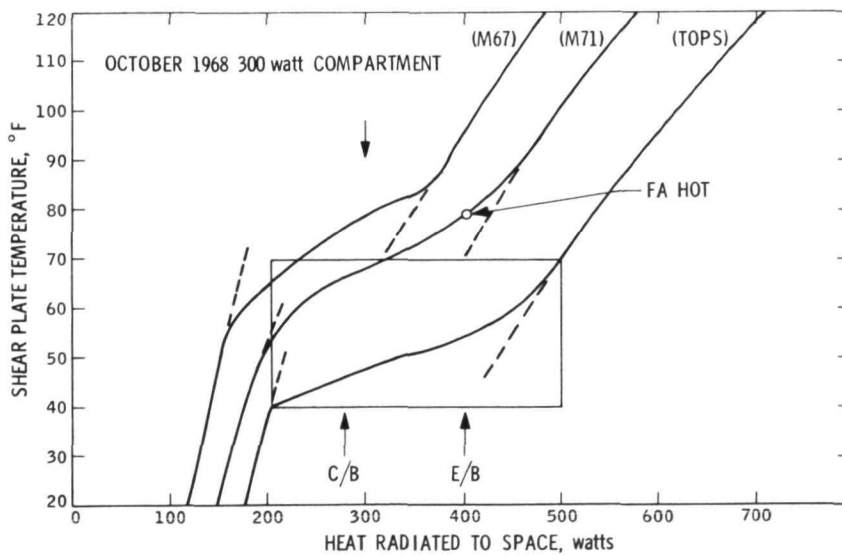


Fig. 56. Electronics compartment

Figure 57 shows a typical digital packaging for a 41-W bay (encounter power). The particular spacing of the bosses allows a gradient between the shear plate and the assembly to vary from 2.2°C (4°F), where there are two bosses, to 5°C (9°F) where there is one boss, to 9.5°C (17°F) where there is no boss. The shear plate is not isothermal, but has hot spots which allow the compartment temperature to exceed the 21.1°C upper limit.

i. High-gain antenna. The various thermal environments encountered by the high-gain antenna are the solar, the RTG, the deep space, and that caused by conduction from the propulsion bay. Early predictions were made for a deep space environment and for that inside a thermal vacuum chamber. Table 27 shows the results.

Table 27. Variation in equilibrium temperature^a

Space-craft position	Case 1, solar heating, no blanket		Case 2, solar and RTG, no blanket		Case 3, solar and RTG with thermal blanket		Case 4, thermal vacuum effect, wall temperature -280°F		
	Temperature, °F	Gradient, °F	Temperature, °F	Gradient, °F	Temperature, °F	Gradient, °F	Temperature, °F	Gradient, °F	ΔT
Near Earth	75	3.63	90	3.79	219	0.06	220	0.07	1
1.5 AU	-25	1.60	1.5	1.23	91	0.02	93	0.03	2
Jupiter	-225	0.14	-126	0.58	-160	0.01	-151	0.01	9
Saturn	-285	0.04	-142	0.70	-236	0.01	-215	0.01	21
Uranus	-337	0.01	-147	0.74	-296	0.01	-255	0.01	41
Neptune	-362	0.01	-148	0.74	-319	0.01	-265	0.01	54

^aTemperature gradients around a 1-in. -OD grey-body antenna rib, 0.020-in. wall thickness, 6061T-6 aluminum.

The RTG's major effect on the ribs is increased rib temperature and temperature gradients as the solar intensity decreases. Some ribs are warmer on the back, others on the front, and some on the side, depending upon the look angle between the RTG and the individual ribs. As a result, the ribs are bending in different directions.

Computer analysis shows that, when a 15-layer blanket is used, the rib temperature gradients are greatly reduced. When the antenna is needed to support the data rates at Jupiter encounter, rib temperature gradients are about 0.006°C (0.01°F).

A computer analysis was made to predict antenna temperatures inside a thermal vacuum chamber having an effective cold wall of -173°C (-280°F). The effects of a weak Sun, an RTG, and a thermal blanket were also assumed. Analysis showed that thermal vacuum antenna temperatures would be high because even a -173°C cold wall was not cold enough. Antenna temperatures at Neptune conditions inside a thermal vacuum chamber would be off as much as 30°C (54°F) from those expected in flight (i. e., -265°F to -319°F).

Stress studies determined that small temperature gradients cause significant surface errors. However, gradients of no more than 0.006°C around the rib result in small surface errors of about 0.0013 cm. To minimize the gradients, it was then decided to use a thermal blanket and leave the front side of the antenna Sun-dependent.

If the tapered ribs are wrapped with an ideal (no loss) thermal blanket at 21.1°C , the rib temperature would remain 21.1°C throughout flight. However, a practical thermal blanket will always have some heat leaks. Thus, without an internal heat source, it is impossible to predict what the rib temperature may be. For this reason, the blanket was placed behind the ribs, leaving the ribs Sun-dependent and isolated from the RTGs. Further, low-conductance supports were used from the warmer electronics compartment and propulsion module to the rib support ring. The contact area of the pickup points of each rib where the ribs come into the ring is critical, because a large gradient at the base of the rib could cause large movement in the tips of the ribs.

The ribs, the trim ribs, and the sunlit side of the thermal blanket are white. To reduce the energy-focus problem, the subdish is also white, as is the fixed portion of the main dish. A metallized subdish would send much

more specular energy to the feed than a white subdish. The mesh is gold because of the RF requirement. For this set of conditions, temperatures have been determined for each of these items for the JUN and JSP trajectories. These temperature data are being processed in structural computer programs to predict the surface error.

Other antenna studies were made to determine the effect of the subdish shadow on the ribs. The Sun angle 50 days prior to Jupiter encounter is approximately 11 deg, so that the shadow cast by the subdish strikes about 5 ribs, and the pattern is about 2.54 cm long. Fifty days after Jupiter encounter, the Sun angle is 8-1/2 deg, and the subdish shadow is off the ribs and on the fixed portion of the main dish. These temperature data can be used to predict distortion.

Using one Earth-Sun and a 0-deg Sun angle, feed-heating studies were made for the subdish supported by (1) a tubular structure and (2) a fiberglass cone. When the tubular structure is used, there must be an aperture cover for the S-band/X-band feed.

Figure 58 shows a specular solar-ray trace. It is assumed that the white thermal blanket has a 5% specular reflectance to solar energy. With 5% of one Earth-Sun reflected as shown in the figure, and 5% of that 5% reflected as shown, a feed-heating problem develops and creates, in effect, a solar furnace, because the ratio of the concentrated area to the receiving area is 1 to 44,000. To protect the feed, a spherical cover is placed about 24.13 cm (9.5 in.) in front of the aperture. The incident area is increased enough so that a white fiberglass surface would be no warmer than 93.3°C (200°F). A cone subdish support, painted white, filters out the solar energy and resolves the feed heating problem; and the intercept area is wide enough to create a cone heating problem.

E. Electronic Packaging and Cabling

1. Objectives

a. Develop a new packaging and cabling system. An increase of functional complexity of the TOPS over Mariners 6 and 7 (1969) was estimated in early studies to be 10 to 1. An increase in connector contact density of 4 to 1 was anticipated. Based on these considerations and other mission

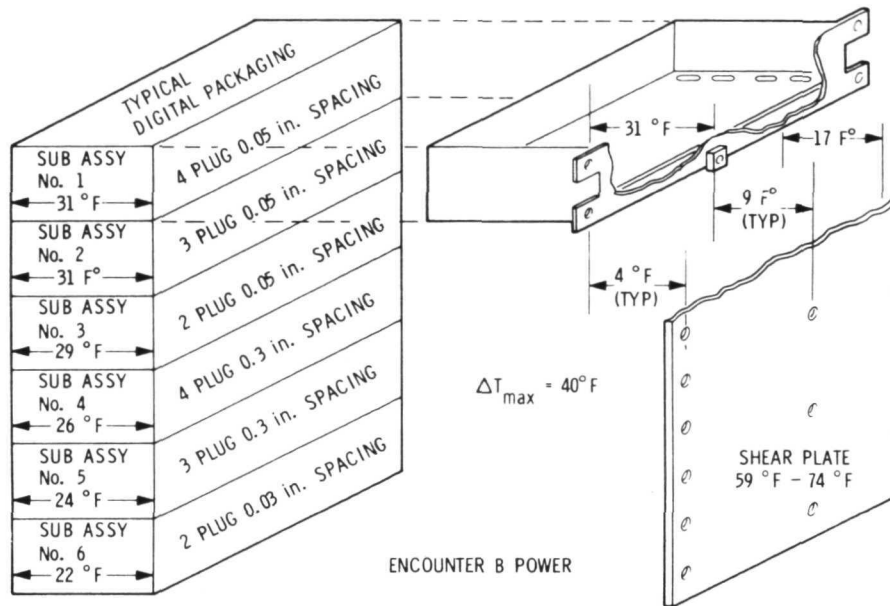


Fig. 57. Thermal analysis of 41-W dissipation bay

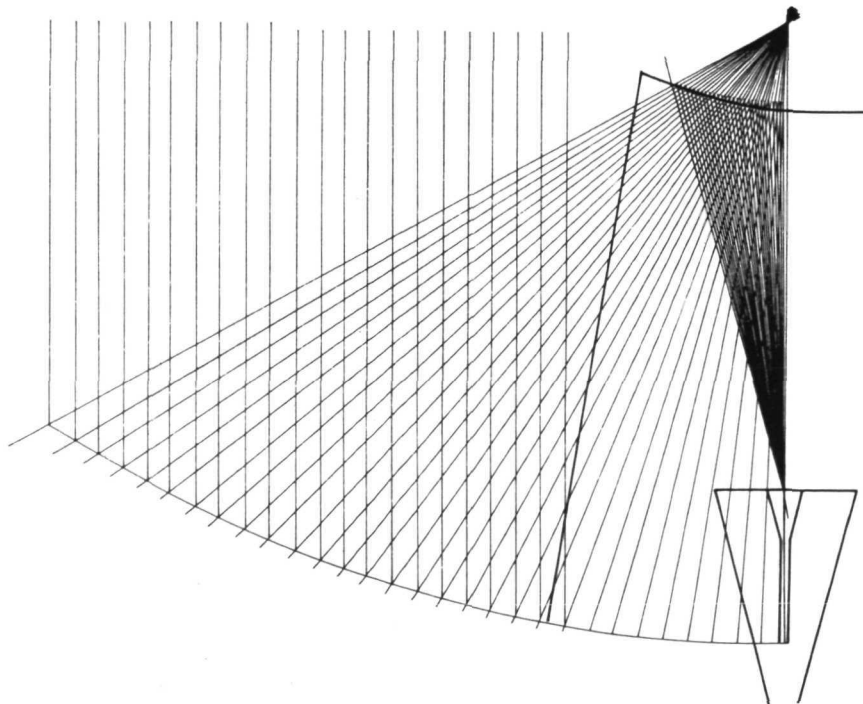


Fig. 58. Specular ray trace

constraints discussed earlier, it was determined that this new packaging and cabling system should have

- (1) Increased density.
- (2) Enhanced electronic part life.
- (3) Environmental immunity.

b. Minimize flight weight. As always in any spacecraft configuration, launch constraints require as low a flight weight as possible. Savings can be realized by more extensive use of removable handling and assembly tooling.

c. Provide parallel operations for mechanical/electrical assembly and test. Previously, mechanical operations have been delayed while electrical systems and subsystems tests were conducted. Parallel operations would increase efficiency during spacecraft assembly and test.

In addition to these broad objectives, there are several physical principles that have formed the basis for JPL packaging designs. These are:

- (1) Use of a hard-mount technique to minimize relative movement between the components and joints at all levels of the system.
- (2) Use of short thermal conduction paths from the heat sources to the primary radiating thermal control surface.
- (3) Use of connector interfaces for each level of interconnect for testing, assembly operations, and field assembly.
- (4) Use of standard assembly and subassembly envelopes to simplify design and to increase the design flexibility.
- (5) Use of the concept of an integrated structure, whereby each additional assembly or item that is added to the system contributes to the overall structural system integrity.
- (6) Use of assembly/handling tooling, which provides temporary fasten-on fixtures to prevent handling damage at all levels of fabrication and installation, and permits certain mechanical and electrical operations to be done simultaneously.
- (7) Emphasis on reduction of volume to effectively decrease weight.

2. Design Features. To meet the preceding objectives and goals, specific packaging features have been incorporated into the design. A part density as high as 24.4 equivalent parts per cubic centimeter (400 equivalent parts per cubic inch) was achieved through some new developments.

A single side-access, plug-in assembly provides a more efficient use of the packaging volume. The increased use of medium-scale integration (MSI) and large-scale integration (LSI) requires a new packaging concept for microelectronics, and much development work was concentrated in that area.

Electronic assemblies have been functionally sized by the use of an iterative loop which considers the electrical function. Two dimensions of the plug-in assembly or chassis are fixed at 17.78 × 36.83 cm (7 × 14.5 in.), and then the chassis thickness is varied, depending upon the size of the individual modules that go into the assembly.

The electronic compartment is separable from the remainder of the spacecraft through the use of fasten-on tooling to aid in the dual mechanical and electrical test and assembly operations. Precision tooling is used for the alignment of the various mechanical interfaces. These interfaces are readily broken by connectors.

The configuration of the electronic compartment permits the use of short cable lengths for the cabling subsystem. Small-gauge wire in the 26- to 32-gage range is used because it decreases weight and volume. Wires that small require careful handling, and therefore plug-in connectors and hard mounting are used to limit handling of the cable bundles.

To increase cabling density, the connectors used in the cabling subsystem, particularly for the electronic compartment, have contacts on 50-mil centers. These connectors are one fourth the size of the Mariner connectors. The impact of the data bus on the cabling subsystem is being examined, and may provide additional improvements in cabling density.

3. Hardware Development

a. Electronics compartment. Figure 59 is a drawing of the electronics compartment assembly, which is approximately 1.22 × 0.61 × 0.61 m (4 × 2 × 2 ft). Each of the four transverse planes which support and align this structure has a mounting rail for connector supports and assembly installation.

The system connectors for the electronic assemblies which plug into each bay are mounted on the connector supports at the rear of each bay. The compartment cabling volume is located in a 10.16-cm (4-in.) deep zone that runs through the entire center of the compartment. The TOPS connector interface differs from that of Mariner in that the OSE connectors are located along this system connector interface. Micrometeoroid barriers are provided on the upper and lower faces.

The design goal for the weight of the compartment structure was 22.23 kg (49 lb). The unit, with 16 connector support brackets and all the shear panels in place, weighs 21.80 kg (48.6 lb). The louver assemblies are included in the thermal control weight.

The compartment volume is approximately 0.197 m^3 (12,000 in.³). Each individual bay has a volume of 0.033 m^3 (2000 in.³), and the interconnect volume in the center is approximately 0.074 m^3 (4500 in.³).

High-power-producing units (e. g., the radio and power conditioning equipment) are placed at opposite corners of the compartment, and units which have a fairly high degree of communication are placed as close together as possible. The unit is designed to take advantage of thermal power sharing by close conductive coupling of the bays to achieve an isothermal compartment. A high degree of structural integration is attained by the installation of the individual assemblies into the compartment. At the time this compartment was originally designed and configured, the spacecraft power, now at 400 W, was approximately 300 W. For this reason, the degree of power sharing has actually increased, and the thermal coupling design has been adapted to satisfy the power requirements of the individual subassemblies.

b. Electronic assembly. The prime consideration for electronic assembly development is the need for improved integrated circuit packaging. As a consequence, work from the beginning of TOPS was oriented toward producing a high-density packaging technique for digital circuitry. Although the design development emphasis was on higher-density packaging, the design provided for use of existing Mariner techniques and could also accommodate "black box" assemblies. The package is installed into the compartment by a single-side plug-in technique which minimizes the volume required for cabling, connectors, and assembly fastening access and makes

efficient use of the volume. Individual assemblies are functionally sized and a single subsystem is kept within a given assembly. In some cases, a subsystem may require more than one assembly, but no more than one subsystem is packaged in any one assembly. Plug-in connectors with contacts spaced on 50-mil centers are used at all assembly interfaces.

The assembly is designed for a high degree of adaptability for thermal coupling. During the initial design, capability was provided to thermally decouple from the temperature control surface to maintain proper subsystem temperatures. This required development and testing of a mechanical attachment design which provided the minimum number of contact points. With the increase in subsystem power dissipation, this feature is probably not required.

Figure 60 shows how the assembly interfaces with the compartment and with the modular subassemblies. The connector support accepts up to 408 contacts to the system harness with one row of connectors.

The entire assembly is handled with a precision fixture which locates the assembly and controls the direct insertion of the assembly into the compartment bay, so that it is fully mated to the interface along the connector row. A tool is then used through the access tube to torque fasteners to the assembly mounting rail to lock the assembly into place. Then the fixture is removed. The master keying shear pin has an offset shoulder boss to prevent accidental 180-deg rotation of the unit, which would damage the connector interface.

The interface between the subassembly and the connectors, which are end-mounted on the assembly itself, is significant. Three techniques have been investigated for installation of the assembly/connector interface. One uses a full plate with permanently mounted connectors. An alternate technique uses a plate with easily removable connectors; i. e., the interconnect harness can be made on the bench and then transferred to the plate. The third technique, applicable to some assemblies which have a small number of connectors, uses a smaller bracket with the connectors positioned wherever they are needed to accept various module configurations that are plugged in. A unit 15.24 cm (6 in.) high, utilized to maximum density of the single-width modules, will accept 10,000 integrated circuits.

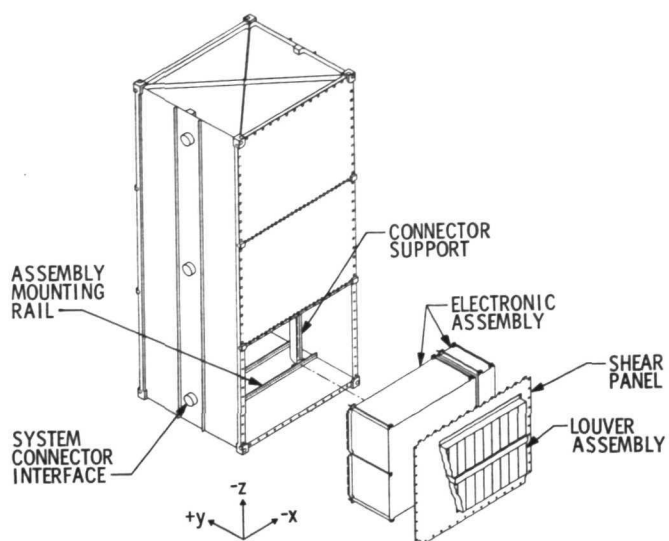


Fig. 59. Electronics compartment assembly

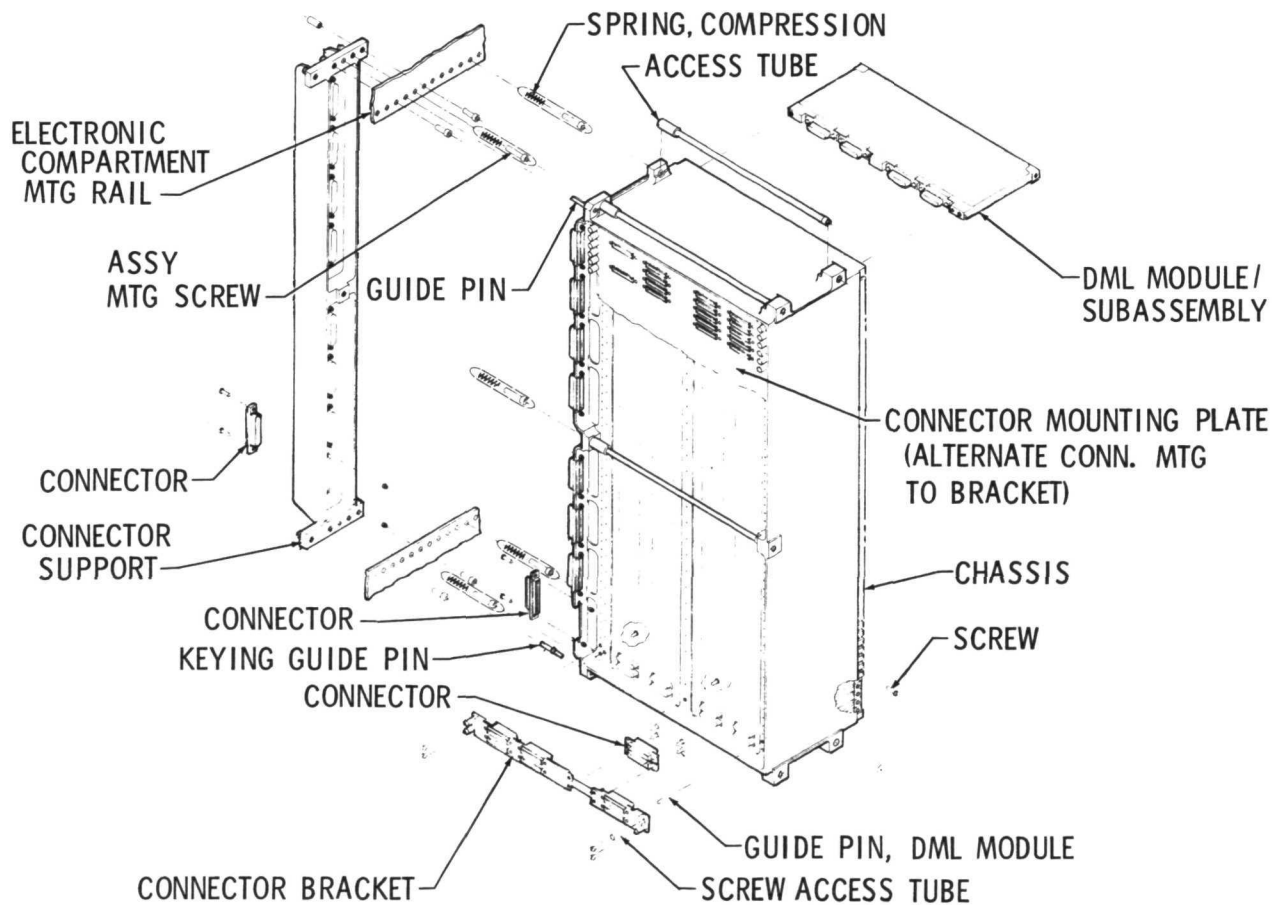


Fig. 60. Electronics assembly, module, and compartment interfaces

The arrangement for attachment of the shear panel for the development assembly provides the minimum mechanical attachments feasible, in order to attain a high degree of thermal decoupling for low-power units. Analysis indicates a temperature gradient from back to front of the compartment for present power levels. The adaptability of this compartment design lies in the capability to change the power sharing to the adjacent assemblies, bays, and the shear/thermal control panel by means of additional attachments to the thermal control panel and/or attachment points to the mounting rail.

In an alternate assembly configuration, the thermal coupling between the individual modules and the shear panel can be increased by inserting the modules in a direction which differs 90 deg from the insertion direction of the other assembly. However, this method decreases the number of pins that can be located in the same envelope and requires a fixed module height.

The hermetically sealed package approach might be used in a fluid-filled subsystem. This package is adaptable to the single-side access by means of the locating pins and a microminiature connector.

A Mariner packaging design was modified by single-side access through a tray-like fixture along the bottom to provide the interconnection zone. These connectors may or may not have the 50-mil centers. Existing Mariner plug-in technology can be used because the unit would be assembled to the tray on the bench before being plugged into the compartment. An early configuration of an assembly wiring harness is shown in Fig. 61.

c. The module/subassembly. In anticipation of an increased use of MSI and LSI in the outer planets project, a module was developed which could be functionally sized and which would allow easy part replacement. One way to do this is by providing increased pin density at the interface.

Figure 62 is a comparison of functional density packaging for several JPL spacecraft. The dashed line represents the maximum package density for digital circuits using various technologies with respect to time. A multilayer board with reflow soldered ICs was used for Mariner Mars 1971 to obtain the density shown on the figure. Mariner 1969 used 110,000 equivalent parts. A 10-to-1 increase was anticipated for TOPS. As a result, a discrete multilayer composite module with significant simplifications is under development. The composite module itself is composed of simple

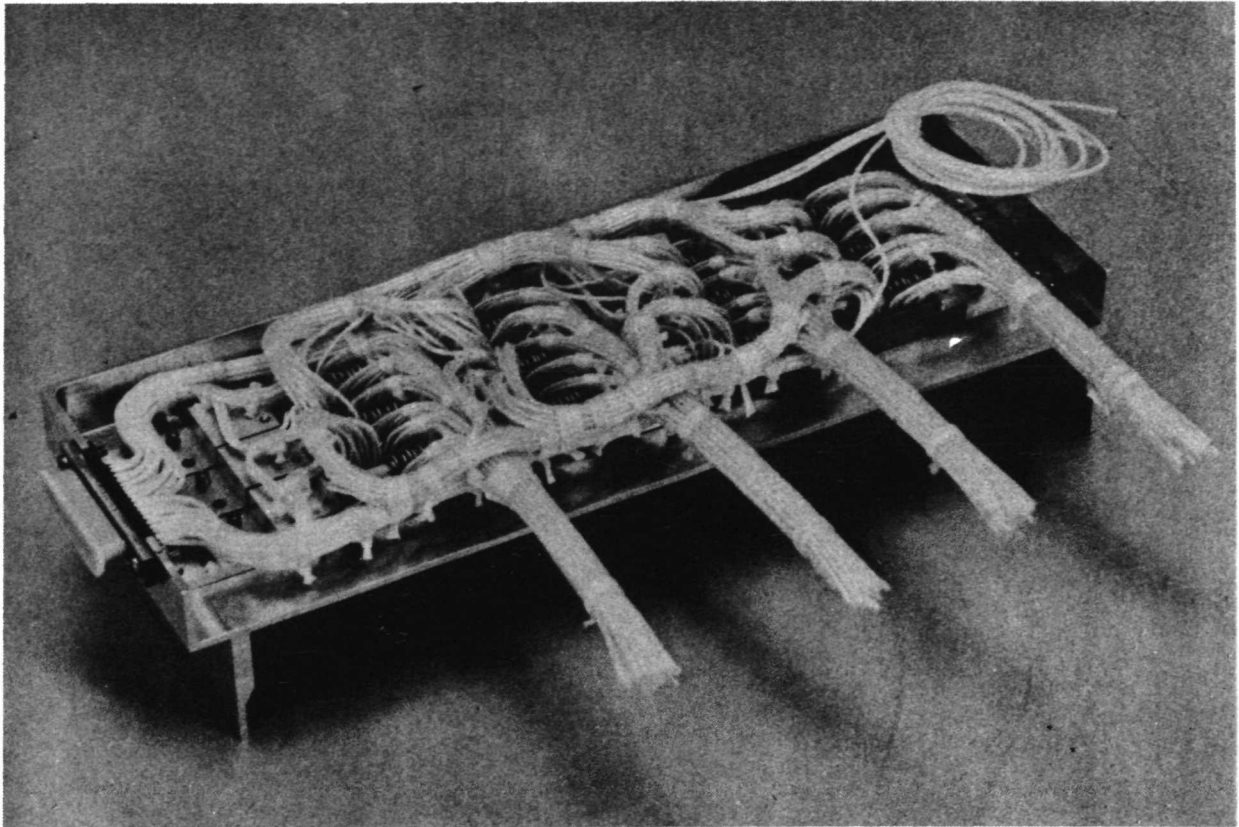


Fig. 61. Electronics assembly harness development

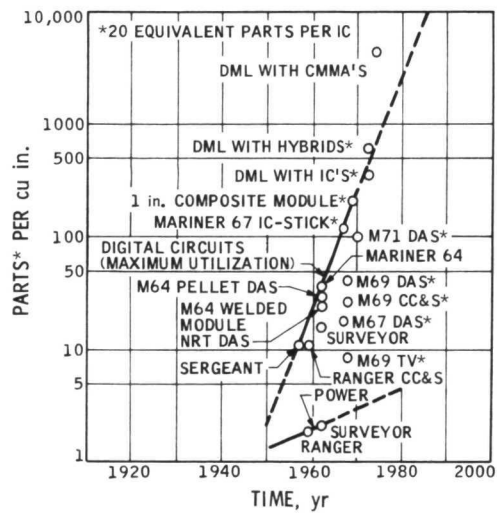


Fig. 62. Packaging functional densities for JPL spacecraft subsystems

components: the 50-mil-center connector, a machined frame, an insulator board, and an interconnect between the components. The interconnect is on a 50-mil node. This node is compatible with a large number of components (e.g., ICs, MSI, LSIs, and discrete). The module is maintainable at the component level, and can be flexibly sized. Nonproprietary manufacturing techniques have been applied to this design, but in a different manner than before.

Figure 63 shows some of the components that make up this module. The frame can have up to four connector installations. The board does not necessarily have to be a matrix board, as shown here. A multilayer or printed wiring board could provide access to the interface which mates to the assembly. The height and depth of this module are flexible.

Figure 64 illustrates the application of high-density packaging of integrated circuits in a discrete multilayer module with nodes of interconnection on 50-mil spacing. The nodes are attached by reflow soldering with a gold/tin solder. However, the interconnect can be welded if necessary. The interconnect is composed of layers of chemically etched metal traces that are discretely insulated with an insulating tape. The terminals themselves are placed in a pattern which accepts any size components. A 14-lead flat pack is shown here, but because of flexibility in terminal locations, LSI or various hybrid configurations can be placed and mixed in the packages at will.

Figure 65 shows the different modes of growth of this assembly. Different numbers of connectors are used with the basic frame. An additional web may be added as the board grows larger. A board about 7.62 cm (3 in.) tall accepts 75 ICs. A unit 15.24 cm (6 in.) tall will accept approximately 200 ICs.

d. Electronic packaging components and parts. In addition to the evaluation of small-gage wire and connectors with high-density configurations, a ceramic, nonmagnetic, microcircuit package in 14-, 40-, and 44-lead configurations has been developed and is now in the procurement stage. Miniature fasteners as small as size 2-56 should be analyzed. Thermal and structural analyses of the module assembly and the compartment interfaces are also necessary to determine how well the fasteners perform.

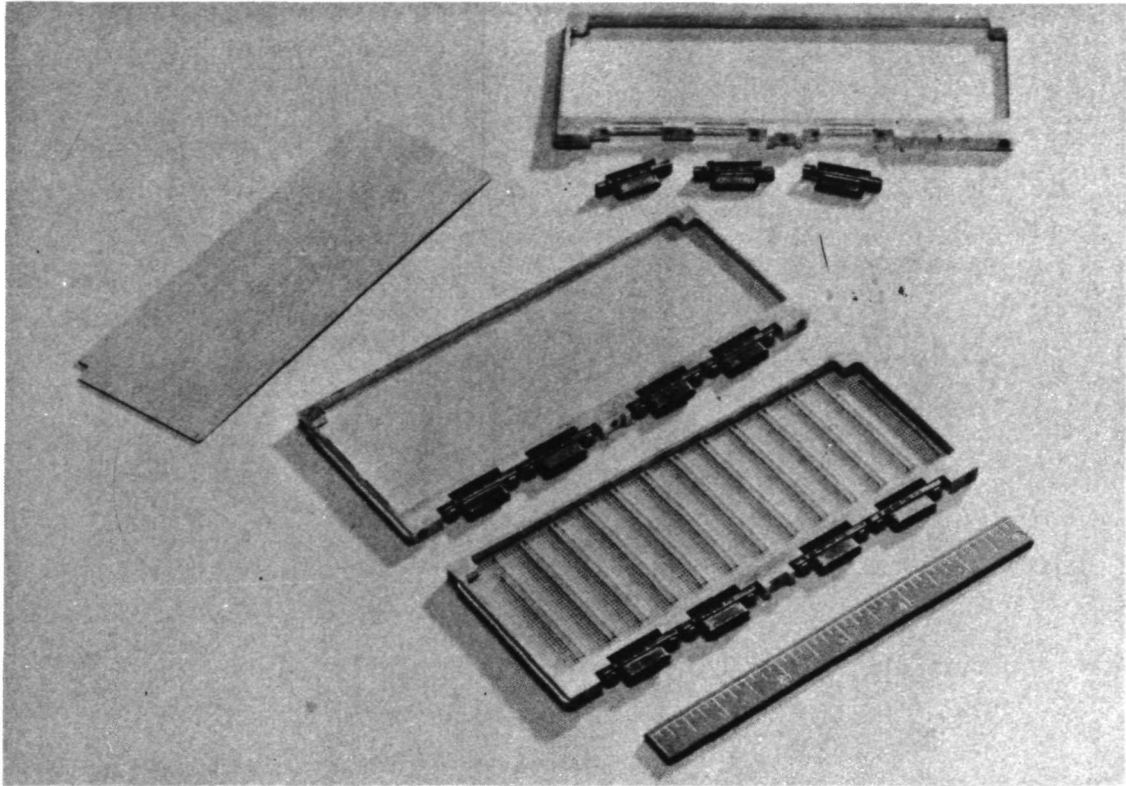


Fig. 63. Composite module components

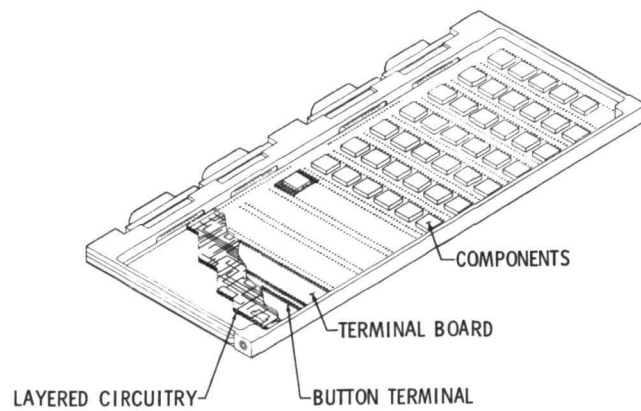


Fig. 64. Discrete multilayer module
(digital-circuit packaging)

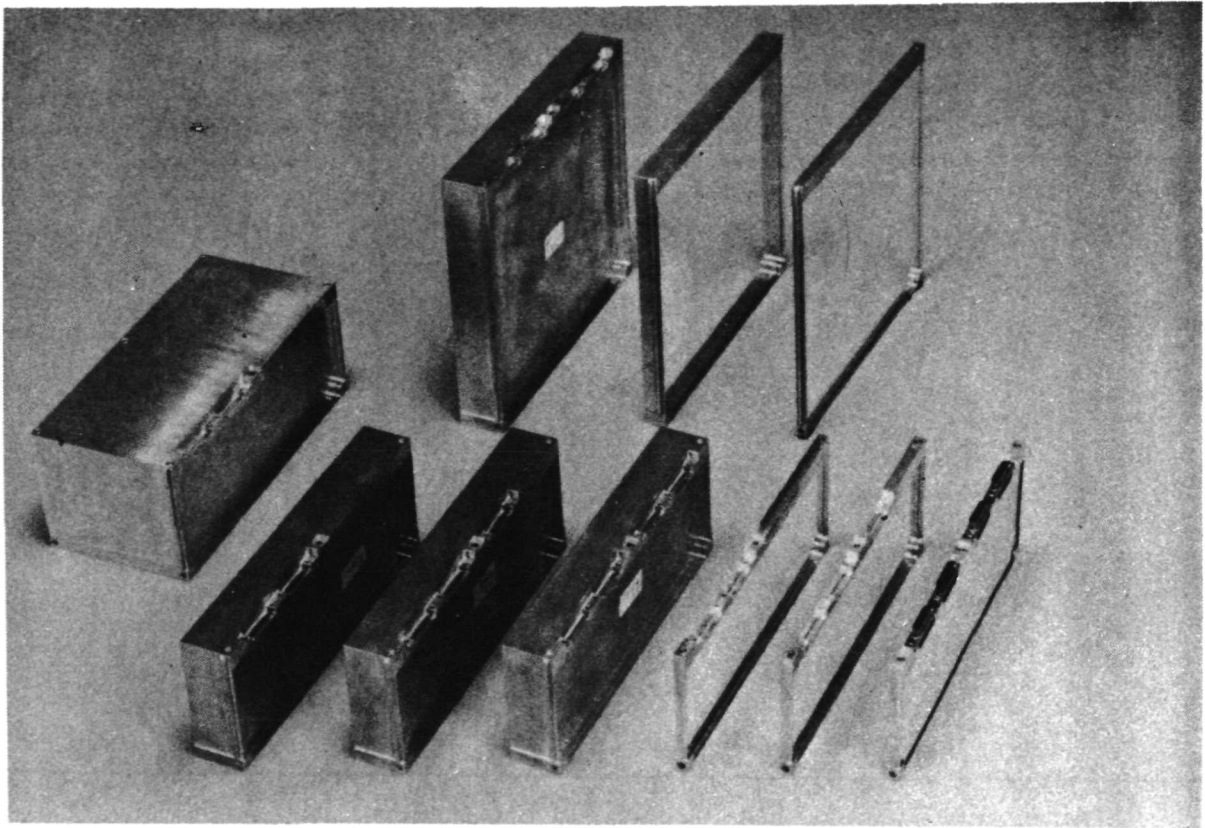


Fig. 65. Module sizing flexibility

4. Summary

a. Hardware

- (1) A composite module with the discrete multilayer module interconnect was built.
- (2) Two electronics assemblies have been fabricated. One was used as an assembly harness development tool. A fit-and-function test of the harness was completed.
- (3) The mockup, full-scale electronics compartment was completed ahead of schedule, and a fit-and-function test with the electronics assembly was scheduled. The interconnect harness that goes in the compartment was not completely developed because the subsystem harness requirements and the impact of the data bus on the harness were not sufficiently well known.

b. Supporting development

- (1) The preliminary selection for both the wires and the connectors has been made. Data on the effects of radiation are not available.
- (2) Specifications and drawings have been prepared for the microcircuit package. The mechanical interfaces for sealing and the package construction are particularly important to reliability. To obtain reliability, test packages for a nonmagnetic, ceramic microcircuit package were procured.

More detailed information is given in Refs. 8 through 11.

REFERENCES

1. E. E. Sabelman, "TOPS Boom Deployment Mechanisms," in Supporting Research and Advanced Development, Space Programs Summary 37-60, Vol. III, pp. 177-180, Jet Propulsion Laboratory, Pasadena, Calif., December 31, 1969.
2. E. E. Sabelman, "TOPS Mechanical Devices," in Supporting Research and Advanced Development, Space Programs Summary 37-66, Vol. III, pp. 148-156, Jet Propulsion Laboratory, Pasadena, Calif., December 31, 1970.
3. E. E. Sabelman, TOPS Magnetometer Booms, JPL Report 701-99, Jet Propulsion Laboratory, Pasadena, Calif., April 1, 1971 (JPL internal document).
4. E. E. Sabelman, "TOPS Thermomechanical Pump," in Supporting Research and Advanced Development, Space Programs Summary 37-64, Vol. III, pp. 37-64, Jet Propulsion Laboratory, Pasadena, Calif., August 31, 1970.
5. J.G. Fisher, "Mesh Materials for Deployable Antennas," in Supporting Research and Advanced Development, Space Programs Summary 37-62, Vol. III, pp. 176-179, Jet Propulsion Laboratory, Pasadena, Calif., April 30, 1970.
6. J.G. Fisher, "Mesh Materials for Deployable Antennas," in Supporting Research and Advanced Development, Space Programs Summary 37-65, Vol. III, pp. 122-125, Jet Propulsion Laboratory, Pasadena, Calif., October 31, 1970.
7. D.J. Starkey, "TOPS High Gain Antenna," in Supporting Research and Advanced Development, Space Programs Summary 37-66, Vol. III, pp. 157-159, Jet Propulsion Laboratory, Pasadena, Calif., December 31, 1970.
8. R.H. Dawe, et al, "Structuring the Outer-Planet Spacecraft," Astronautics and Aeronautics, Vol. 8, No. 9, September 1970, pp. 89-93.
9. R.H. Dawe, "TOPS Electronic Packaging and Cabling," in Supporting Research and Advanced Development, Space Programs Summary 37-63, Vol. III, pp. 143-149, Jet Propulsion Laboratory, Pasadena, Calif., June 30, 1970.
10. J.C. Arnett, "Small Gage Wire for Outer Planet Missions," in Supporting Research and Advanced Development, Space Programs Summary 37-65, Vol. III, pp. 142-147, Jet Propulsion Laboratory, Pasadena, Calif., October 31, 1970.
11. J.C. Arnett, Evaluation of 26-32 AWG Wire for Outer Planet Mission Application, Technical Memorandum 33-463, Jet Propulsion Laboratory, Pasadena, Calif., December 1, 1970.

VI. RELIABILITY

A. System Reliability

1. TOPS Reliability. Because an outer planet mission has a duration on the order of 10^5 h the reliability of parts and functions of the spacecraft is a concern of the greatest importance. The technique for building reliability into a spacecraft follows a known process evolved over the past decade. A list of the major factors required for a reliable design is given below. Since TOPS did not produce flight hardware, the emphasis on each of these factors is adjusted accordingly.

a. Mission requirements. Mission requirements must be translated into the correct functional requirements, including such subjects as data transmission, trajectory correction, and approach guidance.

b. Environment. Adequate margins must be provided in such spacecraft environments as thermal, vibration, arcing, radiation, electromagnetic compatibility, radio frequency interference, voltage, and time in logic (adequate time to consummate a process, and repeat if necessary).

c. Tradeoff studies. Reliability plays a much greater role in determining the best approach to task accomplishment in TOPS than was true with previous spacecraft.

d. Simplex design. The spacecraft is designed in totality, except for redundant systems.

e. Simplification of design and testability. The design is simplified whenever possible; all unnecessary parts are eliminated; and testability is verified.

f. System reliability modeling. Necessary changes in design are determined, based on new developments in the progress of the project.

g. Failure modes, effects, and criticality analysis. Weak points in the design are determined, particularly those with a potential for single-point failure. Such risks are either eliminated or are accepted with justification. A more extensive evaluation would be carried on in a flight project.

h. Redundancy. Redundancy is modeled in the subsystems to bring them to an acceptable degree of reliability.

i. Alternate modes of operation and partial survival capability. An example of this would be the loss, for example, of one or even two RTGs. The onboard computer could be programmed then to sequence between power users — i. e., science instruments, attitude control devices, radio, etc. — again and again so that the spacecraft would continue to function as required and also transmit data back to Earth.

j. Parts. Under the general heading of parts come process control, manufacturing control, understanding of the physics and chemistry of the failure mechanisms, qualification of part types, standardization of parts, screening to determine that parts being purchased are identical to those that qualified earlier, proper derating, and parts application — assuring proper use of parts by circuit designers.

k. Design reviews. The Project designers were able to perform only a cursory system review and a review of only some subsystems. Launch readiness and mission operations reviews were not conducted.

l. Manufacturing of subsystems. Reliability control in this area requires that quality manufacturing must begin with proper parts made of exact materials. An example of the proper choice of materials is that which will withstand radiation; another, that capable of extremely long life.

m. Intensive testing. Functional testing was conducted at the bread-board level to verify that the design performed in practice as well as it did in theory on paper. In an actual flight project, type-approval testing would be required, as would flight approval and system testing. System testing would provide an in-depth understanding of the design and the compatibility of subsystems, design of a proof-test model, and finally a testing of flight units to ensure proper fabrication practices. Throughout design testing an examination of life capability of parts and systems is highly important, with the accent on ferreting out failure areas early enough to effect simple corrections. To accelerate life processes, such measures are undertaken at increased temperatures, or exaggerated vibration.

2. Reliability Analysis. Reliability analyses of spacecraft parts and systems establish criteria for selecting courses of action that effect the ultimate reliability of the spacecraft.

In feasibility studies, reliability analyses first provide inputs to determine whether or not a specific approach should be considered in comparison with alternate approaches, and then provide comparison data for those approaches being considered.

The allocation of reliability requirements to each subsystem in addition to weight, power, volume, and cost assure that reliability is a consideration in subsystem synthesis. As a result of very reliable subsystems, the total system is reliable.

Often reliability analyses are not performed until after the design has reached an advanced state of maturity. When reliability problems are identified late, the impact may be severe. The TOPS reliability analyses identified problem areas early so that the corrective action could be accomplished with minimum perturbation to the program.

In addition to uncovering reliability problems, the performance of reliability analyses often determine that there are deficiencies in existing data on which reliability analyses can be based. Again early identification of data deficiencies allow lead time for the data to be developed in time to be useable on the project.

The results of reliability analyses are considered with such other system parameters as cost and weight during system tradeoffs. As a result the available weight and dollars are applied to additional hardware that provides the largest benefit.

A programmatic use of reliability analyses is to measure progress. It gives management the opportunity to look at the design and decide whether the spending of additional resources is justified.

3. Reliability Block Diagrams. In modeling system reliability, extensive use is made of reliability block diagrams, which are defined by: (1) definition of success, (2) success paths, and (3) hardware involved. As working models in the determination of reliability status, such diagrams describe the result of tradeoff studies and are used as a basis for further studies.

Again block diagrams are used to describe all necessary functions required for system operation. Success paths and alternate paths, including block redundancy and functional redundancy, are illustrated. Single-point

failure situations have been examined at the assembly level and eliminated in most cases, but accepted where the addition of redundancy appeared to reduce reliability. The modeling block diagrams also illustrate reliability relationships between components, assemblies, and subassemblies. Finally, the diagrams provide an understanding of basic reliability problems, design status, and tradeoff changes.

A block diagram illustrating the complete engineering spacecraft is shown in Fig. 66. The basic spacecraft is composed of subsystems (shown in series) required to transmit RF signals from the spacecraft to Earth. To the basic spacecraft are added the remaining subsystems to complete the engineering spacecraft: measurement processor, propulsion, data storage.

In the area of desired reliability allocation, the electrical subsystems were given an allocation of 0.95 for 10^5 h, while mechanical subsystems were given an allocation of 0.99.

B. Reliability Methodology and Failure Rates

1. Reliability Analysis Methodology. The most common use of reliability analysis was in tradeoff studies between alternate designs. A second use was the determination of the required type and amount of redundancy. A third, though infrequent, use of reliability analysis was to generate rough estimates of system reliability.

Most useful of the types of reliability analysis was the reliability prediction, employed in correlation with reliability block diagrams. A second type of analysis dealt with failure mode effect and criticality, while a third type related to single-point failure.

a. Reliability prediction. Predicting reliability by means of block diagrams proves difficult because of the complex redundancy necessitated by long-life requirements. The redundancy necessarily incorporates complex sensing and switching processes, which are additional sources of problems. To overcome these negative aspects, a computer program was developed to generate reliability predictions from reliability block diagrams, particularly in instances of very complex redundancy (Fig. 67). The program employs an analytical derivation of the system reliability equation; it is not a Monte Carlo simulation. Consequently, exact results are obtained and not statistical

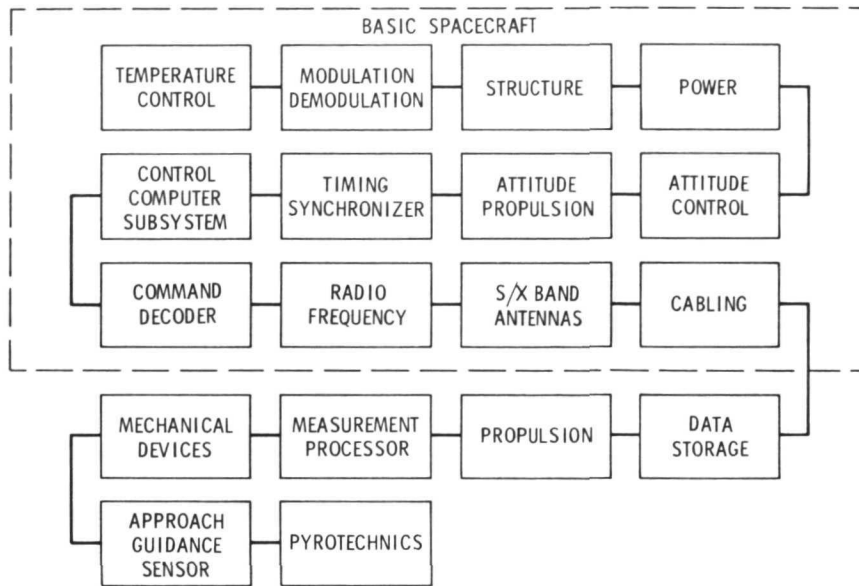


Fig. 66. Engineering spacecraft reliability block diagram

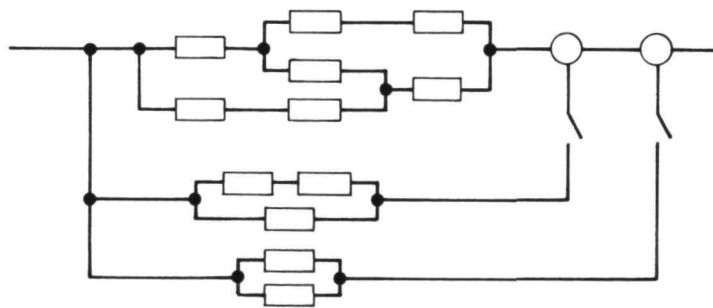


Fig. 67. Computer program example problem

estimates of the results. The method used to generate equations is documented fully in Ref. 1. Main advantages of the computer program are that it permits the use of very complex reliability block diagrams, but still functions with simple computer input/output.

2. Failure Rate Usage. Valid failure rates are required to be established as a major element in determining the necessary hardware redundancy levels to achieve the specified spacecraft performance for the entire mission. In the subsystem design, the use of a failure rate that is too low results in insufficient redundancy with a consequence of a high risk of subsystem failure. Yet, the use of a failure rate that is too high results in unnecessary redundancy with consequences of greater design complexity, greater subsystem weight, and a more complex design verification test program. Variations in the failure rates selected also have a great effect on the effectiveness of predicting the overall spacecraft mission reliability. An error on the low side can result in flying an unreliable spacecraft, and an error on the high side can result in a too costly spacecraft.

The constant failure rate assumption is only a convenient simplifying assumption, and is not applicable to mechanical or electromechanical components because of the influence of wearout failure modes. It is applicable to the majority of conservatively rated and applied electronic parts. An infant mortality problem exists which is corrected through a comprehensive screening program.

3. Relative-Failure-Rate Factor Method for Deriving Failure Rates. To generate failure rates for specific parts where insufficient test and flight experience exists, a technique has been developed that uses a relative-failure-rate factor. The relative-failure-rate is a number that assesses the failure rate of a definitive, optimum part relative to other part types, based on considerations of design, materials, and manufacturing processes. The relative-failure-rate concept can be applied to any part that fits the constant-failure-rate assumption. The relative-failure-rate factor can be used to assign failure rates to definitive part family members when reliability data are available for only the total family population. The method used to develop and verify relative-failure-rate factors for part types on which sufficient data were available to generate failure rates by the classical method is explained in Ref. 2. Table 28 shows the results of this

Table 28. Electronic part failure rates (failures/10⁶ h)

Part type	Study results
Resistors	—
Carbon composition	0.0003
Film	—
Metal	0.002
Carbon	0.003
Wirewound	—
Precision	0.02
Power	0.03
Capacitors	—
Glass	0.0006
Mica	0.002
Ceramic	0.08
Metalized foil	0.006
Interwound foil	0.003
Solid tantalum	0.003
Foil tantalum	0.006
Wet tantalum	0.08
Diodes	—
Lower-power-density	0.002
Zener	—
Low-power-density	0.003
Compensated, low-power-density	0.005
High-power-density	0.008
Transistors	—
Low-power bipolar	0.003
Junction field-effect	0.003
Isolated gate field-effect	0.01
Power bipolar	0.01
Silicon-controlled-rectifier/silicon-controlled switch	0.01
Integrated circuits ^a	—
Bipolar logic	0.03
Bipolar linear	0.05
Metal-oxide semiconductor logic	0.06
^a Does not include medium-scale-integration/large-scale-integration devices.	

failure rate study. The results show good correlation with established failure rate data for part types for which data are available. The study was based on composite parts for convenience in obtaining the required detailed data. This technique can be applied to new or modified parts for which the constant-failure-rate assumption is appropriate. Manufacturers will not have to reveal proprietary parts information, since the required reliability characteristics can be obtained by current analysis techniques.

It must be stressed that due to the long mission time compared to available test time, long-life parts reliability cannot be demonstrated; it can only be accomplished through spacecraft design choices and a comprehensive understanding of the chosen designs and the selected parts.

4. Fault-Tree Analysis for Aiding in FMECAs. A computer program (Ref. 3) was developed for performing reliability computations based on fault trees. This program is not a simulation program, but instead derives the system reliability equation based on the logic inherent in the fault-tree diagram.

C. Reliability Status

1. Introduction. To arrive at the status of subsystem reliability as it existed at the close of the TOPS Project, design engineers had progressed from a beginning of allocated numbers (reliability goals), through tradeoff studies, to a set of designs of various subsystems that bore promise from a predicted reliability standpoint. The important knowledge gained from this activity was not so much numbers as an understanding of alternatives, tradeoffs, weights, costs, etc.

2. Subsystem Reliability

a. Power subsystem. Reliability of the power subsystem, as with other critical subsystems, is created, when possible, through standby redundancy (Fig. 68). The reliability factor, of course, is weighed against such considerations as weight, space, and cost. Power for the spacecraft is supplied by four radioisotope thermoelectric generators (RTGs). The loss of one or even two generators does not necessarily abort the mission, though capability is reduced. Redundancy is evidenced in other components of the subsystem, including quad shunt regulators (internal active parallel redundancy).

Failure mode analysis internal to the RTGs is described in Fig. 69. The study was made using a series parallel array of 500 thermocouples per RTG—some 40% greater than the number actually used in the most recent version of the generator. The series parallel arrangement protects against both an open and a short failure mode. The stair profile configuration to the curves reflects a loss of power from the adjoining couple when one thermocouple is subject to failure. This is a design consideration and can be corrected so that failure in one couple would not affect that adjoining it.

b. Attitude-control subsystem. Considerable standby redundancy was incorporated in this area to enhance long-life reliability. In the cruise mode, the subsystem utilizes three attitude-control electronic units; two power supplies; two reaction wheels each for pitch, yaw, and roll; two pitch and two yaw Sun sensors; two each of pitch, yaw, and roll gyros to provide functional backups to the Sun sensors and Canopus trackers; two Canopus trackers, and two sets of acquisition Sun sensors. The acquisition Sun sensors are parallel redundant--not standby redundant--because long life is not a problem and power requirements are minimal, thus eliminating unnecessary switching. Preliminary data relative to reaction wheel life, accumulated in a TRW study, indicates a possibility that these units have longer life capability than first supposed. Two wheels tested had functioned continuously for more than 75,000 h, although their original duty cycles were 13,079 and 33,436 h, respectively.

c. Attitude propulsion subsystem. Potential valve leakage caused by chemical action of fluid on valve seat materials is the long-term potential problem of this subsystem. In the cruise mode, the leakage factor is countered by dual valves, solenoid and latching, each backing up the other in the system. In the operational phase of the attitude propulsion subsystem, both the solenoid and latching valves must open if the propellant is to discharge properly. However, a backup set of valves can be employed if their operation fails.

d. Propulsion subsystem. The propulsion subsystem of the spacecraft is also subject to valve failure, leakage being the predominant failure mode. Squib valves used only to open and close the line before and after planetary encounters, are backed up by two sets of dual solenoid valves with dual paths leading to the single thruster. The solenoids are also used for

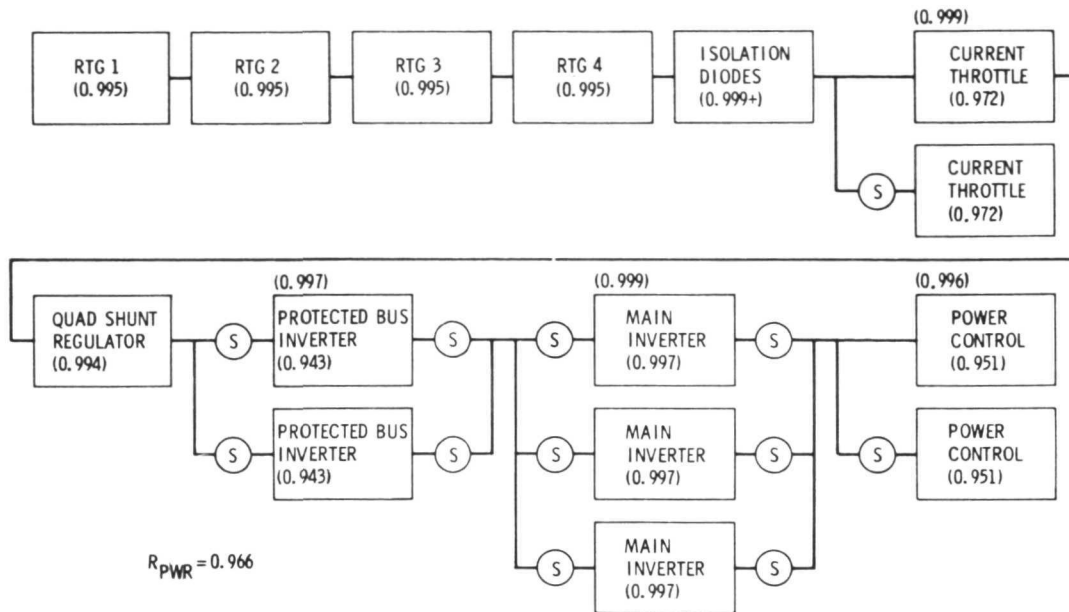


Fig. 68. Power subsystem reliability block diagram

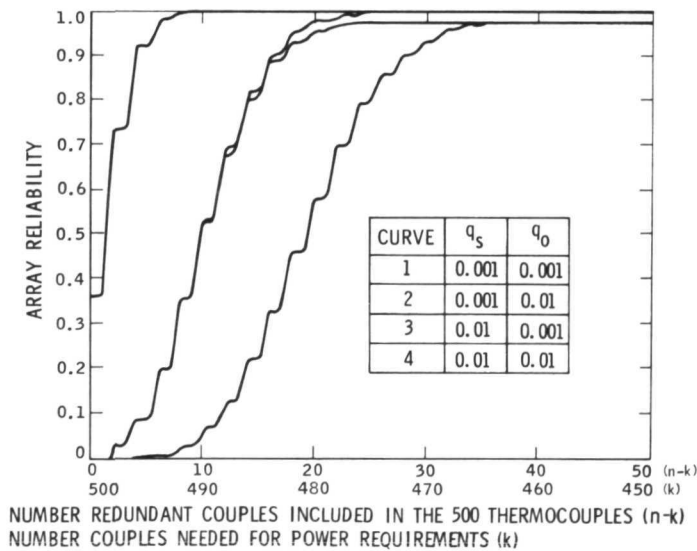


Fig. 69. Reliability for series-parallel array of 500 thermocouples per RTG

trimming during encounter operations. In the start mode (valves open), one of the solenoid sets is functional and is backed up by the other solenoid set on a standby path. The squib valves are in series with either path.

e. Timing synchronizer subsystem. Because this subsystem, the central clock of the spacecraft, is always on and is time-critical, the system is highly redundant in an active parallel configuration, with five oscillators, only one of which is actually needed for successful operation. There is no standby system. While failure is extremely unlikely (0.999+), it can occur. The divider circuitry is triply redundant, and plans were in process to add still greater reliability through additional spare units.

f. Control computer subsystem (CCS). The CCS has the capability of failure detection and repair in all spacecraft subsystems. The hub of the subsystem is the test and repair processor (TARP). To increase reliability, TARP units are broken into two subunits, with interswitching between the halves of the processor. The combining of the halves to singular units may be possible as the design is optimized; this is desirable to eliminate switching. Each TARP subunit is triply active redundant, with two spares. Majority voting their outputs provides internal error checking.

The read-only memory of the CCS has three units (one powered on, the others in standby), as do the interrupt, input/output, logic, and control processors. The read-write memory has three processors and an additional four spares, any one of which may be switched into any of the three locations. The computer also has a standby power supply. The main reliability trade-off with the CCS centered around parts count per processor, reflected in weight and occupation of space.

Reliability studies give the CCS with the self-test and repair (STAR) concept a 96% survival probability at 10 yr, as compared to 40% for a simplex CCS (no redundancy, no STAR), and 8% for an extrapolated Mariner Mars 1969 CC&S.

g. Modular/demodulator subsystem. Employing standby redundancy along with the reduction of on-time to 15,000 h for the command detector unit and accompanying power supply effected a 0.989 and 0.999+ reliability factor, respectively. With the necessary 100,000-h on-time for the block coder, subcarrier generator, and power supply, the reliability factors were 0.999, 0.997, and 0.999, with the addition of a standby unit.

h. Radio-frequency subsystem. Reliability in the low-gain and high-gain receivers was low (0.516, 0.436) because of large parts population, a condition being improved at the close of the TOPS Project by elimination of certain parts types which are major contributors to high failure rates.

In the S-band transmitter power supply, a low reading of 0.607 per unit was offset by adoption of three standby transmitters. Standby redundancy is used extensively in both receiver and transmitter groups. Because of a known high wear-out factor in traveling wave tubes (TWTs) (45,000-h mean life), redundancy was heavily relied upon, including the use of solid-state amplifiers. The failure rate of the TWTA was assumed to be equivalent to 10×10^{-6} failures/h. Reliability varied from 0.03 using two TWTA units, to 0.96 using five.

i. Measurement processor subsystem. Redundancy is heavily used in the subsystem. The various digital units and the A/D converters are in standby redundancy.

In order to obtain a better than 0.98 reliability for the MPS, a tree switch and driver configuration was employed, with field effects transistors in series parallel redundancy. The tree switch commutator controls the various telemetry sensors throughout the spacecraft, utilizing 512 telemetry channels, or six or seven times those used in Mariner-type vehicles. The tree switch concept allowed minimum parts and high reliability; for example, the maximum number of sensors lost through one particular part failure would be four. The reliability factor for the principal functioning areas within the subsystem (programmer, data processor, data conditioner and multiplexer, etc.) is 0.999+.

j. Data storage subsystem. In this critical subsystem the greatest threat to reliability is found in the tape recorders. To meet long life requirements; in particular, to eliminate the many wear-out failure mechanisms that exist in tape recorders, engineers resorted to fluid-filled instruments. There are two such recorders, under constant hydrostatic pressure, either of which is operable on demand. The fluid environment minimizes tape wear and contamination at the record heads. Other failure elimination design features in the data storage subsystem include single-speed, brushless motors; hydrostatic bearings; low-operating tape tension; and absence of drive belts and spring tension devices.

A buffer memory, consisting of 35 modules, offers parallel redundancy. Sixteen modules are required at all times for recording or playback of data, with 32 used during encounter for TV. With 19 modules on standby during cruise, reliability in the buffer area is quite high. The remainder of the units in the subsystem (decoders, controllers, power supply) are in standby redundancy.

3. Subsystem Reliability Summary

a. Numerical summary. A summary of subsystem reliability, with present predictions for 6.6 and 11.4 yr, is given in Table 29. The 6.6 yr flight period corresponds to a Uranus mission, while the longer flight would theoretically carry a spacecraft to the planet Neptune.

Table 29. Summary of TOPS subsystem reliability

Subsystems	Reliability	
	6.6 yr	11.4 yr
Temperature Control (TCS)	0.9993	0.998
Power (PWR)	0.991	0.966
Attitude Control (A/C)	0.958	0.876
Attitude Propulsion (APS)	0.995	0.992
Propulsion (PROP)	0.992	0.990
Timing Synchronizer (TSS)	0.9999	0.9996
Control Computer (CCS)	0.988	0.957
Modulation/Demodulation (MDS)	0.993	0.984
Command Decoder (CDS)	0.9999	0.9995
Radio Frequency (RFS)	0.992	0.960
Measurement Processor (MPS)	0.994	0.982
Data Storage (DSS)	0.961	0.906

b. Mission success probability. The probability of spacecraft success for a 1979 JUPITER-URANUS-NEPTUNE mission (2 launches, 30-day launch period) is shown in Fig. 70. The baseline spacecraft excludes science instruments. The science instruments, assumed in this study to be 11 in number, have an allocated probability of success of 95% in 100,000 h.

c. Reliability summary. To summarize reliability of TOPS, it can be said that the reliability analyses conducted during the TOPS project offered insight into design of long-life systems. TOPS established a confidence in the systems, showing them to be not only feasible but also possible with planned technology. TOPS took steps to eliminate moving surface contact. Based on the failure rates determined and the assumption of random failures, redundancy was shown to be necessary in all critical subsystems. Finally, such analyses demonstrated the usefulness of the computer to enhance overall reliability of the spacecraft.

D. Custom-Metallized Multigate-Array

1. Introduction. The CMMA is a monolithic bipolar integrated circuit that was developed to be the main logic building block for a self-test-and-repair spacecraft computer. The CMMA contains 140 low-power logic gates and gate extenders, which are interconnected—with a custom metal pattern—to provide desired logic functions. The primary objective of the development was the achievement of the required functional and electrical characteristics of the gates consistent with a very high level of device reliability.

The implementation of the CMMA centers around a 12×12 array of gate and gate-extender cells fabricated on a 153×171 mil die. The wafer processing consists of three diffusions, one epitaxial growth, and two levels of metallization, with the second level customized for specific logic functions.

2. Development Contract Description

a. General. Harris Semiconductor, Melbourne, Fla., was contracted to develop the CMMA. The contract provided for the design, fabrication, and test of 300 CMMA devices. The contract also called for the development of a special Product Assurance Plan for the CMMA based on a 10-yr space-probe application. The contract was divided into three phases.

b. Phase I. Phase I was basically a two-part study effort. The first part of the study involved developing the design concepts for the CMMA. In the course of the study, tradeoffs were made in functional flexibility, array size, die layout, gate power, gate speed, wafer-processing methods, and number of leads.

The second part of the study was a parallel effort on developing the reliability concepts necessary to assure the long lifetime. The semiconductor

industry was surveyed for the latest reliability assurance, test, and screening methods for large-scale integrated circuits, and a preliminary reliability assurance plan was prepared.

Phase I resulted in the establishment of a specific approach to the CMMA design and the reliability plan that was documented in an Interim Technical Report.

c. Phase II. In Phase II, the design and reliability approaches were refined, and engineering model CMMAs were fabricated to verify the electrical and process designs. Included in this phase was the generation of the final Product Assurance Plan (PAP), and all documentation necessary to control the fabrication, inspection, and testing of the CMMA.

d. Phase III. Phase III is a prototype production phase, utilizing the PAP, to demonstrate the results of the development.

3. CMMA Design

a. Design objectives. From a functional standpoint, the objective was to design a large-scale integrated circuit that would be a universal building block for a spacecraft computer, and possibly other spacecraft subsystems. The circuit or logic array was to have moderate speed (gate propagation delay of 50 ns), and a power dissipation less than 1 mW per gate. The logic array had to have great flexibility in its internal connections to be useful for any logic configuration that might be required.

The reliability goal of the CMMA development was to meet or exceed the screening requirements of MIL-STD-883, Method T5004, Class A, and the environmental requirements of an outer-planets mission; and to achieve a 10-yr lifetime component.

b. Gate selection. System-application considerations pertaining to logic interfaces, speed/power efficiency, noise immunity, etc., led to the selection of TTL-type logic for the CMMA. Logic flexibility and logic function per chip were examined to determine whether the CMMA should contain flip-flops and gates, or only gates. It was decided that a majority of the required complex logic functions would be more efficiently implemented if the CMMA consisted entirely of NAND gates and gate-input extenders. Most

types of flip-flops can be implemented with 6 NAND gates. Further refinement of the logic requirements lead to the specifications for the circuit design given as follows:

Gate type	No./ CMMA	Fan-in	Fan-Out (Standard Gate loads)
Standard	92	3	10
Driver	24	3	50
Extender	24	3	--

c. Die organization. The organization of the CMMA die affords maximum logic flexibility and packing density. The principal features of the die organization are:

- (1) Gate cells of uniform size.
- (2) A power bussing system which partially frees the interconnect levels for intragate and intergate wiring.
- (3) A two-level interconnect system which provides an X-Y cross-point matrix with greater than 6000 potential low-capacitance crossovers or interlevel connections available.
- (4) A single custom interconnect level to selectively energize and configure the die into any complex logic pattern.

The die is organized in a 12×12 unit cell array as shown in Fig. 71. The standard gate, driver gate, and gate extender occupy one unit cell each. There are 8 columns of standard gate cells, and two columns each of driver gates and gate extenders. Four cells are utilized for test devices. The left side of the die is a mirror image of the right side.

Power-supply voltage and ground are fed to the gate cells through second-level interconnect main busses and a system of diffused distribution busses, as depicted in Fig. 72. The diffused busses are formed using all three diffusions in the fabrication process. These busses have less than 20Ω impedance from the metal main bus to the edge of the die. The use of this

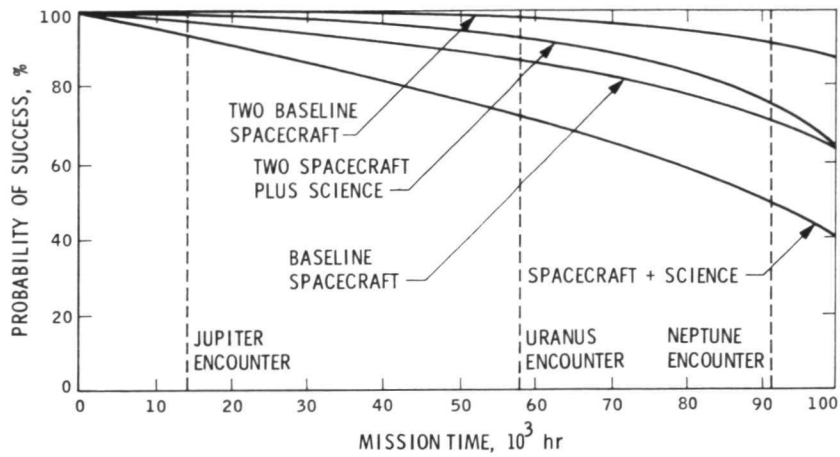


Fig. 70. Spacecraft probability of success for 1979 JUN mission (2 launches, 30-day launch period)

ASTRONICS DIVISION	S	S	E	T	S	D		D	S	T	E	S	S
S = STANDARD GATE CELL (92)	S	S	E	S	S	D		D	S	S	E	S	S
	S	S	E	S	S	D		D	S	S	E	S	S
E = EXPANDER GATE CELL (24)	S	S	E	S	S	D		D	S	S	E	S	S
	S	S	E	S	S	D		D	S	S	E	S	S
	S	S	E	S	S	D		D	S	S	E	S	S
D = DRIVER GATE CELL (24)	S	S	E	S	S	D		D	S	S	E	S	S
	S	S	E	S	S	D		D	S	S	E	S	S
	S	S	E	S	S	D		D	S	S	E	S	S
T = TEST CELL (4)	S	S	E	S	S	D		D	S	S	E	S	S
	S	S	E	T	S	D		D	S	T	E	S	S

Fig. 71. CMMA die organization

diffused distribution system leaves the interconnect layers free for intragate and intergate connections. The metal main busses are located in the center of the die with the supply voltage line split so that dual logic functions may be separately energized. The final connection of the ground line to a gate is made at the second level so that only the gates that are used draw power.

d. Fabrication-process design. The epitaxial base/collector diffusion-isolation processing method was chosen during Phase I as the best approach for the CMMA because it is simpler than the conventional epitaxial collector method and allows greater component density. The number of diffusion steps is reduced from five to three by elimination of the base and gold diffusions. The base diffusion is unnecessary since the base epitaxial layer replaces the conventional collector epitaxial layer. Gold doping is normally employed to minimize the storage time produced by hole injection into the collector region which occurs when the transistor saturates. In the epitaxial base structure, hole injection into the collector region is essentially eliminated as a result of the heavily doped collector. As a result, gold doping is not required. Moreover, the N-type emitter diffusion is the only critical diffusion step since it is this diffusion which defines the transistor current gain and resistor sheet resistance.

The epitaxial layer is thin, approximately 4 μm , compared to conventional epitaxial thickness of 6 to 10 μm . Component packing densities achievable are thus higher as a consequence of the reduced lateral diffusion effect and narrow diffusion apertures which result from the shallow diffusions required. Furthermore, junction capacitances are also made small, a significant point in low-power logic, as a result of the small geometries and shallow diffusions which minimize junction sidewall effect.

The basic structures of the CMMA transistor and resistor elements are shown in Fig. 73. The significant aspect of the epitaxial base structure is the absence of the normal epitaxial collector layer. The buried layer diffusion is employed directly as the collector. An epitaxially grown P-type layer forms the transistor base. An N-type diffusion into the buried layer serves the dual function of forming a surface collector contact and completing the transistor isolation. The transistor is completed by a second N-type emitter diffusion. Resistors are formed by the same processing. The large resistor values required in the CMMA are obtained by using the thin P-type epitaxial region

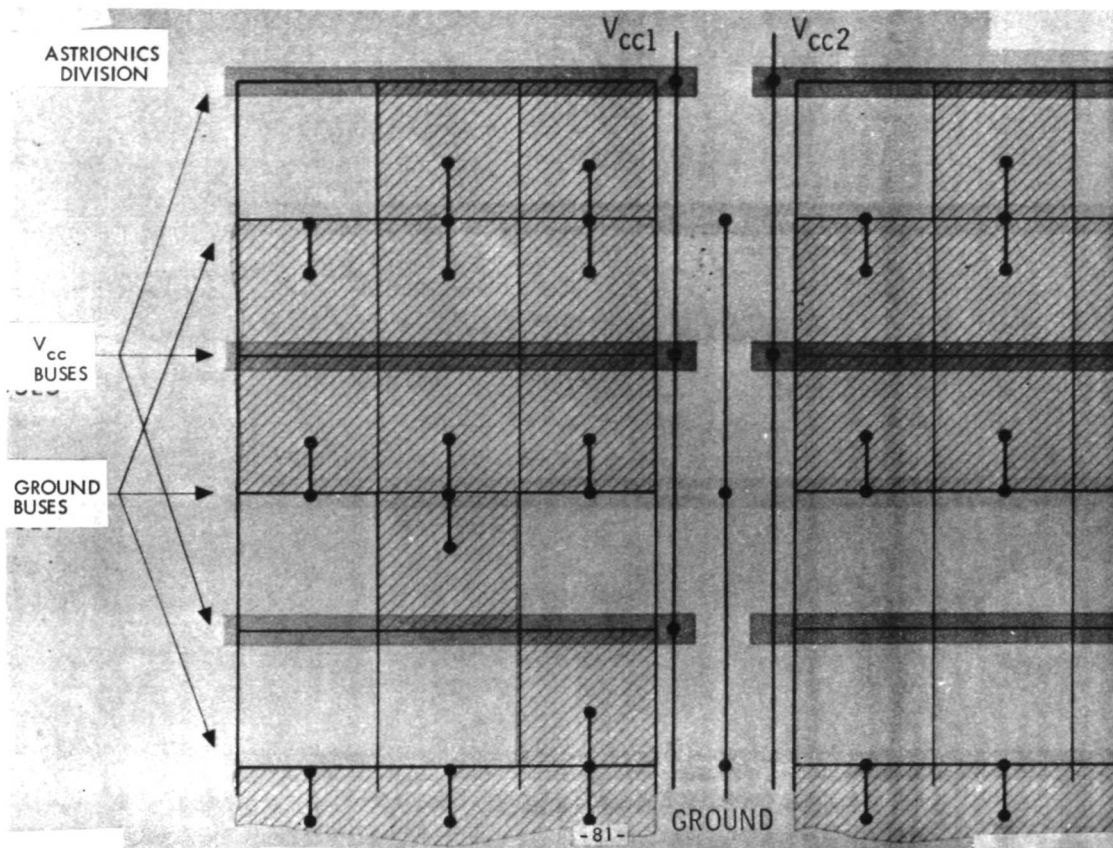
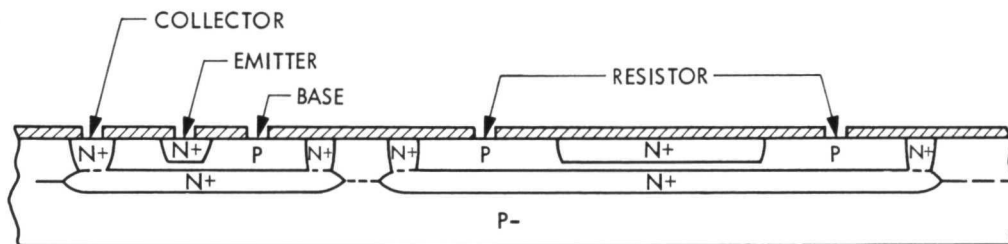


Fig. 72. CMMA power distribution system



TRANSISTOR

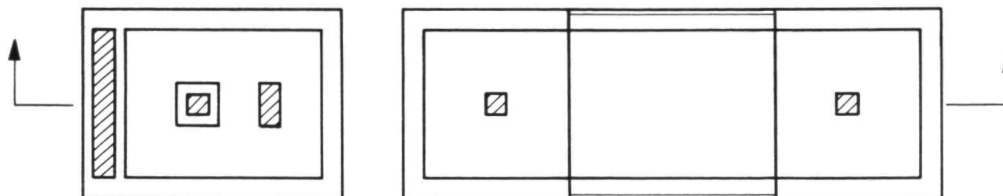


Fig. 73. Epitaxial base structure

formed between the buried layer and the emitter diffusion. The N-type isolation diffusion also isolates resistor elements.

e. Multilevel interconnection. Two alternates to the required two-level interconnection were considered for the CMMA application. The first was an aluminum oxide-aluminum system, and the second an N+ doped polycrystalline silicon oxide-aluminum system.

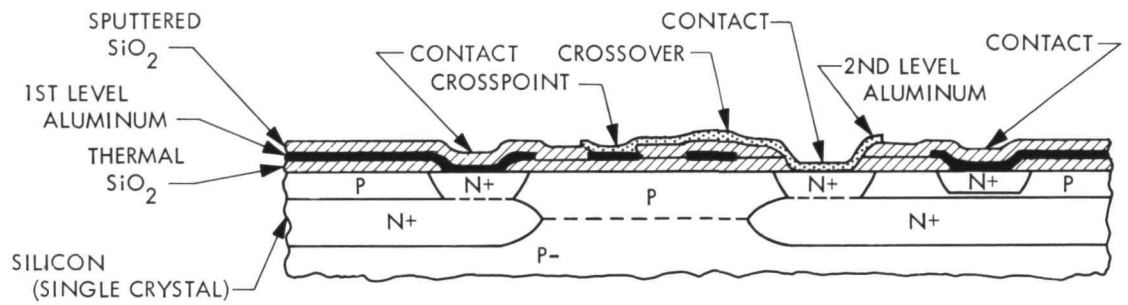
Figure 74 depicts the aluminum oxide-aluminum interconnect system. The two interconnect levels are formed by aluminum evaporations over silicon dioxide. The edges of the first aluminum are beveled to enhance step coverage. The two oxide layers serve as dielectric isolation between the circuit components in the epitaxial layer, first-level aluminum and second-level aluminum.

The oxide layer has a thickness on the order of 1.2 microns. The aluminum evaporations are 1.0 and 1.5 μm .

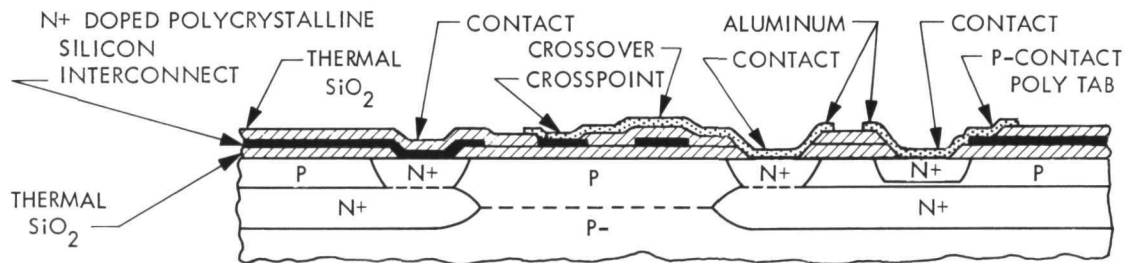
Figure 74 depicts the interconnect structure of the doped polycrystalline silicon oxide-aluminum system. The first-level interconnect is formed by a highly doped N-type polycrystalline silicon layer. This polysilicon layer is formed by deposition of doped silicon onto the oxide layer on the processed silicon wafer. The layer is polycrystalline rather than single crystal since the deposition is on oxide rather than the usual single-crystal substrate. The deposition is accomplished in the usual manner in a reactor system, with the sheet resistance obtained less than 10 Ω /square unit of area. The first-level interconnect pattern is then formed by etching the polysilicon layer. A thermal oxide is then grown over the entire wafer followed by aluminum evaporation and etch to form the second interconnect layer.

The oxide layers employed have thicknesses on the order of 0.6 μm . The poly-silicon layer is approximately 1.5 μm and the aluminum layer approximately 1.0 μm .

Basically, both approaches result in a similar two-level interconnect system. The principal advantage of the polysilicon system is that it eliminates the silane SiO_2 deposition which presents a potential yield and reliability problem. The consideration in this regard is the integrity of the oxide layer. A low pin-hole density in the insulating layer must be obtained to avoid shorting of first- and second-level aluminum. Thermally grown oxide results in lower pin-hole density than deposited or other oxide techniques.



A. THERMAL OXIDE - ALUMINUM - SPUTTERED OXIDE - ALUMINUM SYSTEM



B. THERMAL OXIDE - N+ POLYCRYSTALLINE SILICON - THERMAL OXIDE - ALUMINUM SYSTEM

Fig. 74. Aluminum oxide-aluminum interconnect system

The advantage of the aluminum-aluminum system is a lower interconnect resistance and a simpler first-level to P-type silicon contact. That is, since the poly-silicon is N-type, a second-level aluminum tab must be employed to accomplish an ohmic poly-silicon to P-type silicon contact as shown in Fig. 74.

The polycrystalline-silicon aluminum-interconnect system was abandoned due to contact resistance problems. The all-aluminum system was selected after it was shown that low pin-hole densities could be achieved with the silane oxide.

f. Gate design and layout. Schematics of the standard gate and driver gate cells are shown in Figs. 75, 76, respectively. The circuits are standard TTL configuration with three exceptions. First, a collector-base resistor was added to the input transistor. The epitaxial base transistors have a relatively large inverse current gain as a result of the non-gold-doped and high-concentration collector structures resultant from the selected fabrication process. The shunting resistor serves to hold the input transistor in very light saturation and still maintain noise margin.

A second circuit variation from the conventional TTL structure is the output of the standard gate. The pull-up transistor has been omitted to allow output AND-ing.

The third circuit variation is Q3 of the driver gate. It has an additional emitter diffusion which is tied directly back to its base. The purpose of this diffusion is to control the inverse gain to optimize the saturation characteristics.

The schematic of the gate extend/pull-up cell is shown in Fig. 77. Each cell contains a three-input extender, a standard load pull-up, a five-standard load pull-up, and a string of diodes to clamp the standard gate output. The pull-up resistors and diode clamps are used to speed up the output of the standard gate.

The design of the standard and driver gates was fairly straightforward. The power-consumption requirement of the standard gate essentially determines the values of R1 and R2 and the forward diode characteristics of Q1, Q2, and Q3. Power consumption for the driver gate is somewhat more complicated since some trade-offs are available in the choice of R1 and R4 which,

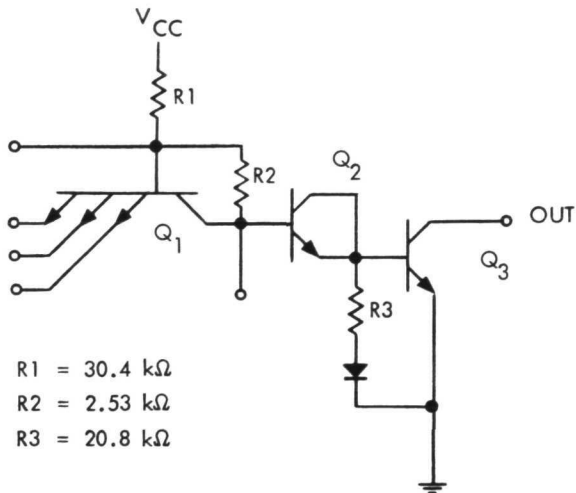


Fig. 75. Schematic of standard gate cell

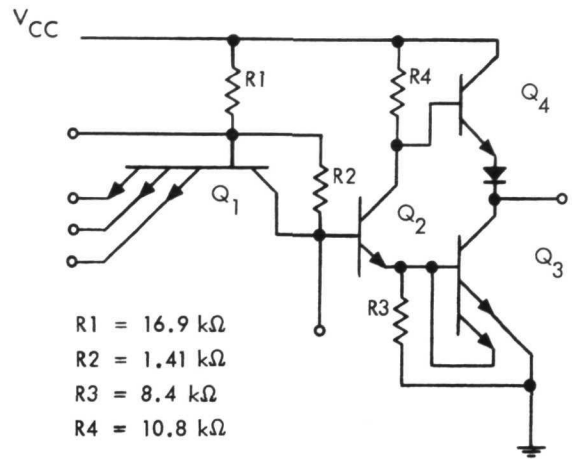


Fig. 76. Schematic of driver gate cell

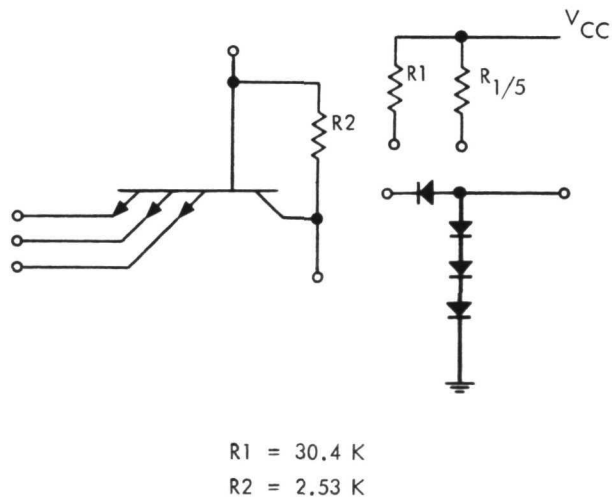


Fig. 77. Schematic of extender gate cell

along with the diode characteristics of Q1 and Q3 and the saturation characteristics of Q2, define the power consumption of the driver gate. From a propagation-delay standpoint the worst-case situation is associated with T_{pd1} because of the total capacitance at the base of Q4. This consideration indicated a minimum value for R4 consistent with power objectives.

The component layout for the standard gate, driver gate, and gate-extender cells are shown in Figs. 78, 79, and 80, respectively. These figures are microphotographs of the cell areas that were taken after the diffusions were completed, but before silicon-contact etch. The light areas at the top and bottom of the photographs are portions of the ground and V_{CC} busses, respectively. Resistors that are connected to V_{CC} are built on the V_{CC} bus. In the driver-gate cell (Fig. 79) transistor Q4 is also on the V_{CC} bus. Resistor R2 in each of the cells is a part of the three-emitter transistor whose base-collector junction it bridges, and can be identified by the pinch diffusion to the right of the three-emitter diffusions. Other resistors can be identified by their pinch diffusions also. The transistors are identified by emitter diffusions within the collector isolation moats.

Figure 81 is the standard first-level-metal pattern for the CMMA die. All intragate connections are made on the first level. Left to right side, and Y-axis crossunders are also on the first level.

The CMMA function is established by the intergate connections on the second level of metal. Input and output connections are made to bonding pads. The second level also has the gate-grounding tabs (to energize each gate), and the main power busses. Figure 82 is the second-level metal-pattern for a 4-bit adder/subtractor. This CMMA uses 66 standard and 23 driver gates. Prominent features of Fig. 82 are the bonding pads around the edges and the thick ground bus in the center.

Other functions that were implemented in Phase II were: a dual, 8-stage shift register, a 10-stage counter register, and a general-purpose logic element. These functions are representative of logic functions that would be used to implement the spacecraft computer subsystem.

g. Design and fabrication problems. As might be expected, a variety of design and fabrication problems were encountered during Phases I and II. Some of the problems were anticipated and some were not. This section will highlight some of the more important problems that were encountered.

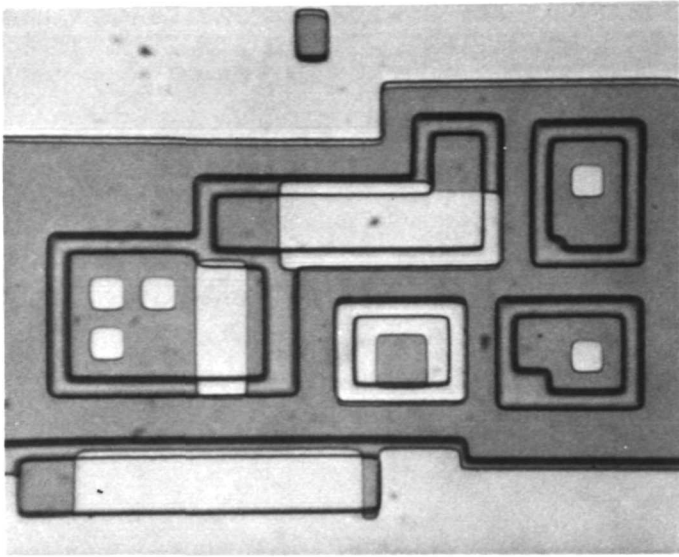


Fig. 78. Microphotograph of standard gate cell

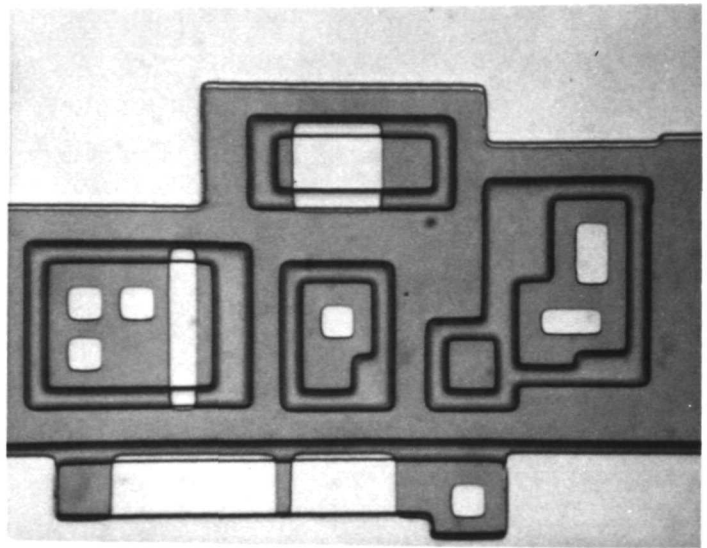


Fig. 79. Microphotograph of driver gate cell

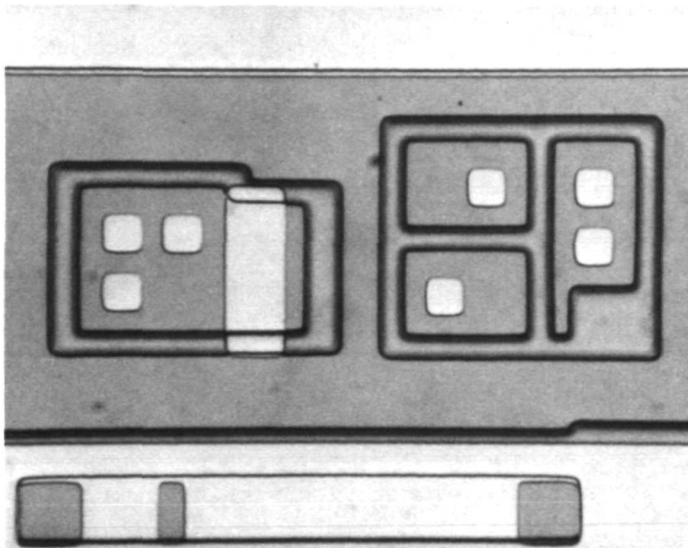


Fig. 80. Microphotograph of extender gate cell

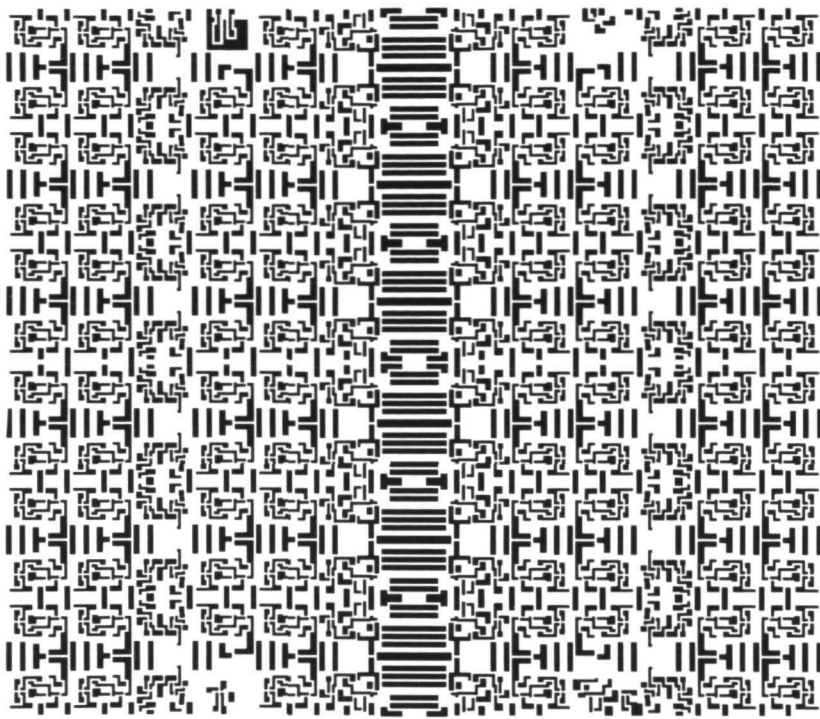


Fig. 81. First-level interconnect pattern for CMMA

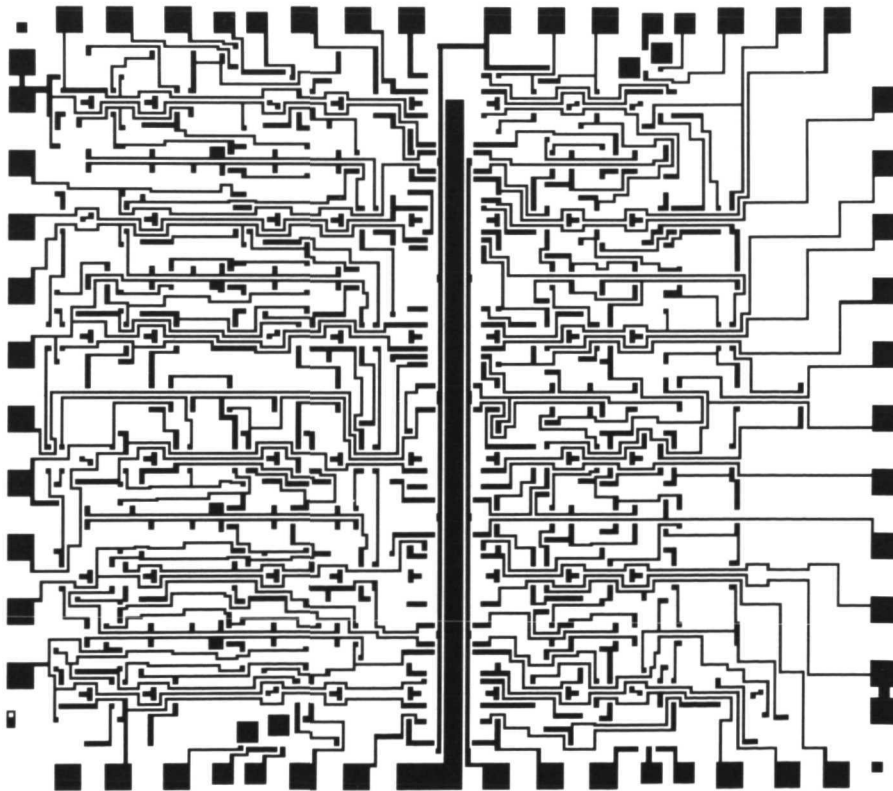


Fig. 82. Second-level interconnect pattern for four-bit adder/subtractor CMMA

During Phase I, it was recognized that the epitaxial base process chosen for the CMMA had a basic problem. Since the base layer is epitaxial, it is uniformly doped, resulting in a low surface concentration. This makes the surface prone to inversion. A boron deposition over the entire surface of the wafer was added to the process to eliminate surface inversion. Although the boron is subsequently diffused in slightly, it remains primarily at the surface and does not reduce the lifetime of the minority carriers in the active base region or the injection efficiency of the active emitter area. An added feature of the boron deposition is that the lateral injection of the emitter is reduced. This reduces lateral current gain between adjacent emitters in the three-emitter transistor. Increasing the base-surface concentration reduces the reverse breakdown voltage between collector and base which, in turn, brings the collector-emitter breakdown down to 7-8 V. Although lower than conventional logic circuits, the 7-8 V BV_{CEO} is acceptable for the CMMA.

The multilevel interconnection part of the process caused several problems. The continuity of the second-level-metal paths where they crossed stops at the edges of the first-level metal was identified as a problem early in the development. The second metal was made thicker than the first metal, but that alone did not assure continuity; so the contractor applied a proprietary process of theirs to "bevel" the edges of the first metal to slope the step. The "beveling" results in a slope of about 45 deg at all edges of the first metal, which solved the continuity problem.

The insulation oxide between the metal layers must have a very low density of pinholes. The contractor demonstrated that silane oxide could be deposited with a low density of pinholes; however, when the time came to fabricate the engineering model CMMAs, shorts through the insulation oxide were a major yield factor. Getting repeatable good results in the silane deposition was a major problem until the cleanliness of the deposition chamber was improved and other quality-control measures were applied. These measures have been incorporated into the PAP, and it is now believed that the oxide pinhole problem is under control. It is recognized, however, that the silane oxide probably still has a low density of pinholes which will continue to be a minor yield factor.

Near the end of Phase II it was discovered that excessive "micro-alloying" at the aluminum-silicon contact areas was causing emitter-base

anomalies in the CMMA transistors. This problem, which had apparently been masked by more serious yield problems in the previous engineering model process runs, was most pronounced in the three-emitter transistors. Some of the E-B junctions exhibited "soft" forward characteristics similar to a Schottky diode, and others were completely shorted.

Micro-alloying or sintering of aluminum-silicon contacts is a universal practice in the industry to insure good ohmic contact. Typically, the wafers are baked at about 500°C for 20 min to 1 h. This causes silicon at the contact area to diffuse into the aluminum leaving voids in the silicon which are filled with aluminum. The diffusion is time and temperature dependent, and usually localized at defects in the silicon surface, where the atomic binding energy is lower, or at grain boundaries in the aluminum, rather than being uniform over the area of the contact. The resultant effect is that of tiny aluminum spikes penetrating what was the surface of the silicon. The spikes vary in size and number due to the irregularities mentioned above, and can approach 1 μm in depth. The E-B junctions were nominally 1.2 μm deep on the CMMA, but in some cases the junctions were as shallow as 0.9 μm . The shallowness of the emitter diffusion combined with a normal amount of spike "growth" was the cause of the problem.

The first steps taken to cure the problem were the elimination of the 450°C 20-min contact bake, and the reduction of the silane oxide deposition temperature from 450 to 420°C. The 420°C is considered to be the lower limit for a quality silane oxide deposition. The other post-metal processing temperatures are low enough to have very little effect. It was believed the two 20-min silane depositions would be sufficient to form small spikes, for good ohmic contact, but not cause spikes large enough to affect the E-B junctions. The next process run, with these changes, had much better yield (of good junctions), but the spike depth was not reduced enough to have confidence in the CMMA for the intended application. The lack of confidence was borne out by high-temperature stress tests which brought on the poor junction condition within 48 h (at 350°C). Other solutions were then sought for the problem.

Two approaches that were considered at some length were doping the aluminum with enough silicon (2 to 5%) to satisfy the solid-state solubility requirements at 420°C, or placing a barrier metal, such as molybdenum,

between the aluminum and silicon to block the silicon diffusion. Both approaches are feasible, but somewhat complex in their implementation. The simpler solution of increasing the nominal E-B junction depth from 1.2 to 1.8 μm was chosen. This approach is simpler because the only process changes necessary are an equal increase in the epitaxial layer thickness and longer times for the collector isolation and emitter diffusions. The validity of the deeper emitter solution was demonstrated with a process run of CMMA wafers which were tested for temperature stress, as before, and for the electrical characteristics of the transistors and gates. The results of the temperature stress testing indicate greatly reduced degradation of the junctions. It was concluded that the effects of emitter spikes are negligible with the deeper emitters. Evaluation of the electrical characteristics show negligible differences between the old process and the new. It was concluded that the CMMAs built with the thicker epitaxial layer and deeper emitters would meet the specification.

4. Product Assurance Plan. Quality assurance on a device of the size and complexity of the CMMA is a difficult problem. The requirement for a ten-year lifetime compounds the problem. The Product Assurance Plan developed by the contractor during Phases I and II starts with a device designed for reliability, utilizes rigorous process control and visual inspections, adds special test devices as sensitive indicators of trouble, and finishes with powered burn-in to eliminate infant mortality.

a. Time-dependent failure-mode detection. The prime ingredient of a product assurance plan that is sufficient to assure confidence in a ten-year lifetime is some means to detect, correct and screen highly time-dependent failure mechanisms. Since the classical approach of life-testing devices for a period of time equal to the expected mission requirement prior to the mission is not possible, some alternative means must be developed. The approach taken in the development of the CMMA was to determine the characteristics of all time-dependent failure mechanisms inherent in the technology to be used in fabricating the CMMA, and to develop test devices that correctly and accurately reflect these failure mechanisms in such a manner that they can be detected in a more reasonable period of time.

These test devices were placed on special test die of which there are five per CMMA wafer. At the conclusion of wafer-processing the test die

will be separated from the CMMA die, on a lot-by-lot basis, and evaluated by the quality control department for insulation-oxide integrity, aluminum coverage at oxide steps, via resistance, surface stability, and electrical characteristics. A quantitative measure of device stability can be determined in a few days by using advanced high-temperature-stressing techniques. The information obtained from these tests can be used to qualify CMMA device lots for high reliability.

b. Standard test devices. In addition to the special test devices described above, each CMMA die contains a few standard test devices to aid in determining the quality and reproducibility of the fabrication processes. Transistors, diodes, and pinched resistors are used to determine parametric characteristics and deviations. Simple gate cells are also directly accessible at bonding pads for gate characterization. Data from these test devices will, of course, be used to regulate the fabrication processes, and will provide an excellent measure of the process control.

5. CMMA Performance. The performance of the CMMA standard and driver gates was predicted by computer simulation during the design phase using the Sceptre Program. Worst-case variations of electrical and environmental parameters were included in the circuit simulations. The nominal, simulated performance characteristics for the standard gate are compared in Table 30, with measured data from a small number of Phase II engineering model CMMAs. Also shown in Table 30 are the parameter limits that were agreed upon for Phase III. Where there is disagreement between the simulated characteristics and the specified limits, it is the result of difficulties in obtaining the right device parameters for the computer simulation. Test results from actual CMMAs fabricated during Phase II indicate that the parameter limits listed can be met.

The parameters listed in Table 30 are:

- (1) Power dissipation when the output is at 0 logic level.
- (2) Power dissipation when the output is at 1 logic level.
- (3) Average power dissipation for 50% duty-cycle operation.
- (4) Propagation delay time with a fanout of 10:

t_{pdo} time for output to reach 1.1 V from the 1 level

t_{pdl} time for output to reach 1.1 V from the 0 level

Table 30. CMMA standard gate performance characteristics

Parameter	Pre-radiation computer simulation			Phase II E. M. measured at 25°C		Specified limit	Units
	-35°C	+25°C	+100°C	Min	Max		
Power DISS (0)	0.66	0.55	0.44	0.34	0.60	0.78 Max	mW
Power DISS (1)	0.91	0.71	0.48	0.43	0.77	1.0 Max	mW
$\frac{PD(0) + PD(1)}{2}$	0.785	0.63	0.46	0.385	0.685	0.89 Max	mW
Propagation delay time:							
$t_{pd}(0)$	58	43	33	Not measurable		60 Max	ns
(Fanout = 10) $t_{pd}(1)$	18	24	56	15	25	30 Max	ns
$\frac{t_{pd}(0) + t_{pd}(1)}{2}$	38	33.5	44.5	-	-	45 Max	ns
I_0 at $V_0 = 0.3$ V	4.2	6.5	5.4	2.35	4.3		mA
V_t with fanout = 1	1.01	0.91	0.78	-	-		V
V_t with fanout = 10	1.12	1.0	0.86	1.03	1.06		V
Conditions: Supply voltage = 5.0 V.							

- (5) Average propagation delay time for 50% duty-cycle operation.
- (6) Fanout current measured at $V_0 = 0.3$.
- (7) Input switching threshold voltage.

The minimum output current that the standard gate must have for a fanout of 10 is 1.4 mA at +25°C, 1.9 mA at -35°C, and 1.1 mA at +100°C. It can be seen that the design allows considerable margin in fanout current. Part of this margin was designed in to allow for degradation of transistor current gain (from 100 to 30 typically) as a result of the expected radiation environment. Gain degradation is the major radiation effect in the CMMA.

Similar performance data is given in Table 31 for the driver gate. The minimum output current the driver gate must have for a fanout of 50 is 7.1 mA at +25°C, 9.4 mA at -35°C, and 5.4 mA at +100°C. There is considerable design margin here also for radiation effects and manufacturing tolerances.

a. Array performance. Only a limited amount of performance data was taken on the engineering model CMMAs, because they were not considered to be typical of normal production, and because the small quantity of working units did not provide a good statistical sample. Full electrical characterization of the CMMA circuits was to be done on the Phase III production units. The array data that follows will, however, give some indication of the performance of the complete CMMAs.

The dual 8-stage shift register uses 90 standard and 22 driver gates. The power-dissipation vs temperature-and-supply voltage of one of these registers is shown in Fig. 83. The register was clocked at 100 kHz, and the data fed to the register was 50% duty cycle (101010--). The power dissipation increased above 100 kHz due to capacitance effects. At 1 MHz (5.0 V and +20°C), the power was 160 mW. These registers operated up to a maximum clock rate of about 4 MHz at +20°C. The typical propagation delay time from clock transition to settled output was 160 to 185 ns. The delay time increased by 30 to 40 ns at +100°C, and decreased by 20 to 25 ns at -35°C.

The propagation delay time of the 4-bit adder/subtractor, from the carry/borrow input to the fourth sum/difference output was 210 to 240 ns at +20°C. The carry/borrow output occurred 210 ns after the carry/borrow input. Using a ripple-through adder, it is therefore not particularly fast.

Table 31. CMMA driver gate performance characteristics

Parameter	Pre-radiation computer simulation			Phase II E. M. measured at 25°C		Specified limit	Units
	-35°C	+25°C	+100°C	Min	Max		
Power DISS (0)	3.68	2.88	2.25	1.8	3.0	4.0 Max	mW
Power DISS (1)	1.64	1.27	0.86	0.78	1.4	1.8 Max	mW
$\frac{PD(0) + PD(1)}{2}$	2.66	2.07	1.56	1.29	2.2	2.9 Max	mW
Propagation delay time:							
$t_{pd}(0)$	28	28	36	35	37	40 Max	ns
(Fanout = 50)							
$t_{pd}(1)$	32	44	53	25	30	40 Max	ns
$\frac{t_{pd}(0) + t_{pd}(1)}{2}$	30	36	44.5	30	33.5	40 Max	ns
I_0 at $V_0 = 0.3$ V	10.3	10.6	10.5	8.7	10.4		mA
V_t fanout = 1	1.06	0.99	0.86	—	—		V
V_t fanout = 50	1.08	1.05	0.92	1.02	1.11		V
Conditions: supply voltage = 5.0 V.							

b. Radiation performance. Test samples of CMMA transistors and gates underwent electron and proton radiation tests during Phase II to demonstrate that the design was adequate for the intended application. Electrons and protons at Jupiter are thought to be the main radiation hazard of the mission. The radiation tests are summarized in Table 32. Early in the design it was determined that transistor current gain (beta) would be the parameter effected most by radiation. This proved to be true as indicated by data on the output transistor. Note that the beta initial and beta final values given in the notes will accommodate the degradation experienced in the tests. It was concluded that the CMMA would perform as specified after receiving the full radiation dose.

6. Current Status. Work on the CMMA contract was suspended shortly after the beginning of Phase III due to a major redirection of the outer-planets mission. Several hundred wafers were being processed. The contractor was allowed to complete work on 40 wafers to assess the effect of the PAP. The effect of the PAP on the CMMA yield was severe. Twenty-three electrically good CMMAs were completed and delivered. Only one conformed to all the requirements of the PAP.

At this time there is no plan to use the CMMA at JPL. The Goddard Space Flight Center is, however, planning to use the CMMA in an advanced on-board processor (computer) being developed for Earth-orbiting spacecraft. The basic processor has been partitioned into 66 CMMAs consisting of 26 types. Harris is building prototypes of these CMMAs for the processor breadboard. Other CMMAs are intended for the I/O section. Goddard is planning a CMMA-environmental test program to qualify it for spacecraft use. Assistance in using the CMMA is being given to Goddard wherever possible.

E. CMMA Reliability

The long life requirements for CMMA reliability were realized through: (1) proper design, (2) proper process control, and (3) proper screening tests. Proper design is critical to successful development of any device, while screening tests must be conducted as a backup to process control, which is never 100% perfect. Each of these topics will be examined in the following pages.

Table 32. Summary of radiation testing for CMMA output transistor

Test no.	Radiation type	Fluence	Energy	Shielding	β_F/β_I
1	Electrons	$1.2 \times 10^{14}/\text{cm}^2$	3 MeV	Alumina lid	0.77
2	Protons	$1.2 \times 10^{12}/\text{cm}^2$	2 MeV	None	0.35
	Combined effect of above 2 tests				0.30
3	Protons Gamma	$9 \times 10^{12}/\text{cm}^2$ 5×10^4 rad	140 MeV —	Kovar lid	0.35 to 0.42

β_I & β_F Measured at emitter current density = 1.45 mA/mil²

$\beta_I = 90 - 120$

β_F Min for max gate load = 22 at +22°C

No change in BV_{CBO} , BV_{EBO}

Small changes in V_{SAT} , BV_{CEO} , τ_S

In CMMA gate circuit:

Small changes in $I_{IN}(1)$, $V_{OUT}(0)$, $I_{OUT}(0)$

No change in propagation delay or power dissipation

1. Design Factors. One of the first considerations in design of the CMMA was the use of extensive design analysis. In contrast to a normal cut and dried approach to circuit design, engineers in this instance worked extensively with device characteristics and with circuit design configuration before attempting to build the device. Consequently, results realized through actual measurement of devices after fabrication correlated well with predictions made through computer simulation during the design phase. The result was a well-designed CMMA.

Process simplicity was another design factor. Simplicity was achieved, for example, in reduction of critical diffusions within the CMMA from several (normal in bipolar processing) to only one. This was the emitter diffusion, which determines the beta of transistors. Again, design simplicity reduced critical alignments to only two: alignment of the emitter to the collector, and alignment of the aperture to the emitter. Gold doping also was eliminated through the epibase process. Gold doping is not considered to be well controlled, and there is reason to believe that a radiation environment may adversely affect devices which employ that process.

Another factor in design simplicity was the use of a power/ground bus which was formed primarily with diffusions. The power/ground bus did, however, require the use of some metallization. Electromigration could have presented a reliability hazard in this metallization but the problem was circumvented through carefully limiting the current density allowed. The greatest consideration is that, if diffusions in the power/ground bus had not been used, a third level of metallization would have been required--hardly within the concept of process simplicity.

Long life consideration was given to proper step coverage as shown necessary in Fig. 84. The figure shows a patterned piece of oxide deposited over patterned aluminum on silicon dioxide. The oxide forms into a bulbous configuration as it dips over the rims, or steps, of the depression. If a second layer of metal were deposited over this region, the bulbous oxide might easily cause inadequate metallization immediately above it, and result, over a long life situation, in cracking and resultant discontinuous conduction.

Fabrication methodology generated to overcome the above potentially hazardous condition within the CMMA is illustrated in Figs. 85 and 86. Here, the sides of the basic aluminum metal have been bevelled, and the oxide strip

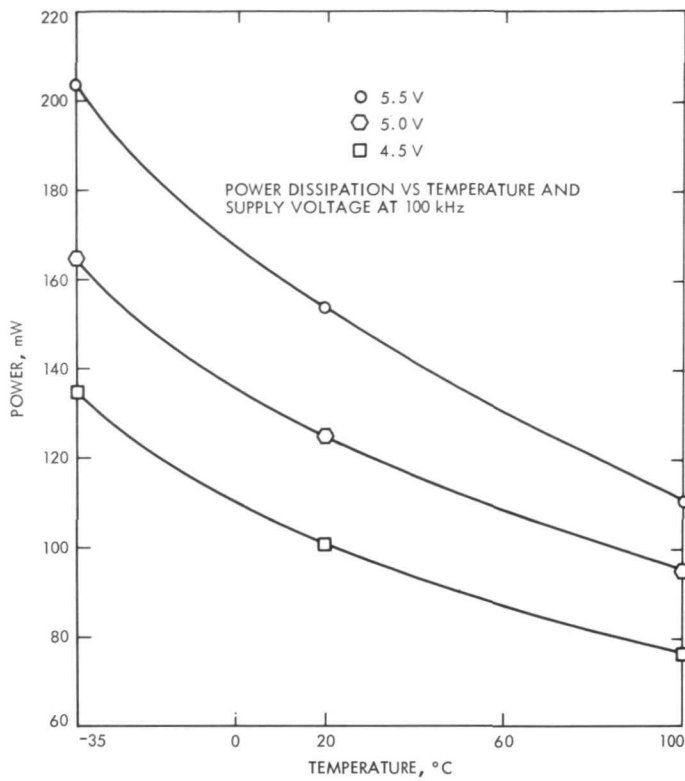


Fig. 83. Dual 8-stage shift register

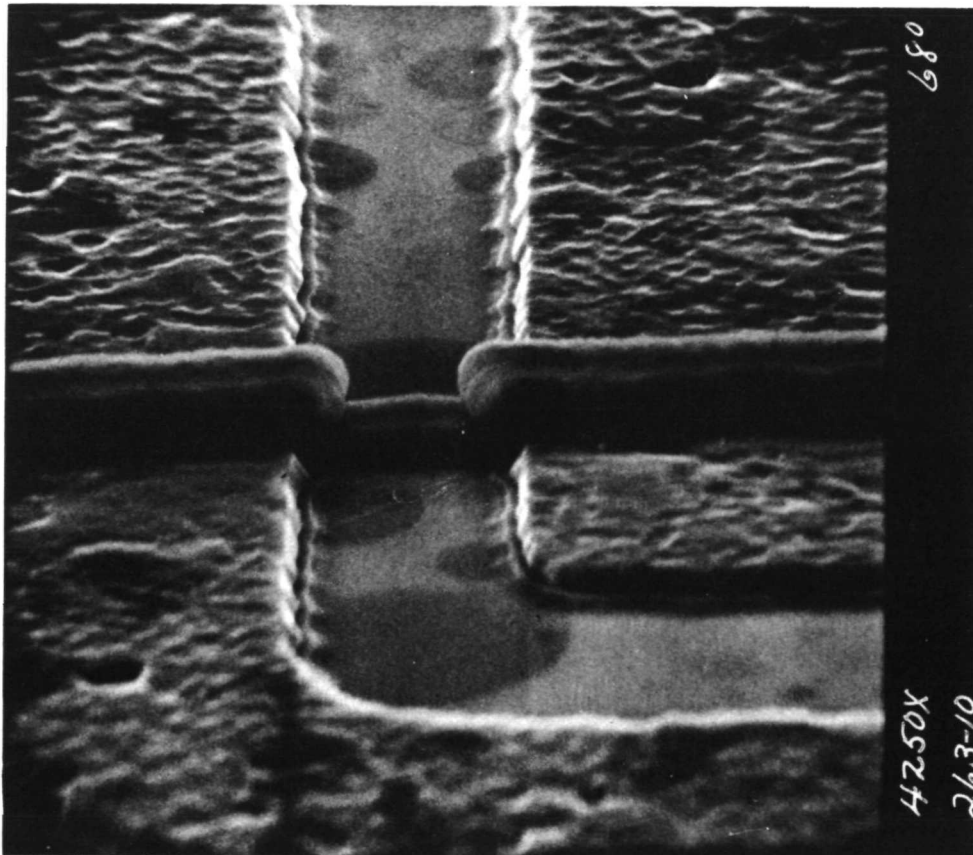


Fig. 84. Deposited SiO₂ stripe crossing patterned aluminum

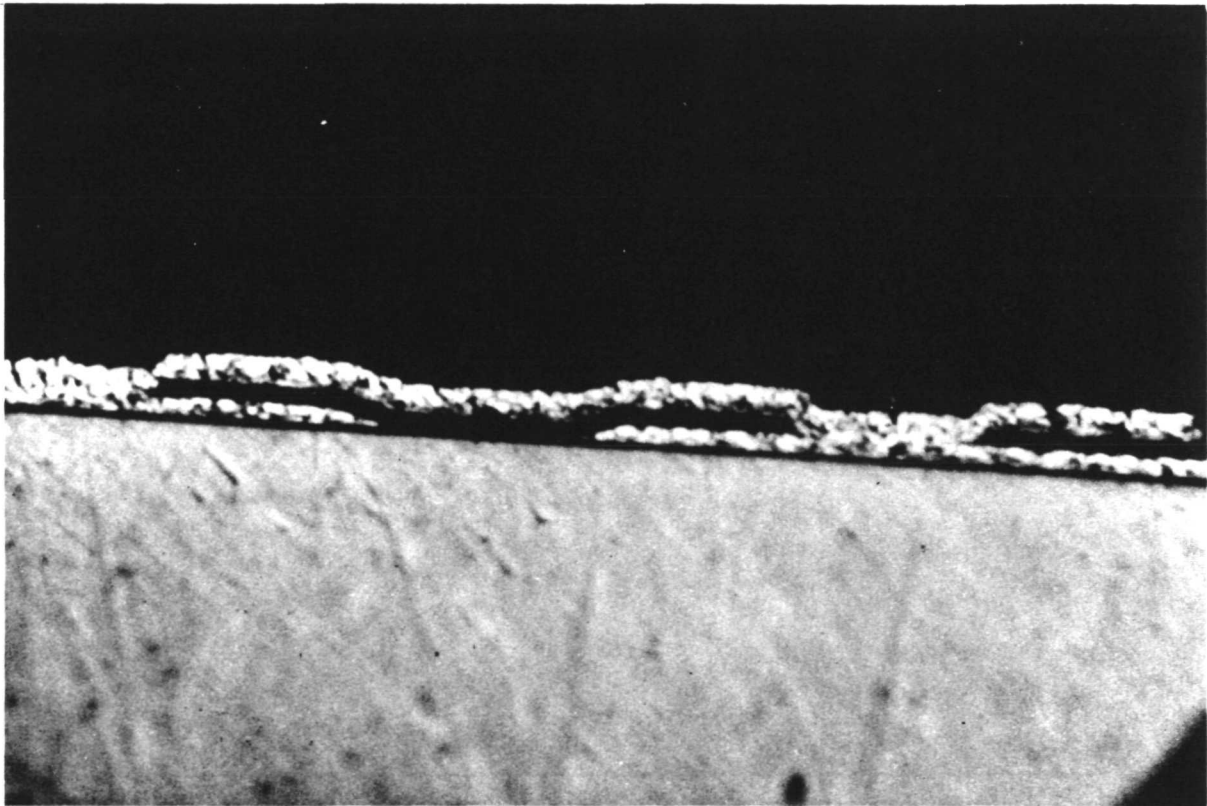


Fig. 85. Microsection of CMMA 2-level aluminum

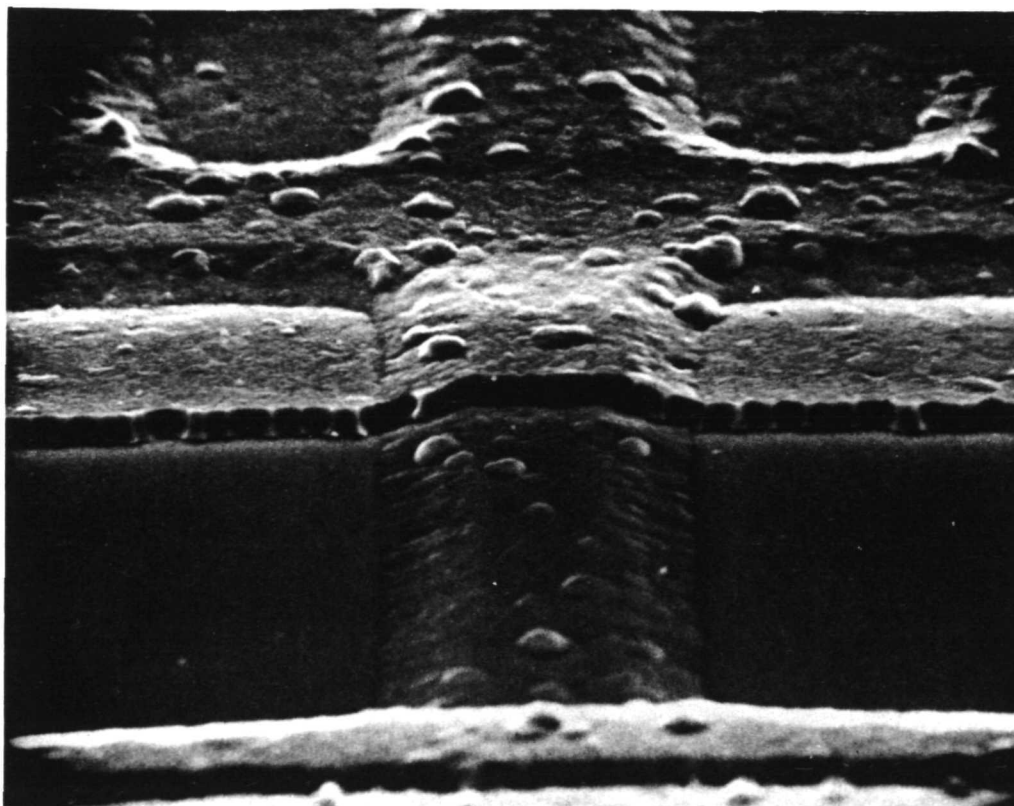


Fig. 86. CMMA second-level aluminum over beveled first level

deposited upon it shows no signs of bulging at the steps, but simply follows the contours of the gentle slope. There has been no reduction in metal thickness across the step, and there is little likelihood of the appearance of cracks.

2. Process Control. A control feature for processing CMMA material was the control wafer. Wafers were used in two functions: first, as controls; second, as pilots. In the control function, the wafers were run through the processing operation alone – without other materials – simply to check calibration of the whole processing system. In the second function, the pilot wafers accompanied the material being processed, and were used for test purposes. The pilot wafer could reveal damage to the batch, but could not, of course, be instrumental in preventing damage, as could the control wafer.

Another feature of process control was the use of five user in-process inspections. The first inspection was made prior to deposition of the first level metal. The second inspection followed such deposition. A third inspection was made after the device had been scribed and broken. The fourth examination was made following all bonding and before sealing. The last inspection followed the sealing process. The large number of these qualifying measures attests to the criticality of the CMMA to successful performance of the outer planet spacecraft.

Again, process control was strengthened through a scanning electron microscope metallization inspection that insured, through sampling of dies from each wafer, that metallization was being put down in proper fashion.

Finally, test patterns were included for both die and wafer certification. These were used to locate systematic and local problems.

3. Screening Tests. In the test die and test cell hierarchy within each CMMA wafer there are five test dice. For convenience these dice are identical in size to the CMMA dice. The test dice can be broken out, bonded separately, and tested for information concerning the wafer. Within each CMMA die there are four test cells, which were padded out on second level metal and can be probed to provide information concerning the die.

Test die structures (5/wafer) include a standard gate, a driver gate, and an extender gate; also discrete transistors and resistors; a via contact test structure consisting of 120 0.0127 mm (0.5 mil) vias connected in series;

a crossover test structure, consisting of 240 0.127 mm crossovers between first and second level metallization layers; and finally, a metal oxide/metal capacitor.

Of the four test cells on each CMMA die, one is devoted to the driver gate. The other three contain the following test structures: multi-emitter input device, driver gate output transistor, minimum geometry transistor, a resistor, and a large geometry field-plated transistor.

The test structures have several uses. One applies to device characteristics; devices can be bonded and their stability observed over a long period of time. Similarly, gate characteristics may be studied, and stability observed. Via structures permit evaluation of oxide and metallization, as do crossover structures. Again, test structures enable engineers to determine contact resistance and stability between first and second layers of aluminum. Insulation oxide may be examined with the metal oxide metal (MOM) capacitor, while the geometric field plated transistor facilitates study of thermal oxides.

In the area of acceptance and screening tests, evaluation and tests are performed with consideration to three principal criteria: wafer acceptance, die acceptance, and CMMA acceptance.

a. Wafer acceptance criteria. Before a wafer may be accepted for further processing toward becoming a CMMA, it must be examined and evaluated by the scanning electron microscope. If the wafer shows inadequate metallization, it is rejected. A test die evaluation is performed which may indicate problems based on test dice and, again, reject the wafer. A high stress test is conducted on the test dice to expedite turnaround and eliminate time lost on speculation as to whether a wafer is to be processed further. A final criteria applies to yield limits: if the yield falls below a preset limit, the wafer is considered unsuitable for further processing.

b. Die acceptance criteria. A test cell evaluation is performed at the probe level. Should nonstandard results be obtained, the corresponding die is rejected. Secondly, the die acceptance criteria must be based upon CMMA die performance.

c. CMMA acceptance criteria. These criteria are based upon a sequence of environmental tests, burn-in tests judgements on electrical

performance and stability maintained throughout the tests, and, finally, upon the types of failure mechanisms observed.

4. Summary. To summarize the CMMA reliability approach, JPL engineers believe they have a reliable design. The bipolar processing system is satisfactorily simple, given a reasonable chip size and two-level metal structure. Process control has been emphasized. There is test vehicle wafer certification. Plans have been adopted to screen test each array. Finally, a total data review of the entire CMMA reliability package is envisioned.

REFERENCES

1. Chelson, P. O., and Eckstein, R. E., Reliability Computation from Reliability Block Diagrams, Technical Report 32-1543, Jet Propulsion Laboratory, Pasadena, Calif., Dec. 1, 1971.
2. Sicol, R. L., and Chelson, P. O., "Development of Electronic Part Failure Rates for Long-Duration Space Missions", in Proceedings of the 22nd Electronic Components Conference, Washington, D.C., May 15-17, 1972.
3. Chelson, P. O., Reliability Computation Using Fault Tree Analysis, Technical Report 32-1542, Jet Propulsion Laboratory, Pasadena, Calif., Dec. 1, 1971.

VII. PROPULSION

A. Trajectory Correction Propulsion Subsystem

1. Functional Requirements. The functional requirements for the trajectory correction propulsion subsystem (TCPS) are shown in Table 33. The tank will be sized for the greatest trajectory correction velocity and will be loaded as necessary for missions requiring less propellant. The nonpropulsive spacecraft mass is the total spacecraft mass less the propulsion system mass. The engine thrust is limited by spacecraft dynamics considerations; the less thrust, the less perturbation of the 15-m booms and other appendages. For this reason and because several engines in the desired range are already developed for military programs, a 111.206 N (25 lbf) engine was selected. The system will be man-rated so that personnel can work around it while it is fueled and pressurized.

Table 33. TCPS functional requirements

Specific requirements	Nominal value
ΔV (mean + 3σ) for 714 kg	$\left\{ \begin{array}{l} 205 \text{ (JUN 79)} \\ 167 \text{ (JSP 76, JSP 77)} \end{array} \right.$
Non-propulsive spacecraft mass, m/s	
Minimum number of maneuvers	9
Time from launch to last maneuver, yr	9
Minimum maneuver ΔV , m/s	1
Engine thrust, N	<444.82
Minimum service life (fueled), h	10^5
General requirements	
Environment: Space vacuum Radiation (RTGs, Jovian belts) Particles (asteroid belt) Man-rated system	

A study of mass, reliability, and cost was made to determine whether the system should be monopropellant or bipropellant. The results, shown in Table 34, have been normalized to the monopropellant values.

Table 34. Monopropellant versus bipropellant system

Mass	$(M_M - M_B) / M_M = +6.5\%$
Reliability	$(R_M - R_B) / R_M = +1.6\%$
Cost	$(C_M - C_B) / C_M = -62.5\%$

The mass difference between the two systems is small, with the bipropellant system slightly lighter, but slightly less reliable, than the monopropellant system. The major difference is that the monopropellant system costs less; and our experience with the monopropellant is greater than with the bipropellant system. The monopropellant system has less leakage potential; a cooler, more benign exhaust; requires less power; and integrates easier with the attitude propulsion system. For these reasons, the monopropellant blow-down system was selected.

2. Configuration. The TOPS reliability goal is 95% for the propulsion subsystem. One-year reliability data was used for comparative and relative studies because long-term data was inadequate, and there was no generally accepted model to extrapolate the short-term data to ten years. Several independent sets of reliability data were gathered from the literature, and the mass and reliability were computed for five configurations, using the different sets of data. The widest range, using any one set of data, was 3.8% in mass and 2.0% in reliability. Because the difference was small, the original baseline was retained; this permits evaluation of both the solenoid and the pyrotechnic valve technologies.

Figure 87 is a schematic of the baseline system for a three-planet mission. Two pressure transducers are used to make the important tank pressure measurement. A surface tension device is used for propellant acquisition. Squib valves are used for cruise propellant isolation. One valve is opened prior to the first pre-encounter maneuver, and the corresponding valve, which is normally open, is not closed until after the last

post-encounter maneuver is satisfactorily completed. Flow rate is measured by an orifice. Two parallel series branches, of solenoid valves for engine control and encounter isolation are protected by filters from any contamination that might be generated in the pyrotechnic units. Engine temperature and pressure will be measured, and the catalyst bed temperature in the engine will be monitored to detect any valve leak so that early remedial action can be taken. Gimbal actuators are used to provide thrust vector control.

Table 35 gives the mass estimate for the TCPS. The attitude propulsion subsystem (APS) propellant and tank weight allocation required by the APS are not included here.

Table 35. TCPS mass estimate

Component	Quantity	System mass, kg (lbm)	
Propellant tank	1	19.187	(42.3 ^a)
Propellant acquisition device	1	1.769	(3.9)
Fill valves	2	0.227	(0.5)
Transducers (P, T, F)	10	0.907	(2.0)
Explosive valves (NO, NC)	10	1.814	(4.0)
Filter	3	0.454	(1.0)
Orifice assembly	1	0.136	(0.3)
Solenoid valves	4	1.361	(3.0)
Engine assembly	1	0.680	(1.5)
Mounting hardware (gimbal TVC)	—	2.268	(5.0)
Cable harness	—	0.454	(1.0)
Hardware Total		29.257	(64.5)
Propellant (N ₂ H ₄)	—	73.528	(162.1 ^a)
Pressurant (GN ₂)		2.495	(5.5 ^a)
Subsystem Total		105.3	(232.1)
^a APS portion not included.			

3. Interfaces. The TCPS and the APS comprise the propulsion module. They have a common propellant tank and will probably use some of the same component designs. The pyrotechnic subsystem fires the squib valves and switches the power for the solenoid valves. A modular structure is used for the propulsion subsystem so that the assembly can be fabricated, tested, loaded, and monitored without impacting the spacecraft. The attitude control subsystem operates the gimbal actuators and has an accelerometer to determine the duration of the engine firing time. The control computer issues the engine start, and in response to the accelerometer, stop commands. In addition, the control computer numerically computes the change of velocity from the flow rate, chamber pressure, and thrust and then computes the engine firing time as a backup command to be used in the event that the accelerometer fails. The measurement processor performs the transducer sampling at three data rates: one for cruise, one each for the transient and steady-state portions of the maneuver. Thermal control is required to maintain the propulsion bay temperature between 15 to 32°C (60 to 90°F), except for a stabilization period after engine firing. Either a radioisotope or an electric resistance engine heater will be used to maintain the bay and engine temperatures.

4. Propulsion Bay. The propulsion bay is a truss structure covered with a flexible thermal blanket (Fig. 88). The propulsion module will probably be installed through the end or perhaps through the open sides of the bay, depending upon the location of the other major components near the antenna end of the bay. The center of gravity of the spacecraft is located very close to the antenna end of the tank. The engine has adequate clearance to move freely under control of the gimbal actuators without touching the attitude propulsion subsystem thrusters.

Figure 89 is an artist's conception of the first flight design for the propulsion module based on typical component sizes. The propulsion module mates with the propulsion bay truss at the bottom of the structure, and the system will be cantilevered from the truss.

5. TCPS Evaluation and Development. The 10-yr life requirement was emphasized in the solenoid valve program, whereas in the squib valve program, the emphasis was on the compatibility of construction metals with hydrazine and the elimination of squib particulate blowby in the valve to

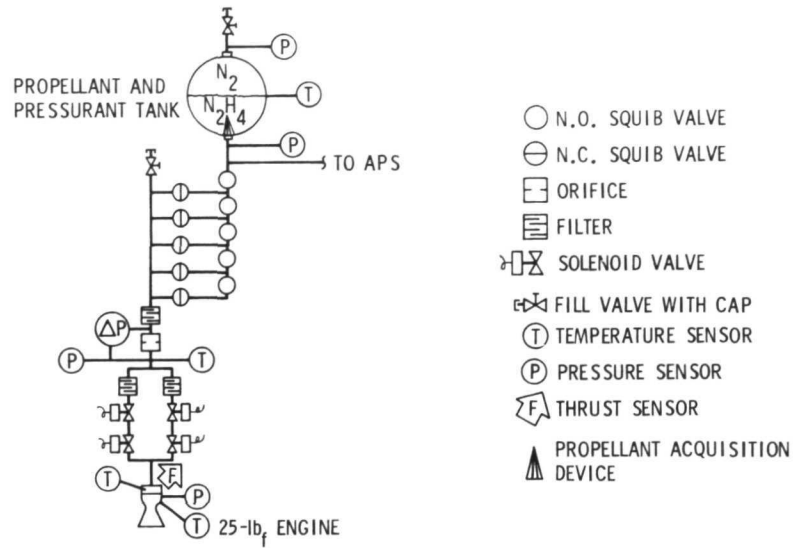


Fig. 87. TOPS baseline system

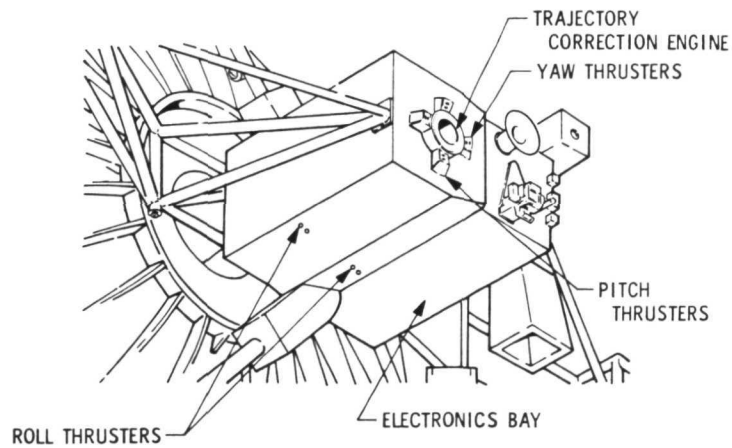


Fig. 88. Propulsion bay

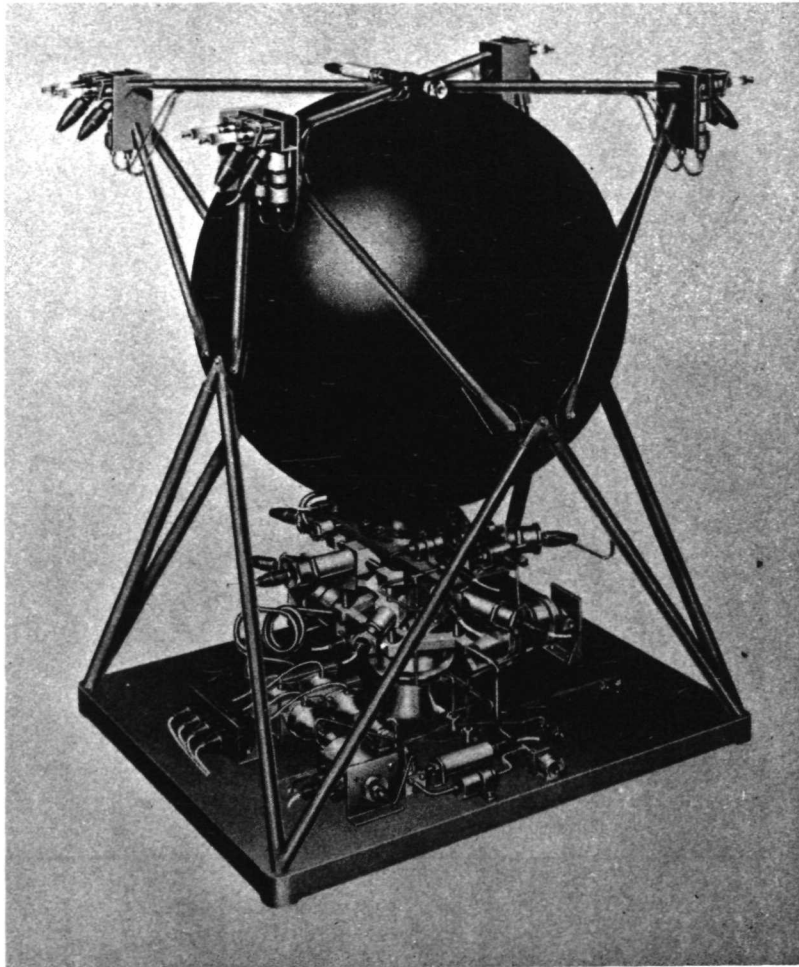


Fig. 89. Propulsion model (configuration 12L/A)

reduce filtration and minimize compatibility problems. Reasonable performance with an adequate margin for the full lifetime was stressed in rocket engine testing. Additional tasks completed were the evaluation of the baseline system configuration and the subsystem interfaces by means of an actual system test using available hardware.

a. Normally closed and latching solenoid valves. The normally closed (NC) and the latching solenoid valves were evaluated by using surplus hardware primarily from the Apollo and Gemini programs. These valves have an initial leakage value of 0.1 to 1 standard cm^3 of helium per hour. The end of mission value has not been determined. The TOPS leakage requirement was not established.

The magnetic field requirement for TOPS spacecraft is $1\ \gamma$ at 0.9 m (3 ft) from the assembly. Although valve designs available differ greatly, none meet this requirement. With development, the requirement probably can be met for the de-energized state only. A waiver from the requirement during engine firing (the energized periods) has been requested. A brief examination of magnetic shielding indicates that a field reduction by a factor of 2 to 5 can be achieved. However, this is not enough for the energized state; so it appears that, if the waiver is denied, spacecraft compensating magnets will be needed.

The current program for testing valve life involves recirculation of hydrazine through cycling valves and storage of hydrazine in contact with the valves.

b. Zero-blowby aluminum squib valve. Figure 90 shows a sectioned NC squib valve which was actuated in a design evaluation test. Products of combustion are isolated by both the O-ring and by the welded bellows. When the piston assembly drives the ram down into the flow tube, the nipples are sheared off and pushed into the retaining space and the hole in the ram allows hydrazine flow. The valve body is made of aluminum, and the bellows and the actuator assembly, of stainless steel. The only particles entering the hydrazine from this valve result from the ram shearing the tube stubs. The flight valve would be much smaller and lighter than this through the use of a smaller squib.

c. Rocket engine life. Table 36 gives the duty cycle for the engine test. The first engine test program concerned the duty cycle for the

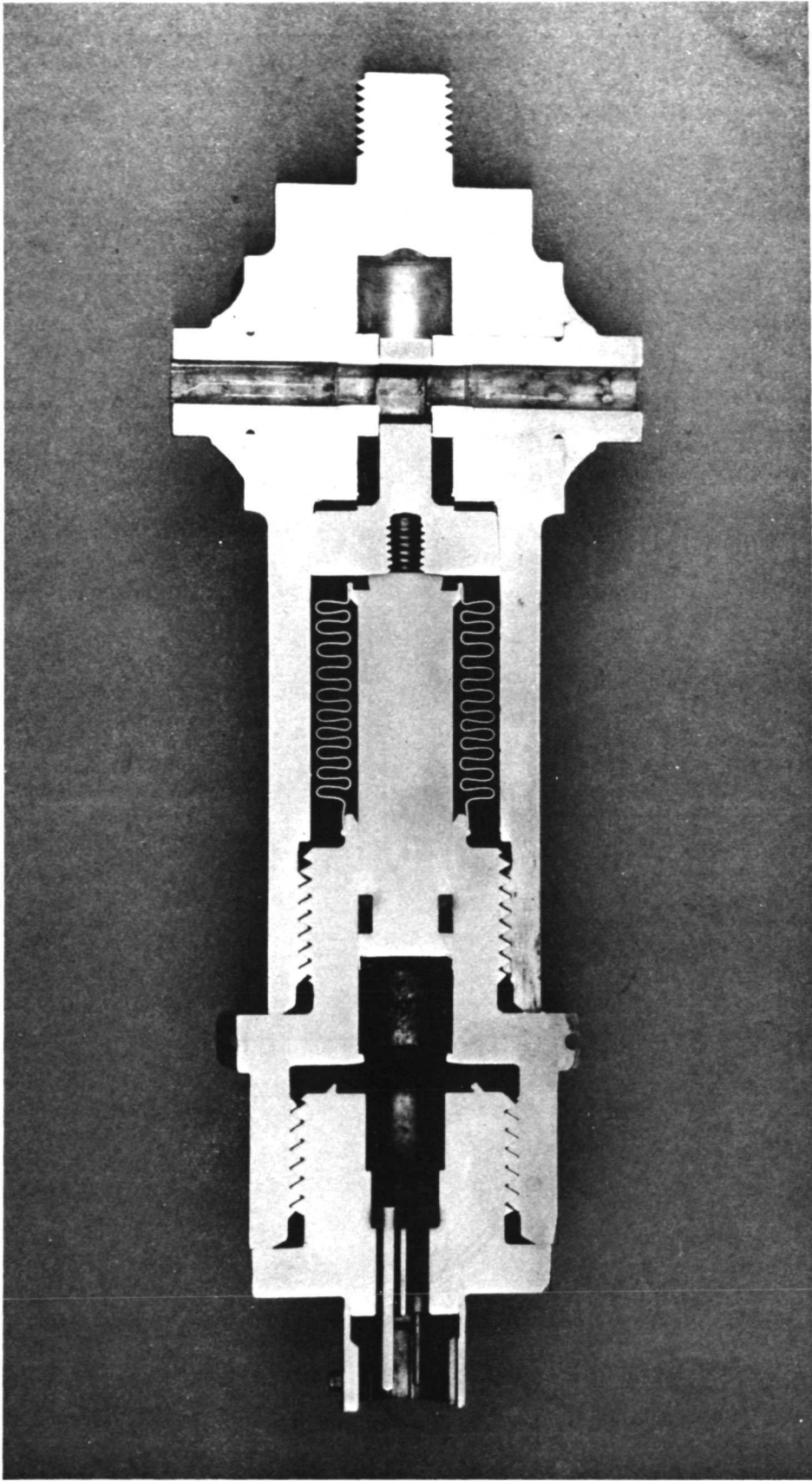


Fig. 90. Normally closed squib valve after actuation

Table 36. Engine test duty cycle

Event	Squib valve firing	Trajectory correction description	Engine burn duration, s
1	NC 1		
2		Post-Earth	99
3	NO 1		
4	NC 2		
5		Pre-Jupiter	22
6		Post-Jupiter	47
7	NO 2		
8	NC 3		
9		Pre-Saturn	56
10		Post-Saturn	749
11	NO 3		
12	NC 4		
13		Pre-Uranus	269
14		Post-Uranus	185
15	NO 4		
16	NC 5		
17		Pre-Neptune	15
18		Margin	158
Total burn time			1600

four-planet mission, and this cycle has been retained for subsequent programs to ensure data comparability and to demonstrate an adequate margin for the three-planet mission. It is now determined that the 1600-s burn time is about the mean plus 3- σ value for the baseline three-planet mission. Nine maneuvers are shown in the table instead of the eight now planned for the four-planet mission, where one maneuver before and one after each planet is assumed because there were originally two pre-Uranus maneuvers. The nine maneuver schedule fortuitously fit the baseline three-planet mission, which requires two maneuvers before each planet and one after.

At the start of the program, engines on hand and borrowed engines were tested. Originally, it was planned to use a hydrazine/hydrazine nitrate blend. No engine was specifically made for the nitrate blend, so standard hydrazine engines were used. These engines suffered mechanical failure of the bed and catalyst failure at high temperatures. Other types of engines which might operate with the nitrate blend needed too much development for TOPS use. As a result, available resources were concentrated on hydrazine engines. Early testing of these engines showed several significant problems, which were subsequently understood. There was a 50% loss of performance during firing; the chamber pressure roughness values were 25%. A later nine-burn test series revealed ignition spikes of as much as 100%. Increases in engine pressure appeared to be caused by catalyst migration into the injector. Nevertheless, it is believed that these engines can meet the TOPS requirements with careful attention to the design of the catalyst bed and to the engine and propellant temperature limits. Because of the test results, the initial thermal control requirement of 4 to 32°C was raised to 15 to 32°C. It was also found that the propellant should have less water than the amount allowed by the current military specification, and a JPL specification with stricter requirements will be written.

Two engines were tested to demonstrate adequate life. Each engine underwent a pre-firing vibration test in accordance with the TOPS specification to test catalyst bed integrity. Each then went through the standard nine-start, 1600-s, cumulative firing-time test. The tests were atmospheric to minimize cost, with vacuum conditioning before and after each firing. No thrust measurements were taken. An initial temperature of 4°C was used to simulate the worst condition for the engine. Two different injector designs were tested to demonstrate the technology while minimizing the cost. Both engines passed the vibration tests with very little catalyst shaken out of the beds. Because of a problem with one of the engine valve combinations, the firing schedule was continued beyond 1600 to more than 1740 s with no resultant problems. The engines were judged on the basis of I_{sp} , ignition delay, the start-pressure spike, and chamber pressure roughness. The performance of both engines was close and was adequate for the TOPS missions.

d. Component development. An all-metal system will be used for propellant acquisition rather than an elastomeric bladder because the surface tension device is simpler, more compatible with the propellant, and can be

made of the same materials as the tank. Such a device, shown in Fig. 91, was recommended for this type of mission after intensive study. V-shaped galleries go around the tank. The TCPS normally starts out with a 50% ullage for the blowdown process. Other designs are now being used, primarily in military flights, and some NASA studies are also in process. The recommended system cannot be Earth-tested, and confidence in the design is gained from flight experience and model drop tests. Because this technology is developing rapidly, a specific TOPS design was not selected.

Some components were not evaluated for various reasons. Transducers currently being developed by other projects will be used or adapted to the TCPS. A type of strain gauge pressure transducer of a material compatible with hydrazine is needed. A filter is being developed by the APS program. Tank and fill-valve technology are available.

e. Demonstration system. The components were integrated and system-demonstrated to verify the performance of the baseline system configuration. Computer simulations of the engine feed system were made. Shock from the hard-mounted squib valve system was monitored to find if it transmits excessive shock to the spacecraft. Data on the post-firing thermal soak-back from the engine were obtained, the gimbal actuator system tested, and transducer response checked to provide experience in determining whether or not the engine firing time can be computed and controlled on board with the proper accuracy. The demonstration tests were run in a vacuum cell at the JPL Edwards Test Station, Edwards, California. The firing was vertical because an acquisition device was not available. This was the first test in which a continuous tank pressure blowdown was achieved in the TOPS program.

Figure 92 shows the assembled TCPS demonstration system. The component support plate is located at the head of the tank because the tank has no side tabs to support the structure. The system went through its final calibration check, and it was tested in the second quarter of FY'72.

f. Final TCPS work. Work completed included:

- (1) System demonstration tests and reduction of the data obtained.
- (2) Fabrication and evaluation of titanium squib valves.

NAS7-754 STUDY
RECOMMENDS CENTRAL
PILLAR OR POST WITH
COMMUNICATING
CHANNELS AROUND
TANK (IN TWO
ORTHOGONAL PLANES)
FLIGHT SYSTEMS
CANNOT BE EARTH TESTED
DESIGN CONFIDENCE FROM
MODEL DROP TESTS AND
FLIGHT EXPERIENCE

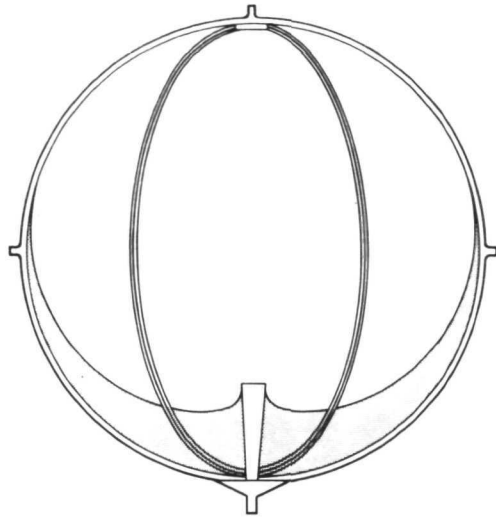


Fig. 91. TCPS propellant acquisition

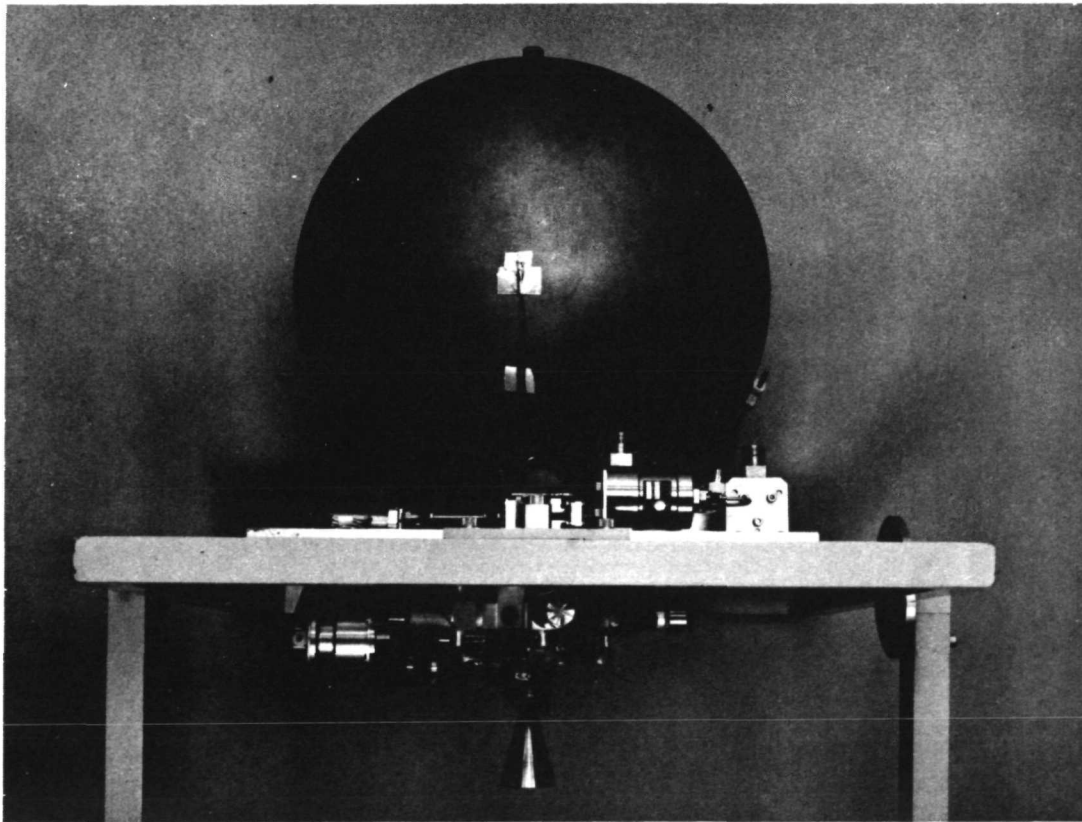


Fig. 92. TCPS demonstration system

The following tests on the titanium components were planned but not completed during the TOPS Project because of schedule and funding limitations:

- (a) Radiation tests on all constituents of the valves.
- (b) Storage tests, using hydrazine with less contaminants than allowed in the military specification.

6. TCPS Design Status. The evaluation program disclosed that today's technology will meet the TOPS TCPS requirements. However, component design changes are necessary to achieve better material compatibility, lower power consumption, a lower magnetic field, and less mass. Selected material must be compatible with hydrazine and must meet the power, magnetic field, and mass requirements. New designs are needed to improve the normally closed and latching solenoid valves in all of these areas. A propellant acquisition device must be designed for the selected TOPS tank. Squib valves as well as transducers should be reduced in mass and made of a material compatible with hydrazine. The filter material is of prime importance (see Paragraph VII-B-2-e). Data from the program to date indicates that titanium and aluminum are the most compatible materials for the system: Titanium has the additional advantage of superior strength and low mass. All component passages in constant contact with the hydrazine should be made from titanium, if possible.

A detailed report of the engine test program is given in Refs. 1 through 3. Reference 3 is in a classified volume, although the paper itself is unclassified. Results of a NASA study on acquisition devices are discussed in Ref. 4, and Ref. 5 is a general discussion of the TCPS and the attitude propulsion system. A more detailed report on the TCPS is given in Ref. 6.

B. Attitude Propulsion System

1. Baseline Requirements. The APS must reduce the turning rate at separation (tipoff rate) and perform acquisition immediately after spacecraft launch, and it must perform turns on command throughout the mission life of 10 years. Further, it positions the spacecraft for nine trajectory corrections. A total of 90 science calibration maneuvers are performed. Sixty are roll maneuvers occurring at a rate of one every 1/2 AU. The other 30 are yaw maneuvers, one every 1 AU. The APS provides for twenty

reacquisitions in the event that the spacecraft should lose synchronization with the reference star. In addition, because reaction wheels are used for the primary attitude control of the spacecraft, the APS will provide reaction wheel unloading and, if the reaction wheels fail, will provide a backup limit cycle. Originally, the reaction wheels were to perform the commanded turns. However, it was found that approximately 5 kg (12 lbm) could be saved by trimming some mass from the wheels and assigning the commanded turn function to the APS. The commanded turns require 408 N-m-s (300 ft-lbf-s) in total torque impulse and 0.136 N-m (0.1 ft-lbf) of torque in the pitch axis, with 0.272 N-m (0.2 ft-lbf) in the yaw and roll axes. Because of a slight imbalance between the center of pressure and center of mass of the specific spacecraft configuration, the yaw axis requires 2520 wheel unloadings. About 1000 to 1500 unloadings in pitch and roll axes are required.

2. Implementation. To meet these requirements, the thrust level at the beginning of the mission is 0.444 N (0.1 lbf). Using a 2 to 1 blowdown system, thrust at the end of the mission is about 0.222 N (0.05 lbf) for the APS type of laminar flow control device. The moment arms necessary to meet the torque requirements is 0.3 m in roll, which will be implemented as a couple; and 0.3 m in pitch and 0.6 m in the yaw axis, both implemented as noncouples. Eight of the 16 thrusters are active, and eight are redundant. The total subsystem mass of 14.5 kg (32 lbm) comprises 6 kg (14 lbm) of propellant mass and 8 kg (18 lbm) of dry mass.

As shown in Fig. 88, the thrusters are clustered around the trajectory correction engine. All pitch and yaw thrusters are shown in the figure. An equal number of roll thrusters are located on the other side of the bay, which cannot be seen in this view. The thruster locations were selected to minimize plume interference with other subsystems.

The APS is shown in Fig. 93. Figure 94 is a schematic diagram of the APS. The upper leg of the schematic represents the active APS and the lower leg represents the spare. Two isolation valves are located in proximity to the tank so that the entire branch can be isolated if a catastrophic failure occurs, e. g., a meteoroid striking and breaking a line. However, the redundancy concept allows for a normal replacement of a failed component on a one-to-one basis with the latching valves located near the thrusters in

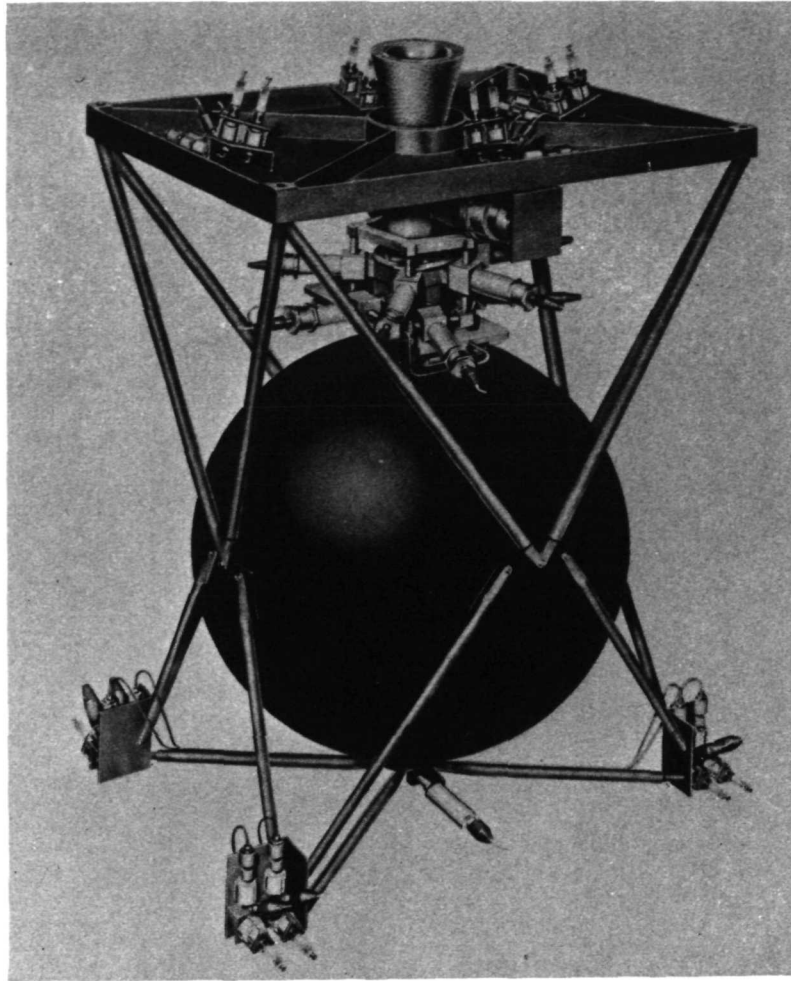


Fig. 93. Attitude propulsion subsystem

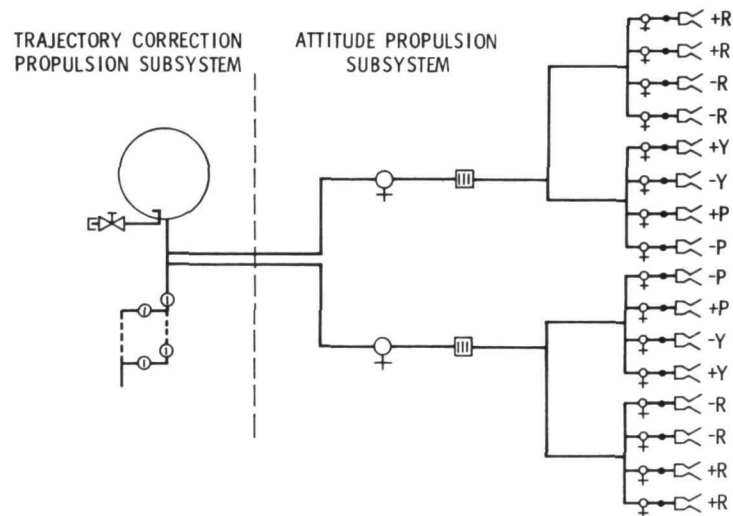


Fig. 94. Attitude propulsion subsystems schematic

the individual branches. For example, if the plus pitch unit failed, it would be replaced by the redundant plus pitch.

Figure 95 is a schematic diagram of a typical "leg" configuration. The latching valve is bistable, and the thruster valve is a continuous duty valve.

3. APS Studies

a. Selection of thruster system. Approximately two years ago, an intensive thruster tradeoff study was made of various types of thruster systems, such as vaporizing ammonia, hydrazine plenum, cold gas nitrogen, and liquid hydrazine catalytic thruster. The primary reason the liquid hydrazine system was selected is that the TCPS propellant is liquid hydrazine, which increases substantially the available reserves which can be used by the APS. Another reason is that, for the given torque impulse required by the mission, the higher I_{sp} of the catalytic thruster, along with the higher thrust itself, permits the thrusters to be located within the propulsion bay in consonance with the modular concept. This location eliminates the need for thermal control for the feed lines because they are all contained within the thermal blanket. Additionally, the lines are not exposed to meteoroid hits. Deployment flexures are not needed because the lines are now very short. Further, the lines do not affect other subsystems because they are not routed through them. The thrusters now can be located where the plume interference with other subsystems is minimum.

The liquid hydrazine system has fewer active components than the hydrazine plenum or gaseous nitrogen system, and it does not require high pressure tankage. Because the valves are sealing a liquid, rather than a gas, the leakage rate is much lower. Also, the liquid hydrazine system has a lower mass.

b. Reliability. For reliability purposes, it is desirable to evolve a simple system which would minimize wear on individual components and maximize thruster life. In addition, the system should not be prone to leakage and valve failure, and, at the same time, should be as flexible as possible. The conclusions from the reliability tradeoff study are that a standby redundancy mode with a one-to-one replacement of failed components and series redundant valves would offer the greatest probability of mission success.

c. Thruster evaluation. A study is being made at JPL to demonstrate the feasibility of the 0.444 N (0.1 lbf) catalytic thrusters. Four designs (three purchased and one JPL design) are being used. The objectives of the study are:

- (1) To verify design agreement with acceptance test data.
- (2) To characterize the thrusters, i. e., to define the limits by tracing or mapping them in both pulse mode and steady state.
- (3) To demonstrate how well they meet the functions and requirements of the TOPS duty cycle. For example, the tipoff rate reduction represents a burn of about 7-1/2 min. The on-time for the commanded turns ranges anywhere from 23 s to 7-1/2 min, depending on the type of turn. Each wheel unloading requires a minimum of 13 pulses in a pulse-mode operation at a 10% duty cycle.
- (4) To accumulate 1000 cold starts on all four designs, i. e., at a temperature of less than 32°C (90°F).
- (5) To accumulate 2600 cold starts on one design after 1000 cold starts for all designs are completed.

Two of the JPL thrusters were integrated with a portable propulsion module in support of the TOPS pitch axis attitude control validation tests in the JPL stellar simulation facility. This program has been completed. In a similar JPL design, the catalyst bed was modified and the thruster then life-tested. During this test series, 1532 cold starts were made consuming a total of 5.1 hours to determine how many cold starts can be achieved. The first phase, and part of the second, were completed for the purchased thrusters. The results of the first phase were in agreement with acceptance test data. The second phase comprises characterizing the thrusters at four different temperatures: 4, 21, 32, and 49°C (40, 70, 90, and 120°F). To date, the work is completed for 21°C, and implementation of a heat exchange system to lower the temperature to 4°C is in process. Approximately 1000 cold starts have been made on three of the engines. Performance as indicated by characteristic exhaust velocity and I_{sp} is steady, and all three engines have successfully completed the tests.

d. Valve evaluation. Approximately two years ago, letters were sent to more than 80 valve vendors to ascertain the availability of valves which could meet the following APS requirements:

- (1) Activation power of 1 to 3 W.
- (2) A maximum liquid flow-rate of about 2.27×10^{-4} kg/s (5×10^{-4} lbm/s).
- (3) Internal leakage on the order of 0.01 standard cm^3 of helium per hour.
- (4) Operation with 2760 kN/m^2 (400 psia) maximum upstream pressure.
- (5) A response time of less than 10 ms.
- (6) All materials compatible with hydrazine.

Because several of these requirements were mutually exclusive with the existing technology, such a valve is nonexistent. However, valves that meet some of these requirements are available and were included in the evaluation program. The general conclusion of the evaluation is that a development program would be necessary during a project phase to develop a valve to conform to these requirements.

Two kinds of actuation units are being considered: (1) the in-line solenoid and (2) the externally actuated. The type of operation is either continuous duty or bistable (latching). The in-line solenoid valve is smaller than the externally actuated and also can be designed with a self-aligning poppet. However, a disadvantage of in-line solenoid valves is that ferrous materials have to be used internally somewhere in the valve actuator, and they would often be in contact with the propellant unless some new design can be devised to avoid this. Sometimes plating is used, but plating involves risks. Externally actuated valves can be designed so that no incompatible materials are ever in contact with the propellant. However, they are larger, and the alignment is more critical because it requires a pivot-point configuration. Two types of bistable latching valves are under consideration: mechanical and magnetic. The mechanical latch mechanism is analagous to a Belleville spring. Once the latch changes its position, it stays there until reactivated. When a magnetic latch is actuated, it is held in the open position by a magnet

until it is commanded to close. A normally closed, continuous duty valve would be used for the thruster valve itself.

In addition to the valve studies, valve sealing designs are being evaluated. The hard-seat valve has been flown extensively. However, it is prone to contamination effects, and the leakage over a long period of time could be a serious problem. For these reasons, the elastomeric, soft-seat seal was selected as baseline for TOPS. The elastomeric seal can be either in the valve body, as in the Marquardt R4D valve, which has been flown on Apollo and Lunar Orbiter, or the seal can be on the poppet itself, as in the Wright valve, which is flown on many Naval Research Laboratory satellites. The poppet geometry that carries the sealing part can be either flat; e. g., in torque motor valves, where alignment is critical; or it can be spherical, as in Rocketdyne Gemini valves; or it can be conical as in the Marquardt R4D valve.

Evaluations of solenoid valve sealing materials are also being conducted. Six seat designs made of TFE Teflon and one of Teflon FEP were evaluated. Teflon is compatible with hydrazine, and if implemented with a retained seat, the cold flow problem can be overcome. However, the radiation fields which are defined for TOPS are severe, and Teflon itself is approximately 1 or 2 orders of magnitude more sensitive to radiation than other types of polymers. The Parker EPR (ethylene propylene rubber) (E-515-8), which has been used on ground support equipment, is compatible with hydrazine, although some swelling does occur. Its lifetime would probably be limited, making it useful only for a mission of about one or two years, rather than for ten years. The E-515-8 is a proprietary compound, which makes quality control difficult. Some EPRs are good, and probably compatible with hydrazine, whereas others, even from the same batch, are not. To eliminate this difficulty, the USAF and JPL have made extensive studies on the various types of polymers, specifically, the EPT (ethylene propylene terpolymer) series. EPT 10 was developed at JPL. The HYSTL-filled EPT or the AF-E-102 appears to be one of the most promising polymers for a long mission and a hydrazine propellant. Four valve-seat designs are being evaluated with this particular compound. Because HYSTL is a hydrocarbon, rather than a fluorocarbon, it is much less sensitive to radiation environments, and its mechanical characteristics are good. Another promising compound, DuPont AF-E-124D, is being investigated. This

fluorocarbon is similar to Teflon and is compatible with hydrazine. Its mechanical characteristics are good. Preliminary radiation tests indicate that it is much more tolerant of radiation environment than TFE or FEP Teflon. However, it is too early to know whether or not its tolerance is as good as the AF-E-102. Wright-Patterson Air Force Base is the organization responsible for investigating these polymers. Two seat molds have been designed to form and test the AF-E-102 compound and the AF-E-124D Teflon in conjunction with the Marquardt R4D valve.

The conical seating arrangement is shown in Fig. 96. The conical valve seating configuration is one of the better designs because the poppet makes a metal-to-metal contact with the polymer seal located upstream. The valve poppet/seat shown is slightly different from that of the Marquardt R4D valve in that if this valve incorporates a 90-deg poppet cone angle whereby the seat and cone meet perpendicularly, there is no sliding.

e. Filter evaluations. The sintered metal filter was one of the first to be considered, but it was eliminated because it sometimes tends to generate more particles than it filters. The wire mesh filter, in particular, the 5- μm absolute is considered state-of-the-art. The stacked disk filter with a labyrinth filter element design was selected as baseline. Specifications for a 1- μm absolute labyrinth filter were defined, and procurement was initiated. The filter was developed, assembled, and evaluated, using a flowrate of about 0.0009 kg/s (2×10^{-3} lbm/s), which is approximately 4 times the normal APS single-leg flowrate. The reason for the high flowrate was to determine if the filter could sustain a maximum or worst-case condition, i. e., a tipoff rate reduction when the thrusters for three axes could be firing simultaneously. This specific filter sustained approximately 345 kN/m^2 (50 psid) change in pressure. The actual etched depth versus flow rates and pressure changes is not yet determined. However, there was no media migration in excess of 1 μm absolute; there were some microscopic erosion patterns on some of the disk elements, which are being investigated. The filters themselves were vibration-tested to the TOPS specification and were found to have a 1- μm rating (actually less than 1 μm absolute) inasmuch as a 1- μm glass bead never passed through. Further investigation may prove the real rating to be about 0.5 μm .

f. Flow control evaluation. The TCPS feed system goes from 2760 kN/m² down to 1380 kN/m² (400 to 200 psia) and has an APS injector inlet pressure of about 1035 ±345 kN/m² (150 ±50 psia), depending on the thruster design. Obviously, some form of flow impedance device is needed. In addition, the APS subsystem has a low mass flowrate of 0.00027 kg/s (5×10^{-4} lbm/s). A flow impedance device eliminates the necessity to meter with a valve, which would require a very high valve response. A flow impedance device also provides the means whereby final trim for thrusters can be obtained. For example, the impedance device can vary the output of one thruster so that it is equal to the output of another thruster.

Orifice devices were eliminated early in the study because the small diameters required makes them prohibitively susceptible to contamination.

A capillary tube, which appears to be feasible, has an internal diameter of about 0.25 mm (10 mil) and a length of about 25.4 to 38.1 cm (10 to 15 in.) in a coiled configuration to form a compact package. Although the internal diameter is the same throughout, an 0.18- or 0.20-mm (7- or 8-mil) particle could get jammed in the tube; thus, it is susceptible to contamination. Another promising device, the Lee Company Viscojet, was evaluated at JPL, and one is being used now in tests. The Viscojet has a minimum passage of 0.38 mm (15 mil), and it is similar to several orifices in series. The liquid has to follow a rather tortuous flowpath through a wafer, and energies are dissipated in several expansion and contraction passages.

4. Areas for Further Investigation

a. Propellant and system contamination. Contamination studies include propellant cleanliness, both chemical and particulate, and the type of system contamination which is tolerable.

b. Filtration. Filtration requirements must be defined. A 1- μ m absolute filter may not be feasible or necessary. Probably, a filter should not be used if it must be constrained to the degree that it will clog up during the mission. Perhaps use of a 5- or a 10- μ m absolute filter would be better.

c. Thruster life expectancy. As discussed in Section VII-B-1, the thrusters must perform the backup limit cycle mode if the reaction wheels fail. If a failure occurs at the end of five years, the thrusters and valves would have to be actuated for approximately 75,000 starts in a limit cycle mode for the remainder of the mission. In view of this performance

requirement, it appears that the thrusters would have to be augmented by a heating source, either a radioisotope or an electrical heater whose energy could be diverted from the reaction wheels. This type of backup limit cycle would occur only in the event of a double reaction wheel failure.

d. Compatibility of material with radiation and propellant. Compatibility of polymers with propellant and radiation must be investigated further. Polymer life-expectancy beyond two years has not been investigated to any extent, nor has long-term polymer compatibility with hydrazine been demonstrated.

e. Failure detection. A failure detection scheme should be developed, e. g., bed temperature could be monitored or a thermocouple mounted near the injector to detect any increase in temperature, which might indicate that a leak has developed; or, conceivably, a reaction-wheel rate change, such as an increase in the number of unloadings in a certain axis, might mean there is a failed open valve or a leak of some kind.

f. Magnetic interference. Conceivably, a valve could be developed to meet the magnetometer requirements when it is de-energized but, when it is energized, special shielding or compensating magnets would be used to meet the requirements.

g. Valve seat life. Study of valve seat life-expectancy should be expanded to include particle absorption capability to determine whether or not the seat will be scored, if it absorbs a particle remaining or generated in the system.

h. Effects of the exhaust plume. Although the APS was implemented to have minimum impingement on any other subsystem, the exhaust plume should be investigated further. References 7 through 10 discuss in detail the JPL thruster evaluation, the 1- μ m absolute filter, and the APS subsystem technology, respectively. A more detailed report on the APS is given in Ref. 11.

C. Long-Life Liquid Propulsion Technology

The long-life liquid propulsion technology includes the investigation of hydrazine compatibility with materials for 10-year missions, a radioactive, nondestructive test method for determining hydrazine feed performance, and radiation effects on hydrazine. The study of radiation effects was initiated before the inception of the TOPS Project.

1. Hydrazine Compatibility With Materials for Ten-Year Missions.

A literature search and a survey of the data available on material compatibility revealed that 10-yr data are lacking and that data from different sources are inconsistent. As a result, it has been necessary to project 1/2 to 2-yr data to a 10- or 12-yr application.

A current testing program at Edwards Test Station is under way to verify various material compatibility data. The program is also being used to investigate new areas; e. g., purified hydrazine. After available information is surveyed and verified, the materials are rated for a 10-yr application with hydrazine.

Several types of rating systems can be devised: a percentage system, a point system, or a letter system. JPL is using a system of two ratings and two qualifiers. Materials that are acceptable without any qualifications for mission applications are rated "A". Materials not acceptable under any conditions are rated "N". Some materials are acceptable with qualifications. Materials with compatibility over a portion of the environment only are qualified "R" for restricted applicability. For example, some materials are limited to a given temperature. If data are incomplete, the rating is qualified "I". In this instance, it may be that the specimen only was analyzed, not the propellant; or it may be found that no analysis was made to determine whether or not the constituents within the propellant were at the minimum or the maximum rate, as defined in the specification. In some cases, documentation is incomplete.

Table 37 gives the compatibility ratings and qualifiers for the basic materials as applied to the TOPS. The rating "A" for aluminum is qualified "I" because the data were insufficient for extrapolating. The 300 series of corrosion resistant steel, qualified "R", is restricted by a temperature limitation. Titanium is qualified "I" because the data are incomplete.

Table 38 lists the basic materials and the components in which they would most likely be used. This information should not be construed as limiting the choice of material for a specific component.

Figure 97 shows a typical hydrazine specimen-capsule used in the JPL verification test program. Three hundred and seventy-six of these specimen capsules are stored at the JPL Edwards Test Station. All contain specification-grade hydrazine except for 24 that contain purified hydrazine. The metallic

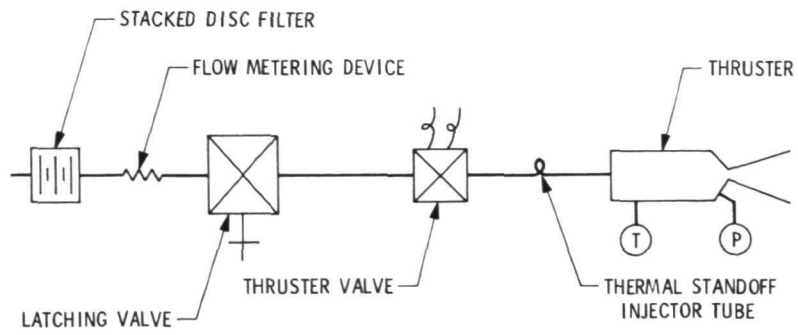


Fig. 95. Attitude propulsion subsystem, typical leg configuration

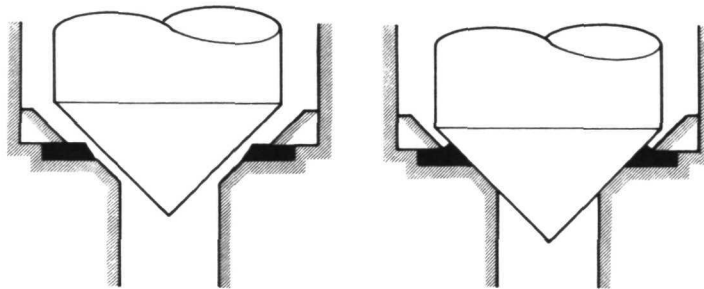


Fig. 96. Conical valve seating configuration

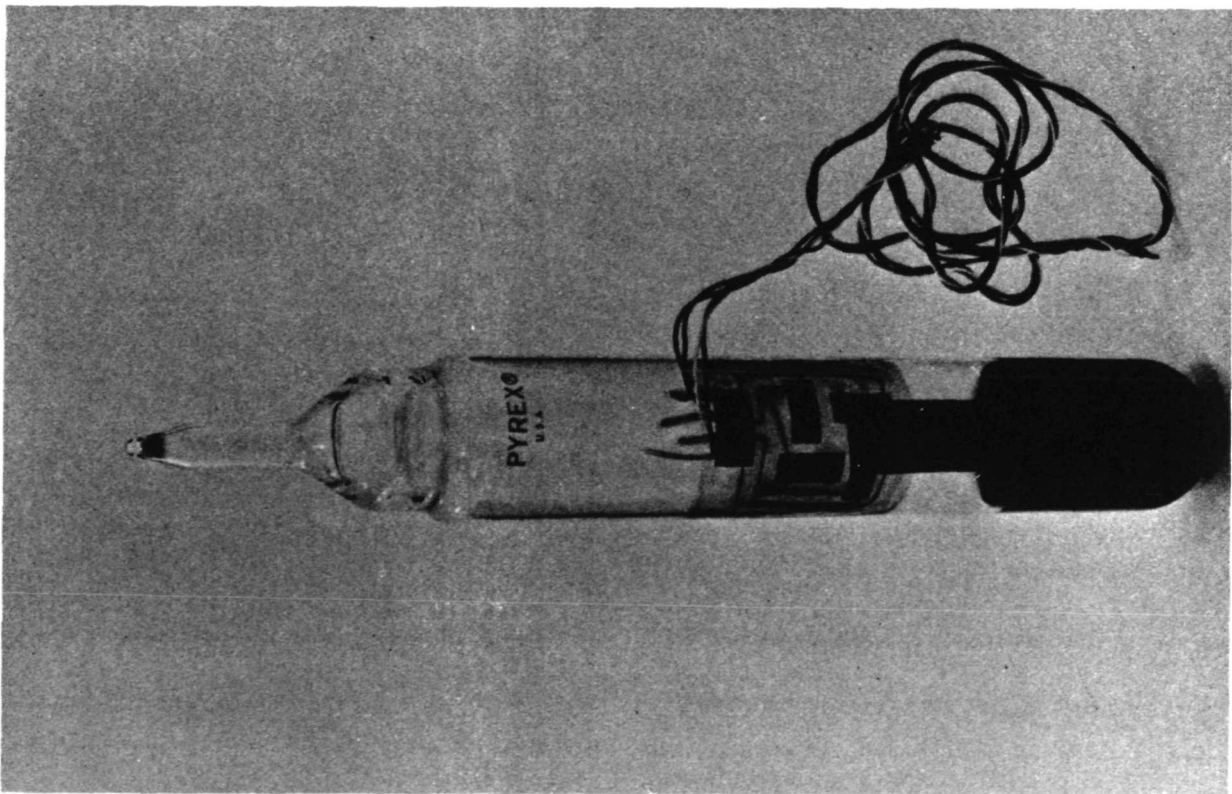


Fig. 97. Material compatibility, specimen capsule

Table 37. Compatibility rating of materials in contact with hydrazine

Material	Rating	Qualifier
Aluminum		
6061-T6	A	I
1100	A	I
Corrosion-resistant steel		
304L, 316L, 347	A	R, I
430, 446	A	I
17-7 PH	A	I
Titanium		
6Al-4V	A	I
Other		
Chrome plate	A	I
Teflon (TFE)	A	I

Table 38. Materials in contact with hydrazine

Material	Component
6Al-4V Titanium	Propellant tank
	Propellant acquisition device
6061-T6 Aluminum	Propellant fill valve
	Explosive valves
	Filter
	Orifice assembly
	Propellant lines
1100 Aluminum	Metallic seals
304L CRES	Transducers
	Capillary tubing or Viscojet
316L CRES	Transducers
347 CRES	Filters
	Solenoid valves
430 CRES	Solenoid valves
446 CRES	Solenoid valves
Chrome Plate	Solenoid valves
Teflon (TFE)	Solenoid valves

test specimen shown in the figure is called a slug specimen. Only certified materials are used; and the fabrication procedures, etc., are documented so that at all times complete traceability is maintained. Thus, if corrosion occurs, it is possible to retrace the procedure to determine the cause. The transducer consists of four strain gauges attached to the outside of the Pyrex glass capsule. This transducer monitors the internal pressure within the capsule so that if the pressure goes above 345 kN/m^2 (50 psia), the capsule can be removed. The transducer also transmits the information to the remote control room, where the data are recorded and evaluated. The top of the capsule is hermetically sealed to isolate the elements within the capsule from outside influences, with the exception of temperature. The capsules are stored at a constant temperature of 43°C (110°F), and they are removed periodically from test, or as required. Post-test analyses of both the specimen and the residual hydrazine are then made. The level of the post-test evaluation varies from specimen to specimen, depending on the interest in a specific test, which can be extended at this test facility for an indefinite period of time. Some specimens have now been in test for two years. The large number of specimens not only increases the amount of data and permits replication, but makes it possible to use semiproduction techniques during the preparation phase.

Figure 98 shows the various kinds of test specimens used in the JPL program. The slug specimen is used as a basis of comparison with the other types of specimens shown. Two types of bi-metal specimens, made of dissimilar metals, are used to investigate galvanic corrosion: (1) dissimilar metals held in contact with a glass clip, and (2) dissimilar metals separated by a special glass separating device. Stress specimens are mounted in special stress fixtures and are stressed to 67% yield. Welded and braised specimens are being tested, as well as slug specimens which are first plated and coated with lubricant.

The long-term storage characteristics of purified hydrazine compared with those of specification-grade hydrazine are being investigated. First, a definition for purified hydrazine was developed, and then the permissible quantities of aniline, water, and ammonia were reduced to trace amounts. Further tests may indicate that one of these constituents may, at a certain desirable level, improve the long-term hydrazine storage. In this event, the specification would be rewritten to improve 10- or 12-yr performance predictions.

The initial lot of specimens for the study of the purified hydrazine problem are shown in Table 39. These specimens were placed in test the latter part of 1971. Several slug specimens were added to the basic materials. Twelve hydrazine specimens were added as controls. Specimen capsules will be withdrawn periodically for post-test evaluation.

Table 39. Long-term storage specimens, purified hydrazine

Materials	Number in test	Type
6Al-4V Titanium	4	Slug
6061-T6 Aluminum	4	Slug
304 Stainless steel	4	Slug
Hydrazine (control)	<u>12</u>	
	Total 24	

A recent post-test finding was hydrogen embrittlement in 6Al-4V titanium, caused by a primary reaction between residual Freon, which was used to clean the specimen, and the hydrazine, which was later added to the capsule. A secondary reaction took place with the titanium forming the embrittlement. A NASA Pre-alert (Ref. 17) has been published to describe this incident, and the use of isopropyl alcohol, rather than Freon, is recommended as a cleaning or rinsing agent with the titanium because the isopropyl alcohol is better than Freon for removing inorganic material and does not interact with hydrazine or titanium.

2. Radioactive Nondestructive Test Method. The formation of gelatinous material which contributes to flow decay has been observed in some propellants. One published reference describes the formation of gelatinous material in hydrazine. Test instrumentation at present is not sensitive enough to detect the onset of this flow decay. Therefore an ultrasensitive method of measurement called the radioactive tracer technique has been used to test TOPS components. This technique consists of thermal neutron activation to make the constituents radioactive, then sensing the gamma rays. The technique has been demonstrated using TOPS capillaries and screen filters. The internal diameters of the capillaries were 0.203 mm

(0.008 in.) and 0.330 mm (0.013 in.); the filter was 10 μ m absolute. To date, no flow decay has been found. The radioactive tracer technique can detect less than 1 ppm of a given constituent, with estimations as low as 1/100 ppm.

3. Radiation Effects on Hydrazine. Data available in the published literature were surveyed and inquiries were made by the contractor at various government agencies to obtain unpublished information. Results of the survey disclosed a lack of data about radiation effects on hydrazine. It was decided to perform some verification testing in this area.

For the purpose of these tests, a cobalt 60 source was used to irradiate capillary tubes and a stacked-disk filter. Figure 99 shows the radiation test specimen used during these tests. The capsule can be filled to various fractions of the volumes shown. Control specimens were placed outside of the radiation field to detect any autodecomposition of the hydrazine or any reaction which might take place between the hydrazine and the capsule wall. The results were then subtracted from the overall radiation result to get radiation effects only.

The data obtained during the test, shown in Fig. 100, revealed radiation-caused gas formation. The curve on the right shows the high dose rate; the curve on the left is the low dose rate. The low dose rate caused more gas to form than the high dose rate. For this reason, the TOPS requirement for a low dose rate, as well as the total dose for the entire program, should be reexamined. Data are available for hydrazine in aluminum capsules, and it agrees closely with the high dose-rate curve shown on the right side of the figure.

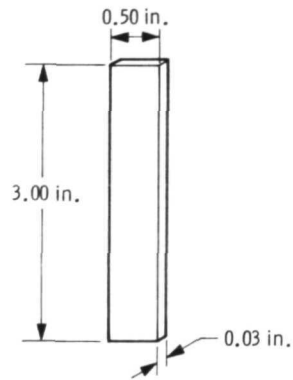
It is believed that the feasibility of using hydrazine in an RTG-radiation environment has been established because the TOPS total dosage is low, similar to the values used in the test program. No hydrazine radiation problem is foreseen. However, additional tests on radiation effects should be made using the actual total radiation dose and the dose rate which will be experienced by the hydrazine feed system.

References 12 through 19 give further details of the long-life liquid propulsion technology.

D. Pyrotechnic Subsystem

The Pyrotechnic Subsystem provides control and switching circuitry for firing squib-actuated devices, enabling release of electromechanical

• CONFIGURATION
(SLUG-TYPE)



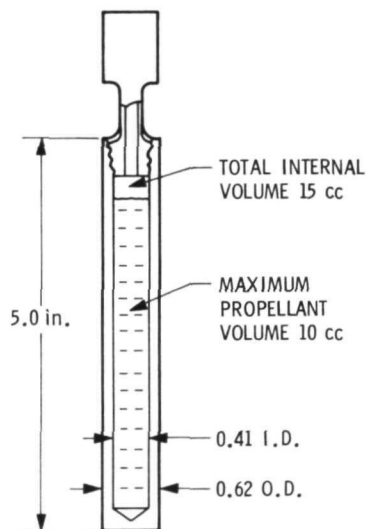
• METAL SAMPLES

- SLUG (Ref)
- BI-METAL CONTACT
- BI-METAL SEPARATED
- STRESSED (67% YIELD)
- WELDED
- BRAZED

• COATINGS

- PLATING
- LUBRICANT

Fig. 98. Hydrazine material compatibility, test specimen description



• PROPELLANT

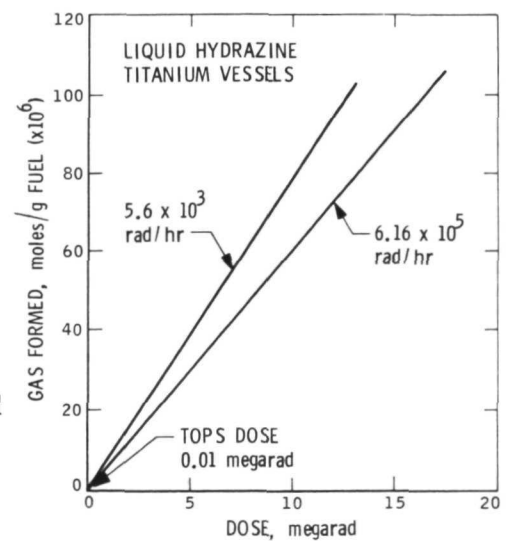


• CAPSULE MATERIAL

- TITANIUM
- ALUMINUM

Fig. 99. Radiation test specimen

Fig. 100. Radiation-caused gas formation



devices, and telemetry monitoring of critical spacecraft pyrotechnic events. Platform and boom unlock and propellant valve operate are typical of the 20 squib-actuated functions performed by the subsystem. Typical of the 12 electromechanical functions are latching and nonlatching valve operate and solenoid release operate.

The Pyrotechnic Subsystem consists of various pyrotechnic devices, including pinpullers and spacecraft release, the squibs to actuate the devices and valves, and the devices to enable the rocket engine propellant valve during maneuvers and to release the encounter science platform, antennas, and booms for the RTG, science, magnetometer, and plasma wave detector. A pyrotechnic control unit (PCU) contains the control and switching circuitry to actuate squibs and electromechanical valves.

The design assures that no single-component malfunction can cause a catastrophic mission failure. The concern over spurious signals led to a design with two switches in series requiring two commands to initiate an event. In addition, the second switch is an electromechanical stepping type, which assures the order of events.

A parallel redundant unit is included for high subsystem reliability. Thus, all devices are redundantly initiated on command from the PCU and achieve internal redundancy either through the use of two single bridgewire squibs or a single squib with two bridgewires. Voltages and stepping switch position are telemetered and used by the CCS for monitoring subsystem operation and determining any necessary corrective action.

The TOPS Pyrotechnic Subsystem design is constrained by radiation immunity, magnetic cleanliness, weight, power consumption, assurance that no single-point mode of failure will be catastrophic, selection of materials and electronic parts from approved lists, and compliance with provisions of the range safety manual.

Consistent with the TOPS Project philosophy, two specific areas were designated for investigation in the Pyrotechnic Subsystem: a reliable squib-firing circuit and prelaunch checkout of the subsystem over the communications link.

Reliability in squib firing is achieved by a two-step actuation of squibs, and a maximum of two bridgewires to be fired simultaneously. The design

philosophy prefers small events because of the reduced stress placed on the system and because they eliminate the need for stored energy. TOPS pyrotechnic events can be scheduled during the mission when excess power is available. To this end, 75 W for 50 ms was allocated for each event.

Figure 101 illustrates two-step actuation of squibs. Two switches are located between the power source and the squibs. In the first step, the desired squib is selected through the enable switch. In the second step, the selected squib is fired by the fire switch. Proper operation of the enable switch is confirmed by telemetry before the fire switch is commanded. The two switches are operated by independent commands.

As shown in the block diagram of the baseline squib firing circuit (Fig. 102), commands are received through the remote decoder arrays, and the command pulses are broadened to usable duration by signal conditioning circuits.

The enable switch must be an electromechanical set-reset type that provides extremely high confidence that the desired squib is being enabled and in reading out the switch position. It should hold the set or reset position with little expenditure of power.

The fire switch must be a momentary, solid-state type, and it must act as a constant-current source of power, thus protecting the spacecraft power supply from shorted squibs. The squib current is independent of changes in harness or cabling resistance.

The two alternate mechanizations of the enable switch are shown in Fig. 103. The upper sketch illustrates a stepping switch, the lower sketch an array of relays. Representative stepping switches and relays were successfully tested at 8.0 A, which is twice the TOPS nominal squib current. This type of current switching is not difficult for an electromechanical device because switching does not occur while current is flowing.

Some alternate mechanizations were considered but rejected. The Mariner circuit lacks series redundancy in the main switch, and also contains some radiation-sensitive components. All solid-state enabling switches investigated were considerably more complex than their electromechanical counterparts.

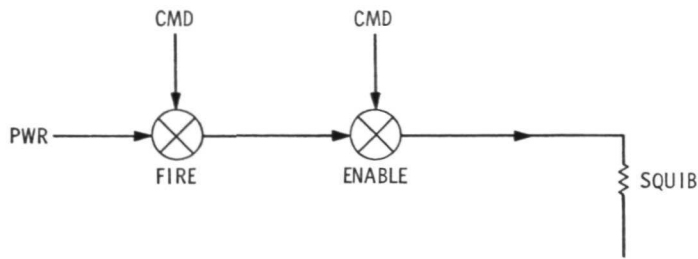


Fig. 101. Two-step actuation of squibs

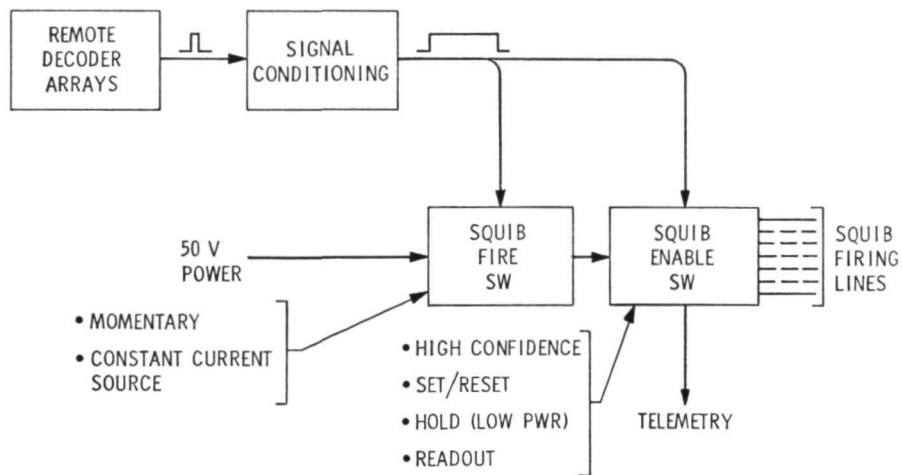


Fig. 102. Baseline squib firing circuit

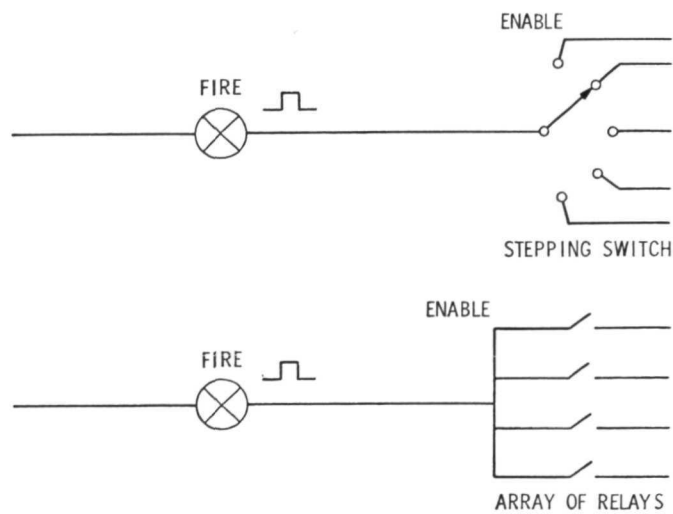


Fig. 103. Alternate mechanizations of enable switch

The TOPS Project also studied the subsystem checkout over the communications link. Only basic concepts were determined; the final mechanization was not established.

It was considered desirable to avoid the electrical anomaly of direct-access wires during subsystem checkout. Subsystem voltages and switch positions will be available through telemetry, and it is believed that adequate subsystem checkout over the RF link could be accomplished if the energy in the squib-firing pulse could be quantized. The capacity of the measurement processor is not sufficient to quantize the squib-firing pulse directly along with other functions simultaneously being required of it. Therefore, the baseline subsystem contains circuitry to quantize the energy of the squib pulse for readout through the processor.

E. Pyrotechnic Devices

Because some of the TOPS subsystems and science experiments were in the conceptual design phase at the end of the Project, the pyrotechnic devices to be used lacked specific definition. For this reason, specific designs are not discussed in this section.

Figure 104 shows the TOPS spacecraft with some typical pyrotechnic devices. A pyrotechnic device is defined as both the electrical squib device and the pyromechanical device installed into it; e.g., a pin-puller, a release nut, of a squib valve.

1. Functional Requirements

- (1) Four hardpoint devices are required to release the spacecraft from the launch vehicle. All four must operate; V-bands will not be used. Structural requirements forced this configuration.
- (2) Eight squib valves, two for each RTG, are required to dump gas.
- (3) Two simple pin-pullers/pin-pushers in the latching mechanism are necessary to release the RTG boom.
- (4) One hardpoint device is used to release the science platform.

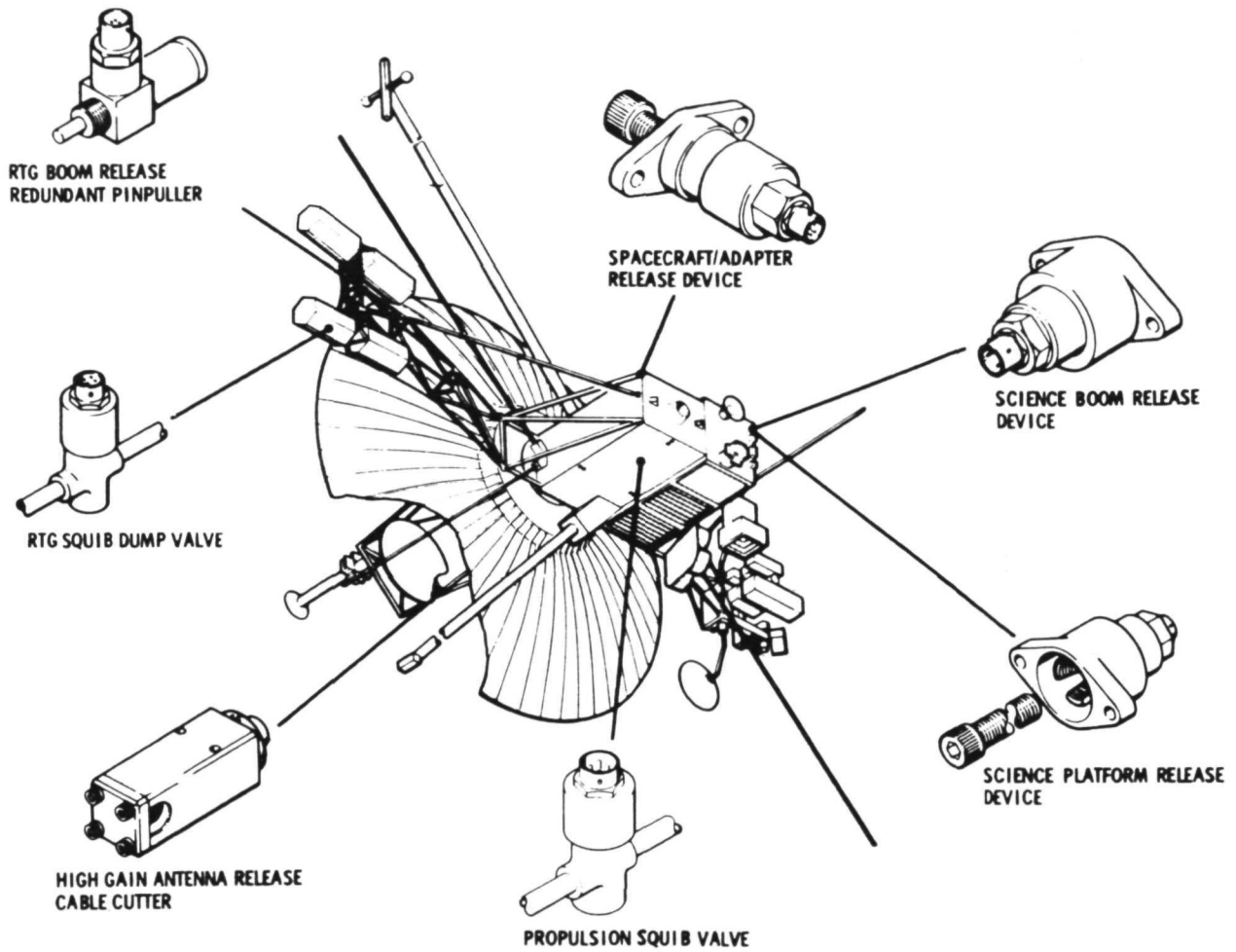


Fig. 104. Typical pyrotechnic devices

- (5) One hardpoint device releases the science boom. The devices in (1), (4), and (5) are all preload tension devices at 6804 kg (15,000 lb), 4530 kg (10,000 lb), and 2268 kg (5000 lb) of tension, respectively.
- (6) Either of two cable cutters releases the high-gain antenna.
- (7) A simple clevis pin-puller/pin-pusher mechanism, like the RTG boom release, releases the medium-gain antenna.
- (8) Ten squib valves for propulsion propellant isolation.

The functions in (1) through (8) all take place quickly after launch. The only pyrotechnic function that will be performed in deep space (after 10 yr of mission life) is the propulsion valve actuation. The propulsion valve squibs are, at the present time, dual-bridge wire, high-pressure cartridges.

2. Constraints. In addition to the TOPS-unique constraints, such as weight, etc., the following basic constraints apply to the pyrotechnic subsystem:

- (1) The propulsion valve squibs must have the capability to survive the long-term environment of RTG radiation and the proton radiation environment in the Jovian belt. This constraint could seriously affect the selection of the pyrotechnic material in the squib.
- (2) The failure of any single pyrotechnic device must not cause science or mission failure. This is particularly important in a four-hardpoint separation system, where all four devices must work.
- (3) The squib devices must be magnetically clean.
- (4) Devices must generate minimum shock to spacecraft structure. Experience with the Viking spacecraft indicates that the TOPS electronics density and the proximity of electronics to the hardpoint pyrotechnic mechanisms is such that this constraint could be severe. The devices must be selected, designed, and qualified to generate a minimum shock. Minimum shock is yet to be defined.

- (5) The devices must not emit any pyrotechnic gasses or particles upon actuation. A large percentage of pyrotechnic devices being presently used on spacecraft do generate pyrotechnic gases into a propellant system, or into the atmosphere, or around the science instruments.

3. Subsystem Approach. The general approach to resolving the constraints and meeting the functional requirements is to use dual-mode pyrotechnic devices for each function. A dual-mode pyrotechnic device is one pyrotechnic assembly that encompasses two independent pyrotechnic mechanisms, each of which operates under a distinctly different mechanism. Thus, the failure modes would be uncommon. An example of this type of device is the lunar module descent engine, which has an explosive-bolt explosive-nut dual-mode mechanism. Commercially available and JPL-designed devices like this are presently being evaluated.

The devices are to remain hermetically sealed after actuation, i. e., a leakage no greater than 10^{-6} standard cm^3/s . A design goal is that the devices be capable of preflight pneumatic testing. Actuation reliability must be demonstrable at a minimum of 0.999, and the confidence level must be 90%. It is planned to establish design guidelines whereby the energy needed to actuate a device and the energy of the squib or pressure cartridge can be determined. Reliability margins can then be established. In the past, a squib was fired with a 50% undercharge and then with a 50% overcharge, and the actual margin was unknown.

Devices which require swaging, spalling, or plastically deforming cylinders are not recommended. Instead, the devices should be simple, piston cylinder devices. Because of the shock constraints, detonating materials or devices are to be avoided unless a detonating device mounted in a particular configuration can successfully solve a functional requirement. Pressure devices are to be actuated by the JPL standard squib or its equivalent. This standard squib is a high-pressure electro-actuated device which can be used in either a single-bridge-wire or dual-bridge-wire mode. The squibs, to be flown, should be built, selected, and qualified after being electrothermally nondestructively tested. During the past three or four years, JPL has been developing and refining an electrothermal nondestructive test technique to examine the inside of an assembled squib for certain failure mechanisms that

cannot be uncovered by the common bridge-wire resistance technique, X-ray, weight, etc. Basically, this technique consists of pulsing the bridge wire of a squib with about 0.4 A or one half the level of the no-fire pulse for about 100 ms on and 100 ms off. Because of the temperature coefficient of resistance of the bridge-wire material, a heating curve of that bridge wire can be displayed on the oscilloscope, and the thermal time constant of the squib can be quantitatively determined. Certain failure mechanisms like nonhomogeneity of the pyrotechnic material on the bridge wire are easily observable.

4. Status. The status of the pyrotechnic device is as follows:

- (1) A study of the effects of radiation on pyrotechnic materials and squibs has been in progress for about 18 months.
- (2) Development of electrothermal nondestructive techniques has been completed. These techniques were used on the Mariner Mars 1971 project, and it is planned to use them on the Mariner Venus-Mercury 1973 project and on the Viking program.
- (3) Dual-mode devices are currently being analyzed and evaluated.
- (4) Pyrotechnic shock-reducing techniques are being reviewed, analyzed, and evaluated. Experience on the Viking program indicates that the way to reduce shock is to change the structure configuration rather than to change the inside of the device itself.
- (5) The post-actuation hermetic seal using the bellows device, which can either expand or contract and can completely contain the pyrotechnic gases, is being examined. This concept is in the detail design stages and it appears to be good.

5. Radiation Study. A TOPS study was made of the effects of radiation on pyrotechnic squibs and materials. A literature search made about 18 months ago indicated that little was known of low flux rates on pyrotechnic materials. Most of the data was taken at a fast rate, within milliseconds or microseconds, rather than over a long period of time. To obtain some quick engineering information on whether or not there was a serious radiation

problem, typical pyrotechnic materials were selected, and the materials and the squibs were irradiated with neutrons and gamma rays at two different rates: 5 and 25 times the present profile for TOPS. Protons were excluded from the study because it is believed that the damage they might cause could be inferred from an analysis of neutron- and gamma-ray damage. In the gamma ray tests, approximately 1400 evacuated Pyrex test tubes were used with approximately 200 squibs and with pyrotechnic materials, like zirconium, potassium perchlorate, etc. Materials both with and without binders were tested. The 1400 test specimens are presently in accelerated damage temperature environments. Periodically, samples from both environments are taken out and either test-fired or examined against control units to determine any damage caused by the radiation. Damage evaluation techniques are, for the most part, established and consist of the differential scanning calorimeter for the pyrotechnic materials; nondestructive test techniques, previously described; gas evolution for the pyrotechnic materials; and thermoluminescence. Preliminary data to date reveal physical and chemical changes. The significance of the changes is not yet known, but will be determined during the next three months.

Further details on pyrotechnic devices are given in Refs. 20 through 24.

REFERENCES

1. Heidenreich, G. R., "TOPS Trajectory Correction Engine," in Supporting Research and Advanced Development, Space Programs Summary 37-63, Vol. III, pp. 227-235. Jet Propulsion Laboratory, June 30, 1970.
2. Heidenreich, G. R., "TOPS Trajectory Correction Engine Testing," in Supporting Research and Advanced Development, Space Programs Summary 37-64, Vol. III, pp. 153-157. Jet Propulsion Laboratory, Aug. 31, 1970.
3. Heidenreich, G. R., Development of Advanced Monopropellant Reaction Control Systems for Outer Planet Missions, paper presented at the 12th JANNAF Liquid Propulsion Meeting, Las Vegas, Nov. 17-19, 1970.
4. Investigation of Space Storable Propellant Acquisition Devices, Final Report under Contract NAS7-754, MCR-70-171, Vols. I and II, Martin Marietta Corp., Marietta, Ga., October 1970.
5. Baughman, L. E., "TOPS Spacecraft Propulsion Subsystem," Aeronautics and Astronautics, Vol. 8, No. 9, pp. 77-82, September 1970.
6. Long, H. R., and Bjorklund, R. A., Trajectory Correction Propulsion for TOPS, Technical Report 32-1571, Jet Propulsion Laboratory, Pasadena, Calif., Nov. 15, 1972.
7. Nunz, G. J., "Experimental Evaluation of a Miniature Catalytic Hydrazine Thruster," AIAA Paper No. 71-706, presented at AIAA/SAE 7th Propulsion Joint Specialist Conference in Salt Lake City, Utah, June 14-18, 1971.
8. Test Report-Evaluation of DuPont LRV 448 as a Seat Seal Material in the Marquardt R4D Engine Valve, Final Report, Report No. S-991, The Marquardt Company, Van Nuys, Calif., January 1971 under JPL Purchase Order GK-541658-01.
9. Evaluation Test Report Filter Assembly Fluid, 1 Micron Absolute, Disc Labryinth Part No. 9-580, Report No. 247, Wintec Corp., Los Angeles, Calif., May 1971 under JPL Purchase Order AQ-541 867.
10. Moynihan, P. I., "TOPS Attitude Propulsion Subsystem Technology," JPL Quarterly Technical Review, Vol. I, No. 3. Jet Propulsion Laboratory, Pasadena, Calif., October 1971.
11. Moynihan, P. I., Attitude Propulsion Technology for TOPS, Technical Report 32-1560, Jet Propulsion Laboratory, Pasadena, Calif., Oct. 31, 1972.
12. Advanced Spacecraft Valve Technology Compilation, Volume I, Mechanical Controls, Group Report No. 12411-6012-R000, TRW Systems, Redondo Beach, Calif., under NASA Contract NAS7-717, July 1970.

REFERENCES (Contd)

13. "Material Compatibility - Phase II," in Supporting Research and Advanced Development, Space Program Summary No. 37-60, Vol. III, Dec. 31, 1969; No. 37-61, Vol. III, Feb. 28, 1970; and No. 37-65, Vol. III, Oct. 31, 1970. Jet Propulsion Laboratory, Pasadena, Calif.
14. Results of Long-Term Storage Tests for Compatibilities of Spacecraft Materials with Hydrazine and Hydrazine Mixtures, Report 951581-6. Stanford Research Institute, Menlo Park, Calif., Oct. 1, 1967.
15. Specimen/Capsule Preparation Used on the JPL Material Compatibility Program, Final Report, PSI Report No. 525902-1, Pressure Systems, Inc., Los Angeles, Calif., April 1970.
16. Pullen, K. E., Application of Radioactive Tracer Techniques to Flow Decay Problems, Final Interim Report, No. D 180-12741-1. Boeing Aircraft Co., Seattle, Wash., December 1970.
17. Kircher, J. F., and Vaughn, D. A., Radiation Effects on Liquid Propellants, Part 2, Final Report, NASA CR-109767, Battelle Memorial Institute, Columbus, Ohio, Jan. 22, 1971.
18. Dolder, M. P., et al., Chemical and Metallurgical Analyses of 6Al-4V Titanium Test Specimens Exposed to Hydrazine (N₂H₄) Liquid Propellant, Report No. SRI-951581-11, Stanford Research Institute, Menlo Park, Calif., April 15, 1971.
19. Test Specimen, Metallic, 6Al-4V Titanium, Immersed in Hydrazine, and Glass Encapsulated, NASA Pre-Alert, Alert No. E4-70-03A. National Aeronautics and Space Administration, Washington, D.C., August 10, 1971.
20. Mitchell, D. H., "Flight Separation Mechanisms," NASA Space Vehicle Design Criteria (Structures), NASA SP-8056. National Aeronautics and Space Administration, Washington, D.C., October 1970.
21. Rosenthal, L. A., and Menichelli, V. J., Nondestructive Testing of Insensitive Electroexplosive Devices by Transient Techniques, Technical Report 32-1494. Jet Propulsion Laboratory, Pasadena, Calif., Oct. 2, 1970.
22. Rosenthal, L. A., and Menichelli, V., Terminated Capacitor Discharge Firing of Electroexplosive Devices, Technical Report 32-1521. Jet Propulsion Laboratory, Pasadena, Calif., Feb. 15, 1971.
23. Varsi, G., "Radiation Effects on Pseudostable Materials for Long-Term Space Missions," Trans. Amer. Nucl. Soc., Vol. 14, No. 2, pp. 549-51, October 1971.
24. Menichelli, J. V., and Rosenthal, L. A., Interrelationship of Nondestructive Testing to Fault Determination, Seventh Symposium on Explosives and Pyrotechnics, pp. 11-5-1 to 11-5-7. Franklin Institute Research Laboratories, Philadelphia, Pa., 1971.

VIII. SCIENCE EXPERIMENTS

A. Science Instrumentation

When the science objectives for the first exploratory missions to the outer planets were discussed in Section II of this report, little was said about the scientific instruments themselves. Because of weight and power limitations, all worthwhile experiments proposed for a mission cannot be flown. For this reason, a balanced payload of instruments, which together can meet all or most of the scientific objectives, was selected for TOPS.

It should be stressed that the TOPS payload is a single, rather than the only, payload for the outer planet missions. When NASA conducts the final competition for the selection of flight payload, there may be some significant changes from this set of instruments based on additional knowledge gained in the last two years. However, these instruments are sufficiently representative for the design of the spacecraft and the subsystems that directly support the science.

The instruments associated with each experiment (shown in Table 3) gather useful data throughout the life of the mission with peaks occurring at the time of the planet encounters. Where there is more than one instrument for a particular experiment, the instruments cover different dynamic ranges or measure different aspects of the observed phenomenon. The following paragraphs identify instruments and their characteristics that affect spacecraft integration.

1. Fields and Particles

a. Energetic particles. To meet the objectives discussed in Section II-B-3, performance goals have been set for the energetic particle instruments. These three instruments (the trapped radiation detector, the trapped radiation instrument, and the charged particle telescope) will measure electrons in an energy range of 0.1 to 30 MeV, protons from 0.1 to 250 MeV, and alphas and other nucleons in a range from 0.1 to 50 MeV. The energetic particles instruments are sensitive to the RTG radiation and

to the magnetic environment of the spacecraft itself. Thus, they require two special procedures: (1) shielding from the RTGs, and (2) spacecraft roll maneuvers. When the spacecraft is rolled with the instrument in place, any detectable signal which accompanies the roll can be associated with the spacecraft rather than with the environment. For example, the magnetic field surrounding the camera should rotate with the camera, and the energetic particles instruments would detect this field as a dc signal. The spacecraft roll also gives the instruments a 4π -steradian view of space.

b. Plasma. The plasma probe, required to measure the intrinsic and extrinsic properties of the solar wind (Section II-B-3-a), must be sensitive to electrons and protons and have an accuracy of 1%. The probe also requires shielding from the RTGs and a spacecraft roll calibration.

c. Plasma wave. The plasma wave detector is a simple dipole and a magnetometer used to measure the Alfvén waves and their properties by monitoring the electromagnetic field associated with the waves; the electric field, from 3 to 30 kHz, and the magnetic field from 3 to 300 kHz.

d. Magnetic fields. Magnetometers are used to study the magnetosphere at Jupiter, to determine the details of satellite interaction with the magnetosphere, to search for magnetospheres at the other major planets, and to gather data on the particle populations and magnetic fields to the boundary of the heliosphere (Section II-B-1-d). The magnetometers, with eight ranges up to $5 \times 10^5 \gamma$, are quite sensitive and detect signals of $<0.01 \gamma$. Therefore, they require a magnetically clean spacecraft. The magnetometers are located on a long boom, and the uncertainty in orientation caused by boom flexure could make the data difficult to reduce.

e. Meteoroids. The meteoroid experiment is performed by two instruments, the micrometeoroid detector and the meteoroid-asteroid detector. The micrometeoroid detector is a type of impact and puncture instrument, which has a large number of pressurized cells. The cells can be penetrated by particles down to a nanogram. The pressure transducer

in the cell detects the fact that the cell has been broken and counts a particle. The meteoroid-asteroid detector is an optical detection instrument using four telescopes. If a particle passes through the fields of view of at least two of these telescopes, velocity and range from the spacecraft to the particle can be determined. The telescopes can detect particles to +6 visual magnitude (a bolometric magnitude of about +2). Another measure of sensitivity is the ratio of the particle-to-spacecraft range to the particle radius. The range/radius ratio is expected to be about 10^6 divided by the distance to the Sun in AU. The meteoroid-asteroid detector requires spacecraft roll calibration from time to time, and has a preferred sensor orientation.

f. Planetary radio emissions. A radio-emission detector is used to measure the Jovian decametric radiation, which is the longer wavelength source believed to be associated with the surface of the planet. These emissions, with the character of a noise storm, are correlated with the presence of certain meridians on the planet. This implies strongly that the source is localized on the planet's surface, but the position of the source is highly uncertain, even though large interferometers have been used to measure it from the ground. A better measurement of the localization of the source would help in the evaluation of some of the theories offered to explain the origin of the radio emissions. The radio-emission detector will take measurements in the 20-kHz to 20-mHz range. The frequency spectrum of these sources as detected from Earth is about 3.5 to almost 40 mHz. The bandwidths are narrow, from 5 to 10 kHz. The instrument will be capable of detecting left or right circular and linear polarizations, and it can be operated in several modes to optimize the detection of polarization or for a quick sweep of the frequency spectrum.

2. Planetology. Planetology includes the experiments concerned with the structure and composition of the planets and with their origin and dynamics. The instruments often provide two-dimensional information from a distance away from the spacecraft and close to the planet as opposed to many of the fields and particles instruments, which take samples at the spacecraft.

a. Imaging. The television is probably the best reconnaissance instrument in the planetology category. As discussed in Section II-B

of this report, it is desirable to determine the basic properties of the planets and their larger satellites and to study the atmospheres of the major planets. Measurements of the vertical structure of permanent dense cloud layers, and studies of smaller, less coherent, turbulent motions of the atmosphere would be valuable. Television monitoring of the cyclonic systems of major planets for periods of several days, and in a wide range of colors, would enable physicists to determine the dynamics of the clouds. Observations of satellite surfaces should help to determine whether or not any of them retain even a tenuous atmosphere.

The television will observe the geological features of the satellites (Section II-B-2-c) to provide evidence from which the history of the satellites can be deduced. For these observations, the camera should have a minimum resolution of 10 km.

Television pictures of the rings of Saturn from phase angles not available from Earth should resolve the question of the density profile of the scattering. An optical search will be made near the rings of Saturn for unknown satellites (see Section II-B-2-a). Ground-based instruments view the outer planets and satellites at small phase angles and must view the satellites of Saturn in the vicinity of the bright rings. However, as the spacecraft approaches the planet at a point above the terminator and the phase angles become larger, the contrast of features increases and the albedos can be measured at different angles.

To achieve high resolution, it will probably be necessary to have a fairly narrow field of view, which requires a high degree of pointing accuracy. Also, the camera system will generate large amounts of data in a short period of time, which requires the full capability of the data system.

b. Infrared radiometry. The infrared experiment as conceived for TOPS has two goals: (1) to measure the thermal anomaly at Jupiter and Saturn, and (2) to provide thermal maps of the atmosphere.

From Earth, Jupiter and Saturn appear to radiate about two and one half times as much thermal energy as they receive from the Sun. Some possible explanations are: (1) the experiment is wrong; (2) the cause is simple cooling of these bodies; (3) there is some mechanism for the conversion of gravitational energy to thermal energy, etc. It is difficult to

measure this energy from Earth because, for one reason, the planet can be observed only when it is in a full-phase condition. The signal-to-noise ratio can be significantly improved with proximity to the planet, and the quality of the data is better when the phase angles are larger. In fact, the planets are radiating thermal energy at some level around the night side also. A major objective of the TOPS mission is to confirm or refute this Earth-based measurement and to discover whether or not Uranus or Neptune has similar properties.

The thermal map of the planet atmospheres will be in three dimensions. From Earth-based observations, it is known that the atmospheres of the major planets are dynamic. In addition to the rotation of the planet, one major driving force must be thermal. The maps may also disclose some localized thermal sources on the surfaces of the planets.

The infrared radiometer measures thermal radiation without high spectral resolution for identification of species. The spectral range of the device is from 0.5 to 100 μm and the resolution is 0.5 deg. The radiometer scans in one direction with a mirror and uses the motion of the spacecraft to scan in the other direction.

c. Ultraviolet photometry. The purpose of the ultraviolet photometry experiment is to identify the molecular and isotopic composition of the atmosphere at the major planets and to determine the abundance of the major constituents. Some of the performance goals are shown in Table 40.

Table 40. Ultraviolet photometry experiment performance goals

Elements	Photometric settings, Å
Atomic hydrogen	1216
Neutral helium 584	584
Helium ion 303	303
Oxygen 1304	1304
Plus: N, Ne, Ar	
Resolution is 1 deg.	

It should be possible to determine whether or not there are significant differences in composition between the zone belts seen in the major planets. This is a key experiment. Jupiter and, probably, Saturn are large enough and sufficiently cool to have retained most of the atmosphere they had at the time they were formed, whereas the terrestrial planets, Earth and Mars, have lost most of their lighter gases. A probe below the region of turbulent atmospheric mixing may identify some of the composition and abundances of the various light elements which existed at the time these planetary systems were formed. Such knowledge applied to theories of the origin of the solar system would be invaluable.

d. Radio science. The radio science experiment uses the RFS to measure:

- (1) Refractive index profile of atmospheres.
- (2) Electron density in magnetospheres.
- (3) Magnetic field strength in ionospheres.
- (4) Scattering in rings of Saturn.
- (5) Interplanetary medium.
- (6) RF reflectivity of surfaces.
- (7) Planetary radio emissions.

The spacecraft RFS, as designed, will include both S- and X-band, permitting measurement at two frequencies. Earth occultation of the spacecraft by the planet is a special requirement in obtaining the refractive index profiles of atmospheres, and an occultation at the rings of Saturn would measure radio depth.

e. Celestial mechanics. The celestial mechanics investigation also uses the radio system, but in this experiment, the accurate tracking of the spacecraft provides data from which the forces acting on the spacecraft can be determined. Planetary mass and gravitational potential, and improved information about the ephemerides of the planets and their satellites will be collected. A long-term relativity experiment, similar to that of Mariner Mars 1969, will be made as the spacecraft leaves the solar system. The experiment uses both S- and X-band and the normal extended range and rate tracking of the spacecraft.

B. Science Instrument and Interface Engineering

The TOPS general engineering task is twofold: (1) to integrate a baseline payload with the spacecraft, and (2) to identify and resolve problems associated with the science instrumentation, spacecraft configuration, and the mission requirements.

The following is a brief description of some significant problems encountered during the integration of the baseline payload.

1. Nonimaging Instruments

a. Vector helium magnetometer. The vector helium magnetometer (VHM) sensor is located at the end of a 9.14 m (30 ft) extendable boom and the electronics are contained within the spacecraft bus.

Significant problems associated with this experiment are:

- (1) Temperature control of the sensor complicated by the heat transferred back to the spacecraft bus by the signal and control wires running along the boom.
- (2) Possible RFI problems due to the 100-MHz RF excitation generated within the VHM electronics and carried to the sensor.
- (3) An overall spacecraft problem of magnetic cleanliness in order to reduce the magnetic field at the sensor to 0.01γ .
- (4) Proper orientation (± 0.33 deg) of the sensor after the boom is extended. This problem of sensor orientation is not one of actually orienting the sensor in a given direction but rather knowing its orientation to within ± 0.33 deg.

b. Plasma wave detector. The plasma wave detector (PWD) sensor is located on a boom similar to the magnetometer boom. The electronics are located in the spacecraft bus, with the exception of a preamplifier mounted at the end of the PWD boom.

The only significant problem associated with the PWD is the temperature control of the preamplifier on the boom. Since only a small amount of heating is required, temperature control can be achieved by use of a radioisotope heater, such as plutonium.

c. Plasma probe. The plasma probe presents the most serious drawback in the TOPS payload. The instrument design has not progressed beyond the conceptual stage; however, the choice of this instrument was made over others, such as the Pioneer F & G instrument, because it does not require a spinning spacecraft.

The major problem in the plasma probe is the utilization of 40 channeltron sensors oriented in a circular pattern.

Channeltron lifetime is on the order of 10^{11} total counts, thus with an average count rate of 400 counts/s the expected sensor lifetime is less than one year.

Several methods of extending channeltron lifetime are available, such as lowering the supply voltage during periods of high counting or turning the instrument off when within the influence of the Jovian radiation.

These alternatives have an impact on the science value of data lost during these periods and the operational aspects of changing instrument modes, both of which have not been examined in detail.

d. Micrometeoroid detector. This experiment is the same as the Pioneer F & G experiment, the only difference being sensor area. The experiment consists of some 600 pressurized cells covering an area of about 2.0 m^2 . As a dust or meteoroid particle strikes the sensor surface a cell is punctured causing a gas discharge which is indicated as an event to the data system.

It is important to mount the sensor panels on the spacecraft such that they are oriented in the proper direction to be penetrated by particulate matter.

The orientation problem gives rise to the problem of temperature control of the sensor panels. This concern for temperature control is in respect to possible cracking of the sensors due to differential expansion.

It is not apparent that differential expansion is a problem but without further investigation it is planned to provide electrical power for heating through Saturn encounter only.

e. Meteoroid asteroid detector. Weight is the prime problem with the meteoroid asteroid detector (MAD). The problem is caused

by: (1) the increased size of the telescopes required at great distances from the Sun and, (2) necessity to use logic other than the Pioneer CMOS. CMOS logic is very lightweight and low power but cannot survive the Jovian radiation encountered on the JSP'76 trajectory.

f. Radio emission detector. The radio emission detector (RED) with its high sensitivity and broadband capability will be very susceptible to interference from other spacecraft subsystems. It is anticipated that this experiment will require a detailed examination, both analytically and experimentally, of its RFI characteristics.

g. Charged particle telescope, trapped radiation detector, trapped radiation instrument. These instruments presented no significant problems in integration. They are all Pioneer F & G instruments. The only integration problem with these instruments was that associated with adapting the instruments to the TOPS configuration in order to obtain the proper fields of view unobstructed by spacecraft structure.

h. Ultraviolet photometer. The UV photometer is an encounter instrument located on the scan platform.

It is a relatively noncomplex instrument and does not present any integration problems. The instrument does utilize channeltron sensors and there is a concern regarding sensor lifetime (see Plasma Probe, Section VIII-3-C).

i. Infrared multiple radiometer. This instrument is in the conceptual stage only. It is a three-channel device, one of which must be cooled to 80 K at Jupiter and about 20 K at Neptune and Pluto.

Planet scan is accomplished through the use of a motor which steps a mirror. As the stepping motor is actuated, the power dissipated in the motor may increase the temperature of the cooled sensor such that it is out of the calibration range or even out of the proper operating range.

Another area that needs further definition is the planetary scan sequence. As the instrument scans a planet, the mirror steps in one direction ± 10 deg in 1/2-deg increments, and then requires the scan platform to move over to allow the instrument to scan back up. This sequence could interfere with the television sequence.

2. Instrument calibration. The spacecraft will be commanded into a roll mode approximately every 1/2 AU for purposes of calibrating some of the cruise instruments. The effects of this roll maneuver have not been addressed in detail as of yet; however, it is recognized that these maneuvers will affect several other spacecraft subsystems, mainly attitude control and its gas supply.

Another aspect of instrument calibration that is recognized but has not been examined in any detail is that of sensor degradation. It is simple to calibrate instrument electronics by injecting test signals behind the sensor; however, over the lifetime of this mission sensor degradation will be of considerable concern and methods of determining sensor characteristics and calibrating instruments will be required to be developed.

Table 41 is a list of the TOPS baseline payload indicating: (1) the source of the instrument, (2) instrument weight, and (3) power consumption.

C. Radiation Effects

The two main objectives of the study of radiation effects are: (1) to determine the maximum allowable radiation levels consistent with acceptable radiation interference and damage levels in the science instruments, and (2) to design ways to effectively reduce radiation effects to acceptable levels for the science instruments.

1. Determination of Maximum Allowable Radiation Levels. Figure 105 shows the approach to the problem. The radiation sources are shown on the left of the figure. These levels are fixed for each specific trajectory. The source radiation is attenuated for any instrument through the inherent spacecraft shielding to get the no-shield actual radiation environment. Working from the right side of the figure, the experimental objectives are defined; the instrument is designed; and then components and sensors are selected.

The experimental objectives directly affect the acceptable radiation environment and the instrument design, and the various components and sensors affect the acceptable environment through a radiation response function which must be determined. The no-shield actual environment is compared with the acceptable environment; and, if the actual is less than or equal to the acceptable environment, the next instrument is considered.

Table 41. Baseline payload instrumentation

Experiment	Source	Weight		Power, W
		kg	lb	
Imaging	JPL	40.8	90	50.0
IR radiometer ^a	JPL	8.2	18	10.0
UV photometer	Judge, USC Pioneer F/G	1.4	3	2.0
Radio emission detector	Alexander, GSFC Pioneer F/G	2.7	6	3.0
Vector helium magnetometer	JPL	2.2	4.8	4.1
Plasma wave detector	Scarf, TRW Pioneer F/G	2.7	6	2.0
Plasma probe ^a	JPL	4.5	10.0	12.6
Trapped radiation	(1) Fillus, UCSD Pioneer F/G	4.5	10.0	5.0
	(2) Van Allen, UI	1.5	3.2	1.2
Cosmic ray	Simpson, UC Mariner 71	3.6	8.0	4.0
Micrometeoroid	(1) Soberman, G. E. Pioneer F/G	7.3	16.0	2.0
	(2) Kinard, LRC Pioneer F/G	4.5	10.0	1.0
TOTALS		83.9	185	96.9
^a Conceptual only.				

However, if it is not, it is then determined whether or not practical amounts of additional shielding will reduce the no-shield actual environment to less than or equal to the acceptable environment. If it will, the desired radiation environment is obtained. If it will not, it is necessary to repeat the process through both paths to see whether the limits of the acceptable environment can be raised or those of the actual environment lowered.

The acceptable radiation level is determined in the following manner: First, the experimental objectives and the backgrounds expected in the absence of RTG interfering radiation are determined. Then, from a preliminary estimated assessment of the instrument design and of what the most sensitive components may be, the response functions of the instruments and the components are defined. It is assumed arbitrarily that the acceptable RTG-induced interference level is equal to all other background sources of that particular instrument because an infinite amount of shielding would be required for the ideal case in which there would be no interference.

Figure 106 shows the gamma and neutron design constraints and the expected fluxes and fluences.

Figure 107 shows the Jupiter radiation model. For both the upper limit and the nominal models for electrons and protons, fluxes and fluences in the equatorial plane change as the inverse third power of the flyby distance from Jupiter.

Table 42 gives the maximum acceptable radiation level for the TOPS baseline instruments. In some cases, the neutron acceptable levels are at the lower limit of the best estimates; and the protons are, in all cases, less than the design constraint level.

The table also includes the radiation degradation for the electronics. Non-TOPS instruments, the cosmic and X-ray detectors, are included for completeness. The cosmic ray detector was used on Pioneers F and G, and the X-ray detector is a "combination" of a proportional counter and a silicon detector instrument.

The response functions for the various instruments were obtained by first determining the component response function through literature search and experimental testing, and from this inferring the instrument response function. Literature searches were made by contractors (e.g., Boeing) and by the JPL Library and individual JPL personnel.

Figure 108 shows the results of the Boeing report on proton-damage thresholds in electronic components. The proton radiation which can be received by seven of the twelve TOPS baseline instruments is limited by the damage to the electronics. It is estimated that the electronics can be

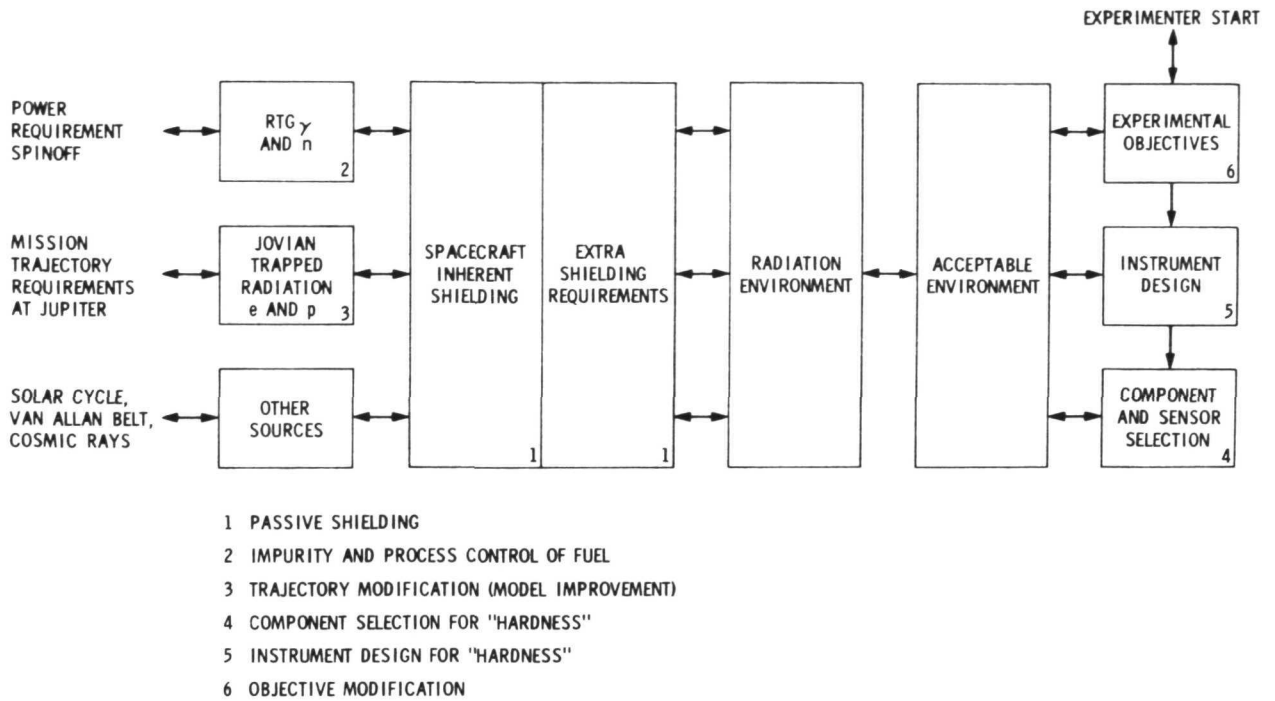


Fig. 105. Approach to radiation problem

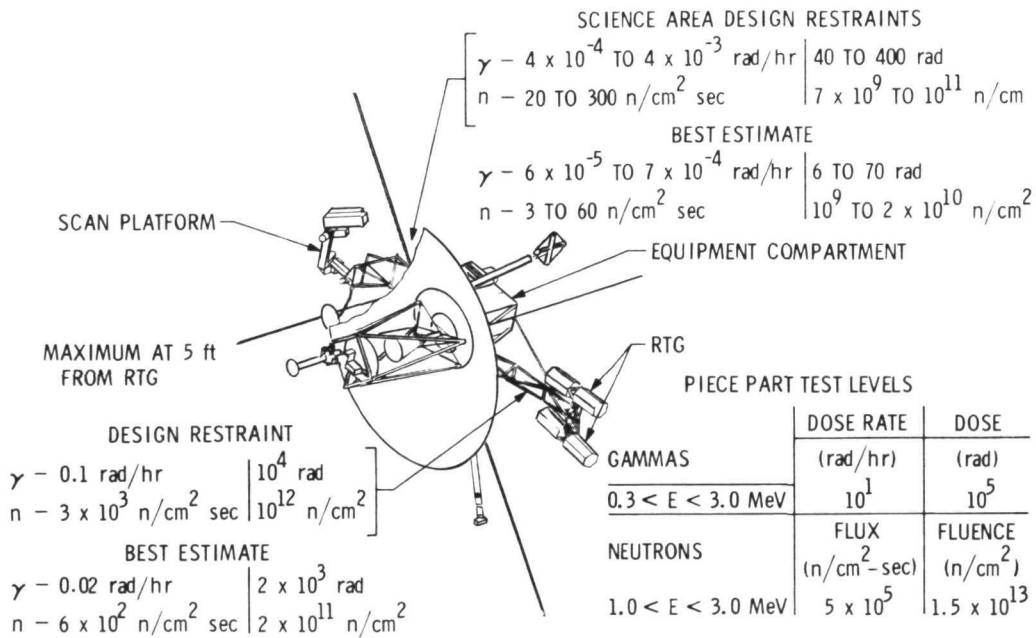


Fig. 106. Gamma and neutron design constraints and expected fluxes and fluences

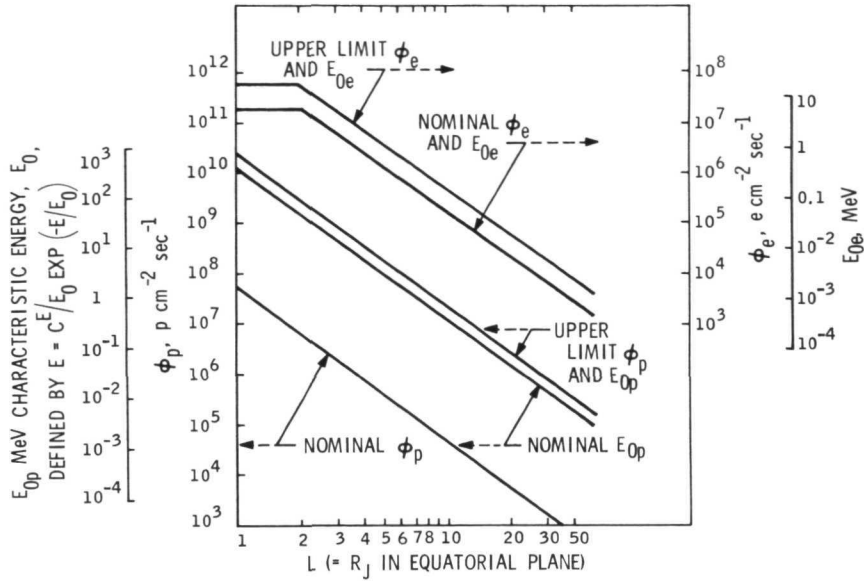


Fig. 107. Jupiter radiation model

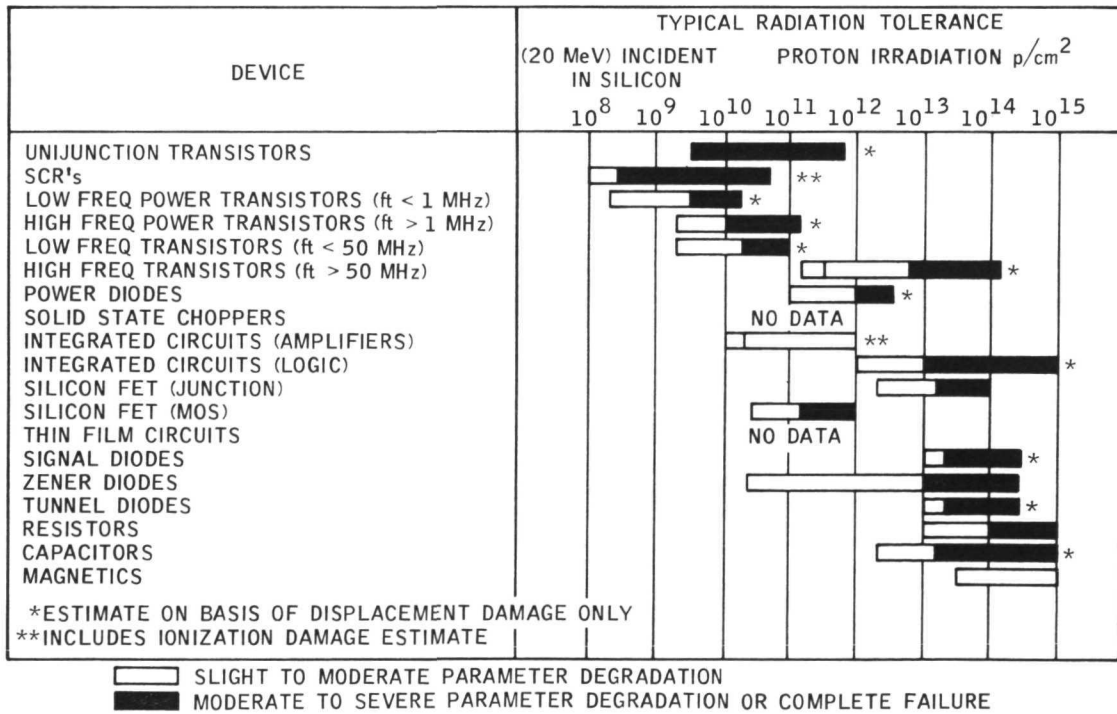


Fig. 108. Electronics, proton degradation

Table 42. Maximum acceptable radiation levels

Instrument	p, 20 MeV	e, 10 MeV	γ , RTG "spectrum"	n, Fission
Charged particle telescope	$<10^9 \text{ cm}^{-2}$ dynamic range limitations		$\left\{ \begin{array}{l} <350 \text{ cm}^{-2} \text{ sec}^{-1} \\ (<8 \text{ cm}^{-2} \text{ sec}^{-1} \text{ on part}) \end{array} \right.$	$<10^9 \text{ cm}^{-2}$
Television	$<10^6 \text{ cm}^{-2} \text{ sec}^{-1}$	$<10^6 \text{ cm}^{-2} \text{ sec}^{-1}$	$<10^4 \text{ rad}$	$<10^{12} \text{ cm}^{-2}$
Infrared multiple radiometer	$<10^{10} \text{ cm}^{-2}$	$<5 \times 10^{12} \text{ cm}^{-2}$	$<500 \text{ cm}^{-2} \text{ sec}^{-1}$	$<10^{11} \text{ cm}^{-2}$
Meteoroid asteroid	$<10^{10} \text{ cm}^{-2}$	$<5 \times 10^{12} \text{ cm}^{-2}$	$<10^4 \text{ rad}$	$<10^{12} \text{ cm}^{-2}$
Meteoroid detector	$<10^{10} \text{ cm}^{-2}$	$<5 \times 10^{12} \text{ cm}^{-2}$	$<10^4 \text{ rad}$	$<10^{12} \text{ cm}^{-2}$
Plasma probe	$<10^{10} \text{ cm}^{-2}$	$<10^{10} \text{ cm}^{-2}$	$<5000 \text{ cm}^{-2} \text{ sec}^{-1}$	$<10^{11} \text{ cm}^{-2}$
Plasma wave detector	$<10^{10} \text{ cm}^{-2}$	$<5 \times 10^{12} \text{ cm}^{-2}$	$<10^4 \text{ rad}$	$<10^{12} \text{ cm}^{-2}$
Radio emissions detector	$<10^{10} \text{ cm}^{-2}$	$<5 \times 10^{12} \text{ cm}^{-2}$	$<10^4 \text{ rad}$	$<10^{12} \text{ cm}^{-2}$
Trapped radiation detector	$<10^{10} \text{ cm}^{-2}$ dynamic range limitations		$<10^3 \text{ cm}^{-2} \text{ sec}^{-1}$	$<5 \times 10^{10} \text{ cm}^{-2}$
Trapped radiation instrument	$<10^9 \text{ cm}^{-2}$ dynamic range limitations		$<10^3 \text{ cm}^{-2} \text{ cm}^{-1}$	$<10^9 \text{ cm}^{-2}$
Ultraviolet photometer	$<10^{10} \text{ cm}^{-2}$	$<5 \times 10^{12} \text{ cm}^{-2}$	$<10^4 \text{ rad}$	$<10^{12} \text{ cm}^{-2}$
Vector helium magnetometer	$<10^{10} \text{ cm}^{-2}$	$<5 \times 10^{12} \text{ cm}^{-2}$	$<10^4 \text{ rad}$	$<10^{12} \text{ cm}^{-2}$
Cosmic ray detector	$<10^9 \text{ cm}^{-2}$ dynamic range limitations		$<500 \text{ cm}^{-2} \text{ sec}^{-1}$	$<10^9 \text{ cm}^{-2}$
X-ray detector	$<10^8 \text{ cm}^{-2}$	$<5 \times 10^{10} \text{ cm}^{-2}$	$<0.5 \text{ cm}^{-2} \text{ sec}^{-1}$	$<10^9 \text{ n/cm}^2$

designed to sustain radiation to levels of about 10^{10} protons/cm², but at the 10^{12} or 10^{13} level, the electronics are endangered.

Figure 109 shows the proton-damage thresholds for some typical science components. The information in the figure was derived from a combination of experimental work and literature search. At levels of about 10^9 to 10^{10} , there is a probability of no serious component damage, but at 10^{12} to 10^{13} , most of the science components will be experiencing difficulty.

The study showed that specific proton and electron shielding is not practical. The reasons for this conclusion are:

- (1) Shield mass increases rapidly with proton energies greater than about 20 MeV and for electron energies greater than a few MeV.
- (2) The dependence of the variation of the fluxes and the energies on the inverse cube of the radius implies a severe penalty on the higher periapsis missions, if the design is based on the closest periapsis mission.
- (3) Because large uncertainty still exists in the models for both fluxes and energies, use of the upper limit models results in a severe spacecraft penalty in shield weights.

To shield instruments from gamma or a neutron radiation, 4.53 kg (10 lb) were allocated. This amount appears to satisfy the requirement that the actual environment be less than or equal to the acceptable environment. However, after this requirement is met, the radiation effect must be reinvestigated, if any one of the following four events occurs:

- (1) If the spacecraft configuration changes. In this event, it is reasonable to expect the actual gamma and neutron environment to change.
- (2) If the RTG fuel loading changes. As indicated in Section VII, there is a good probability of such changes.
- (3) If the Jupiter model changes. Any change in the model would mean change in the actual electron and proton environment. The model might be changed because of data received from Pioneer 10.

- (4) If the instrument itself changes. Alteration of the instrument would change the acceptable radiation environment for all four types of radiation.

2. Protective Techniques. There are various means of protection against radiation. For convenience, these methods may be divided into two categories: (a) ways to protect the instruments from damage, and (b) ways to protect them from interference.

a. Protection from damage

(1) Shielding. Figure 110 shows an example of shielding from neutron damage by using a 5% borated polyethylene mass for the shielded area. For a typical TOPS baseline instrument, the area to be shielded is about 100 cm². For an order of magnitude neutron reduction, approximately 2 kg (4.5 lb) of 5% borated polyethylene are required.

Materials other than the borated polyethylene are being investigated for spot shields located at the instruments. For instruments located on the scan platform, it is necessary to shield almost 4π steradians.

(2) Inherent Electronic Shielding. Although no specific proton and electron shields are provided, the electronics in many of the sensors are inherently shielded by spacecraft and instrument shells, which afford protection against protons with energies less than approximately 20 MeV and against electrons with energies less than about 1-1/2 MeV.

The RTG separation distance and orientation also effectively reduce the gamma and neutron environments. The electronics and the propulsion bays for the instruments located behind them provide additional shielding on the side opposite the RTG. To take advantage of inherent shielding, it is necessary to determine what the optimum operating conditions for a specific component are. For example, some components and sensors will receive much less radiation damage when the power is off than when it is on. Different levels of bias may affect a component's sensitivity to radiation.

(3) Selection of Jovian Periapsis. The advantages here are obvious from Fig. 107.

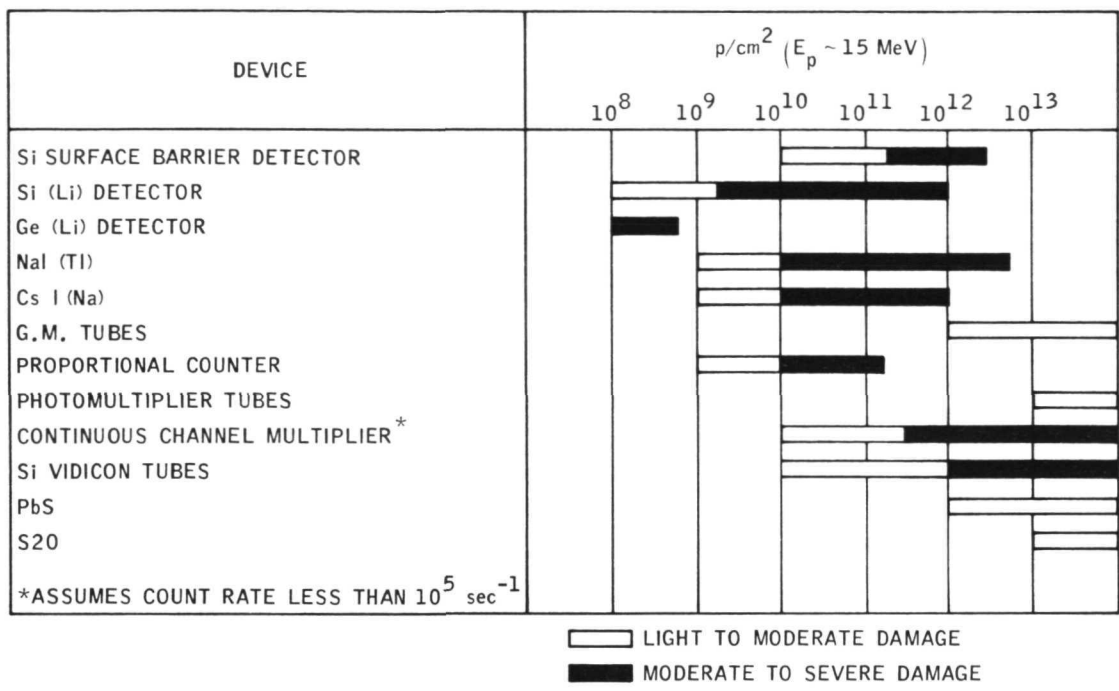


Fig. 109. Proton damage to science components

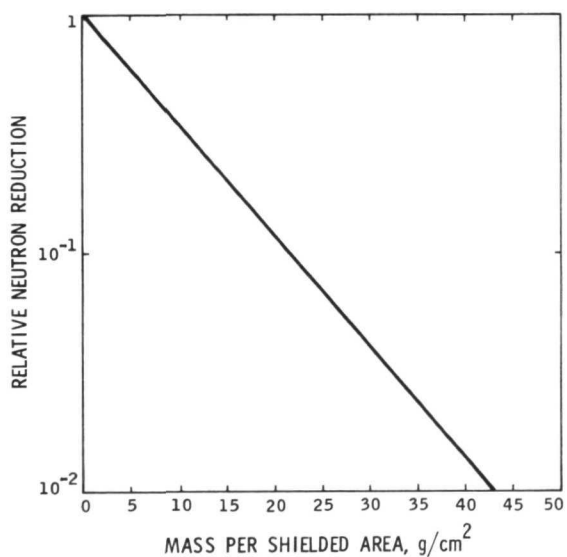


Fig. 110. Shielding from neutron damage with 5% borated polyethylene mass per shielded area

(4) Selection of Components. Gamma-neutron-hardened electronic components have been proven. Tests to determine their resistance to the proton and electron environment are under way. There is some choice in sensor selection; e.g., a silicon detector, a channel multiplier, a photo tube or a proportional counter could be used for the X-ray detector. Each has its own advantages and disadvantages, but one consideration should be the radiation effects on the various components.

(5) Redundancy. The redundant component must be maintained in the optimum operating condition to provide any real advantage. Two parts in the same environment will both deteriorate at the same time.

b. Protection from interference. Protection from interference can be obtained by shielding, by taking advantage of inherent shielding, and by the Jovian periapsis selection. In addition there are electronic techniques (using pulse size and durations, rise time, etc.) to determine the differences between the noise signal and the desired signal so that the desired signal can be discriminated. Directional discrimination (anticoincidence shields) are effective, particularly against RTG radiation.

Table 43 lists the shield masses required to protect the science instruments against gamma/neutron radiation.

Figure 111 shows at what point a particular instrument will cease to become useful because of interference effects or the effects of permanent radiation damage occurring as the spacecraft travels on a 1.1 R_J periapsis trajectory. The Xs correspond to the upper limit trapped radiation model, and the circles to the nominal model. For example, X^B indicates the B telescope portion of the trapped radiation detector which, because of damage effects in the upper limit model, will no longer be satisfactory at about 8 R_J . Using the standard model of the meteoroid/asteroid detector, as an example, the entire instrument will no longer be useful at about 3.5 R_J because of interference effects. The dashed line indicates the R_J at which 10^{10} proton/cm² (20 MeV equivalent) will have emerged through a 1-g/cm aluminum shield. The line on the right represents the upper limit model and that on the left, the nominal model.

3. Status of Study. The proton and electron radiation will not cause serious instrument damage at Jovian periapsis of 6 or 7 R_J in the upper

Table 43. Science instrument shield masses

Instrument	γ Shield, kg	n Fluence, n/cm ²	n Shield, ^a kg of 5% borate polyethylene
Charged particle telescope	1.1	<10 ⁹ ^b	1.3
Trapped radiation detector	0	<5 x 10 ¹⁰	0
Trapped radiation instrument	0	<10 ⁹ ^b	2.0
Cosmic ray detector ^c	1.9	<10 ⁹ ^b	1.9
X-ray detector	~22 Proportional counters or 2.5 Si detectors	<10 ⁹ ^b	3.3 0.4

^a Does not include the effect of γ shield in reducing neutron flux. Assumed neutron flux levels are: (1) 20 n/cm² sec on CPT and XRD; (2) 150 n/cm² -s on TRD; (3) 50 n/cm² -s on TRI and CRD.

^b These damage limits for Si (Li) detectors are not presently firm, but may become recommended levels if data warrants their adaptation.

^c Assumes 1-HET, 1-MET, and 1-LET.

limit model. This means that the JUN 1979 missions will not have any serious difficulty caused by radiation problems. Present data are not complete for the JSP 1977 mission, however.

The instrument designs used in this study do not afford adequate radiation protection for the science instruments at Jovian periapsis of less than $3 R_J$ in the nominal model. This means that the JSP 1976 mission with the $1.1 R_J$ periapsis is in difficulty. Radiation hardening and in-flight calibration for science instruments will maximize the amount of scientific data returned, if there is slight radiation degradation.

The proton and electron shields are not practical in the trapped radiation model under consideration. Gamma-neutron shields are presently required in most energetic particles instruments, and designs have been studied. The gamma and neutron environments are dependent upon spacecraft configuration.

Radiation effect data are insufficient. Interference and damage data must be obtained by experiments, in many cases.

D. Imaging Subsystem

1. Requirements and Goals

a. General. Reliability is a prime requirement of the imaging subsystem. Storage lifetime must be 12-1/2 years, including the 9-to-10 year mission life as well as a possible 2-to-3-year lapse between the time when the components were manufactured and launch time. An operating time of 2400 h and 4500 h of powered standby are minimal. Because encounter periods at planets are long, from 30 to 100 days, it would be possible to exceed the number of operating hours before Jupiter, for example, is passed.

The imaging subsystem must be resistant to radiation. It must also have the capability to meet the navigational requirements imposed on it, whether it is to make appropriate measurements for approach guidance or to provide some type of backup to a separate approach guidance instrument, if one is necessary.

The subsystem must have high resolution. High resolution is difficult to obtain because the light level at the outer planets is low, and the flyby

altitudes at some of the points of closest approach are as high as 500,000 km. Figure 112 shows the brightness of the outer-planet scenes. The camera exposure equation (Lambertian surface) is:

$$E = \frac{10^6 N D^2 \cos \theta}{4 R V F L^3} \int_{\lambda_1}^{\lambda_2} H_{\lambda} A_{\lambda} T_{\lambda} d_{\lambda}$$

where

- E = sensor exposure, erg/cm²
- N = number of picture elements of image smear
- D = optics diameter, cm
- θ = solar zenith angle
- R = sensor raster frequency, scan line/mm
- V = smear velocity, rad/s
- FL = optics focal length, cm
- H = solar spectral irradiance, W/cm²-μm
- A = surface spectral reflectance
- T = optical system transmission

The lower the sensor exposure, the more sensitive the sensor has to be to create any kind of picture. Of these parameters, the only two that the system designer can significantly influence are the optical system focal length and the optical system diameter. (To get high surface resolution from a long distance, it is necessary to use a long optical system focal length.) The functional dependence of exposure on focal length is in the inverse third power. Therefore, very small increases in focal length cause tremendous decreases in the sensor exposure. It is desirable, then, to fly an optical system with the largest diameter possible. This approach is limited by weight.

Figure 113 shows the estimated weight of the optical system as a function of aperture diameter. Previous studies indicate that weight

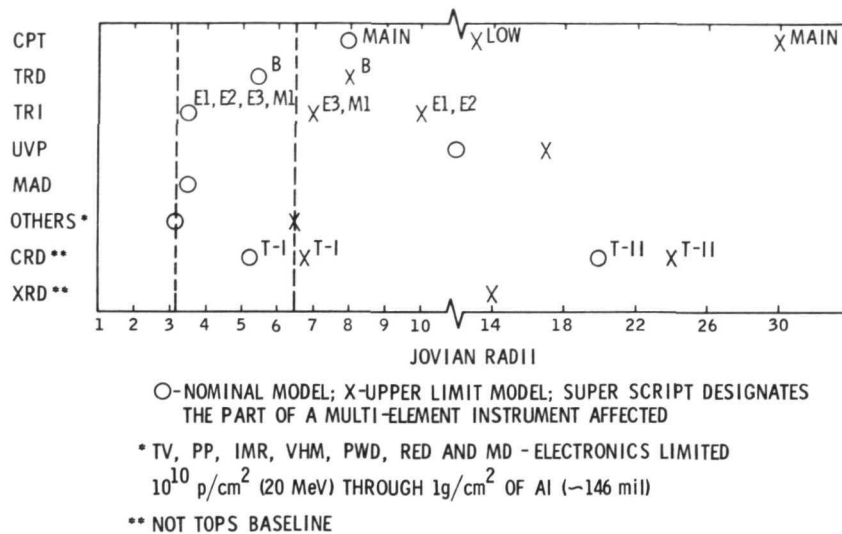


Fig. 111. Jupiter interference or damage radii, 1.1 R_J periapsis

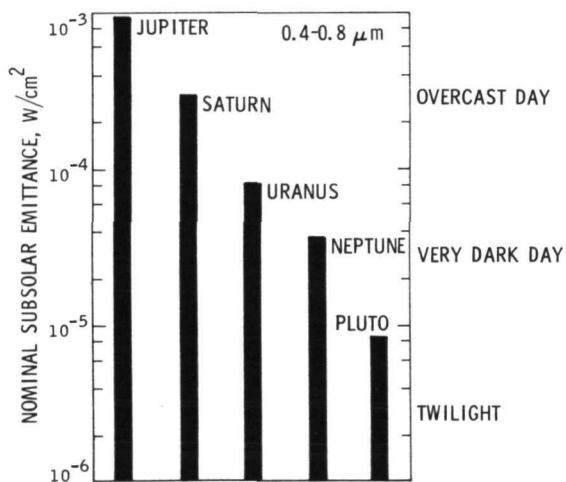


Fig. 112. Brightness of the outer planet scene

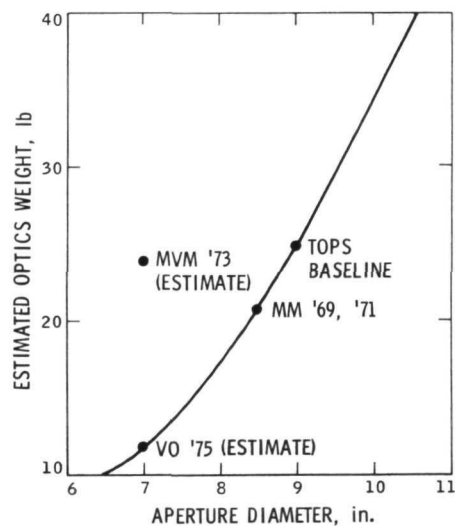


Fig. 113. Estimated minimum weight of optics

increases roughly as the third power of diameter, other things being equal. It can be seen that a slight increase in aperture diameter increases the weight of the optical system completely off scale. For the TOPS Project, a 22.86-cm (9-in.) aperture optics weighing 11.34 kg (25 lb) is probably the largest that can be flown because of weight. The combination of a constrained aperture diameter and the use of long focal lengths for high resolution necessitates the use of sensors which can work at extremely low light levels.

b. Specific performance goals. Some specific performance goals for TOPS are:

- (1) A 10-km surface resolution, which corresponds to between 5 and 15 μ rad per scan line angular resolution, depending upon the actual flyby distance. The angular resolution on the narrow-angle Mariner cameras has been about 25 μ rad.
- (2) To extend phase coverage of the outer planets from 1 or 2 deg to within at least 5 deg of the terminator to produce properly exposed pictures at 85 deg solar zenith angles.
- (3) To obtain a large format for the cloud dynamic study. A minimum of 800 scan lines per frame has been selected for the TOPS project.
- (4) To be compatible with the data rate of 131 kbps, which is imposed by the spacecraft.

2. Systems Considered. Several different system approaches to meet these goals have been considered.

a. Film system. Film systems appear to be impractical because of radiation fogging on the film and because developing chemicals would have to be stored for 10 yr. The mass of shielding required to survive the proton environment of Jupiter would probably exceed the entire weight of the baseline imaging system (see Fig. 114).

b. Point scanning system. The reliability of point scanning systems, such as an image dissector camera, is high because of their great simplicity. A target is not used on a point scanning system, and the

thermionic cathode is eliminated. However, the system has a relatively low performance because of its limited sensitivity, which necessitates a resolution-frame-time tradeoff (Fig. 115). For the image dissector camera to achieve the performance of the baseline system would require a frame-time of more than 24 h at Pluto. In 24 h there would be geometrical distortion because the planet would probably have revolved several times. Also, not much information can be returned with a 24-h frame time.

c. Dielectric tape system. The built-in storage feature of dielectric tape systems would simplify the spacecraft data system. Unfortunately, working models of this concept have not been successfully demonstrated, so that the feasibility of using such a system is uncertain; it is considered a high development risk.

d. Television system. The television system was selected as having the lowest development risk and the highest potential for high resolution because television sensors are among the most sensitive detectors currently available. The entire field of available television imaging sensors was then surveyed. The conclusions are that silicon target sensors, in particular, a silicon vidicon and a silicon intensifier target vidicon, are the most promising, although no currently available off-the-shelf imaging sensor can meet the reliability requirements of the mission. Silicon target sensors have a potential long life because of inherent target stability and because they can be baked at very high temperatures, which reduces the residual gas pressure thus extending the cathode lifetime. Also, the silicon intensifier target vidicon has the highest resolution potential because it is the most sensitive single-envelope sensor available.

Because there is always some development risk with a new type of technology such as this, a selenium photoconductor sensor of the type used on the Mariner and Surveyor missions was selected as a backup to the silicon target sensors. The selenium sensors have a proven slow scan capability which interfaces with the spacecraft data system. If, however, some unforeseen problem in the development of silicon targets should necessitate the use of the selenium photoconductor sensors, some compromise in the performance objectives would have to be made because the selenium sensors have a relatively low sensitivity.

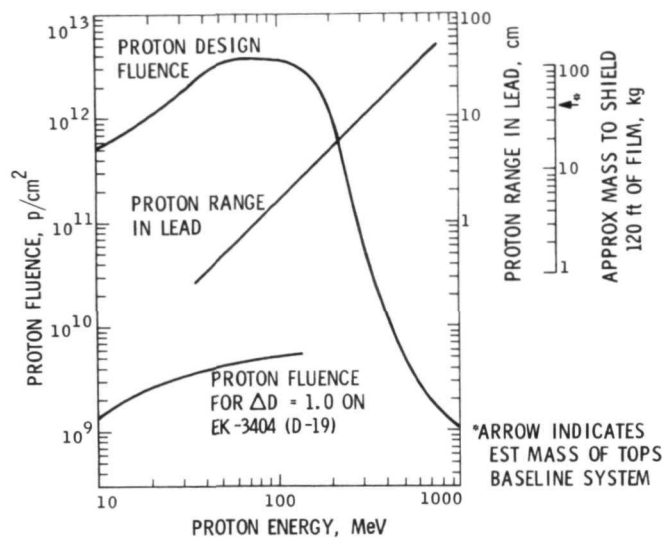


Fig. 114. Estimated film shielding, primary proton radiation

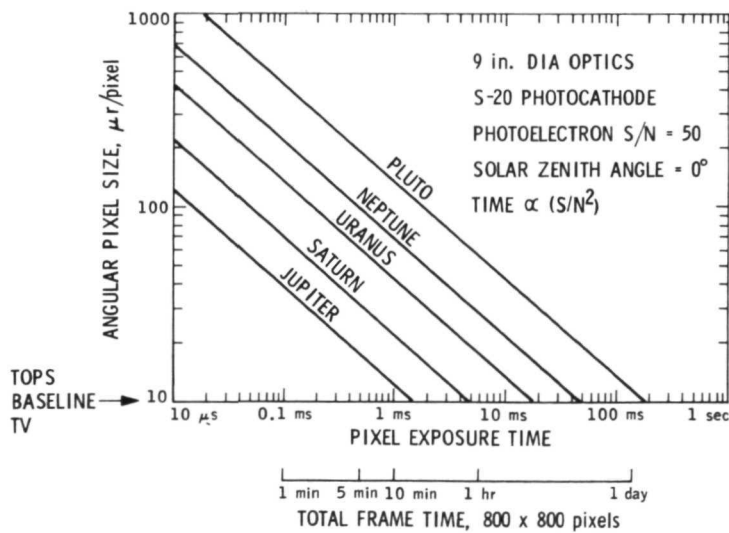


Fig. 115. Image dissector camera, resolution/frame-time tradeoff

3. Baseline Imaging System. The characteristics of the baseline imaging system using the silicon target sensors are summarized in Table 44. The two-camera system is composed of a narrow-angle camera and a wide-angle camera. The narrow-angle camera has 22.86-cm (9-in.) diameter optics with a 2-m focal length and a 3.81-cm (1.5-in.) intensifier target vidicon which produces an 800×800 format, i. e., 800 scan lines per frame and 800 samples per scan line. The wide-angle camera, which has ten times the field of view of the narrow-angle camera, uses a 3.81-cm (1.5-in.) nonintensified silicon vidicon with the same output characteristics as the intensifier vidicon. The two cameras, operating together, will consume an estimated 50 W of power.

Table 45 gives an estimated mass breakdown for the baseline imaging system.

Figures 116 and 117 estimate the performance parameters for the baseline imaging system.

As can be seen in Fig. 117, all of the planet encounters except at Saturn meet or exceed the 10-km surface resolution set as the TOPS goal. If a longer focal length were used to increase the resolution at Saturn, other problems would arise. The exposure values, especially at high phase angles, would become very low for Uranus and Pluto because of the spacecraft velocity and the low illumination level, which produces a very low signal-to-noise ratio. The effect of this on resolution is shown in the figure. If the target surface features were of infinite contrast, the signal-to-noise ratio would be optimum and the resolution would continuously increase as the spacecraft approached the planet. In fact, however, the signal-to-noise ratios become so low that very small low contrast objects will become submerged in noise. When this happens, one of two things can be done: (1) the shutter can be left open longer to increase the exposure, which will increase the image smear, or (2) when the data are received on the ground, the pixels can be averaged to increase signal-to-noise ratio. Either method will degrade the resolution. Therefore, it is desirable to use a shorter focal length for encounters at the farthest planets to increase the exposure value and a longer focal length at Saturn to increase resolution. For this reason, a 2-m focal length was chosen as a compromise for the baseline system. As

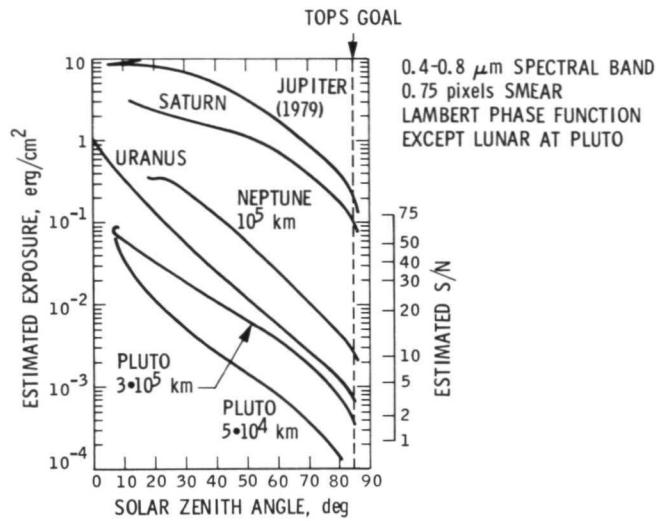


Fig. 116. Baseline imaging system, estimated exposure and signal-to-noise for narrow-angle camera

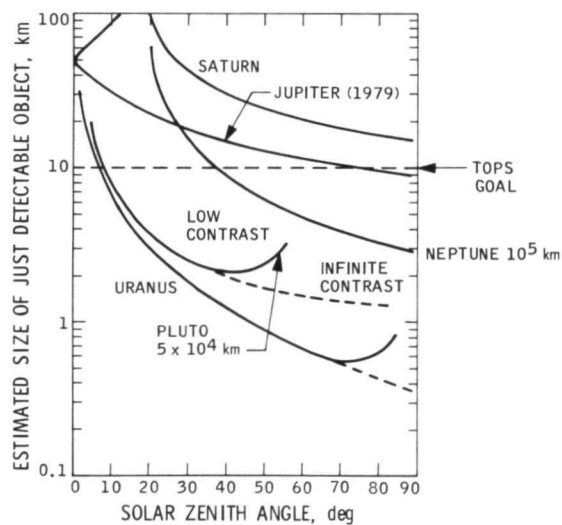


Fig. 117. Baseline imaging system, estimated surface resolution of the narrow-angle camera

Table 44. Baseline imaging system characteristics

Parameter	Narrow-angle camera	Wide-angle camera
Focal length	200 cm	20 cm
Aperture diameter	23 cm	6 cm
Focal ratio	f/8.7	f/3.3
T/Number	T/12.3	T/4.0
Angular field of view	0.5 × 0.5 deg	5 × 5 deg
Angular pixel size	10 μrad	100 μrad
Sensor type	3.81-cm silicon intensifier vidicon	3.81 cm silicon vidicon
Target size	18 × 18mm	18 × 18 mm
Scan line/frame	800	800
Samples/scan line	800	800
Bits/sample	8	8
Bits/frame	5.1×10^6	5.1×10^6
Frame time	41 sec	41 sec
Output data rate	131 kbps	131 kbps
Exposure control	Electronic shutter variable gain	Mechanical shutter ND filter
Shutter range	5 ms - 10 s	10 ms - 10 s
Power consumption	28 W	22 W
Envelope size	25.40 × 25.40 × 102 cm	12.70 × 12.70 × 38.10 cm

Table 45. Baseline imaging system, estimated mass

Instruments	Mass, kg (lb)
Narrow-angle camera	
Optics	11.34 (25)
Camera head	13.15 (29)
Wide-angle camera	
Optics	2.27 (5)
Camera head	9.53 (21)
Total on scan platform	36.29 (80)
Spacecraft electronics	4.54 (10)
Total Subsystem	40.83 (90)

a result, focal lengths are longer than desired at the outer planets and somewhat shorter at the nearer planets.

4. Study and Development of Silicon Target Sensors

a. The study. Although the silicon target sensors have the greatest potential for meeting the TOPS requirements, there were three questionable areas to be investigated:

- (1) The feasibility of slow scan, necessary to get a low data rate, had to be demonstrated.
- (2) The radiation effects on the entire sensor and, in particular, on the target had to be determined.
- (3) The standard 2.54-cm vidicons available could not support 800 scan lines. A new configuration of 3.81 cm (1.5 in.) had to be developed.

When silicon target sensors are slow-scanned, dark current builds up as a function of time. When frame-time is extended, the dark current eventually builds up to a point where it completely saturates the target and erases the image information. Two methods were tested to solve this problem: (1) a charge transfer technique wherein some of the image charge is transferred onto the silicon dioxide insulator on the target to eliminate

dark current buildup; and (2) target cooling to reduce the dark current. It was concluded that the charge transfer technique was not practical because it has a complex and critical operating sequence which requires additional internal light sources. Further, performance is poor in that defects in the silicon dioxide insulator, (pinholes and scratches) degrade the output image. However, the study showed that the dark current buildup problem can be eliminated by simple target cooling. Figure 118 is a plot of the tradeoff between the target temperature and the data rate. Any place along the operating line, on the left, the peak output current of the target would be five times the dark current. Along the other line, the entire output signal would be composed of dark current and no image information could be read out. At room temperature, the tube does not display much slow scan capability; the maximum frame time is only a few seconds. It is desirable to operate in the region where the signal-to-dark current ratio is greater than five. Figure 118 is plotted for a target with no radiation damage. Actually, radiation damage increases the dark current, and the lines in the figure would be moved left. The tube is not destroyed by radiation, but it can no longer operate at a frame-time and temperature compatible with the TOPS baseline design. In this event, the data rate would have to be increased or the temperature decreased, or both.

b. Development. Silicon sensors are being developed by RCA at Lancaster under JPL Contract Number 953106. The principal development objectives are:

- (1) To increase the size of the silicon targets to 25 mm to support 800 scanlines and to maximize the signal-to-dark current ratio in an attempt to offset the effects of radiation damage as much as possible.
- (2) Incorporate a dispenser cathode in the vidicon. The thermionic cathodes are unreliable for long-life missions because positive ion bombardment eventually destroys the cathode. The dispenser cathode under investigation has a self-healing capability to extend the lifetime.
- (3) To redesign the electron optics to accommodate the 3.81-cm (1.5-in.) envelope and the dispenser cathode.

- (4) To study environmental effects. The component must be designed to withstand the shock, vibration, and temperature environments.
- (5) To determine the effects of the radiation environment on the performance of the entire sensor, particularly on the targets.
- (6) To fabricate and test a prototype 3.81-cm silicon vidicon and a 3.81-cm silicon intensifier target vidicon.

c. Current status. There are 12 months of the 16-month contract remaining. RCA is fabricating the 25-mm targets and investigating the effects of changes in the processing and geometry of the diode structure, etc., to try to increase the signal-to-dark current ratio. Design of the electron optics has not been started. Some preliminary radiation testing of the standard silicon targets has been completed, but more data are needed before firm conclusions can be drawn. However, some tentative conclusions can be drawn at the present time about survivability of the sensor past Jupiter. The term "survivability," as used here, does not include possible interference effects which might cause the sensor to cease operating sometime during the approach and then restart as the spacecraft departs from Jupiter. On a simple survivability basis, the effects of the RTG neutron and gamma radiation are probably negligible. The effects of electron radiation from Jupiter are also probably small or negligible, depending upon the actual trajectory and the amount of inherent shielding. No special shielding is contemplated. The effect of the proton radiation is uncertain. Proton radiation is, to a great extent, mission-dependent and, within a mission, dependent upon the trajectory selection. The proton radiation effect on the JSP 1976 mission is probably very severe.

5. Study and Development of Selenium Target Sensors. Although there has been more experience with selenium sensors than with any other type of television sensor, their lifetime capability on missions of long duration, their resistance to radiation, and their stability are uncertain.

a. Lifetime characteristics. Thirty-nine surplus Surveyor vidicons, between five and seven years old, were tested to see whether or not they were still operational. One had an open filament; two could not be fine-focused; but 36 of the 39 were functional and had a reasonable video

level. Because the vidicons were not tested before they were stored, no quantitative data about performance degradation are available. Photographs taken from five of the vidicons before they were stored were blemished, and there was no increase in the number of large blemishes after storage.

Five surplus Mariner 4 vidicons and two complete Mariner flight cameras, between seven and eight years old, were tested. All were functional. Previous photographs were available from two vidicons, and, again, the large blemishes had not increased.

b. Resistance to radiation. To date, one surplus Surveyor vidicon has been irradiated with 2-MeV electrons. The test showed no significant permanent changes in the operating parameters at about 25 times the TOPS levels, but there was a temporary (two-day) beam landing problem. After the beam began landing on the target again, there was severe shading and geometrical distortion with eventual recovery. There was no permanent change, and it is believed that the problem was possibly caused by envelope charging, which affected the electron optics.

c. Stability. The principal uncertainty in the stability of these targets is that the photoconductor is an amorphous selenium material. Crystallization of the material destroys its photoconductive properties. RCA at Princeton has just started a stability study under an eight-month contract (JPL Number 953194). The objective of the study is to characterize stability and aging in relation to crystallization of the amorphous selenium compounds. Preliminary results indicate that microcrystallization with attendant dark-current increase can be induced by exposure to light as well as by the normal thermal activation expected at room temperature. It is hoped that the study will lead to the capability to quantitatively predict the operating drift, etc., and, thus, the stability of the target performance over the ten-year mission life.

6. Approach Guidance Study. A very important aspect of the imaging system is the approach guidance capability. A study was made to investigate the feasibility of using the science imaging cameras to satisfy the approach guidance requirements (see Section XI for a detailed description of the subsystem).

a. Requirements. The principal requirements are shown in Fig. 119. To obtain approach guidance data, pictures of the satellites of the planets will be taken against the star background to determine the pointing vector between the spacecraft and the planet. The dynamic range must be sufficient to expose dim stars and bright satellites simultaneously.

b. Status. Because the sensors under development were not available, laboratory measurements were made using a commercial 2.54-cm (1-in.) silicon vidicon at standard television rates. Based on these measurements, the star detection threshold for the silicon and silicon intensifier target sensors to be used on the baseline system were estimated as follows: (1) a silicon vidicon with 22.86-cm (9-in.) optics and a 50 percent transmission with a 1-s exposure time could detect a seventh magnitude star and (2) a silicon intensifier vidicon with a gain of about 1000 could detect a star between the eleventh and twelfth magnitude. The only actual data available are from two tests. The first was a JPL test of the Mariner Mars 1971 breadboard camera, which uses a selenium vidicon. The same estimation procedure was used as for the silicon vidicon. Estimates are that the selenium vidicon should have been able to detect a star of about four and one-half magnitude. The camera actually did detect a fifth-magnitude star.

The second test was made by RCA on the breadboard Apollo SIT color camera. Rough, conservative estimates are that this camera should be able to detect between fifth- and sixth-magnitude stars. They actually can detect eighth-magnitude stars.

By using these data points, then, for any other combination of optics diameter and exposure time, it is possible to estimate what magnitude of star the camera can detect.

Figure 120 shows the results of these estimates for various combinations of focal length and the diameter of the optics for a silicon intensifier target sensor. From a selected focal length and optics diameter, it is possible to read the maximum spacecraft attitude drift rate which allows an exposure time long enough for detection of two stars of the required magnitude in the field of view. With a drift rate of a little less than $30 \mu\text{rad}/\text{sec}$, the baseline narrow-angle camera should be able to detect two stars in the field of view. Geometric accuracy is a stringent requirement. The

separation of the stars should be measured to an accuracy of 15 arc-s. In the past, objects within a field of view have been located to one or two picture elements. Six picture elements on the narrow-angle camera subtend 15 arc-s. Therefore, the 15 arc-s accuracy requirement should be possible. The major uncertainty is that blooming will occur because of the wide exposure difference between the satellites and the stars. What effect this will have on geometrical accuracy is not known.

Figure 121 shows the same information for the wide-angle silicon vidicon camera. It is estimated that, if the spacecraft attitude drift rate is less than about $20 \mu\text{rad/s}$, this camera can also see two stars in the field of view but, unless the objects can be located to less than one picture element, which is unlikely, the geometrical accuracy requirement cannot be met.

c. Conclusions. Conclusions of the study are that (1) the baseline narrow-angle camera has the potential for meeting the approach guidance requirements, and (2) the baseline wide-angle camera has a backup capability, but with a reduced accuracy. The major area of uncertainty is the effect of blooming on geometrical accuracy. A blooming problem is expected at the brighter satellites of Jupiter and Saturn, but how much the effects will reduce accuracy is unknown.

7. Requirements Imposed by Imaging Subsystem

a. Spacecraft attitude and scan platform control. The imaging subsystem places the following requirements for stability and control on the spacecraft and the scan platform:

- (1) Attitude drift rate, $20 \mu\text{rad/s}$ (about $25 \mu\text{rad}$ at Pluto).
- (2) Pointing accuracy, ± 0.2 deg of a desired angle.
- (3) Platform step size, 0.1 deg to control the amount of overlap for mosaics.
- (4) Viewing directions, 4π steradian for continuous viewing of satellites, planets, rings of Saturn, etc. The location of the satellites is not as certain as that of the planets, and a new satellite could appear anywhere in the field of view. Sections of

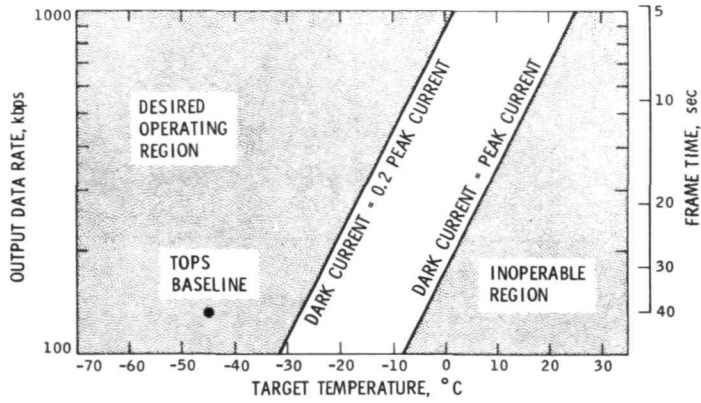
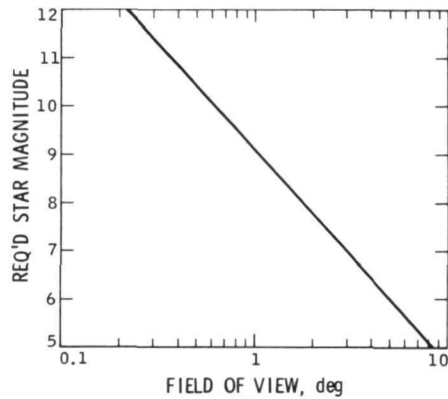


Fig. 118. Silicon target sensors, temperature/data rate tradeoff (no radiation damage)

- SUFFICIENT SENSITIVITY TO DETECT TWO STARS PER FIELD OF VIEW



- ABILITY TO MEASURE ANGULAR SEPARATION OF STARS AND SATELLITES TO ± 15 arc sec
- SUFFICIENT DYNAMIC RANGE TO EXPOSE STARS AND SATELLITES SIMULTANEOUSLY

Fig. 119. Principal requirements, approach guidance study

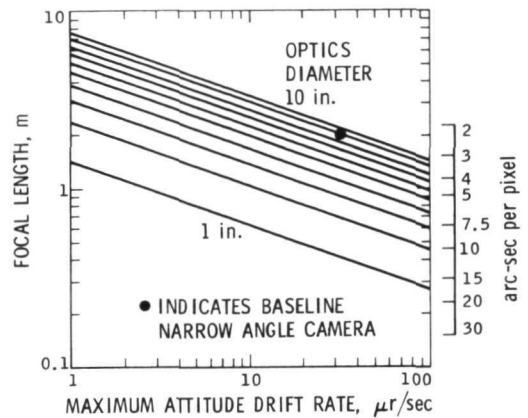


Fig. 120. Approach guidance camera design, 3.81-cm silicon intensifier target sensor

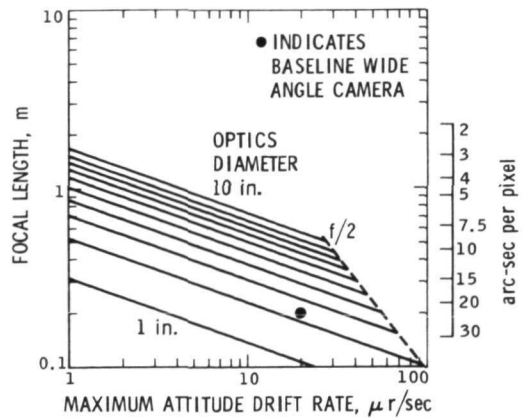


Fig. 121. Approach guidance camera design, 3.81-cm silicon vidicon

the 4π steradian field of view may be eliminated later when better data about satellites are available.

- (5) Slew rate, 0.5 deg/s, both axes, to permit slewing between the satellite and the planet without losing significant amounts of data.
- (6) Settling time, 1 min to 20 μ rad/s after slewing to prevent loss of more than one or two frames.

b. Spacecraft data system. The following requirements are placed by the imaging subsystem on the spacecraft data system:

- (1) Data rate, 131 kbits/s minimum.
- (2) Ability to transmit data without using tape recorder to prevent loss of data if recorder fails. A data buffer has been incorporated which can store or transmit, and, because the buffer cannot hold an entire frame of uncompressed TV data, a TV data compression mechanism will be used on board.
- (3) Mass storage, 400 frames (2×10^9 bits uncompressed).

c. Miscellaneous

- (1) Target cooling, -45°C max temperature, possibly by thermally isolating the sensor, deflection coils, and preamplifier from all other electronics and heat-producing components in the camera head and then passively cooling the entire package.
- (2) In-flight calibration using the Sun or some onboard source.

IX. SPACECRAFT DATA ACQUISITION

A. Spacecraft Data Subsystem

The TOPS data handling system comprises five individual subsystems, which together form the basic function of spacecraft measurement and control: (1) timing synchronizer, (2) control computer, (3) command decoder, (4) measurement processor, and (5) data storage.

The principal responsibilities of the data system in measurement and control are: (1) control of the state of the spacecraft, (2) distribution of commands, (3) computation and analysis of data, (4) fault detection and correction, (5) provision of a common timing source, (6) control and sequencing of the science payload, (7) processing of measurement data, (8) encoding, formatting, and buffering of measurement data, and (9) storage of science and engineering bulk data.

The design of the data system was strongly influenced by the unique requirements of an outer planet mission. The 10- to 12-yr lifetime, several times the span of near planet mission, necessitated a data system capable of recovering from permanent internal faults. The unknown hazards of the flight imposed on the data system a recovery capability from externally induced transient faults. The 8-hr communication delay which occurs at the outermost planets, Pluto and Neptune, and the weekly data dump necessitated an onboard decision-making potential. Finally, physical limits to the weight and power of the data system, as well as its extreme complexity, placed a requirement for extensive use of low-power, large-scale integrated devices.

The components of the data system and their relationship are illustrated in Fig. 122. The Timing Synchronizer Subsystem (TSS) is a highly redundant oscillator centrally located within the data system. The TSS provides synchronized clock signals to all spacecraft subsystems including the data system itself. The Control Computer Subsystem (CCS) functions as spacecraft control, fault detector, and data analyzer. The CCS also detects and executes ground commands. The Command Decoder Subsystem (CDS) decodes and executes ground commands as a redundant function to the CCS. Either subsystem can accept a ground command and, depending

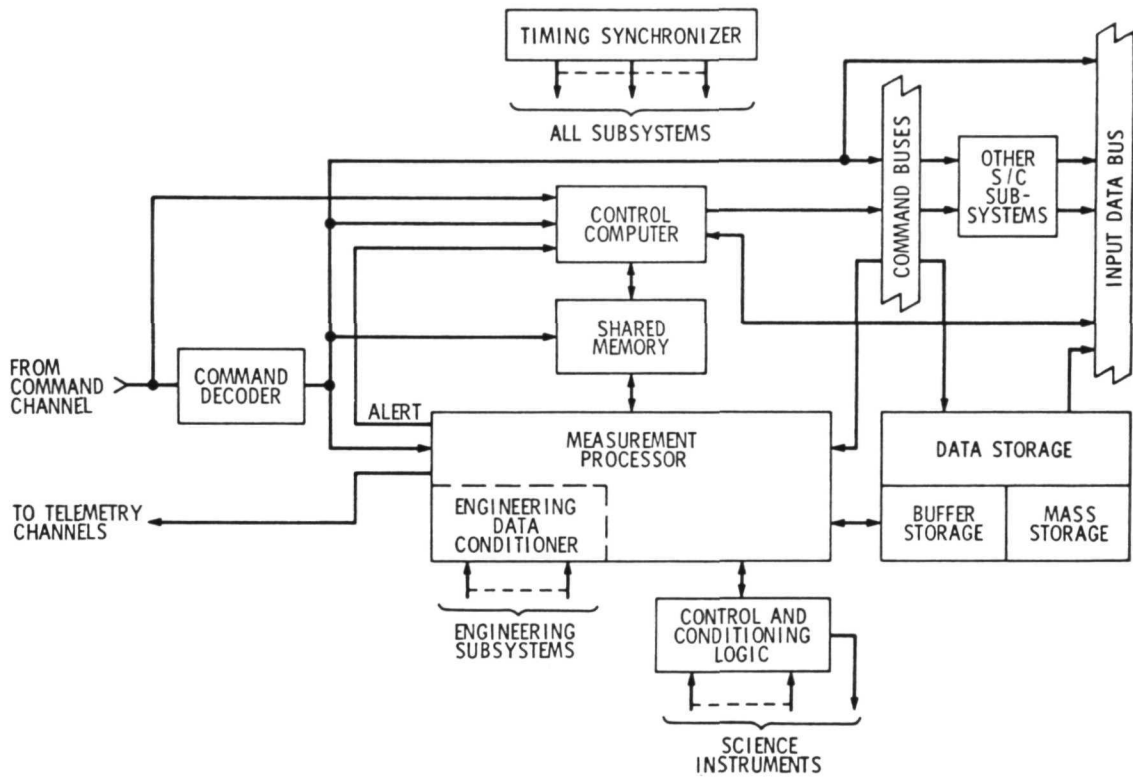


Fig. 122. Data system

upon the current mode, one or the other system will execute the command by way of the command busses.

The Measurement Processor Subsystem (MPS) is responsible for the sequencing and formatting of all science and engineering data. A stored program machine, the MPS is capable of data editing and data compression. Engineering data enters into the MPS by way of a data conditioner, consisting of a 512 channel multiplexer. Science data, on the other hand, enters the MPS through a special interface called Control and Conditioning Logic. The CCS and MPS interact and work together by means of a shared memory. Computer programs as well as latest sample data values are stored in the MPS memory bank and are available to the CCS, for whatever purpose, on call. The fifth and final constituent of the data system, the Data Storage Subsystem (DSS), consists of two parts, a buffer storage and a mass storage. The mass storage is a tape transport (2×10^9 bits), while the buffer storage is a solid-state device primarily used as a rate buffer to the tape transport, but also available as back-up storage for image frames.

Two of the above subsystems of the TOPS data system (CCS and DSS) bear further, more detailed discussion. First, the principal subsystem, key to the functioning of all others, is the Control Computer Subsystem (CCS). This special-purpose computer, employing about 100 instructions in its instruction set, is a serial operating machine functioning at a clock frequency of 500 kHz and an add time of 36 μ s. Memory requirements are 4 K word read only, 8 K read-write, and 4 K shared memory also read-write. Memory transactions are made at 32 bits per word.

The computer employs a highly advanced regenerative concept developed at JPL. Known as STAR, for Self-Testing and Repair, this innovation incorporates standby redundant processors and a test and repair processor. The latter monitors other processors in the CCS and switches to a standby unit when a processor is identified as nonoperating.

Finally, the computer features two types of interrupts: 3 hard-wired and 20 software. The hard-wired interrupts, one from power, one from the MPS, and the third to start command decoding, force immediate transfer

of program control. The others are serviced according to predetermined priorities stored in the CCS memory.

The mass storage facility of the Data Storage Subsystem has two fluid-filled tape transports, each with a capacity of 10^9 bits. This provides a storage capability of 390 images based on an $800 \times 800 \times 8$ frame. The primary function of buffer storage is to rate buffer data in and out of the tape transport. Storage is provided in 35 modules, each with a 65-kilobit capacity, for a total of 2.3×10^6 bits. Since this total is roughly half of that required to store a full, uncompressed imaging frame, an onboard 2:1 compression ratio is implied. The data input rates to data storage are between 0 and 150 kbits/s on the average, while data arrives in bursts up to 1 MHz. Plated wire is the baseline technology selected for buffer data storage.

The Control and Conditioning Logic (CCL) of the data system is a special-purpose interface that mates the MPS with the varying and unique interfaces of each science instrument. Complexity ranges from a few logic elements to several hundred, providing a flexibility that permits last-minute changes in payload without effecting major impact to the data system. The basic functions of the CCL are micro control and sequencing. The CCL also performs special-purpose processing required by science instruments, including data compression, data editing, and data encoding.

The flow of command and control though the data system is executed in three ways. The first method is based upon programs stored in the CCS prior to flight or updated during flight. These programs are executed as a function of mission time in a normal predetermined sequence. The second method of executing command and control is by way of ground commands, reaching the spacecraft through either the command decoder subsystem or the control computer subsystem. Commands reaching the command decoder are executed upon receipt, while those passing through the control computer can be stored and executed at a later date. The third method of executing command and control is dependent upon real-time events aboard the spacecraft. This method involves interruption of the CCS by either the MPS, the power subsystem, or others. In event of a power failure, for example, the critical nature of the event justifies a

direct alert from the power system to the CCS, where immediate remedial action is taken.

Measurement data is processed through the data system via two channels. The first of these is a low-rate, fixed format channel with a data rate between 8 and 32 bits/s in ratios of two. This flow may be governed (commanded) from the ground. The output consists of nonimaging science and engineering data. The second channel is a high-rate variable format channel, with a data rate between 8 K and 131 kbits/s. This channel, too, can be commanded from the ground. Data flowing through the second channel is of two types: real-time nonimaging science and engineering data; and data from the data storage. Again, storage data consists of two types: imaging data (compressed, or not compressed), and nonimaging science and engineering data. Data streams from both channels are time division multiplexed, with suitable PNs and subframe IDs added, and are stored in the data storage.

The primary high-rate format for measurement data, as processed through the data system, consists of 3,584 bits. The data block is headed by a 15 bit PN code and 13 status bits. The remaining part of the primary frame consists of the real-time and stored data blocks just discussed.

Stored data consists of imaging and nonimaging data. Each data block is headed by its own 24-bit PN code plus identifiers. Because the data are compressible, the data blocks are both variable, resulting in an overall variable length format.

The status of subsystem development of the TOPS data system at close of the project was as follows: All subsystems had progressed through the conceptual and functional phases except for the control and conditioning logic (CCL) and data storage, which were still in functional design. An exception was the image data compression algorithms of the CCL which had progressed through detailed design, breadboarding, and were in the testing phase. The control computer and timing synchronizer subsystems were in detailed design. The command decoder had been functionally designed and was ready for detailed design. The measurement processor had progressed through detailed design and breadboarding and was in preparation for testing.

B. Measurement Processor Subsystem

1. Introduction. The measurement processor subsystem (MPS), in conjunction with the control computer subsystem (CCS), forms the heart of the TOPS data system.

The MPS is a special-purpose computer that gathers data from all spacecraft sensors and instruments and multiprocesses these data into CCS alerts, science and engineering real-time data formats, and science and engineering stored data formats. The MPS controls the control and conditioning logic (CCL) which interfaces with the science instruments. All MPS functions are programmable by either the control computer subsystem (CCS) or the command decoder subsystem (CDS).

a. Output channels. The MPS has four output channels: high rate, low rate, nonreal time and CCS.

The high-rate channel has a wide variety of data rates that allow optimizing the signal-to-noise ratio for the various planetary encounters and cruise modes. This channel is used for nonreal-time data dumps, CCS memory data dumps, transmitting TV data, and is time shared with varying percentages of programmable real-time data. The data rate varies from 8 to 131,072 bits/s in 3-dB steps.

The low-rate channel contains fixed formats of real-time data from all spacecraft measurements. It is not programmable. In event of loss of programmable formats, a definite set of data from each measurement is available to attempt reconfiguration. The data rate varies from 8 to 64 bits/s in 3-dB steps.

The nonreal-time channel transmits data from the measurement processor subsystem (MPS) to data storage at a 1-mHz clock rate as needed.

The CCS channel provides recent measurements of all sensors through the shared memory. In addition, alerts are provided through this compressed channel when critical measurements are out of limits.

Any measurements that the MPS can access may be outputted on any combination of the four channels.

b. MPS tradeoffs. The MPS differs from Mariner telemetry in that it has:

- (1) A highly programmable capability for sampling sequences for all data sources.
- (2) On-board data processing and compression.
- (3) Interactive relationship with the CCS.
- (4) A self-test and repair capability, backed up and enhanced by the CCS's self-test and repair capability.

The MPS/CCS combination is more efficient than a single CCS with speed adequate to do both jobs.

c. Data processing rationale. Throughout the mission data will be transmitted in real time, on the low-rate channel, for monitoring as desired. In cruise mode, monitoring will be performed periodically — perhaps once a week. Storage space is limited and efficiency is an absolute requirement. At the same time, high sampling rates are desirable in order that no data are missed. These conflicting requirements are best met by the use of onboard data processing.

d. CCS-MPS relationship. Another point of departure from Mariner design was the CCS-MPS relationship. The CCS monitors the MPS periodically to check its performance. The CCS reprograms the MPS in response to changes in mission phase, or to interrupts from the MPS. The CCS can control MPS redundancy switches if necessary, and can provide optional and/or backup capabilities to the MPS. The MPS provides spacecraft data to the CCS shared memory. Finally, the MPS will alert the CCS if data goes out of limits.

e. MPS redundancy. Most units in the MPS contain alternate processing paths; thus, the MPS can be programmed not to use functions that have failed. Most functional units of the subsystem are standby redundant, with power switching of standby redundant spares. Within the MPS program, a rollback structure is provided to prevent error propagation in the case of transient error. If error is permanent, the MPS will switch to redundancy. Error detection is enhanced by the use of coded words.

f. Fault checks. The MPS makes use of many internal checks to detect a fault in the system. A list of such checks follows:

- (1) A residue coding technique checks on words accessed from memory.
- (2) Following transfer of data from the memory into a register, the register is rechecked by circulating the data and determining that the code was intact.
- (3) Excessively long strings of ones or zeros in the data stream are detected; they may be caused by data bits stuck in the register.
- (4) Proper data response to known inputs is checked by placing test samples at various places in the sampling program. When a sample appears, a particular response is expected. If this fails to happen, an interrupt occurs.
- (5) Tests for proper bit combinations in key registers.
- (6) Coincidence tests controlled by a hard-wired counter.

Because of the unique structure of the MPS, the detection circuits described above created no more than a 3% increase in system complexity, yet detected an estimated 85% of failure modes. This contrasts with the near 100% fault detection capability of the CCS (STAR Computer), and indicates why the MPS is much lighter than the other mechanism and requires less power.

g. MPS adaptivity. With CCS support, a high degree of adaptivity exists in the MPS. This capability allows more efficient use of data storage resources and provides for quick response to unexpected science events. This is important because scientists cannot predict with assurance what phenomenon is to be expected in the reaches of space beyond Jupiter. Eight-hour turnaround time would not permit immediate changes in data rates, for example, or allow necessary activities for manual sampling.

High adaptivity also provides for quick response to unexpected spacecraft malfunctions, and reduces chance of lost data caused by MPS malfunction.

h. MPS function. Data from engineering sensors enters the MPS through an engineering data conditioner (Fig. 123). Data from analog sensors enter through an analog tree switch. Data from science instruments are introduced into the MPS via the control and conditioning logics (CCL).

The micro control of this input operation is performed by the sequencer module. Again, the overall macro control of the MPS is the province of the mode-I/O module.

Once incoming data enters the multiplexer module (MUX), it is sent to the data processor module. There it is compared with previous samples from the contributing sensor (brought up from memory) and a decision is made to its significance. If the data has changed from previous measurement, i. e., is significant, it either triggers a CCS alert (if error is suspected) or the data are sent into storage.

If, on the other hand, the data are to be sampled with a real-time format, the multiplexer module sends it to the real-time buffer module, thence to the formatter module where it is mixed with stored data. The resulting data are then sent out on high-rate channel A to the mod/demod subsystem (MDS). Simultaneously, low-rate real-time data from the multiplexer formatter module are being outputted on Channel B. The composite sampling rate to support all the foregoing activities can be as high as 14 samples per second.

2. Mode I/O Module (MIO). The MIO controls the mode-timing, self-testing, and redundant unit coordination within the MPS. It interfaces with the CCS, CDS, timing synchronizer, power system, and shared memory. Basically, the mode I/O is a hardware module, and consequently cannot be backed up by the CCS.

3. Sequencer Module (SEQ). The sequencer module determines the order in which samples are taken. It can accommodate samples from as many as 1024 different sensors, at rates up to 14,000 samples per second. Because, in the nominal TOPS configuration, commutation structure has

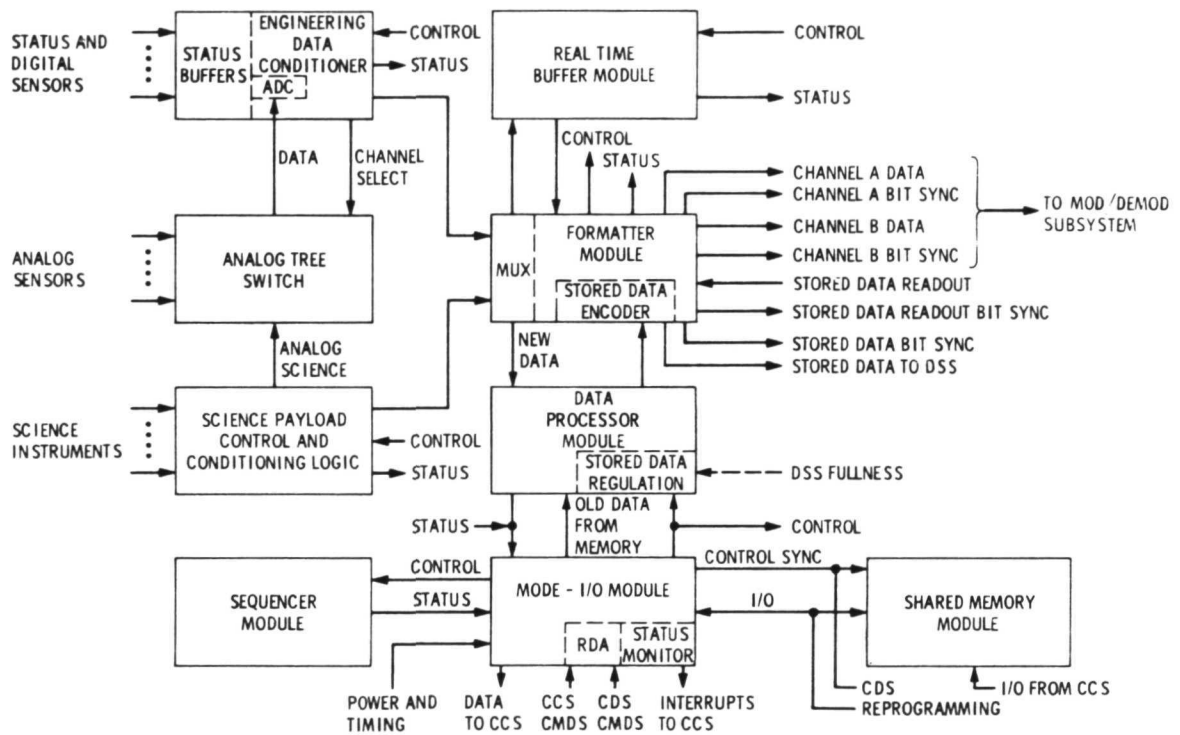


Fig. 123. Functional block diagram measurement processor

been provided for 512 sensors, two algorithms can be related to each sensor within a given program. Consequently, there is provision for one set of limits, e.g., for computer alerting, and a second set of limits for memory outputting. In addition, real-time editing is carried in the same control words, thus providing a third capability for each of the 512 sensors.

Within a format the sampling rates vary 32,000 to 1. This permits sampling of some sensors at 100 times per second, and others at 10 to the hour. The base rate can be varied over a very wide range also.

The sequencer module has a 100% self-test capability, as well as CCS backup.

a. MPS instruction word types. The MPS memory organization uses three types of instruction words: index words, control words, and data words.

Index words control timing. These words establish the number of samples that can be taken at given rates: one word per sampling rate. They furthermore set up do-loops which access a second type of words (control words) to memory. Control words are distributed one to the sensor, or for every sensor-algorithm combination, a maximum of 1024. In controlling data accessing and processing, control words allow a unique algorithm to be related to each sample taken, and allow any combination of sampling order. Even as index words establish the number of samples to be taken at given rates, control words direct the samples into slots that have been allotted.

Data words are connected with each sensor and are accessed simultaneously with samples being taken from the sensor. They provide reference data: tallies of the number of significant samples taken from a sensor within a given interval and previous data values from the sensor. One data word is related to each sensor.

If the CCS, for some reason, required more than two previous sample values from a particular sensor, it would be expected to store within its own memory earlier values, then periodically transferring the data value from these words. These words would provide the CCS with the most recent sample value from each sensor.

The MPS can change the location of data and index words, but not control words. Because each word carries an error detection code, it is impossible for a change to occur in the MPS program without the MPS error detection device noting the change. An exception is where the change has been predetermined and properly placed in the memory, either from ground commands or by the CCS under control of a prescribed program known to the ground. Changes in the program are described to the ground, and the ground, knowing the initial program, will thereby be constantly aware of the status of the spacecraft.

b. Data processor module. The data processor module provides several types of algorithms that are principally of use for engineering data. It provides a maximum-minimum type of algorithm with limits variable in 3% steps. The algorithm sets limits whereby data values above or below the limits is considered significant. It is particularly useful for CCS alerting.

Engineering telemetry relies heavily upon a zero-order compression algorithm. This algorithm designates a data sample significant if it changes from a previous sample by more than a certain percentage. The percentage is widely variable, and the choice of the algorithm on the percentage apertures can be made in each control word for each sensor, uniquely determined.

The capabilities of the data processor module allow efficient use of the DSS, CCS, and the RF channel. In addition, it provides output regulation on the telemetry channel, unimportant because of the wide variation of sample rates. For example, if samples are being harvested at a rate too swift to store or transmit to Earth, the sampling rate can be retarded, and conversely, if more samples are desired, the rate can be increased. Provision is also made for confidence samples—samples transmitted at fixed intervals, say every 50th sample taken. One such sample would be generated for each pass through an MPS format.

The data processor module is capable of 100% self-test, and has CCS backup. A failure in the module results in noncompressed data.

c. Multiplexer formatter module. The multiplexer formatter module provides the fixed-sequence generation on the low-rate channel. It also provides engineering data formatting and encoding effective for compression ratios from unity to 1000 to one or more. Limitations are established by the mandatory confidence samples.

The module interfaces with data storage, the modulation-demodulation subsystem, the control conditioning logic, and the engineering data conditioner. The module is 85% self-testable, and 70% of it is capable of being backed up by the CCS. The parts not capable of backup are the unique gating and the multiplexing structures that interface for the instruments.

In failure circumstances of the MPS, the multiplexer-formatter module and the mode I/O module alone can accomplish a useful mission. This can be done in two ways: either the CCS backs up the sequencing function; or fixed program data are generated, and the CCS utilizes the interface provided to obtain required samples. Two-thirds of the modules of the MPS can fail, and yet useful information will reach the Earth.

d. Real-time buffer module (RTBUFF). The RTBUFF edits and buffers programmable real-time data and mixes the data with engineering data from storage. It is 90% self-testable and has 45% backup from the CCS. A failure in this module results in loss of programmable real-time data. Failure does not affect output of TV data, stored data, or real-time data transmitted on the high-rate channel.

e. Tree switch module. The tree switch analog commutator multiplexes analog measurements. This commutator incorporates extensive internal redundancy, using complementary paths for critical measurements. Complementary paths, with some branches distributed to other subsystems, diminish the failure hazard; a short in one path will not affect the complementary path. It is believed that the tree structure will lose less than 1% of its paths over a 10-yr period, despite the large number of sensors subject to sampling.

f. Engineering data conditioner (EDC). This module contains ADS, analog conditioning, and digital status measurement buffering as needed. A breadboarded EDC generated in the TOPS program consisted of ADC and MPS telemetry circuits.

g. Shared memory. The seven shared memory modules aboard the spacecraft allow the CCS and the MPS to have effectively unlimited access. Access is provided through two parts, each with its own address and data registers. Access to the core plane itself is provided, with two MPS cycles for every CCS cycle.

The shared memory module is 100% self-testable and repairable. Although the seven MPS modules may all be used for shared memory, normally only one is so powered, for the MPS and two are powered for the CCS only.

h. MPS design flexibility. Design structures stipulate that most changes in the MPS will be in software only. Hardware is designed modular to permit easy switching around a failed unit. Again, changes required in a particular function are limited to a specific module; the interfaces with other modules do not change, providing cost effectiveness.

Flexibility allows late definition of detailed sensor requirements. With engineering sensors this involves software programming, with science instruments modification of CCLs.

The MPS is highly flexible as to number of sensors, types of sensors, instruments, sequences, sampling rates, and types of processing. Sensors can be added or deleted from a sequence, and sequences and sampling rates can be changed. Importantly, such changes do not affect other sensors. Any number of sensors can be sampled at any rate desired, with limitations only in the degree of compression, in the data storage capacity, and in the composite rate on the real-time channel.

Processing and rate can be individually optimized. New or unknown requirements can be adapted. The alternate path capability in the command system permits new improved programs to be installed in the CCS, an important consideration in a 10-yr flight profile.

i. MPS Development Status. At close of the TOPS project the MPS breadboard design and construction was complete. The breadboard had been debugged. Ground support software had been flow-charted and written. A test setup was being designed that would allow simulation of other TOPS subsystems for the purpose of conducting MPS interface tests.

j. Control and Conditioning Logic (CCL). The primary function of the CCL is to provide control and sequencing commands to instruments based on the coded control word it receives from MPS. In this sense, the MPS acts as executive over the CCL. Long-term commands from the CCS are sent to the MPS, then to the various CCLs. Short-term commands are included within the words the MPS is utilizing in do loop sampling in its programs. The same address used for addressing a CCL for sample purposes can be used for control purposes; a different algorithm will be mentioned, in such case, in the MPS control field.

A second function of the CCL is to perform analog-to-digital conversion or pulse counting on the instrument data, and data editing and data compression unique to the instrument. Again, the CCL is used to transfer the digitized data and instrument status to the MPS at a predetermined time.

Finally, the CCL provides signal interface between the instrument and other spacecraft subsystems when required.

k. CCL interface function. The block diagram shown in Fig. 124 illustrates CCL interface with instruments having pulse data.

Data from the instrument's detectors goes to accumulators within the CCL, then to the digital multiplexer and address decoder. Data from the instruments status register reaches the multiplexer directly. From the multiplexer the data proceeds through a data compressor where the pulse data are scaled, providing a limited degree of floating point arithmetic. For example, the five most significant bits would be taken out of 24, and the five tagged to learn how many zeros had been dropped. From the compressor, data are diverted to the MPS.

Analog data from the instrument of course bypass the CCL. Other mechanism within the CCL include timing control logic, multiplex sequencer, and a control word holding register.

l. Compressor restraints. The television CCL is the most complex on the spacecraft. The MPS, through a control word, instructs the TV CCL to initiate a data line. Through this process the MPS determines the worst-case time required to output data from the CCL; thereafter, while TV data are flowing, the MPS allocates its time to sampling, or other

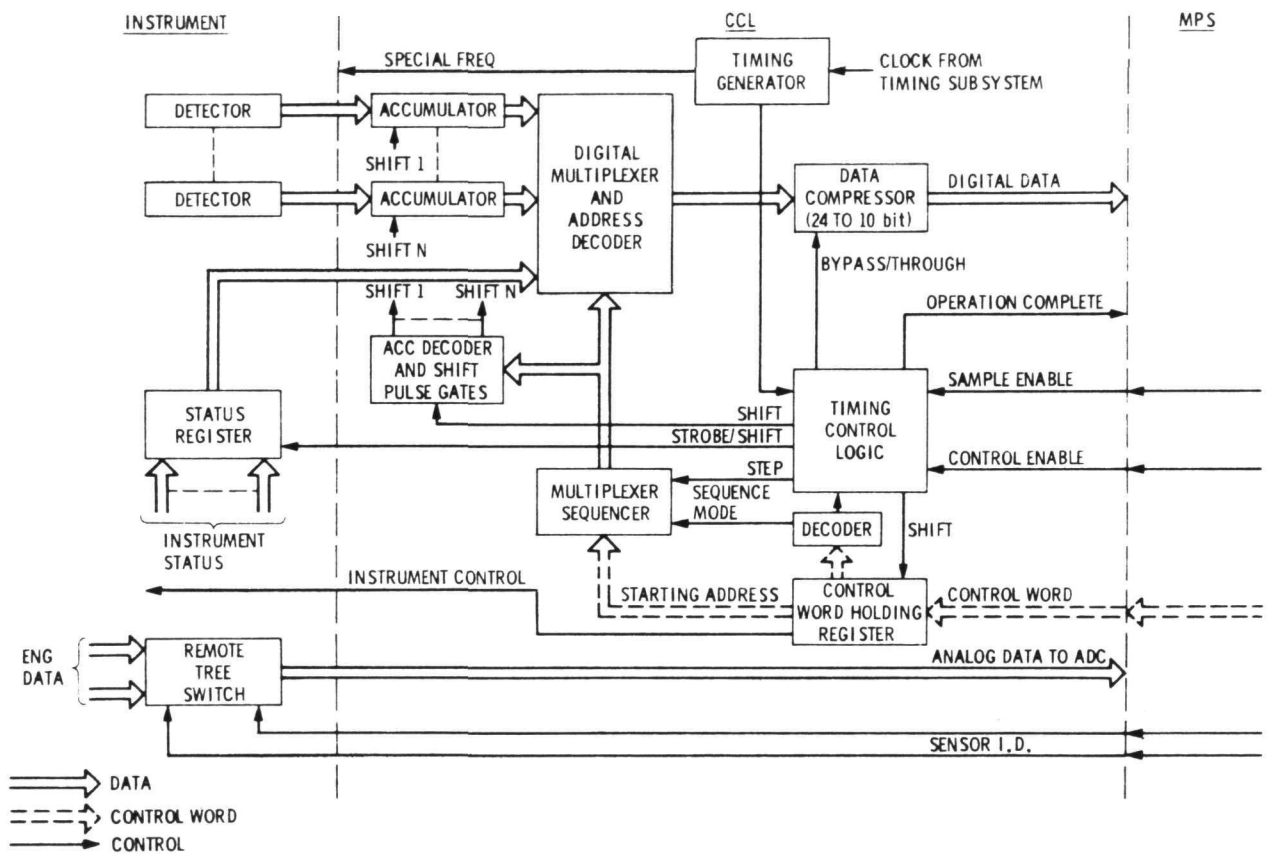


Fig. 124. CCL functional block diagram for interfacing instrument with pulse data

activity that does not involve transfer of storage data, or perhaps it simply idles. Then during flyback time of the TV data the MPS might interleave its own data from the various other science instruments and engineering sources as needed.

The TV CCL contains a television compression algorithm of unique properties. The compressor algorithm preserves information under noiseless channel conditions and is simply implemented. Again, it must perform efficiently through a broad spectrum of picture types, handling all manner of images effectively.

m. TV Compressor features. The compressor adapts to rapid changes in data activity by automatically selecting one of four codes in each block of eight pixels. It examines the data in each pixel and modifies itself to each group of data.

The compressor adapts to slow changes in data activity by automatically adjusting its operating mode on a line-to-line basis. It has a commandable selection of pixel quantization on a picture basis. The algorithm performs within 0.2 to 0.3 bits per pixel of the minimum possible. It is automatically bypassed if it cannot improve on the data reaching it; if none of its codes are data compressed the compressor simply sends straight uncompressed data.

The compressor has three basic operating modes. One involves a fundamental sequence; the others are coded versions of fundamental sequences. The basic compression functions well to an entropy of slightly more than 4 bits per pixel. However, by running only the most significant bits of each pixel through the compressor, up to eight bits may be accommodated. The remainder is either stripped away, ignored, or outputted uncompressed.

In an encounter situation, at far encounter the compression ratio may be 11:1. Halfway into near encounter the ratio drops to 4:1. At the nearest approach, the ratio is 2:1. Past encounter, the ratios build up again.

The inner processes of the TV compressor are illustrated in Fig. 125. After passing through the controlling CCL, data from the camera is either outputted uncompressed, or is sent into two input buffers and an 8-pixel grouping made. The buffers contain two 64-bit shift registers, one to hold

incoming data from the camera, the other to accommodate data in process.

The difference calculator consisting of two 8-bit accumulators computes differences between adjacent pixels as they come from the buffer.

The fundamental sequence generator, an 8-bit binary down counter, generates a sequence of zeros and ones which represent the differences calculated by the difference calculator.

The coder and code selector consists of shift registers and a 3-bit coder which stores, codes, and counts the length of the fundamental sequence based on the length of the coded sequence, and selects the shortest output.

The output data selector selects reference pixel on coded data followed by split pixel (if any) on back up uncompressed data.

C. Data Storage Subsystem

The primary functions of the data storage capability aboard TOPS were to permit noncontinuous tracking during cruise and provide storage of science data during encounters.

1. DSS Size Considerations. On a 10-year mission, during cruise mode a tracking effort is desirable perhaps once a week. Consequently, in determining the size of the data storage subsystem (DSS), engineers assumed a week's storage capacity, or approximately 3×10^8 bits. This information requires a dump period of 4 to 8 hours. Another consideration was an adequate number of imaging pictures. Roughly, a capacity for 200 to 400 pictures of 5×10^6 bits each, or upward of 2×10^9 bits overall, was desired. A total capacity of 10^9 to 10^{10} bits for the DSS was considered to be realistic.

2. Functional Requirements. The DSS was allotted two tape recorders of 10^9 bits capacity each, or 2×10^9 bits in all. A lifetime survival requirement of the mechanism was 12 yr (100,000 h). This assumed a continuously "on," or operating condition for most electronics in the cruise mode, including buffers. The tape recorders, which need not operate continuously, required a 5000-h lifetime. Input data rates varied from 0 to 150 kbits/s,

with a burst capability of 1 mbits/s. The output data rate varied from 0 to 131 kbits/s.

A desirable, more than absolute, requirement of the DSS was simultaneous recording and playback. Another desirable feature: ability to access certain portions of data as desired, rather than waiting necessarily for the normal, full complement of data in storage. Finally, the DSS was expected to perform data quality tests with the control computer subsystem (CCS) to determine DSS failures and data bit error rates. The last, of course, constitutes a self-check capability.

3. DSS Constraints. Weight and power constraints of the DSS are listed in Table 46.

It should be noted that the recording constraint of 61 W is negotiable, not absolute. A lower power requirement would be desirable if attainable. Attitude control of the spacecraft may be affected by stopping and starting the tapes; the uncompensated $I\omega$ of this activity, however, has yet to be determined. Finally, control of the DSS must be subject to CCS or command override.

Table 46. Weight and power constraints for Data Storage Subsystem

Parameter	Maximums
Power	
Record	61 W
Playback	41 W
Record and playback	102 W
Weight	59 kg (130 lb)
Volume	0.053 m ³ (3200 in. ³)
Uncompensated $I\omega$	To be determined
Control	CCS or COMMAND OVERRIDE

4. Why Tape Recorders? After detailed study, tape recorders were chosen for TOPS data storage for several reasons. For one, other possibilities—cores, for example, or solid-state patterns produced on substrates—proved too costly. At upward of 10 cents to the bit, a 10^9 bit capability was beyond serious consideration. Again, alternative storage devices proved too heavy, required excessive power, or were not sufficiently developed. The tape recorder, finally, is well developed; its problems are known and can be addressed immediately.

To be sure, problems inherent in the tape transport are formidable. The recorder is a complex device with moving parts and built-in wear-out mechanisms. Tapes, heads, and bearings wear out and debris accumulates. Chemically complex tapes demonstrate long-range instability. Nonetheless, recorders tested in the TOPS Project functioned well, and although performance over a 10-yr period cannot be demonstrated in real time, it is believed the devices will survive such a flight.

The TOPS approach has been to simplify the mechanical system by use of more electronics, to eliminate consumables, eliminate known wear mechanisms, reduce chemical complexity (no polymeric tapes), and, if possible, to provide limited backup of tape recorder storage with a solid-state buffer mechanism.

5. DSS buffer. The use of a buffer presents a problem of size. A minimum capacity of 8×10^6 bits/s was desired, but proved infeasible; a 2×10^6 device is within possibility and would accommodate a compressed picture.

The advantages of using a buffer are found in maximized efficiency of tape recorder utilization. The recorder can be run at constant speed, with variations of data input or output being accommodated by the buffer. This allows for reduced complexity in the tape recorder, eliminating belts, speed changing, servo switching, etc. Again, input data rates can be increased or decreased by a large factor over that possible with the recorder alone.

The use of two or more buffers has been considered, despite the problems of size and weight, to permit optimum operation of the tape

recorder. While one buffer was filling, for example, the other would be dumping its load into the recorder.

Carrying this a step further, upward of 32 parallel buffers could be employed to feed the recorder serially and sequentially. Eight buffers would be filled in this manner — the number required to feed parallel into the recorder; then the input would be switched to the next buffer group while the full buffer dumped onto the recorder. This permits parallel read into the tape recorder in multitrack fashion and also allows for modularization of the solid-state buffer. In addition to the 32 buffers, provision is made for three spares.

The size of the buffers, as already mentioned, is of concern. The requirement for tape buffering, sufficient to operate a single machine discontinuously, is 10^5 bits. One TV frame and associated science requires 8×10^6 bits. If TV data is alternately stored, 5×10^6 bits are required. One compressed TV frame, compressed at more than 2:1, uses 2×10^6 bits. Of all the foregoing bit requirements, the final size (2×10^6 bits) was chosen for TOPS, for reasons of available technology, cost, size, and weight.

6. Static memory requirements. To summarize requirements for the solid-state buffer capability, the TOPS baseline design is comprised of: (1) 32 modules at 2×10^6 bits each, (2) 3 spare modules, (3) serial access to the tape recorder, (4) data rate input-output of 0 to 10^6 bps, (5) 100,000 h combined reliability of 35 devices, assuming 3 failures, and (6) volatility has yet to be determined.

7. Plated wire memory. While core, flux ring, CMOS, PMOS and MNOS concepts were examined for the buffer memory, the decision was made to use plated wire. Wire was chosen over core partly because it is not desirable to have a core memory that must be read out destructively and then reread back into the memory; the chance exists of losing a bit. Other considerations included favorable factors of power, weight, and size.

The TOPS approach at close of the project was 2-mil plated wire requiring 2 W at 10^6 bits/s read in or read-out. Weight of the stack was estimated at 1.1 lb, and volume 3.3 in.^3 , excluding case and harness.

8. Tape recorder. The design approach for the tape transport incorporates a coplanar reel-to-reel device, with reels driven directly by the motor, thus eliminating belts or gears. The tape itself is of metal, 1 in. \times 0.0005 in. \times 1300 ft. The TOPS approach stressed elimination of all contact between moving surfaces anywhere in the tape recorder. To reduce or eliminate friction, fluid is to be pumped between all wearing surfaces, and hydrostatically pumped pressure (fluid) supports all moving elements, including the tape and its guides, motor rotors, tape reels, etc., in effect, resulting in noncontacting heads and noncontacting bearings. Other design features are simultaneous recording on 8 tracks, and a total of 32 data tracks on a 1-in. tape resulting in 8 tape passes per load/unload cycle of the recorder.

Linear recording density is approximately 2000 bits/in. on each track. This low count is attributed to the lack of contact between head and tape; a lower bit density results.

Certainly a unique feature of the recorder is its fluid environment. Since fluid is everywhere and a reservoir of some type was necessitated, it was decided to make the entire case of the recorder the reservoir. Thus, the tape recorder itself is filled with fluid and then sealed shut. The recorder works in a liquid environment throughout its ten-year mission. The fluid is circulated and filtered by a redundant pump/filter system associated with the tape recorder.

The reel and pump motors are brushless dc motors using Hall-effect commutators.

The open-loop tape is driven by the take-up motor, in other words, pulled. The tape is tensioned by the supply-reel motor, servo controlled to obtain constant tape speed. The speed is controlled by a servo using a tachometer signal prerecorded on the tape.

9. Tape recorder electronics. Electronic features of the recorder include: (1) a self-clocking code that eliminates skew problems, (2) end-of-tape sensors, (3) redundant optical end-of-tape sensors for backup, (4) mechanical sensor to indicate overload of reels, (5) tape position indicator and controller which allows access to 128 tape positions, (6) a ground commandable tape pass sequencer, which allows access to any

of 4 tape channels, and (7) redundant pumps—2 or 3 pumps which are "or"-ed.

10. Hydrostatic transport status. At close of the TOPS project, a breadboard transport was in the design stage, with a math model in development. Tests on fluids were under way to acquire an acceptable candidate fluid. Modeling and analysis were in progress on components of the tape recorder, including the hydrostatic head and bearings. These developments would lead to study of internal parameters.

11. DSS control and interfaces. Electronic interfaces of the DSS are relatively simple, comparable to many extant data systems. Complementing CMMA components would be used. Partial redundancy in electronics would be employed, to a degree not yet determined. Performance checks will be performed periodically, using the CCS and ground command.

DSS control and interfaces requirements for the buffers include control and sequencing of the 35 buffer memories and 2 tape recorders, generation of logic signals for the CCS and MPS, override control by the CCS or ground commands, and engineering telemetry measurements of significant conditions.

D. Command Decoder

The function of the command decoder subsystem (CDS) is to back up the control computer subsystem (CCS) when required, thereby assuring that ground commands reach the appropriate subsystems and are acted upon (Fig. 125). In practice, the command decoder receives digitized command signals from the MDS, classifies them, decodes those where the user subsystem uses very few commands, passes the others, and distributes all signals to the proper subsystem.

The command decoder can insert words into the CCS memory, using CCS hardware, and into the shared memory, using MPS hardware (paths are not shown in illustration). Although the command decoder operates when necessary, i. e., when the CCS is overworked, malfunctioning, or not trusted by ground control, it is not expected that the decoder will be used at all during the first three years of flight and only sporadically thereafter. The design philosophy of the subsystem, obviously, it to make the command system fail-safe.

1. Constraints

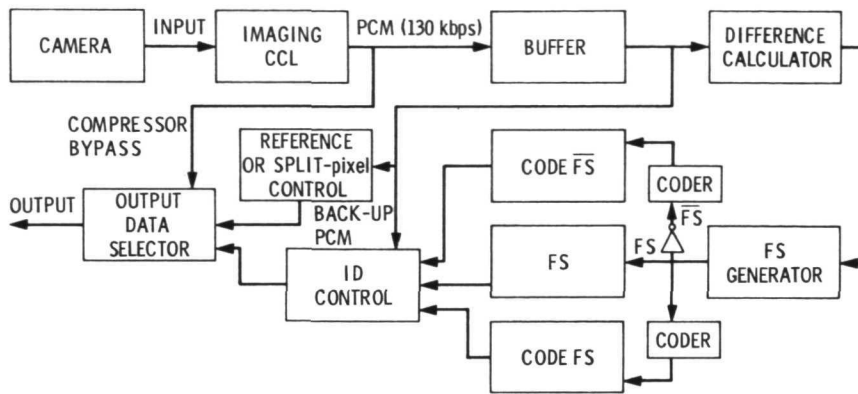
- (1) The command decoder is fault intolerant (one wrong data bit disables it). There is no error correction in the subsystem, making it a simpler and more reliable device. This constraint does not negate the decoder, but places command responsibility on the ground: commands transmitted with errors must be transmitted again, until they are error-free.
- (2) A fixed format is required for all commands. This requirement makes the command decoder less efficient when receiving discrete commands, but the diminished capability is warranted in consideration of a simpler device.
- (3) A third requirement is duplicate command bus systems, one for the CCS, the other for the CDS. These buses duplicate the command bus by which coded commands reach the various subsystems aboard the spacecraft.
- (4) The user subsystems will each carry two or more remote decoders to receive and decode the signals off the buses; the decoded results are merged in the user subsystem.
- (5) The physical characteristics of the command decoder follow:

Power: 4 W

Weight: 1.1 kg (2.5 lb)

Volume: 1650 cc (100 in.³)

2. Formats. The command data stream starts with a mode control prefix (MCP), which specifies the hardware and software configurations used to accommodate the sequence of commands that follow it (Fig. 126). A guaranteed blank space (of 52 zeros) after the MCP simplifies the logic; these are followed by a word sync prefix (WSP). Commands progress after the WSP in 52-bit groups. Commands terminate with arrival of 52 zeros. A new command sequence requires a new word sync prefix.



INPUT BUFFERS:
 DESCRIPTION: • TWO 64-bit SHIFT REGISTERS
 FUNCTION: • OUTPUTS pixels TO DIFFERENCE CALCULATOR
 • OUTPUTS BACK-UP PCM, ref. OR SPLIT pixels

Fig. 125. TV compressor block diagram

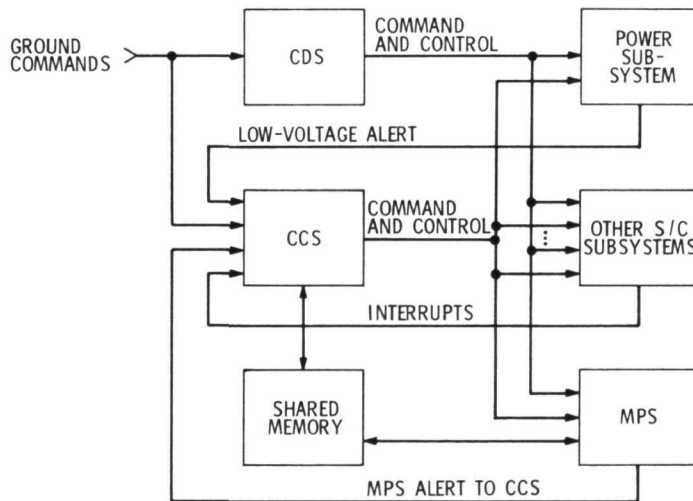


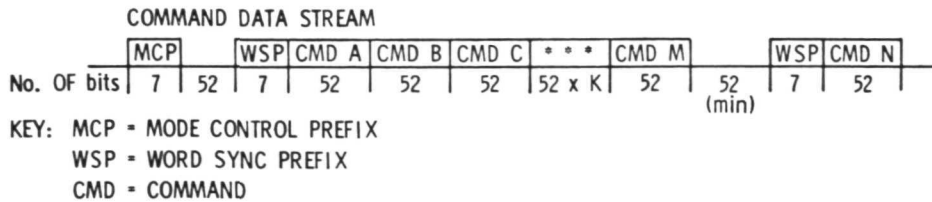
Fig. 126. Command decoder subsystem interface

The processing mode remains constant until the information on the command channel is disturbed in such manner that the command detector goes out of lock. At that point the subsystem requires a new mode control prefix to reestablish the processing mode.

Commands are handled in the command decoder (and in the CCS) in terms of 4-bit bytes in a standard format, as shown in Fig. 127. Bytes 1 through 13 are in order of reception. The address field, bytes 1 through 5, specifies a CCS memory address, if needed. Bytes 6 through 13 are identical to a CCS word. The portion of the word that may be passed directly to the command bus consists of bytes 9 through 13: either a coded command or a short data word. Coded commands contain a zero in byte 12. Short data words contain a nonzero binary number (1–15) that designates the destination of the data. A fail-safe feature requires that every address and word have a 4-bit check byte (bytes 5 and 13), which must be identified before the command decoder will process a command.

3. CDS Function. The overall command decoder subsystem contains a constantly powered mode control decoder (MCD) and two switchable decoder units (Fig. 128). Normally these are in a standby condition until arrival of the mode control word at the start of a command sequence. The mode control decoder analyzes the 7-bit MCP and determines which of five modes (A, B, C, D, or E) has been designated. Appropriate signals are sent to the CCS and power subsystem to switch on either command decoder "A" (CDA) or command decoder "B" (CDB).

In mode A, the normal mode, the CCS decodes ground commands. In modes B and C, one of the decoder assemblies does the decoding, and the CCS monitors the data stream, counting bits to determine when commands are likely to be issued. Modes D and E instruct the CCS to become idle — a condition necessary to reset the CCS if it enters into undesirable activity; for example, issuing wrong commands, or becoming trapped in an endless loop. In this case, following the mode D or E control prefix, the command decoder makes required changes in the CCS memory to break the loop and restore the CCS to its proper role.



COMMANDS

WORD (DATA)								ADDRESS					COMMAND CONTENTS
13	12	11	10	9	8	7	6	5	4	3	2	1	
R	0	x	x	x	0	0	0	R	0	0	0	0	CODED COMMAND FOR COMMAND BUS
R	w	x	x	x	0	0	0	R	0	0	0	0	DATA WORD FOR COMMAND BUS
R	x	x	x	x	x	x	x	R	1	a	a	a	ADDRESS AND WORD FOR RWM1 (CCS)
R	x	x	x	x	x	x	x	R	2	a	a	a	ADDRESS AND WORD FOR RWM2 (CCS)
R	x	x	x	x	x	x	x	R	3	a	a	a	ADDRESS AND WORD FOR RWM3 (MPS)

KEY: x - ANY HEXADECIMAL DIGIT
0 - UNUSED byte; MUST BE ZERO
w - ANY NON-ZERO HEXADECIMAL DIGIT
aaa - ADDRESS WITHIN RWM MODULE
R - MODULO-15 RESIDUE CHECK byte

Fig. 127. Command decoder subsystem, command formats

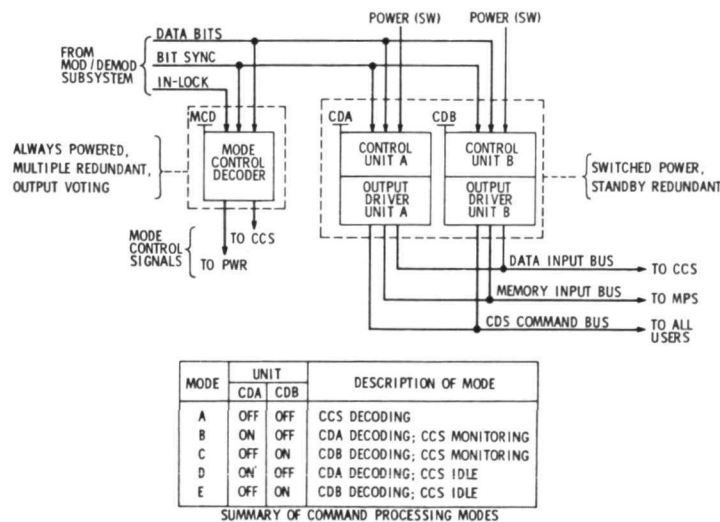


Fig. 128. Command decoder subsystem, functional block diagram

4. Mode Control Decoder. Because the MCD is constantly powered and operative throughout the mission, it is multiply redundant, with possibly triple or fivefold redundancy, and voting circuits in all the outputs (Fig. 129).

The most critical feature of the MCD is the idle signal. Should an erroneous idle signal be sent to the CCS, the mission itself may be aborted. Consequently, rather than one "idle" output, as indicated in Fig. 129, there are as many as five, to ensure a communal decision and provide insurance against failure of one.

Data bits entering the holding register are compared with a dictionary of five possible acceptable prefixes. When a prefix is recognized, activity in one of the five modes is initiated, and a "done" signal is sent to the sequence controls to inhibit further action of the MCD. The MCD then sits idle until next called upon. A signal from the MDS indicating that command lock has been broken reactivates the decoder.

5. Command Decoders - CDA and CDB. Whenever the command decoder subsystem (Fig. 130) is functioning in a command traffic mode, either the CDA or CDB will be in operation, counting bits to determine the decoder's position in the data stream and searching for a word sync prefix. Data bits entering either command decoder are directed to a word sync detector. When the detector recognizes one pattern that will be standard, i. e., a word sync prefix, it directs the main sequence controls unit to take over. Data bits are then shifted into the storage register. When 52 such bits have accumulated, the sequence control instructs the output driver unit to transmit the data to the CCS, to the MPS, or onto the basic command bus.

Interlocks are required to guard against too many commands being accommodated simultaneously. Prior to sending a command to the CCS an interrupt is dispatched to the unit. The interrupt is noted by the CCS, which responds at a convenient point in its program with a request to transmit the data. Messages to the MPS must wait upon an interlock signal signifying that the subsystem is not using the memory during the next two or three microseconds; thereupon, the message is dispatched to the memory.

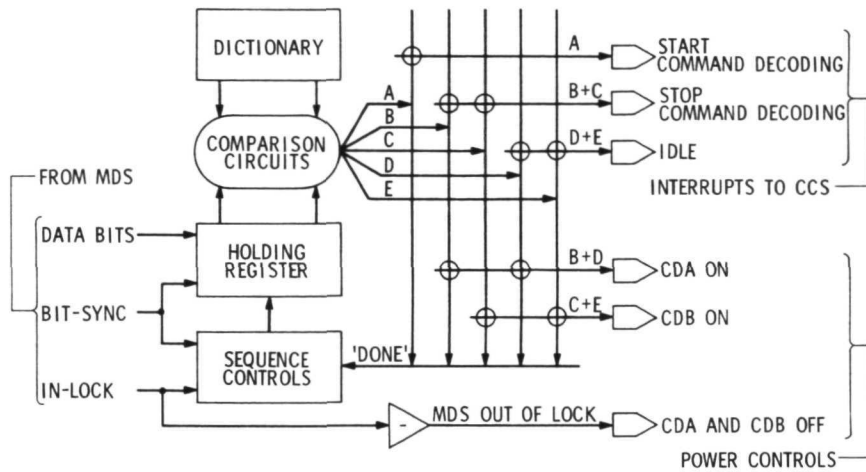


Fig. 129. Command decoder subsystem, mode control decoder

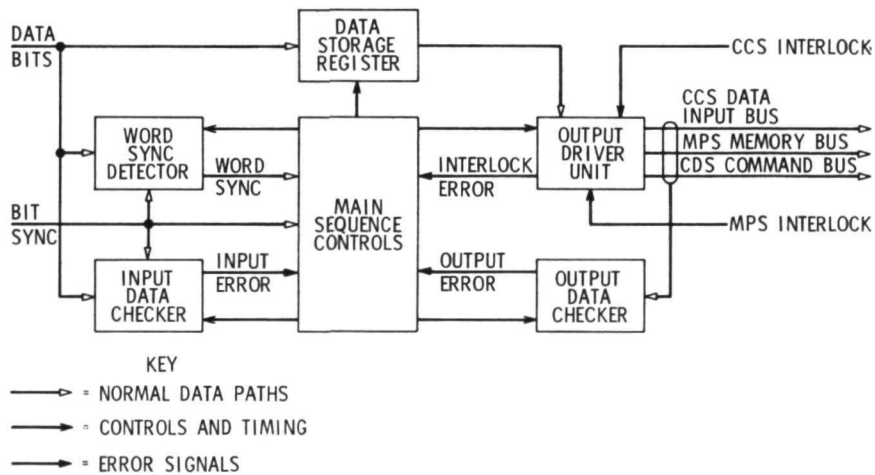


Fig. 130. Command decoder subsystem, command decoders - CDS and CDB

If there is error in the incoming message, the input data checker will detect it and send an input error signal. Again, if any one of the interlocks does not function before arrival of the next bit, there is transmitted an error interlock signal. This serves to prevent the occurrence of undelivered messages. If there is an error in data sent to the buses, it is monitored and will result in an error output signal. The latter locks the sequence control, halting all operation in the CDS. Because no provision was made for unlocking the command decoders from the CCS, or by ground control, the sequencer will remain locked until its power is turned off.

6. Command Buses. Two command buses go to all major subsystems; the CCS command bus, and the CDS command bus. At each subsystem, signals are tapped from these buses into two remote decoder arrays. These remote decoder arrays decode the byte serial pattern on one of the buses and energize a discrete line to the subsystem. Corresponding lines from the decoders are logically OR-ed in the user subsystem. Commands originating in the CCS — maneuver commands, for example — will not be OR-ed, nor are commands that are issued from the ground but not from the CCS. The two decoder arrays will be otherwise identical.

7. Subsystem Status. At termination of the TOPS project, the functional design of the CDS had been completed. No breadboarding or detail logic design had been accomplished.

8. Alternate Mechanisms. The use of a variable command format was examined but because the preponderance of command traffic would be memory loading commands, it was decided to create a single format for those, and thereby simplify the system. An error-correction capability in mode control and in the decoder itself was considered. This, too, was discarded because physically the MCD would be increased by a factor of 4 or 5, making it too complex, and consequently too risky. A third alternate mechanism investigated was a stored program device. The advantage was a maneuver command capability. But second thoughts reminded engineers that the command decoder subsystem was strictly a backup facility. As such reliability was its key feature, and because reliability is equated with simplicity, the resulting complexity of an enlarged CDS was overruled.

9. Special Components. Special components required by CDS include the CMMA, a bus driver to impel commands and data, and isolation switches, photon switches and various forms of bus transformers.

E. Control Computer

The control computer subsystem (CCS) controls the programmed operations of the spacecraft. It also controls the self-test and repair (STAR) functions of the spacecraft. A third function of the computer is the decoding of ground commands.

The STAR approach was chosen for the CCS over two other failure detection and repair concepts—the reconfigurable multiprocessor, and repairable triple modular redundancy (TMR). The reconfigurable multiprocessor was rejected because in relation to STAR it required more hardware and extensive software—resulting in extra complexity, extra memory requirements, and higher design cost. STAR was selected over a hybrid TMR (containing spares) because the latter, like the multiprocessor, required more operating hardware, and, of course, more power. Again, the TMR uses more spares than does the STAR, adding to weight and volume. A third factor militating against the TMR is that it is not self-repairing; repairs must be directed from the ground. This incorporates an 8-h turnaround liability on the system in the outer planet region, and carries the hazard that a second failure may occur before the first is repaired.

1. The STAR Concept. The STAR concept is not a new or unique concept of redundancy. It is rather an optimum combination of selected redundancies. Information coding, control logic partitioning, and internal generation of status indicators are employed to enhance the detecting of failures, when they occur. All information within the CCS and all communication with other subsystems (except interrupt signals) are residue coded. All internal control signals are also appropriately coded. Status signals are uniquely produced by the internal logic at strategic locations and times during the execution of each instruction. These status indicators signify satisfactory operation up to that point in time. The partitioning, or dividing, of control logic helps to ensure that a control failure will produce a faulty code result in the processed information. The test-and-repair

processor (TARP), which is the basic control unit for CCS operation, monitors all of these signals.

Protection from the program errors that some failures may cause before they are detected is accomplished by using selected duplicate and triplicate redundancy.

For repairing temporary or transient failures, the computer resorts to program rollback to achieve temporal duplication of the subroutine. If this is successful, it is assumed the failure was transient. For permanent failures, spares are switched in to replace the failed processor.

This self-test and repair capability is of necessity hardware (hard core) dependent, but so are the alternative systems.

2. Simplifying STAR. The STAR computer previously developed in the Research and Advanced Development program was far too large to incorporate directly into the TOPS baseline spacecraft. The objective was to simplify STAR. Detailed analysis of the computer disclosed two components that could be eliminated completely: the timing processor, and the arithmetic processor. A second hardware-saving operation involved eliminating much of the duplication within the memory, logic, input/output, and interrupt processors. Thirdly, the initial instruction list was reduced from some 200 variants to approximately ninety. This simplified the opcode decoding necessary to implement instructions.

Several basic considerations facilitated the simplification of STAR. The first of these resulted from in-depth analysis of computational requirements, which revealed them to be, after all, quite elementary. All primary functions were performed by simple add, subtract, single-bit shifting. These functions could be incorporated within the logic of the logic processor—thereby eliminating dependency upon the timing processor and the arithmetic processor.

A second consideration was the extensive use of coded commands. By using coded words which could be detected by remote decoders in the spacecraft's subsystems, it was possible to simplify and reduce the need for duplication in the input/output processor, and in the interrupt processor.

Another factor contributing to simplification of the computer related to synchronized interfaces. The Timing Synchronizer Subsystem enables information permits the CCS to be synchronized with pulses in all other subsystems. All subsystems are synchronized with the CCS word time, thereby permitting many basic activities aboard the spacecraft to be synchronous. Consequently, enables and strobes are not required, and again the need for duplication in the input/output processor is reduced.

Other considerations included a capability for detection of spacecraft anomalies by the MPS—relieving the CCS of continuous detection responsibility — and the sharing of memory between the MPS and the CCS. Both of these developments led to simplification of the memory and of the input/output processor.

3. Failure Classification. A final consideration—classification of failures—led to the most marked reduction in the size of the CCS. Primarily, failure classification permitted reduction of memory requirements. Failures were classified in terms of when they had to be detected and in terms of their effect on the spacecraft. Considering the question "when," failures that might prove catastrophic to the rest of the spacecraft were obviously those which must be detected and repaired immediately, say within 100 ms. Such failures may occur within several of the spacecraft subsystems.

Failure occurring within the CCS requires instant recognition, within one instruction time. Immediate detection permits an ability to program around failures after all the spares of any one processor have failed.

Another classification of failures constitutes those which do not require immediate detection or repair. They would cause a loss of some spacecraft data, parameters, and state variables, but not a significant loss. Detection and repair of these dislocations may be delayed for milliseconds or perhaps a week, depending upon the type of failure.

The final classification is of those failures that need not be detected at all by the CCS or MPS, but have alternate means of detection or correction. These form a limited group; most failures will fall within the previous classifications.

The chief simplification resulting from this classification was reflected in the memory. Need for duplicate storage there was practically eliminated. Indeed, 90% of the contents of the read/write memory can be lost without catastrophic consequences to the mission. Thus, duplex memory within the CCS was discarded. The 10% that is needed for spacecraft survival is duplicated.

4. Results of Simplification. The following categories of instructions and variants have been retained in the simplified CCS: (1) add/subtract operations, (2) most jumps, but not all variants, in the STAR repertoire, (3) only one compare register with memory instruction, (4) all register/memory information transfers, and (5) most logical instructions.

The number of register/memory information transfers have actually been increased, for three reasons:

- a. To implement a software self-recovery of the CCS.
- b. To improve the efficiency of rollback segments.
- c. To facilitate programming around failures.

The following instructions and variants from the STAR repertoire have been deleted: (1) multiply/divide, (2) indexed conditional jumps, (3) multiple-bit shifts, (4) right shift (toward LSB), (5) indirect addressing, and (6) normalize (floating point).

5. CCS Characteristics. A comparison can now be made between the characteristics of the baseline TOPS CCS and those that would have resulted from a direct conversion of the STAR breadboard into a flight version (Table 47). The TOPS requirements are also summarized.

It is seen that the TOPS CCS is almost three times as fast as required. This is useful because, in general, computer applications tend to grow as design progresses. Again, some spare capability exists in the TOPS CCS for increasing the size of programs in the memory; additional functions, if any, would be achievable by dint of the excessive speed capacity.

It is believed, also, that 4 K for the TOPS CCS read only memory capability is conservative. The 3.3 K requirement was based on the CCS being responsible for direct monitoring of spacecraft functioning. In reality, the baseline design calls for the MPS to assume this responsibility.

Table 47. Comparison of STAR and TOPS computer characteristics

	TOPS requirements	Flight version of STAR breadboard	TOPS CCS
Operations/sec	10,000	16,000	28,000
Word size, bits	32	32	32
Memory cap:			
Read/write	3.7 K	Up to 65 K	8 K
Read only	3.3 K	4 K	4 K
No. of Interrupts	10	Up to 16 (Expandable)	20
No. of Index reg	1	2	1
Instruction, variants	39	>200	90
Weight, lb ^a	40	66	46 (Includes shared memory)
Power, W ^a	45	55	40
Reliability ^a	0.95	0.4	0.92
^a Same number of spares			

The power requirement in the TOPS CCS – 40 W – is based on an 80% efficiency in the subsystem power supplies and power switches.

6. CCS Function. The most recent version of the CCS is described in the block diagram illustrated in Fig. 131. The test and repair processor (TARP) which controls the operation has three inputs: halt, clock, and power. The dominant philosophy was to keep direct inputs at a minimum; more lines signify more potential failures.

Control of operations by the TARP is accomplished through timing and control pulses outputted to CCS units. Four lines are required to each

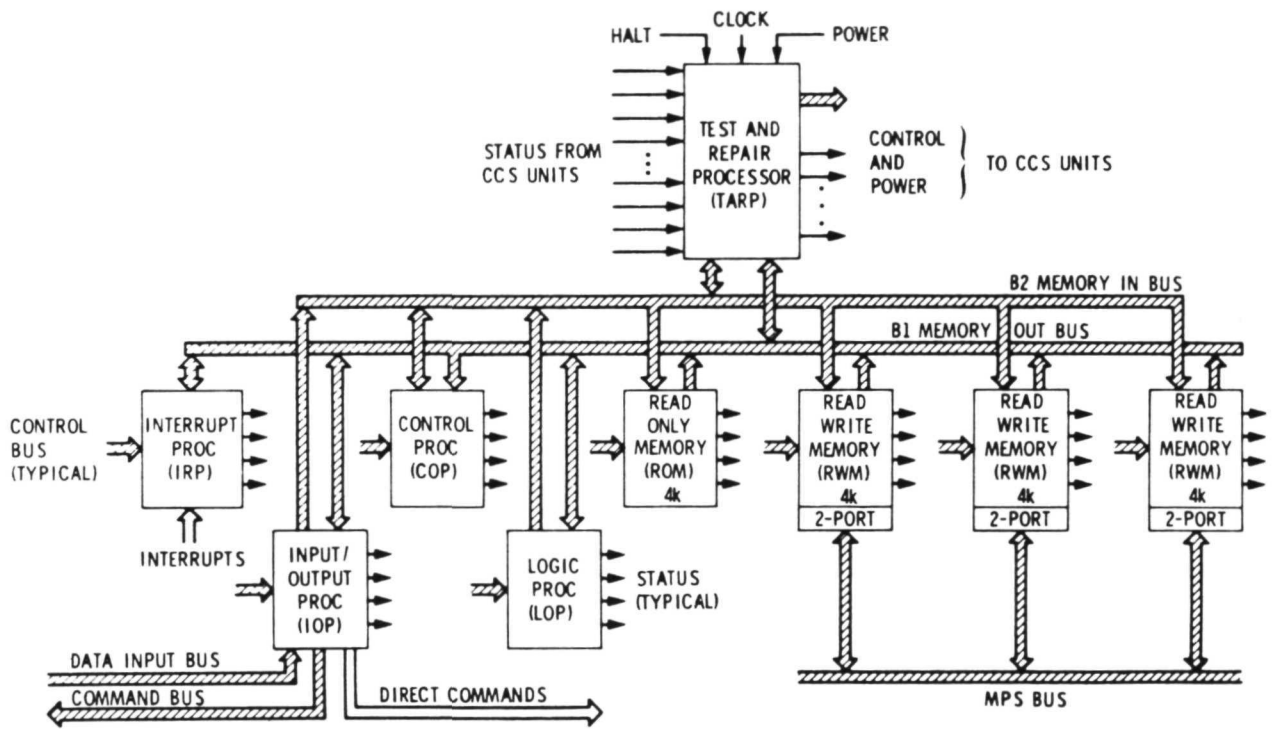


Fig. 131. Control computer block diagram

processor for this. The TARP also controls the power switching of all processors. Because the TARP is hard-wire (that is, it is self-protecting), it is triply redundant, and carries two spares.

The control processor (COP) determines the sequence of instructions fed to the computer. It is responsible for indexing and program counting.

The logic processor performs all logic operations within the CCS — the AND/OR, the exclusive OR of whole words. It also performs arithmetic functions. The logic functions are not code-preserving; the arithmetic functions are. Logic functions are duplicated within the logic processor. This duplication costs very little extra hardware (approximately 5%).

To avoid duplexing, the interrupt processor and the input/output processor are maintained in the CCS as separate and simplified entities (they are duplexed in the original STAR). As such, the simplex devices contribute but 20% more hardware to the CCS, and in effect save 80% of the increase required to duplex the combined interrupt-input/output processor. To avoid the duplex requirement, both processors must be separate and independent. Thus, if failure occurs in one during normal processing of the CCS, an indication of that failure will be detected in the TARP by lack of a corresponding indication from the other processor.

The interrupt processor handles all interrupts sent to the CCS. Of these, 3 are true interrupts; 16 others are basically flags, rather than interrupts. The true interrupts indicate the imminence of catastrophic failure. They interrupt at the conclusion of an ongoing instruction, and a jump immediately is executed to a location in the read-only memory. The other interrupts, upon arrival, are not masked. They are interrogated by a specific instruction in the program in terms of individual bit positions for specific interrupts. If the computer does not interrogate a particular interrupt position, that interrupt can be lost. The ability to handle interrupts in this fashion in the CCS is a direct result of the failure classification policy described earlier.

The input/output processor deals with input and output to the computer. There is a single input data bus and a single output command bus.

There was, at the close of the TOPS project, only one identified direct command — that going to the command decoder during transfer of commands, when the command decoder is decoding ground commands. The desire is to eliminate even that, because direct commands cannot be checked, cannot be easily diagnosed; they increase the amount of software required in the CCS, and they introduce failure modes from which, in the worst cases, there is no recovery.

All processors maintain status lines, four to the unit, by which operational information is sent to the test and repair processor (TARP). Thus, TARP determines if a function has been successfully completed in a particular processor. This capability eliminates much diagnosis that otherwise would be required in the form of software.

The three read/write memories each have two ports, one for the CCS and one for the MPS. They are backed by four unpowered spares, as compared to two spares for the read-only memory and the other processors. The measurement processor subsystem (MPS) is connected to each to the read/write memories, including the spares. One of the operating read/write memories constitutes the shared memory. It is important that the MPS cannot access the other two read/write memories which are not shared. Such access would result in an undetectable failure (undetectable because it would not cause a change in the coding of a word). To prevent this, a control instruction must emanate from the CCS, limiting access by the MPS to the shared memory only. The interactions involved are not yet fully understood.

The CCS communicates with itself by means of two internal buses — a "memory in" bus, which allows all processors to communicate with any of the memories, and a "memory output" bus. The latter also carries outputs from the interrupt and logic processors. The TARP inputs and outputs on both buses in order to have complete control and detection capability.

7. Operation Flow. Essentially, the CCS is involved in event-sequencing. When it is not sequencing events, the computer may move to monitoring the spacecraft—a relatively small, infrequently performed algorithm. Most of the time, the CCS does nothing—it is waiting. With a

capability of 28,000 operations per second, the computer performs most tasks very quickly.

While waiting, the computer will be searching for interrupts. One interrupt normally reaches it every second, causing it to move up to its event-sequencing mode. If there are no events to sequence, the CCS returns to the waiting mode. The computer is, of course, not limited to a one-second cycle: it is capable of a 50-ms cycle or less if required.

Ground command interrupts and operational interrupts are the two nominal forms of interrupt. A third form is the performance interrupt. In the ground command interrupt, a ground command is processed as a result of the interrupt. Bits are accumulated serially at the rate of either 4 or 64 bits/s. The command is processed; when complete, it is either executed immediately, outputted, or stored in memory for later execution.

Operational interrupts occur regularly during normal functioning of the spacecraft. Thus, they are primarily for exchanging data between the CCS and other subsystems. When a subsystem has data for the CCS it first outputs an operational interrupt. The CCS then transmits a command via the coded command bus, instructing the subsystem to begin its transmission. In the following CCS word time, the data are transmitted to the CCS. The CCS processes it as directed by the initial interrupt.

Performance interrupts are executed when performance of the spacecraft is not nominal, i. e., when there is an anomaly. The reaction to such an interrupt is reflexive: a coded command contained in the memory carries instructions designed to correct or circumvent the failure. Then a verification process commences; redundant data within the shared memory are examined to determine whether the failure was indeed that. Other possibilities are: anomalous action of the sensor itself or improper activity within the MPS or some other subsystem.

Once failure is verified, the nature of the failure is determined. Thereafter, repair is made by sending a coded command to the power subsystem to switch off current to the affected unit, and to turn on a spare.

With the crisis over, the CCS status is updated in order that the ground may keep fully informed on the situation aboard the spacecraft. And

with that accomplished, the computer returns to whatever it was doing at the time of the interrupt.

8. CCS Status. The status of the control computer at the close of the TOPS project was as follows: A detailed functional design of the computer and each of the processors had been completed. All algorithms for each instruction had been worked out in terms of timing, information movement, register controls, etc.

Logic design was in process, with basic CMMA configuration and common processor logic about 50% completed. Work on the test and repair processor (TARP) was 60% completed.

Nothing had been accomplished in software design. Nor had TOPS engineers designed the specific TOPS spacecraft power supplies, power switches, or isolation circuits.

F. Timing Synchronizer

The function of the Timing Synchronizer Subsystem (TSS) is to provide basic timing signals for the entire spacecraft (except the auxiliary oscillator — RF carrier frequency source). In concept, the TSS will have an oscillator operating at approximately 8 MHz, and a divider chain from which all frequencies needed are derived. The primary design goal is to achieve the timing signal function with required lifetime capability. The approach is in terms of two problems in the subsystem design; that is, the reliability of the oscillator and the capability to repair the dividers.

The problems in implementing reliable dividers are relatively straightforward. The divider will be operating in a hybrid TMR configuration. That is, three units are operating simultaneously and there are two unpowered spares, which are switched by the computer when an indication of failure is sent to it through the MPS directly from the divider itself.

One way to implement the divider network is as a ring counter. When a counter fails and a spare is switched on to replace it, it is important to minimize the period before the new counter is synchronized with the two operating counters.

A study made by Westinghouse in 1964 showed that the ring counter is the best way to achieve that. It may not be the most efficient in terms of

hardware, but in the CMMA implementation of a ring counter, the cost of a few extra gates is of secondary importance.

The reason for TMR in the dividers is to allow operation to continue during the switching and synchronization of a spare counter. When two counters agree, the voted output will be identical to the correct input. When one counter is either inoperative or emitting pulses at incorrect times, or has just been switched off and a new one switched on, the output will be uninterrupted and nondegraded so that the other subsystems on the spacecraft can continue operating without interruption.

1. Oscillator design. There are three alternatives for the oscillator design. Since the oscillator is the basic timing source on the spacecraft, it would be very difficult to have it checked. The alternatives are: (1) a self-checking redundant oscillator with self-switching of spares, (2) an active redundant set of oscillators with no switching, and (3) a nonredundant oscillator with the CCS monitoring it by means of an oscillator in its own subsystem.

The last alternative was ruled out very early because it would make the CCS considerably more complex and introduce many more failure modes. Therefore, the necessary failure masking or failure detecting capability will be incorporated directly within the oscillators themselves (alternative 1 or 2).

The first alternative is exemplified by three oscillators operating as the minimum required for fault detection and repair capability. The oscillators are synchronized through synchronization circuits.

The outputs are combined within the oscillators themselves or through a summing network. The common output then goes to the dividers. Fault detection circuits monitor each of the three outputs and sense failures. Failures can result in a change in frequency or amplitude of a signal. These conditions are detected and an appropriate three-bit code is placed in a fault register. The output of this register causes a switching matrix to switch in a spare and switch out the defective oscillator.

The second alternative is to use a large number of oscillators and synchronization circuits. Each oscillator will have one or more synchronization circuits to the other oscillators. When one oscillator fails, proper design of the circuit insures that its output becomes ineffective. The outputs are combined at a single point and presented to the dividers. This approach has been identified as the best alternative. Figure 132 illustrates it in simplified form.

Two reasons for choosing the second approach are: (1) the complexity of the first alternative is greater, and (2) the switching transients are expected to be a problem when an oscillator is replaced.

In the chosen approach, the need to synchronize more than three oscillators is a minor difficulty, but one not troublesome enough to outweigh the two disadvantages inherent in the first alternative.

A simple oscillator was studied for the purpose of investigating the problem of synchronizing four to seven circuits. A schematic diagram of the oscillator appears in Fig. 133. It is a modified Pierce oscillator with two phase shifting elements, C1 and C2. The synchronization and coupling element is C3. This circuit gives a common output point for all the oscillators. Consequently, no redundancy is needed in the summing network shown on the right of Fig. 132. It is a single connection.

Behavior of the oscillator was investigated by means of a laboratory breadboard and by digital computer simulations. Four major observations resulted:

First, the number of oscillators N was varied between four and seven. If f_k is defined as the frequency of the k^{th} oscillator operating alone, the synchronized frequency will be very near the highest f_k . It is generally below it. How near it is depends upon the f_k of the other oscillators.

Secondly, the impedance of the coupling network, C3, is inversely related to the difference between the highest and the lowest f_k . The greater the difference, the lower must be this impedance for effective synchronization.

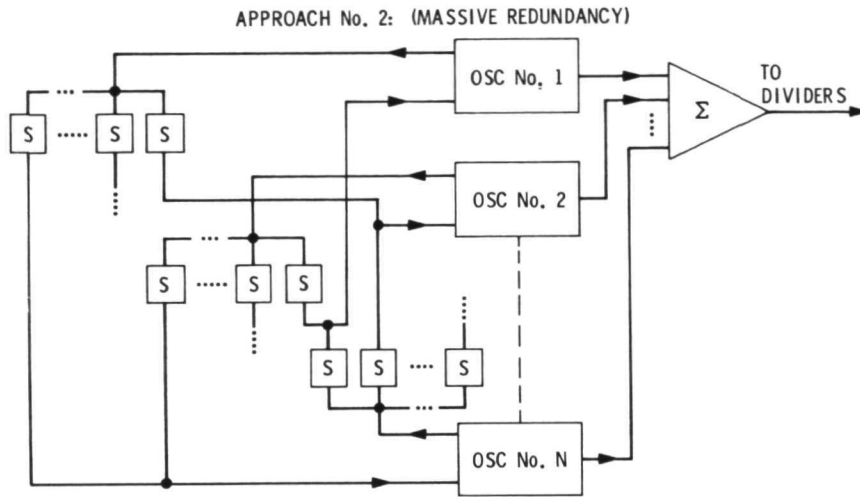


Fig. 132. TSS redundant oscillators, timing synchronizer

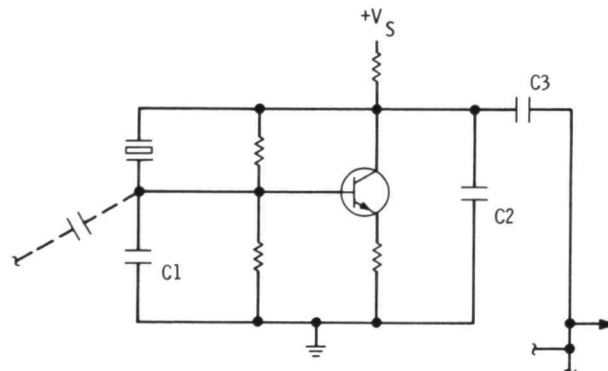


Fig. 133. Oscillator timing synchronizer

Third, it was observed that the common output waveform of N oscillators ($3 < N \leq 7$) was degraded if one f_k was considerably different (on the order of $>0.002\%$) from the other frequencies or from the average.

Lastly, the simulations of the oscillator made it clear that once the circuit has been properly designed, failed oscillators will act primarily as additional loads on the functioning oscillators.

X. TELECOMMUNICATIONS

A. Telecommunications Subsystem Analysis

Space flight to the outer planets calls for a telecommunications subsystem of much greater capability than that which sufficed for inner planets missions. To increase performance of the TOPS spacecraft over that of MM69, an X-band RF capability was adopted, providing an extra 11.3 dB; the high-gain antenna was enlarged from a 101.6-cm (40 in.) -diam dish to a 4.26-m (14-ft) dish (giving 12 dB); transmitting power was increased from 20 W to 40 W (giving 3 dB); and convolutional coding was substituted for the MM69's block coding (giving 1 dB). These advanced techniques and instrumentation accounted for a total of 27.3 additional dBs — sufficient to transmit commands and receive telemetry from the most distant sectors of the solar system.

The TOPS Telecommunications subsystem performs three basic functions: (1) transmits commands to the spacecraft, (2) receives telemetry from the spacecraft, and (3) obtains tracking data. The Earth-based Deep Space Instrumentation Facility (DSIF) transmits S-band RF signals via one of three 64-m-diam antennas (in California, Spain, and Australia), to receiving antennas aboard the spacecraft. The 64-m antennas, in turn, receive X-band and S-band RF signals, carrying telemetry, from the spacecraft. Tracking data are both doppler and ranging.

The spacecraft Telecommunications subsystem — of primary interest to this report — consists of three subsystems: Antenna, Radio, and Modulation/Demodulation (Fig. 134). The Antenna Subsystem comprises a high-gain, a medium-gain, and two low-gain antennas. The Radio Subsystem houses two receivers, two transmitters, hybrid switches, and combining networks. The Modulator/Demodulator Subsystem (MDS) incorporates a command detector and a telemetry modulator.

Of the spacecraft's four antennas, the high-gain antenna receives S-band and transmits both S-band and X-band; the medium-gain antenna transmits X-band only; the forward low-gain antenna transmits and receives on S-band; the aft low-gain antenna receives S-band only.

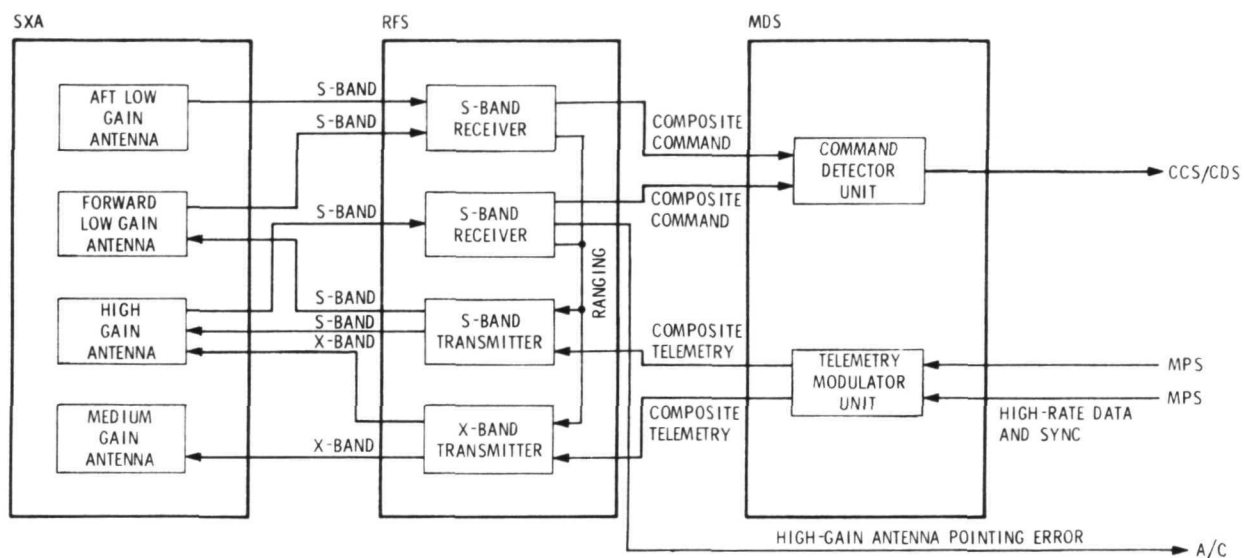


Fig. 134. Functional diagram

Command and ranging signals are received by each of the S-band receivers. The ranging signal and telemetry are transmitted back to Earth by both the S-band transmitter and the X-band transmitter. When receiving over the high-gain antenna, the Radio Subsystem generates error pointing signals to send to the Attitude Control Subsystem. A low-noise preamplifier on the radio generates a system temperature of less than 600 K. The S-band transmits on a signal strength of 20 W; X-band transmission is selectable at 20 or 40 W.

Coherent frequency translation from uplink to downlink is accomplished in the transponder, and functions, of course, only with an uplink signal. The translation ratio is 240 over 221 for S-band, and 880 over 221 for X-band. When the spacecraft transmits without receiving an uplink signal, the downlink frequency is generated by an auxiliary crystal oscillator in the Radio Subsystem. A programmed local oscillator located at the DSIF adjusts uplink frequencies to compensate for varying Earth/spacecraft courses and speeds.

The MDS contains a command detector unit and a telemetry modulator unit. The command detector unit receives composite command signals from either of the S-band receivers and relays these commands to the Control Computer Subsystem/Command Decoder Subsystem (CCS/CDS). The telemetry modulator accepts data stream from the Measurement Processor Subsystem (MPS), modulates both the S-band and X-band signals, then transmits the S-band through either the high-gain antenna or the forward low-gain antenna, and X-band signals through the high-gain or the medium-gain antenna.

The modulator portion of the MDS utilizes a convolutional coder, employs two digital data channels, and has six modulation indices, three per channel. One channel has a high-rate, flexible format for science data. The other channel has a low-rate, fixed format primarily for engineering data. The high-rate channel is convolutionally coded with a Viterbi algorithm, a constraint length of six, and a rate of one third. Modulation indices for the high-rate channel are $72-1/2$, 65, and 55 deg; for the low-rate channel, 11.5, 22, and 30 deg.

The demodulator portion of the MDS is single channeled, with a bit rate capability of either 4 bits/s or 64 bits/s.

Communication performance between the spacecraft and Earth diminishes as the distance between the two increases. In practice, deteriorating radio performance is offset at some point in space flight by switching from the omnidirectional low-gain to the unidirectional high-gain antenna on the spacecraft, and again from the 26-m to 64-m antennas at DSIF stations. A requirement for the Attitude Control Subsystem is the ability to point the high-gain antenna away from the Sun line and direct its beam toward Earth. The relative cone angle (Sun-spacecraft-Earth angle) varies from 90 deg at launch to 0 deg at about 78 days after launch, and thereafter oscillates to a maximum of 25 deg at approximately 150 days in flight.

Transmission is switched from the low-gain antenna to the high-gain antenna at approximately 100 days after launch, when performance with the low-gain antenna and the 26-m station has dropped from an initial 100 bits/s at the adverse tolerances to 8 bits/s, and in the 64-m station from 1000 bits/s to about 128 bits/s. Thereafter, the high-gain antenna points toward Earth and is used for the weekly data dump.

The high-gain antenna link performance at X-band (40 W) transmission is summarized in Table 48.

Table 48. HGA link performance, X-band modulation mode 1

Planet	Data rate (high rate/low rate), bits/s			
	40 W		20 W	
	Design	Adverse	Design	Adverse
Jupiter	131 k/32	65 k/32	65 k/32	32 k/32
Saturn	32 k/32	8 k/16	16 k/32	8 k/16
Uranus	8 k/16	2 k/0	4 k/8	2 k/0
Neptune	4 k/8	1 k/0	2 k/0	1 k/0
Pluto	4 k/8	1 k/0	2 k/0	1 k/0

The MPS transmits data in binary steps from 8 to 131 kbits/s, or 2 to the n, where n ranges from 3 to 17. This results at Jupiter in a nominal capability of 131,000 bits/s, and at adverse tolerances of 65,000 bits/s. Because there is no continuum of data rates (such rates changing at increments of 2 to the n), the nominal performance is 32,000 bits/s at Saturn and 8,000 bits/s at Uranus. Further degradation in transmission is evidenced at the still more distant Neptune and Pluto. At 20 W output, the high-gain capability is, of course, cut in half.

Design and adverse tolerances performance at 20 W for the S-band high-gain antenna and the X-band medium-gain antenna (MGA) is given in Table 49.

It will be necessary to switch to lower modulation indices, within the constraints of available indices, as range increases or if the medium-gain antenna is used, to maintain adequate power in the carrier.

The command link to the spacecraft functions at two data rates: 64 bits/s and 4 bits/s. At the 64 bits/s rate, capability ends at Saturn ($1.1 \text{ km} \times 10^9$) for transmission via the 64-m, 400-kW DSIF antenna to the spacecraft's low-gain antenna (LGA). Capability extends to $1.25 \text{ km} \times 10^9$ using the 26-m antenna and 10 kW into the spacecraft's high-gain antenna. The command margin in dBs is within tolerances well beyond Neptune, at

Table 49. Link performance

Planet	S-band HGA (high rate/ low rate), bits/s		X-band MGA, bits/s	
	Design	Adverse	Design	Adverse
Jupiter	8 k/16	4 k/8	1 k	512
Saturn	2 k/0	1 k/0	256	128
Uranus	512/0	256/0	64	16
Neptune	256/0	128/0	32	8
Pluto	256/0	128/0	32	8

approximately $10 \text{ km} \times 10^9$, using the 64-m antenna and 20 kW, transmitting into the spacecraft's high-gain antenna.

At 4 bits/s the range is, of course, greatly enhanced. The 64-m, 400-kW LGA capability extends beyond Neptune. Commands are receivable through the 26-m, 10-kW HGA mode to $10 \text{ km} \times 10^9$; while for the 64-m, 400-kW operation directed to the spacecraft's high-gain antenna, command capability extends beyond the solar system.

The Doppler effect, by which velocity of the spacecraft is measured, presents a problem when the vehicle approaches encounter with the planets, particularly Jupiter because of its size and strong gravity. As the spacecraft swings behind the planet, the frequency will change by as much as 200 kHz in 90 min. The rate of frequency change at this point is in the order of 220 Hz/s — posing a real danger of breaking lock. Total frequency shift, then, is in the order of 750 kHz over a 3-h period. X-band suffers even greater fluctuation and, in the worst case, would be close to 3 MHz over a 3-h period.

To offset the potentially hazardous frequency shift, the programmed local oscillator is adjusted to drive the uplink in proportion to the frequency change at encounter. Frequency likewise is upgraded during Jupiter occultation to a calculated requirement for linkage when the spacecraft is again visible. Tracking then will be confined only to error in prediction — error occasioned largely by miscalculation in predicted atmospheric parameters of the planet.

Transmitting in X-band introduces weather degradation, a factor not encountered in S-band. Anticipated degradation in dBs, at Goldstone, California, is as follows:

Weather condition	Degradation, dBs	Measure
Clouds	0.5	80% of the time (20%, worse)
Rain	1.5	0.05 in./h
Wind	0.3	30 mph

Degradation caused by cloud formation will average 1/2 dB 80% of the time at Goldstone; 20% of the time it will be greater. Rainfall averages from 7 to 10 in./year, and results in a 1-1/2-dB loss when falling at the rate of 0.05 in./h. Wind causes a 0.3-dB degradation at 30 mph, though winds of this velocity occur no more than 5% of the time. Theoretically, therefore, a heavy rainstorm at this DSIF site could cause a degradation of 3 dB or more. Weather conditions at other DSIF stations around the world are generally less favorable than at Goldstone. The question arises, then, whether environmental conditions would nullify the advantage of X-band over S-band. Engineers believe that on the whole they would not.

In summary, the TOPS telecommunications subsystem provides the capacity of returning large quantities of data from the outer planets. If working optimally, it will transmit 4000 bits/s from Pluto; while in the worst case, should the high-gain antenna fail, the medium-gain antenna will transmit approximately 8 bits/s from that outermost planet. This compares to an 8-1/3-bit/s return from Mars by Mariner 4; the TOPS secondary system provides equivalent performance at ten times the range.

B. Telecommunication Antenna Structure

The Antenna Subsystem of the TOPS spacecraft contains a high-gain antenna, a medium-gain antenna, and two low-gain antennas. Particulars, constraints and requirements pertaining to the antennas are listed in Table 50.

Major design problems for the low-gain and medium-gain antennas were not anticipated; consequently, little work was expended in those areas. The main endeavor was to design a high-gain antenna capable of meeting the TOPS requirements.

The high-gain antenna consists of a 4.26-m (14-ft) -diam rib and mesh unfurlable paraboloidal main reflector with 48 ribs, and a 64.7-cm (25.5-in.) -diam hyperboloid subreflector with conical flange. The diameter of the subreflector with the flange is 85 cm (33.5 in.). Based on RF performance, the requirement of the rib attachment when furled, and physical interference of the feed hardware with other components, the focal length/diameter ratio selected for the main reflector was 0.42.

Table 50. TOPS antenna particulars, constraints and requirements

Antenna	Type	Antenna orientation	Nominal operating frequency, MHz	Nominal gain relative to isotropic, dB
High-gain	Two-reflector cassegrain design, unfurlable main reflector 4.26-m (14-ft) diam	-Z axis (forward roll axis)	8415 2295 2113	48.9 ^a (55% efficiency) 37.2 ^a (50% efficiency) 35.5 ^a (40% efficiency)
Medium-gain	30.3 in. diam focal-point-fed paraboloid	Two-axis gimballed (except where blocked by spacecraft)	8415	34.7
Forward low-gain	Modified MM69 low-gain antenna	-Z axis	2295 2113	7.8 7.1
Aft low-gain	Undefined	+Z axis	2113	5.0
^a The losses due to surface distortion, RF reflectivity, and subreflector defocusing are not included.				

The Cassegrain System was chosen over a focal point system for three reasons: the Cassegrain provides high aperture efficiency for a reflector as large as 4.26 m (14 ft) by requiring shorter RF feed lines; it permits inflight refocusing without using RF joints; it has a potential to enhance performance by shaping the subreflector.

Under current baseline design, the high-gain antenna utilizes a circularly polarized S/X-band feed (Fig. 135). The coaxial structure (preliminary model) provides a feed efficiency of 69% at 8448 MHz, 43% at

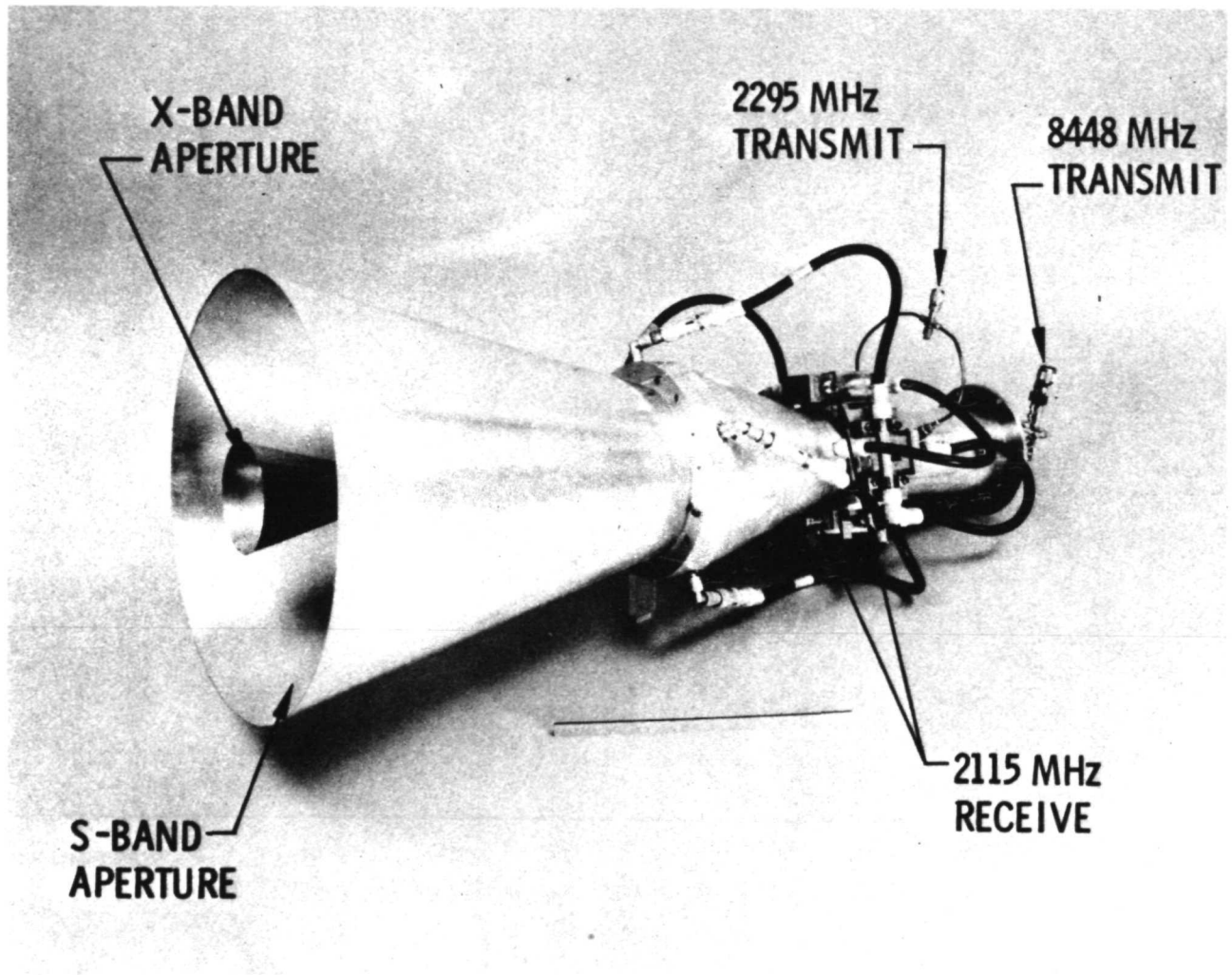


Fig. 135. Circularly polarized S/X-band feed (side view)

2295 MHz, and 57% at 2115 MHz, excluding blockage and dissipation. Both the 8448 MHz and the 2295 MHz are output through 3 dB 90-deg hybrids, which produce circularly polarized signals. Since the circular polarization is produced by 90-deg phase shift between the two transmission lines, the inclusion of an RF switch to provide a path giving equal phase would result in a linear capability. The feed, therefore, is adaptable to circular or linear, polarization.

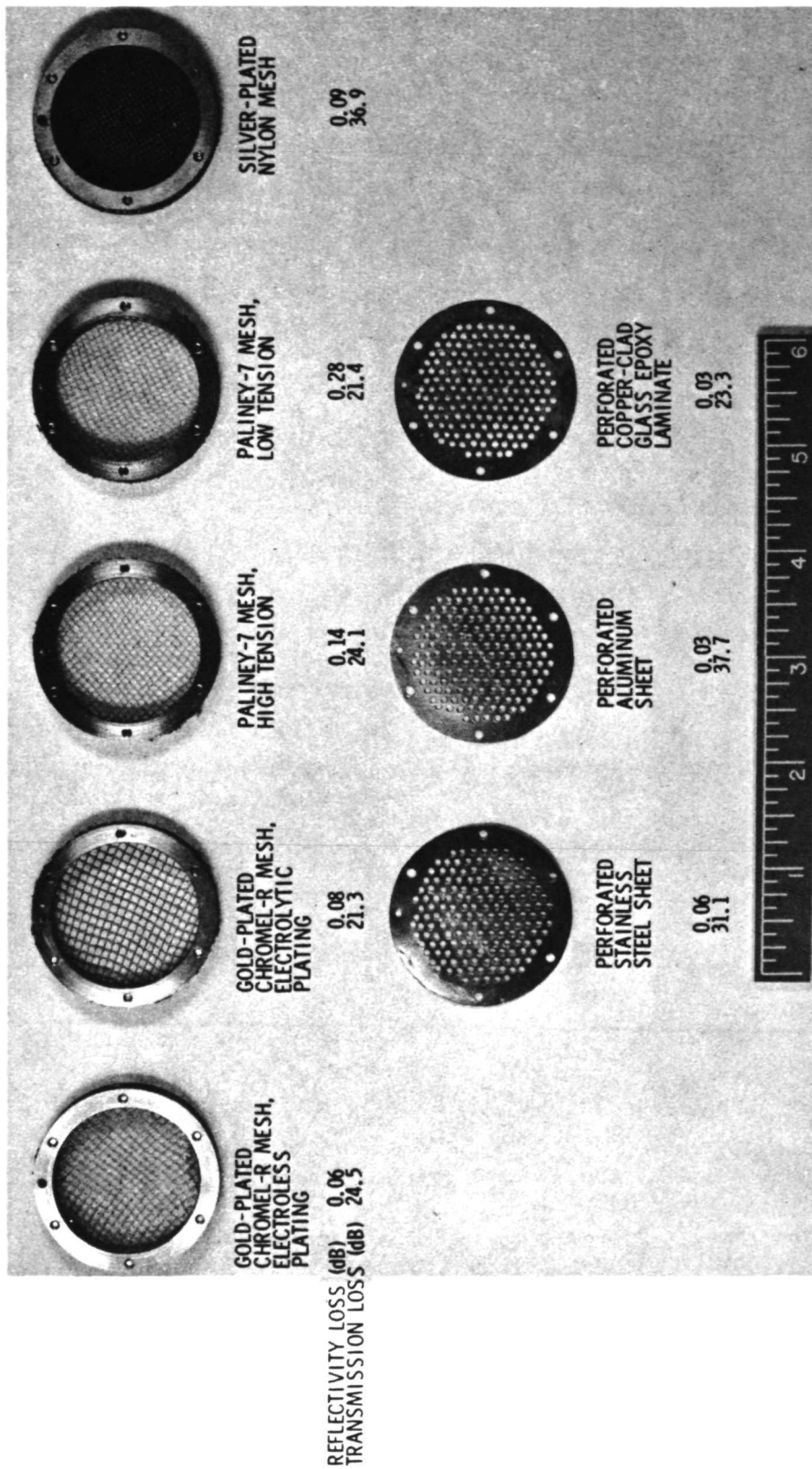
The feed provides two outputs from four probes operating at the S-band uplink frequency. Comparing the magnitude and phase between these two outputs establishes the position of the uplink signal with respect to the bore-sight of the antenna.

An important area of the high-gain antenna development centered about selection of surface and structure materials. The principal objective here was to attain minimum RF loss. A RF study was made of main reflector surface materials, subreflector support structure materials, and thermal control paints using a waveguide method of comparing relative RF performance. Waveguide measurements, in turn, were verified through a free-space method that provided overall RF performance of reflector surface material.

The RF loss for various materials as determined by the waveguide method, is described in Fig. 136. The first surfaces considered were two gold-plated Chromel-R meshes, one with electroless plating, the other with electrolytic plating. Electroless plating has the disadvantage of flaking; electrolytic plating demonstrated better adhesion. Reflectivity loss (RL) of both meshes, less than 1/10th of a dB, was relatively insensitive to variations in surface tension and to direction of the electric field.

To circumvent problems inherent with gold-plated surfaces, a solid precious metal mesh was developed, consisting of silver, gold, and a platinum alloy. This material, called Paliney-7, used the same type of knitting-tricot as the Chromel-R mesh. The Paliney-7 surface had higher reflectivity loss (0.14 and 0.28 dB) than the Chromel-R mesh, and was disposed to be sensitive to variations in surface tension.

Although not suitable for space application, a silver-plated nylon mesh was evaluated for comparison purposes.



$$\frac{P_{\text{refl.}}}{P_{\text{in.}}} = 10^{-RL/10} \quad \left. \begin{array}{l} 98.7\% \\ 0.4\% \\ 0.9\% \end{array} \right\} \text{GOLD-PLATED CHROMEL-R MESH, ELECTROLESS PLATING}$$

$$\frac{P_{\text{transm.}}}{P_{\text{in.}}} = 10^{-TL/10}$$

$$\frac{P_{\text{dissip.}}}{P_{\text{in.}}} = 1 - 10^{-RL/10} - 10^{-TL/10}$$

Fig. 136. Measured results at 8448 MHz by waveguide method

Surfaces consisting of perforated metal sheets were analyzed. Perforations consumed about 50% of the original area, yet tests showed that RF performance was essentially the same for perforated or unperforated surfaces.

Studies were conducted on different types of materials for varying applications on antennas. Serious RF blockage occurs from the use of aluminum struts. Substitution of fiberglass tubes or cylinders proved feasible, using a wall thickness of 0.020 in. or less. Transmission loss (TL) in dB was 0.16 with a 0.015 in. wall but increased rapidly with increasing thickness. Loss was 0.59 dB with a 0.032 in. wall.

The effect of various paints and thicknesses of paints used upon antenna structures was tested. A fiber glass sheet 0.015 in. thick, when painted with Vita Var paint of 0.0027 in. thickness, caused a 0.27-dB transmission loss. When the paint thickness was increased to 0.006 in., the loss in dB was 0.35. Vita Var paint of 0.0027 in. thickness applied to aluminum sheeting of the subreflector resulted in a reflectivity loss of 0.09 dB; with the paint thickness increased to 0.007 in., the reflectivity loss was 0.43 dB. Obviously RF degradation builds up rapidly with increasing paint body.

To summarize the RF study: gold-plated, Chromel-R (electrolytically plated) mesh is suitable as reflector surface material for long life missions; precious-metal mesh (e.g., Paliney-7) as an alternative to gold-plated Chromel-R mesh would require further study; fiberglass tubes or cylinders (wall thickness 0.020 in., or less) are suitable for subreflector support structure.

A major problem with the TOPS high-gain antenna is RF loss caused by the structure supporting the subreflector. If these supports are constructed of aluminum, the resultant loss is an untenable 1.5 dB. Consequently, studies were made of various fiberglass structures and of the use of conical antennas. A thin-wall, painted fiberglass cylindrical shell structure with minimal fiberglass reinforcing ribs proved least subject to RF loss (approximately 0.7 dB). Fiberglass structures also were found to be lighter in weight than other materials, including aluminum. Use of the

fiberglass strut structure (without the cylindrical shell) required an aperture cover with thermal control paint to reduce a solar heating problem for the S- and X-band feed.

Another source of RF loss is defocusing caused by possible movement of the subreflector. Defocusing loss from axial displacement of the virtual feed is shown in Fig. 137, where F is the focal distance, D the diameter of the subreflector, and λ the wavelength. Loss due to lateral displacement of the subreflector, is shown in Fig. 138. Loss caused by subreflector tilting is illustrated in Fig. 139.

C. Radio Frequency Subsystem

To accomplish mission objectives and meet advanced spacecraft design requirements for outerplanet exploration, the TOPS Radio Frequency Subsystem (RFS) as designed proved to be 3 to 5-1/2 times as complex as that of MM71, yet weighed but 85 lbs, or 10 lbs more than Mariner's. The use of microminiature components, particularly in the receivers and exciters, reduced weight and increased reliability. Integrated circuitry in RF receivers was an innovation, as was a S-band solid-state amplifier. Completely solid-state transmitter circuitry is not at this time recommended, but appears feasible in the foreseeable future. The TOPS S-band and X-band downlink systems use a mix of solid state and traveling wave tubes (TWTs). Another generic feature of TOPS design, accommodating parts failure during long term operation, is system redundancy: examples are two exciters and two TWTs in the X-band downlink.

The basic radio functions of TOPS are grouped into three categories: communications, navigation, and radio science. Communications requirements include commands, telemetry functions, and a high-gain antenna pointing error capability to reduce pointing loss during X-band operations. Navigation requirements cover coherent two-way doppler phenomena on S- and X-band, as well as ranging operations on both bands. The S/X-Band System is also utilized in calibration of the propagation medium to achieve navigation accuracy. Under radio science, occultation and propagation experiments are performed at the planets and during interplanetary cruise.

The specific requirements of the RFS are (1) to receive commands over the low-gain antenna to a range of 31 AU, (2) to transmit telemetry

(TM) continuously and ranging modulation when present on the uplink, (3) to transmit simultaneously on S- and X-band, (4) to generate RF pointing error signals, and (5) to transmit engineering telemetry during trajectory correction maneuvers.

A simplified block diagram of the RFS is illustrated in Fig. 140. The forward low-gain antenna (FLGA) and aft low-gain antenna (ALGA) are switched into a low-gain receiver from which commands are sent to the MDS. The voltage-controlled oscillator (VCO) coherent reference and ranging modulation passes through the radio control unit (RCU) to the active transmitters. In the high-gain antenna uplink, the sum and delta channels are processed by the high-gain receiver, which outputs commands, and the VCO coherent reference and ranging modulation, plus pitch and yaw antenna pointing errors. The 20-W S-band transmitter is switched directly into the high gain antenna (HGA), or to the FLGA through a diplexer. X-band is transmitted only from the spacecraft to the Earth, and is switched from the dual-level (20-40 W) transmitter to either the high-gain or the medium-gain antenna.

The RCU provides switching between the coherent and noncoherent modes. In the noncoherent mode, auxiliary oscillators located in the RCU are switched in to provide a stable transmitter signal when neither receiver is in lock.

Power for the transmitter, receivers, and the RCU is supplied directly from the power subsystem; the RCU subsequently provides power to the pointing error electronics and the ranging channels in the receivers.

The RCU processes all radio mode control commands from the spacecraft and from the ground, and processes all telemetry from the subsystem. It also controls the switch modes between the radio and the antennas.

Telemetry from the MDS is processed in the transmitter modulating the downlink signal.

The RFS power demand exemplifies considerable advancement in the technology, effecting low demand and high efficiency. The low-gain receiver operates on 2 W, and the high-gain on 2.4 W. The S-band exciter functions on 1 W, while 1.2 W activate the X-band exciter, and 2.3 W the RCU. These numbers are 1- σ high values. The transmitting equipment, of course,

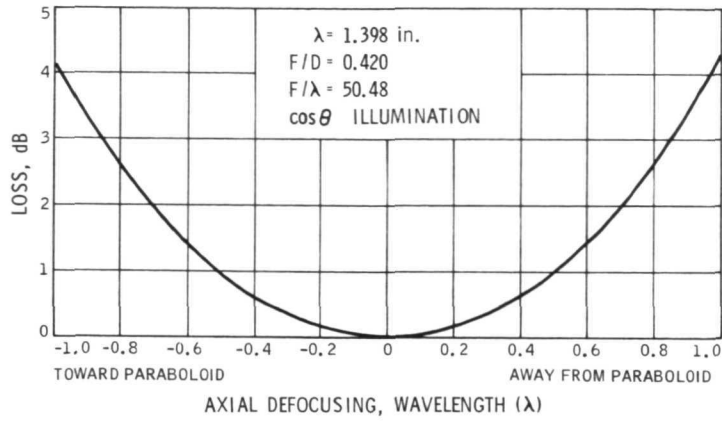


Fig. 137. Main reflector axial defocusing effect

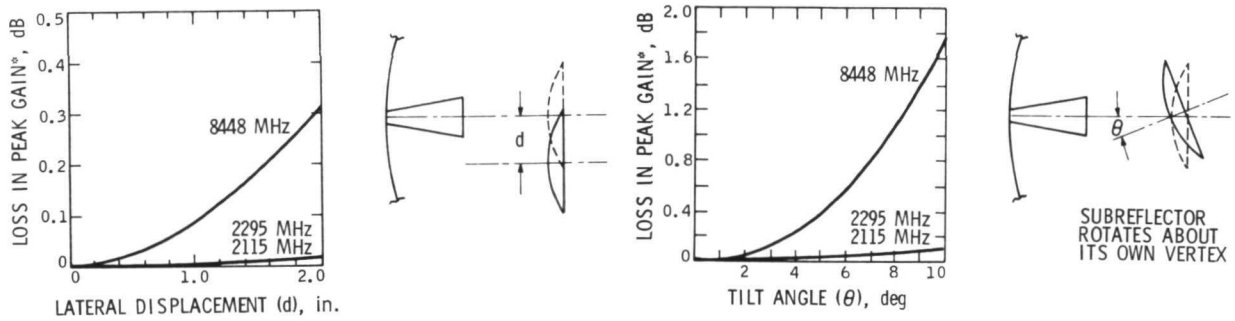


Fig. 138. Loss due to subreflector lateral displacement

Fig. 139. Loss due to subreflector tilting

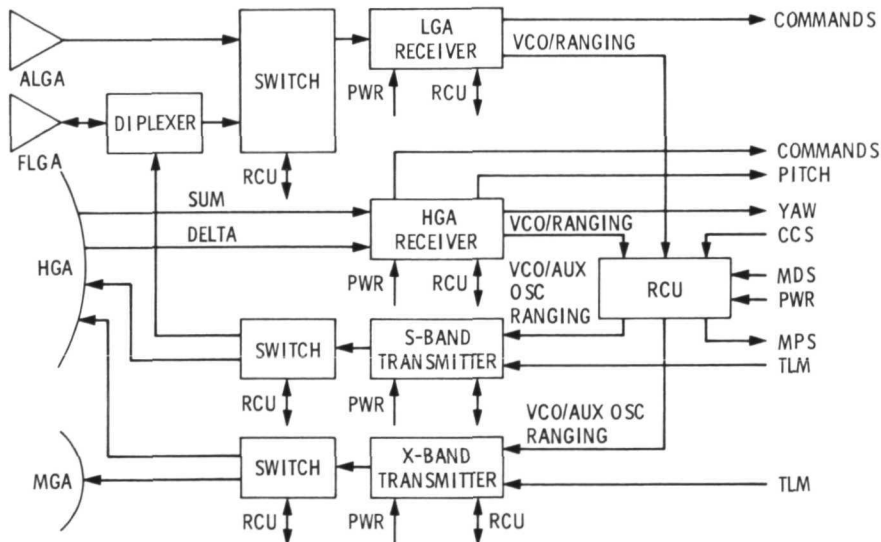


Fig. 140. Simplified RFS block diagram

requires much greater power consumption: 53 W for the S-band solid-state power amplifier, 51 W for the S-band traveling wave tube amplifier (TWTA), 54 W for the X-band TWTA (20-W mode), and 97.5 W for the X-band TWTA (40-W mode). The estimated 1- σ low efficiencies for these units are 38% for the S-band solid-state power amplifier, 39% for the X-band TWTA, about 40% for the X-band TWTA (20-W mode), and 41% for the X-band TWTA (40-W mode).

In arriving at the baseline RFS, several alternate mechanizations were studied and discarded. One of these used the same receiver for high-gain antenna or low-gain antenna uplink. The mechanism adapted for TOPS was a separate receiver for each uplink. The combined concept was rejected because (1) all uplinks necessarily pass through a single switch to obtain the multiple switching modes between the antennas and receivers, and thereby cause an isolation problem between the high-gain and low-gain antennas through that switch as well as creating a single-point failure mode, and (2) the receivers would necessarily be more complex to accommodate a narrow loop for the low-gain function and a broad loop for the high-gain function.

A second alternative mechanism, or tradeoff, concerned the S-band downlink. The system adopted was a TWT/solid-state mechanization. Alternatives were all TWTs or all solid-state. The principal reasons for rejecting all TWTs was a problem of weight: projected life and reliability factors would require five TWTs. An all solid-state concept was not adopted because solid-state technology is not mature enough, nor does an all solid-state system contain the functional redundancy of a mixed mechanization.

Another area where alternate technology was encountered in the RFS was the angle-error channel. The baseline selected was a dual-channel monopulse. Alternates were a single-channel and a three-channel monopulse and sequential lobing. The single-channel concept and sequential lobing were not adopted because in multiplexing the error channel onto the sum channel the basic receiver functions are impacted and receiver performance is lowered. The three-channel mechanism, on the other hand, is unnecessarily complex, and is subject to interchannel drift.

A fourth area of tradeoff pertained to RF switches. Pin diode switches were chosen. Alternatives were circulator switches and electromechanical devices. Circulator switches were not selected because of an isolation factor, magnetic cleanliness, and small power handling margin. The electromechanical devices were rejected for reasons of questionable reliability on long duration missions.

Advanced development was conducted on the following RFS devices and components: receivers, preamps, RF switches, S- and X-band exciters, X-band TWT, S-band solid-state power amplifiers, and a VCO/auxiliary oscillator switch. Developments that have been deferred include the filters, diplexers, and power monitors; a detailed design of the control unit; the X-band switch and transmission components; the S-band TWT; and power supplies.

Advanced development objectives on the RFS receiver included improvement in performance characteristics; receiver threshold (V); doppler and ranging stability; insensitivity to environment; decrease in power and decrease in weight and volume. A principal objective was long life with a desired component life of 10^5 h. High reliability is essential, as is low cost. The cost factor is minimized by basing the TOPS design on multimission compatibility, thus enabling other NASA projects to use a similar design.

The specifications for the TOPS RFS receiver are given in Table 51. The receiver frequency is the DSIF uplink. Long turnaround time from Earth to the spacecraft requires acquisition by automatic sweep of the VCO during out-of-lock operations.

Long term ranging delay stability of 7 ns represents a significant advancement in the state of the art.

A feasibility study was made to determine whether the receiver should be microminiaturized. The stated goals of miniaturization were to (1) achieve a significant reliability improvement, (2) reduce size by 5:1 over a breadboard model, (3) reduce weight by 3:1, and (4) reduce power. In terms of MM71, such reductions would amount to 10:1 for size, 6:1 for weight, and 5:1 for power. Other areas under study were parts and packaging. The parts program included thick and thin film microstrip compatible components,

Table 51. TOPS project receiver specifications

Parameter	Specification	
	LGA receiver	HGA receiver
Receive frequency	2110-2120 MHz	2110-2120 MHz
Turnaround ratios	240/221 880/221	240/221 880/221
Noise figure, maximum (preamp input)	4.0 dB	4.0 dB
RF bandwidth	30 MHz	30 MHz
Threshold loop bandwidth	7 Hz	30 Hz
Acquisition	Automatic Sweep	
Command		
Data rate	4-64 bits/s	4-64 bits/s
Subcarrier	1024 Hz	1024 Hz
Bandwidth	10 kHz	10 kHz
Ranging bandwidth	1.5 MHz	1.5 MHz
Ranging delay stability		
Long term (10^5 h) (0° C to 50° C)	±7 ns (-80 dBm to -144 dBm)	±7 ns (-80 dBm to -139 dBm)
24-h ranging stability (constant temperature, ±7° F; constant signal, ±3.0 dB)	±1 ns	±1 ns
Doppler delay stability (over temperature and signal range)	1 ns	1 ns
Coherent exciter drive (nominal)	19-1/8 MHz	19-1/8 MHz
Antenna pointing error		0.01 sum channel beamwidth
Dc power, regulated	2.0 W	2.4 W
Volume	20 in. ³	26 in. ³

including chip and beam lead resistors and capacitors, and miniature inductors; surface wave filters, and beam lead active devices. In packaging, examination was made of substrates, thick and thin film and their metallizations, and the compatibility of the metallizations. Also studied under packaging were the integration of large discrete devices, such as filter capacitors; partitioning and interconnection of circuitry in this close-packed type of technology, and EMI and module testability.

The desirability of microminiaturizing the RFS receiver is illustrated by the physical characteristics of three different receivers. The MM71 measured 305 in.³ in volume, weighed 8.5 lb, and consumed 8.7 W of dc power. An advanced discrete component breadboard developed by TOPS engineers measured 100 in.³, weighed 4.0 lb, and used 2.0 W. The projected micromin receiver, by comparison, occupies 20 in.³, weighs 1.3 lb, and consumes 2.0 W.

The objectives of an advanced PIN diode switch for TOPS were to improve the isolation and power handling capability, improve reliability and degree of magnetic cleanliness, decrease cost, reduce weight and volume, and effect a reduction in insertion loss.

D. Transmitter Component Development

Development of the RFS transmitter components of TOPS included a VCO auxiliary oscillator switch, S- and X-band exciter, S-band solid-state power amplifiers, and the X-band TWT.

The status of the exciters during the later period of the TOPS project included evaluation of an S-band breadboard with the advanced receiver conducting ranging measurements. A breadboard model of the X-band MVM73 transmitter was utilized for X-band measurements. A primary goal of S- and X-band exciter development was a device that required no tuning adjustments. Other objectives of exciter development included carrier phase and group delay stability, resistance to RF voltage breakdown, and reduction of size to facilitate functional redundancy.

Advanced exciters incorporate high-order first multipliers to minimize thermally induced carrier phase variations. Other exciter advancements include phase modulation by varying the output step recovery diodes bias (to minimize group delay variation), and power amplification at S-band

to avoid power breakdowns. Further areas of exciter development required to meet a TOPS-type baseline are packaging, S- and X-band isolators, and an analysis of starting transients for multipliers to insure turn on when required.

To maintain thermally induced carrier phase variations to a minimum, the first stage multiplier must be as high a multiple as possible. Figure 141 shows curves calculated for the carrier phase shift as a function of temperature for different sequences of multipliers used to construct a multiplier chain. The multiplier in this case was times 440.

In the field of S-band solid-state power amplification, a 20-W bread-board model amplifier was developed. It was used to evaluate a life test configuration for testing RF power amplifiers. This test setup was used to determine what to test, what measurements to use to what degree of accuracy, and what to record. Radiation tests were made of the transistor 5-W amplifier stages using proton, neutron, and electron radiants. With instrumentation capable of detecting changes in power output of 0.2 dB, no changes in output were observed in all radiation tests.

A goal of the S-band solid-state power amplifier design was to achieve 40% efficiency, with voltage and temperature derated. An output of 20 W at 38% dc to RF efficiency was actually achieved. This included the driver stages, power combiner, and isolator. The overall gain was 27 dB using 25 Vdc B+. Junction temperature was maintained at less than 100°C. A negative aspect was the narrow bandwidth: 35 MHz and 3 dB, caused primarily by the low-level input driver stages. The unit output is the combined output of four MSC-3005 transistors, operating at 55% collector efficiency with a 100-MHz, 3-dB bandwidth. A semilumped circuit was used, and microstrip combiners.

Alternate schemes investigated were a 765-MHz power amplifier and a triple multiplier, but direct S-band amplification is believed to be simpler. Different numbers of output stages were considered; four stages were selected. Those stages above four (i. e., five, six, or seven) created too much complexity; three stages would have higher stress.

Further developments of the power amplifier required to meet the TOPS baseline design included (1) total microstrip final packaging, (2) an

emitter ballasting stability/efficiency tradeoff study, (3) more efficient combining schemes with life test data on the solid-state power units, and (4) development of a transistor RF circuit model. An X-band TWT development was initiated to design a highly efficient tube with a dual-power-level capability of 40 W and 20 W. The established goals were 42% efficiency at 25 W, and 45% efficiency at 50 W at the 8.4 GHz frequency. Problems in focusing arose as a result of the difficulty of directing a 16-mil-diam electron beam through a 37-mil-diam helix. Further development is required to meet the TOPS baseline design in the X-band TWT area.

E. Modulation/Demodulation Subsystem

Key functions of the Modulation/Demodulation Subsystem (MDS) are to provide command modulation on the uplink, and telemetry modulation on the downlink.

In the command function, command signals transmitted from Earth to the spacecraft, including background noise, are received by the MDS from the Radio Frequency Subsystem (RFS). The signals are demodulated in sequence: subcarrier, bit sync, and data. A lock status is derived and transmitted with the data to the Control Computer Subsystem (CCS) and the Command Decoder Subsystem (CDS).

In the telemetry modulator function, the high-rate telemetry data are convolutionally encoded, high- and low-rate telemetry data are modulated on subcarriers, and the subcarriers are mixed at appropriate voltage ratios to give correct modulation indices. The resulting composite signal is sent to the RFS.

The MDS contains two redundant command detectors and two redundant telemetry modulators. Maximum power allocated to the subsystem is 6.4 W, maximum weight is 18.5 lb, and the volume of the mechanism is estimated at 100 to 150 in.³, depending upon the ultimate packaging scheme.

Because the established two-channel PN Analog Command System used in conventional near-planet spacecraft is believed to be unreliable from a standpoint of component stability over a 10- or 12-year flight period, TOPS designers generated a largely digital command system. A comparison of characteristics of these two systems is given in Table 52.

Table 52. Comparison of characteristics of two-channel analog system and single-channel digital system

Characteristic	Two-channel analog	Single-channel digital
Data rate, bits/s	1	4 to 512
Detection SNR (ST/N0), dB	16.5	10.8
Acquisition time, min	12.5	0.4
Subassemblies	2.5	2
Power, W	0.72	2.5
Weight, lb	4.2	3.5

The data rate is based on the assumption of a 1-kHz subcarrier. The increased power demand of the digital system reflects increased logic complexity and the high rate at which logic functions are performed.

The command demodulator of TOPS is a sampled data system, incorporating a low-pass analog-to-digital A-to-D converter. This is the only analog circuitry in the system. The acquisition algorithm is a maximum likelihood or correlation receiver, designed to gain fast, reliable, acquisition times. Acquisition of a subcarrier and bit sync by the modulator is performed sequentially. Doppler is tracked using discrete digital tracking of sync references. Power is applied to the command detector only when the receiver is in phase-lock.

Key command characteristics of the MDS are as follows:

- (1) Bit rate: 4, 64 bits/s.
- (2) Command subcarrier: 1024 Hz squarewave.
- (3) Input clock: 2.621440 \pm 0.001% MHz.
- (4) Prefix: SC-SC \oplus BS - SC \oplus BS \oplus DATA, where SC is subcarrier and BS is bit sync.

(5) Required threshold signal: $ST_B/N_0 = 10.8 \pm 0.4$ dB

$$\left[P_{BE} = 10^{-5} \right]$$

(6) Maximum frequency offset: $\pm 0.01\%$

A function flow chart of the command system is given in Fig. 142. At the start of acquisition, 16 subcarrier phases are correlated. Because the correlation curve is symmetric, positive and negative, the operation is actually performed using only eight phases. To make reliable decisions at less than 10^5 error rate on whether a subcarrier is or is not acquired, five bit times are accumulated. If, in Mode 1, the largest value of the 16 phases is less than threshold, the system recirculates to the beginning; if larger than threshold, the operation is repeated. If, at the close of the repeated operation, the largest value is larger than threshold, the phase of the subcarrier is set to the proper value corresponding to the largest value of the accumulated phases. Having acquired a subcarrier, lock is maintained, and arrival of bit sync is awaited. With the arrival of bit sync, Mode 5 is initiated, which correlates for bit sync precisely in the form used for the subcarrier. In the data mode — Mode 8 — three functions are performed: the data interval is set, data summations are made for bit sync and subcarrier, and the absolute values of five data sums are accumulated and compared to a second threshold to determine if the system is in lock (if not, the operation is recycled). A command block diagram is shown in Fig. 143.

The parameters of telemetry modulation are as follows: (1) the convolutional encoder has a 1/3-rate constraint and length 6; (2) the high-rate data channel generates 8 to 131 bits/s in 3-dB steps; and (3) the low-rate data channel operator at either 8, 16, or 32 bits/s. High-rate and low-rate data are selectively mixed to achieve proper modulation indices. Control operations include turnoff of S-band at certain times during X-band data dump, and turnoff of the low-rate channel as required.

A functional description of the TOPS telemetry modulator is illustrated in Fig. 144. High-rate telemetry data passes through the convolutional coder and mixes with the high-rate subcarrier, then is directed to the modulation index selector that selects one of three modulation indices. The

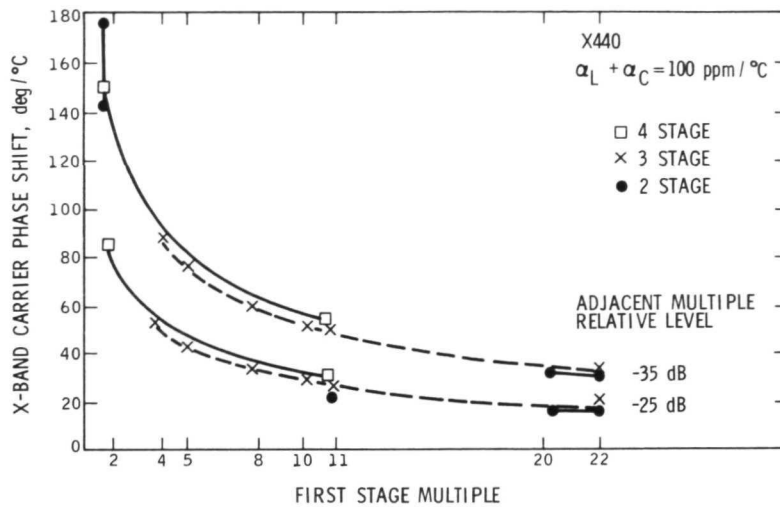


Fig. 141. Multiplier phase shift temperature sensitivity vs first stage multiple

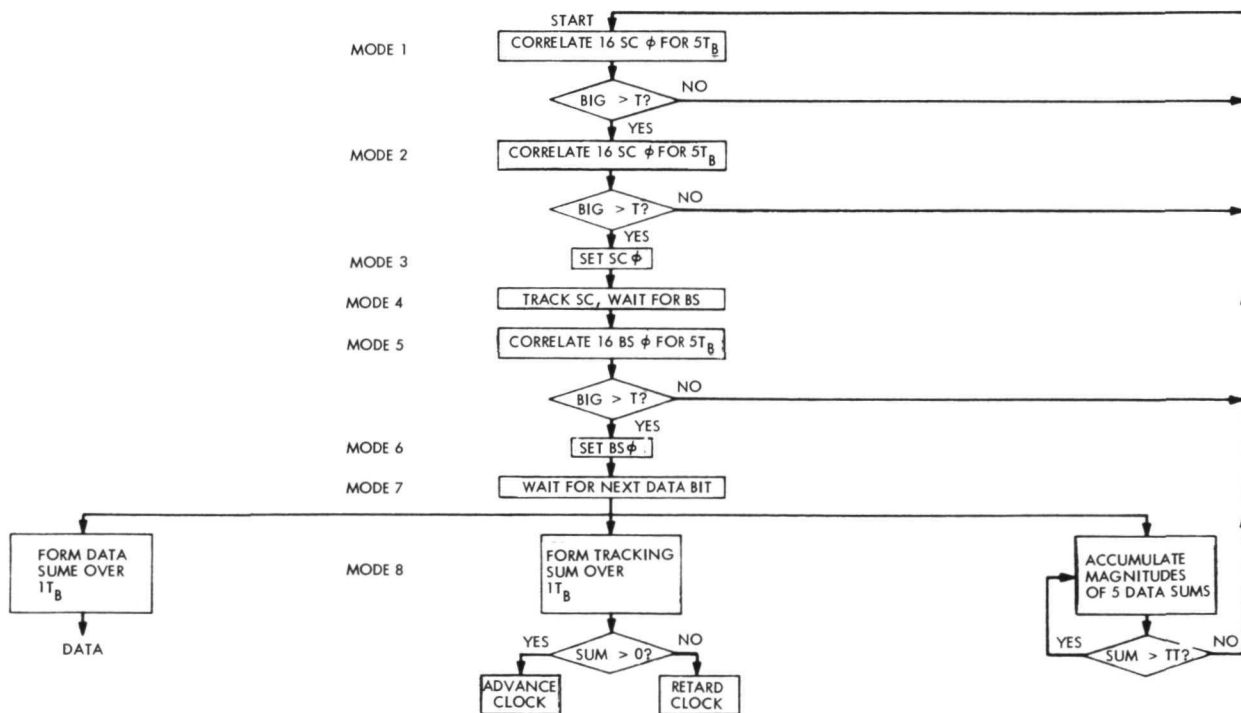


Fig. 142. Command flow diagram

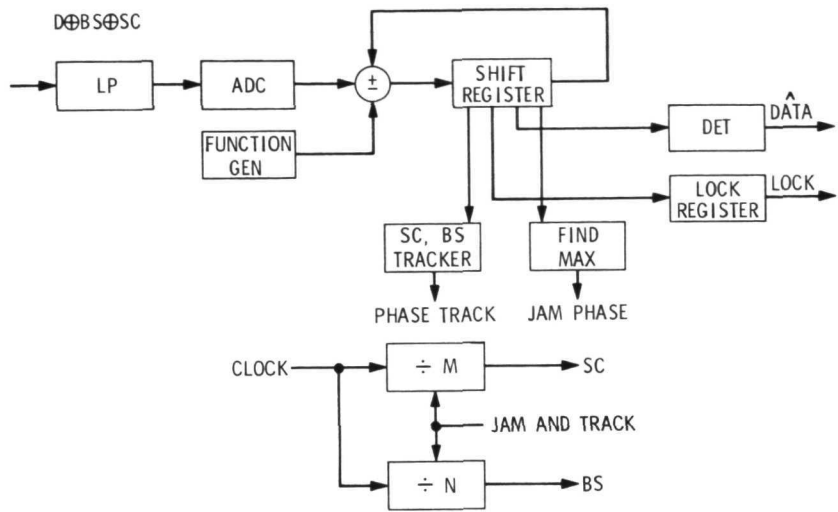


Fig. 143. Command block diagram

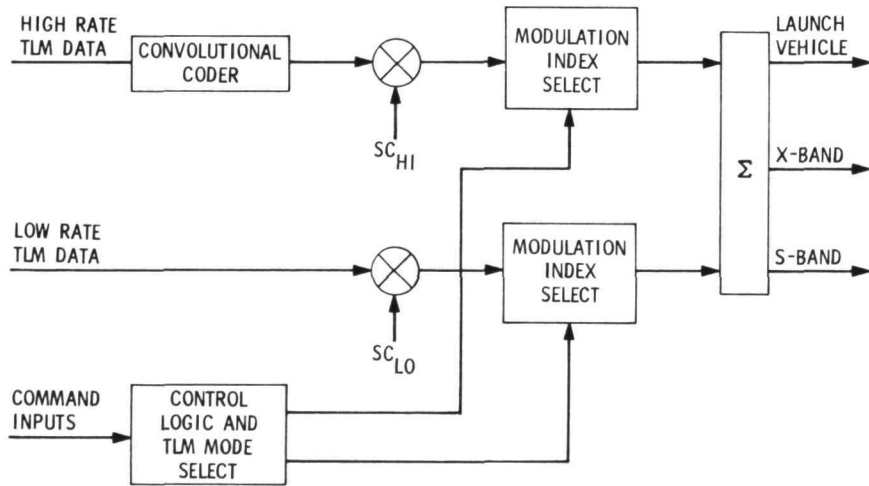


Fig. 144. Telemetry modulator block diagram

summing amplifier adds the high - and low-rate telemetry together and outputs to the launch vehicle for ground operation and to the X-band and S-band modulators.

The command demodulator developed for TOPS was highly successful and will be used, in a slightly differing configuration, for the 1975 Viking Orbiter. A breadboard unit was designed and operated by TOPS engineers. The use of a custom metalized multigate array (CMMA) in the place of current transistor transistor logic (TTL) was studied. No hardware activity was developed or planned for the telemetry modulator.

XI. SPACECRAFT NAVIGATION

A. Navigation Concept

The Navigation Subsystem performs measurements of the spacecraft and target positions, estimates the spacecraft orbit, and decides what maneuvers to make and when to make them. This section is limited to a discussion of the navigation measurements because they are the most important factors differentiating the outer planets navigation concept from earlier missions.

1. Requirements and Constraints. The Subsystem must:

- (1) Deliver the spacecraft to the target with a high probability of success.
- (2) Predict the encounter trajectory relative to the planet and its satellites accurately enough that scientific data can be acquired. For example, in a close satellite flyby, trajectory predictions must be accurate enough that the platform can be pointed to keep the satellite in view.
- (3) Cost of the subsystem should be at a minimum consistent with the available weight and required probability of success.
- (4) The subsystem should have the potential to handle missions not in the current baseline.
- (5) The design risk must be as small as possible for a given development cost.

One figure of merit used for the TOPS Navigation Subsystem is the probability of delivery to the last planet for a given amount of correction capability loaded on the spacecraft. This can also be measured by the correction capability in the m/s needed to assure a given probability of delivery to the final planet, as shown in Table 53.

2. Development of Outer Planets Navigation Concept.

a. Mariner navigation concept and extension to TOPS. Figure 145(a) shows the use of radio tracking to locate the target with respect to Earth; (b) illustrates the use of the ephemerides to locate the target with respect to

Table 53. Correction requirements

Parameter	Velocity increment, m/s
Anticipated performance, $P_N^a = 0.99$	108
Margin for design variations	42
Planetary quarantine biases	40
Satellite flyby option	15
Total	205
^a Probability of navigational success.	

Earth, and (c) shows the use of the combined information from (a) and (b) to locate the spacecraft with respect to the target planet.

The differences between the Mariner and TOPS missions are:

- (1) In TOPS, the most critical target, Uranus, is at a distance of 20 AU, rather than 1 AU. The radio tracking error is proportional to distance, at best. (Some errors are proportional to distance squared.) The ephemeris for the TOPS missions is based on optical data only, whereas the ephemeris for Mariner missions is based on radar as well as optical data.
- (2) Another difference is that the target masses are much larger than the Earth, 15 to 300 times larger.
- (3) The round trip light-time is 3 h at 20 AU, which affects ground tracking to a considerable extent.
- (4) Small, nongravitational accelerations acting on the spacecraft cause errors in the orbit determination filters which, in turn, cause target errors that are proportional to distance. As a result, Mariner System performance would be degraded materially on a tour to the outer planets.

How well the Mariner concept would work without any further development can be measured by examining the JUN79 post-Uranus maneuver. This maneuver is made to correct any errors in the flyby. The principal flyby

errors result from not knowing the planet orbit at the time the final approach maneuver is made. If the ephemeris of Uranus were perfect and the present radio tracking were used for that maneuver, 1400 m/s would be required to correct the total error. If the radio tracking were perfect and the present ephemeris of Uranus were used, 780 m/s would be required.

b. Addition of onboard measurements. It is believed that this radio error can be reduced by a factor of about ten. First, charge particle calibration can be improved through the use of ranging data and through the use of a dual-frequency downlink. The ranging system will be based on experience gained on MM69, MM71, and MVM73. The S/X downlink will be flown on an R&D basis on the MVM73 mission, and significantly improved ranging system accuracy is anticipated. The DSN will have very stable clocks through the use of hydrogen masers. A new type of data, obtained by having two stations track the spacecraft simultaneously, is expected to be advantageous. Improved knowledge of the locations of tracking stations and the pole of the Earth can increase the navigation capability. The ephemeris error can be reduced by a factor of 3.3 by extensive processing of optical observations, the use of flyby data from Pioneers F and G, and from encounters of outer-planet spacecraft flown before the Uranus encounter. The ephemeris will be updated and improved as the mission progresses.

Figure 146 illustrates the performance of an improved Mariner Navigation Subsystem. The anticipated improvements in both radio tracking and ephemeris data are shown in Fig. 146(a). Fuel loading calculations are not based on the worst nor the best case, but on the anticipated performance. It would take 352 m/s of correction capability to accommodate the anticipated accuracy. This number is unacceptably large and does not contain any margin for performance variations above or below the anticipated values (Fig. 146(b)). When the actual performance of the system corresponds to the expected performance, no extra margin would be needed for success. If the ephemeris error is at the higher value, an additional margin of 50 m/s would be necessary. Furthermore, if the radio tracking error were a factor of 2 times its expected value, the margin would have to be increased by 20 m/s. When these sensitivities are considered, a total correction capability of about 400 m/s is necessary. This is about twice as much as can be afforded in available weight. The conclusion is that improving the Mariner Navigation Subsystem is not adequate in itself to accomplish the outer planets mission.

Basically, the Mariner navigation approach consists of traveling a billion or more miles into space, then looking up to see where the target ought to be in an ephemeris, then computing the distance from Earth, and finally subtracting the two to determine what the miss will be. A more natural approach would be to look out the spacecraft "window" to see where it is because the information missing is the location of the spacecraft with respect to the planet.

An onboard subsystem should provide spacecraft/target information where the improved Mariner is weak; i. e., the direction of the planet during the approach phase. To measure the direction to the center of the planet, it is necessary to locate the center of the planet. Then the location of the center of the planet must be measured with respect to some celestial reference(s). One method used to locate the center of gravity of the planet is to take a picture of the entire planet and locate the geometric center of the planet. This method is fundamentally quite limited in its accuracy. A second way of locating the center involves taking a sequence of observations of one or more of the satellites of Uranus over a period of two weeks or more and then fitting the orbit of the satellite. The center of the satellite orbit is used to locate the center of mass of the target planet. Once the center is located, its celestial direction can be measured. One method of measuring the direction is to use secondary references; i. e., examine the telemetry data to determine where the platform is pointing. This method is limited, unsure, and unlikely to deliver any significant improvement over the Mariner system. However, large improvements in accuracy can be made by the use of the star background. In this instance, the band of performance is characterized more by the sensing instrument than by anything else. Tracking of the satellites against the star background is the most promising method. The improvements achieved are shown in Fig. 147, where the direction error is the sum of center-finding and celestial direction errors.

Figure 148 shows the performance of this combined navigation subsystem. If a hypothetical optical subsystem with zero unreliability is put on board, a correction capability of 180 m/s is needed to accomplish the mission and to meet the planetary quarantine requirements, to retain the satellite flyby option, and to maintain an adequate design margin. Although comparison of this 180 m/s with the 394 m/s needed for the improved

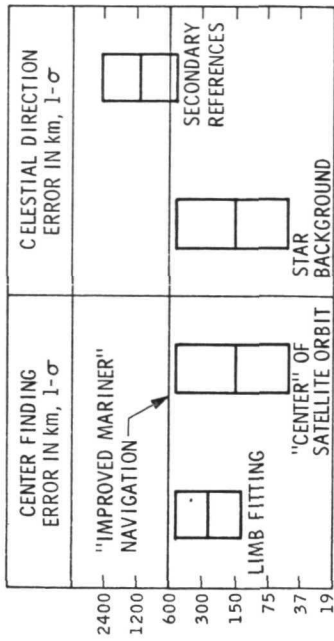


Fig. 147. Accuracy of planet direction measurements

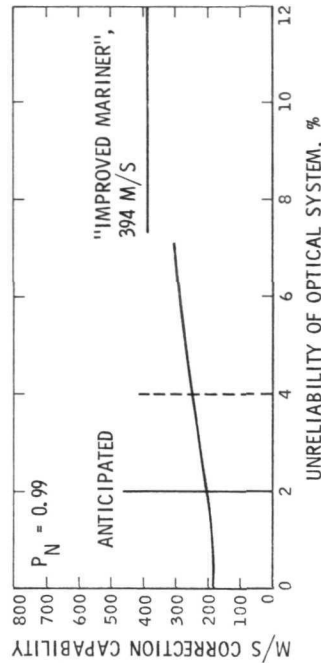


Fig. 148. Performance of combined Navigation System using satellite/star measurements

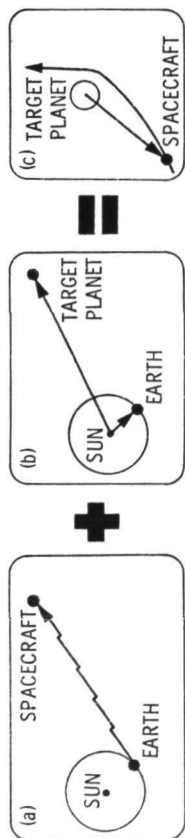
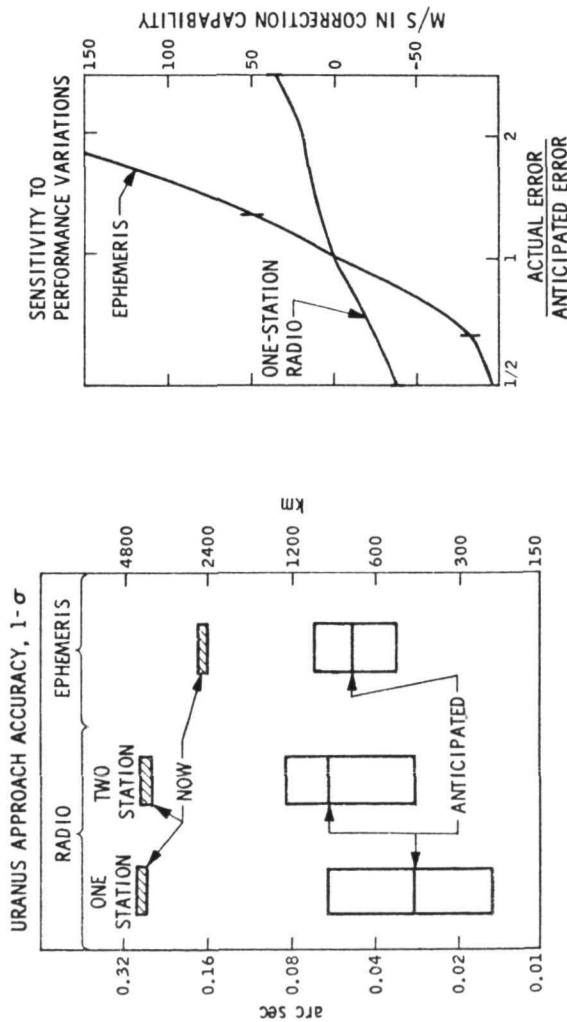


Fig. 145. Mariner navigation concept



- 352 M/S NEEDED IF ANTICIPATED PERFORMANCE IS MET (TOO LARGE)
- HIGH SENSITIVITY TO VARIATION REQUIRES LARGE DESIGN MARGINS

Fig. 146. Performance of improved Mariner Navigation System

Mariner may indicate that the problem is now solved, such is not the case. It is estimated that the unreliability of the optical subsystem will be 2%, in which case a correction capability of 205 m/s will have to be carried to assure 99% probability of navigation success. The function of the additional 25 m/s is to provide a reasonable chance that the radio tracking alone will allow the spacecraft to reach the last planet.

Figure 149 shows the justification for a subsystem using an improved radio tracking, improved ephemerides, and onboard measurements. A comparison of the two curves, one with an improved ephemerides and the other with a unimproved ephemerides, shows a difference of 126 m/s at 2% unreliability. To maintain the same navigational success probability, enough fuel for this additional 126 m/s would have to be loaded on board to compensate for the unreliability of the optical subsystem. The conclusion is that the expenditure needed to improve the ephemeris is justified. Lack of radio tracking improvements has a smaller, but significant, effect.

Figure 150 shows the sensitivity of the combined Navigation Subsystem to performance variations. The center line represents the anticipated performance. If the ephemeris performance is as anticipated, no extra fuel need be carried. If the performance is at the end of the curve, fuel for 20 m/s must be carried. If the optical subsystem performed at the worst end of the anticipated performance curve, extra fuel for a maximum of about 50 m/s would have to be loaded on board. The curves were prepared to obtain an idea of how much design margin is necessary to allow for variations in the expected performance. It can be concluded that this subsystem is relatively insensitive to variations in measurement subsystem performance, which reduces development risk. Because of some parallel paths in the Navigation Subsystem, a degradation of a factor of 2 in most elements within the system will not result in failure, but will, in effect, simply use up all of the margin allowed.

c. Summary of features. The outer-planet Navigation Subsystem concept meets all the requirements for the TOPS baseline mission:

- (1) It is within the allowable weight.
- (2) It has a high success probability.

- (3) It has a low design risk.
- (4) It is likely to be the lowest-cost approach.

The Subsystem has growth potential in that (1) it can perform more demanding multiple-planet missions, and (2) it is capable of relatively close flybys of the outer-planet satellites. This capability results from the method used for finding the center of the planet. In the process of using satellite observations to locate the center of the planet, the location of the satellite is also determined, and the coordinates of the spacecraft with respect to that satellite are accurately known.

3. Status.

- (1) The Science Imaging Subsystem was being used to make the required navigation direction measurements. If it were possible to accomplish this, both development and operational cost savings would accrue.
- (2) Performance estimates were being refined by tests and flight demonstrations. Probably the most important demonstration was the optical navigation demonstration on MM71. Measurements were taken by the Mariner 9 spacecraft as it approached Mars. These measurements of the satellites of Mars have been used to demonstrate the satellite center-finding method, employing the star background and secondary references. The dual-frequency downlink communications will be demonstrated on MVM73. Some two-station tracking experiments have been made on MM71; more will be made on MVM73. The results could contribute substantially to improving the radio tracking system.
- (3) More complete error analysis software was under development for the satellite/star measurement processing.
- (4) Analysis and requirements on the various subsystems were being refined. References 1 through 9 provide additional details on spacecraft navigation.

B. Approach Guidance Sensor

1. Observation Modes. Some of the observation modes needed to either observe the target planet or its satellites are shown in Table 54. The satellites are a reference of the center mass as they orbit the planet. The observations must also be referenced to inertial coordinates, either the background stars or the attitude references on the spacecraft, the Sun and Canopus references, and the scan platform pointing direction. From these references, the pointing direction of the camera is known. Then, when the target, either the planet or the satellites, is seen in that field of view, the inertial coordinates can be determined.

Mode I was rejected for two reasons: (1) the center-finding errors are probably larger than the required measurement accuracy of 15 arc-s, and (2) it is believed that detecting stars within the same plane of view with the planet might be difficult or impossible.

Mode II avoids the problem of detecting stars with the planet in the field of view by using the attitude references, but this mode has larger errors than Mode I. The attitude-sensor errors and the platform-pointing errors, in particular, tend to be much larger than 15 arc-s. It is probable that both Modes II and III, which use attitude references, would have an accuracy as low as 100 or 150 arc-s ($3\text{-}\sigma$). Even with limb-fitting, as in Mode III, there is still the attitude reference problem.

Table 54. Observation modes

Mode	Target	Coordinate reference	Primary error sources
I	Planet	Background stars	Center finding
II	Planet	Attitude references	Platform
III	Satellite	Attitude references	Platform
IV	Satellite	Background stars	Instrument distortions
V	Satellite	Adjacent star field (two cameras)	Instrument distortions
VI	Satellite	Background stars and attitude references	Distortion and drifts

Mode IV uses a satellite and background stars in the same field of view. This mode will be discussed in detail later in this section.

Modes V and VI are modifications of Mode IV. The satellite and stars are used as a reference for the coordinate references. In Mode V, two cameras are used because some of the satellites are much brighter than the background stars. One camera might look at the satellite, and one at the stars, and, because the cameras are hard-mounted together on the same platform, the coordinate system could be transferred from one to the other with a certain degree of accuracy. The accuracy of this mode is much greater than if the attitude references were used to get the pointing direction.

Mode VI uses background stars, but this mode employs some type of scanning device whose total frame readout time is longer than the attitude drift time. As a result, the star/satellite scene is distorted and the drifts have to be removed by the use of gyro data. This method differs from using the attitude references directly because background stars are detected in the field of view, and attitude sensors must be relied on for platform pointing information.

2. Basic Requirements and Constraints. The basic requirements, based on the star satellite observation mode, are:

- (1) To detect one or more satellites and one or more stars per field of view. It is believed that one star will provide enough information for the coordinates of the satellite because information on the orientation of the frame will be obtained by other means so that the orientation of the camera field will be known. Then, when one point is fixed, a coordinate system is obtained. However, it will probably not be necessary to work with one star very often because the vast majority of fields will have up to ten or more stars. The measurement accuracy must be about 15 arc-s; i. e., the right ascension and declination, or equivalent coordinate system, must be read out to 15 arc-s ($3\text{-}\sigma$). If further navigation studies were undertaken, they might indicate

that an accuracy of 30 arc-s may not exact too large a penalty.

- (2) Twenty-four frames per day are required from about 40 to 4 days before encounter (E). A shorter observational period may be adequate, and this requirement is not absolute at this point.
- (3) Measurements must be processed in near real-time so that the measurements can be made within perhaps a day before the maneuver and actually used for the pre-encounter trajectory correction maneuver.

The subsystem constraint is that the navigation requirements must be met with minimum interference with the scientific investigations. During the approach period, the scientific instruments will be able to make observations with much better resolution than can be obtained from Earth. Scientists will not only want the observations to continue as long as possible, but will want as much of the data link as possible for return of the information.

Figure 151 shows the typical approach guidance geometry for the Mariner 9 approach to Mars in November 1971. The size of the area represented is about 6×12 , or 15 deg, and the star magnitudes are from about the fourth down to seventh magnitude stars. (Sixth magnitude is about the faintest star that can be seen with the naked eye on a dark night.) This figure illustrates several points applicable to approach guidance to the outer planets. The first is that two-dimensional information is obtained from the satellite observation. If the spacecraft is deviating from its trajectory out of the plane, the orbit will appear to shift up and down from the predicted values as the spacecraft goes out of the orbit plane. Also, with spacecraft deviations in the plane, the orbits will shift back and forth with apparent motion. As a result, the measurement of the deviation of the spacecraft orbit is essentially isotropic. This is in contrast to the radio tracking, which has a stronger sensitivity to errors in the plane so that it becomes difficult to detect these errors as the spacecraft deviates from the plane of the orbit. Another point that is applicable to the outer planets is that often, when the satellite is being observed and a search is made for faint stars in the field of view, the target planet is close. Thus, stray light can enter the

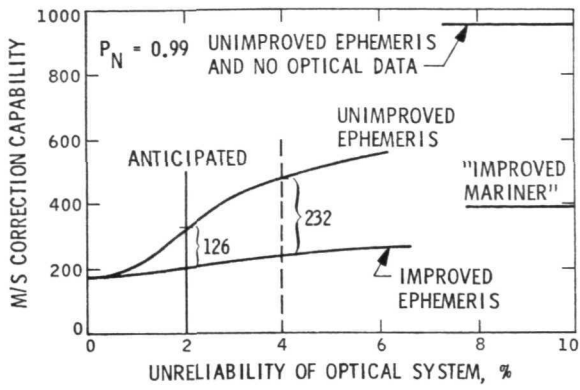


Fig. 149. Justification of improvements

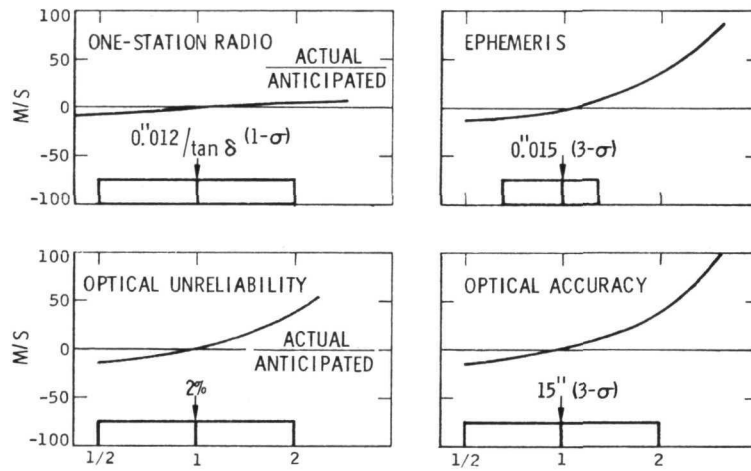


Fig. 150. Sensitivity of command Navigation System to performance variations

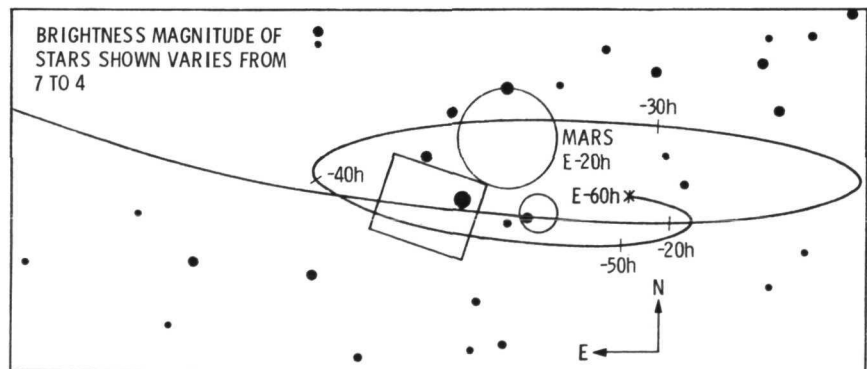


Fig. 151. Typical approach guidance for Mariner 9 approach to Mars, November 11-13, 1971

optical subsystem and scatter over the image plane. The subsystem design must take this stray-light factor into consideration. A third point is that, in any area of the sky, stars are far from evenly distributed. Vast areas have no seventh magnitude stars. It is important, then, that the instrument be sensitive for all anticipated viewing directions.

Figure 152 illustrates the last point. If the dashed lines are ignored, the figure shows the field of view of the instrument vs the star magnitude required to see a sufficient number of stars for some of the poorer star directions. As the field of view increases, it encompasses more stars so that smaller magnitude stars are sufficient. As the field shrinks, much fainter stars are necessary.

In addition to the detection of stars, it is necessary to have the appropriate geometric accuracy to meet the requirements. Geometric accuracy depends on the field of view for a given imaging sensor. Figure 152 is plotted for the standard picture element (PIXEL) for the science camera; i. e., 800×800 scan lines. The geometric accuracy is plotted for two different assumptions: (1) that the satellite can be located relative to stars to within two picture elements, and (2) that it is not possible to do better than three picture elements. The point is that an accuracy of 15 arc-s that intersects the curves at approximately 1.1 or 1.7 deg cannot be achieved with a larger field of view. However, as stated previously, if further studies were undertaken, they might relax the navigation requirements to permit an accuracy of 30 arc-s. On the other hand, an accuracy of one picture element might be obtained by improved calibration. At present, it appears that a 1- to 2-deg field of view will be optimal from the approach-guidance standpoint. The baseline science system has a 5-deg field of view; adequate stars can be obtained, if they are of the sixth magnitude, but the accuracy is not acceptable. Conversely, the 0.5-deg field of view meets the accuracy requirement, but tenth magnitude stars are needed. These numbers indicate that an instrument somewhere between the science narrow-angle and wide-angle cameras is needed.

Another important factor in approach guidance is the brightness of the satellites. Some of the larger satellites of Jupiter and Saturn are very bright during approach, and it is difficult to image them with faint stars. Figure 153 shows satellite brightness during approach. The brightest stars in

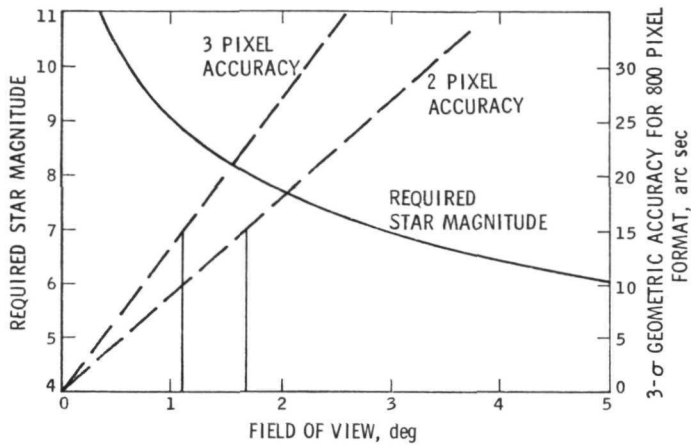


Fig. 152. Required star magnitude and geometric accuracy vs field of view

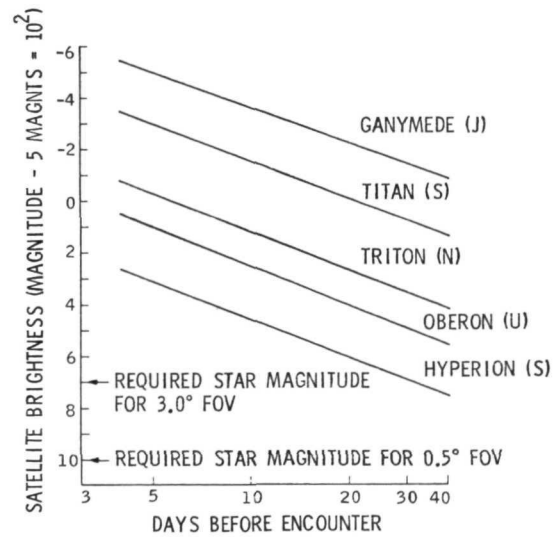


Fig. 153. Satellite brightness during approach for a typical three-planet mission

the sky are about -1 on the magnitude scale; e. g., Sirius and Canopus. Venus, at its brightest, is about -4.4, and the full moon is -12.5. Some of the objects in the sky are very bright a few days before encounter relative to the faint background stars required. There are tenth magnitude stars for an 0.5-deg field of view (FOV), and seventh magnitude stars for the 3-deg field of view. The range between the Galilean satellites of Jupiter and the background stars can be as much as the fifteenth magnitude, a factor of 10^6 in brightness, which is a problem for most imaging sensors. The actual dynamic range requirement for the imaging sensor would be closer to 10^4 because the light from the satellite image is spread over large areas; it is not a point image. However, the dynamic range of most sensors is about 100.

Obviously, special effort is required in this area. One method is not to measure larger satellites. In the case of Jupiter (J), this would mean using no optical approach guidance, which may be feasible. In the case of Saturn (S), one of its smaller moons, Hyperion, is about the third magnitude, which is acceptable if it is imaged with eighth magnitude stars. Like Hyperion, the satellites of Uranus (U) are fairly small and do not present a serious problem. Triton, the only moon that can be used at Neptune (N), is large but quite dim so that the dynamic range problem is not serious. Apparently, the dynamic range problem could be largely solved by forgetting the large moons, if it were not for two considerations. First, in the case of Saturn, perturbations of Hyperion may be very significant because it moves closely to the orbit of Titan, and large perturbations result. It is not clear at this time how these perturbations will affect the navigation determination programs. It may be necessary to use larger satellites, which are not perturbed as much. The second consideration is that, if a flyby is made of one of the larger satellites of Jupiter or Saturn, it is necessary to know where they are going more accurately than can be measured from Earth. Thus, on-board measurements against the background stars are needed. Although approach-guidance might be accomplished without large satellites, there are associated risks involved.

The following areas require special attention during instrument design:

- (1) Dynamic range: dynamic range can be manifested in measurement accuracy, if the satellite image blooms, or, in some cases, by damage to the sensor itself.

- (2) Sensitivity to stars: there are sensors available, such as the silicon intensifier tube, that will detect a sufficient number of stars with even fairly modest optics. However, if other considerations necessitate use of a less-sensitive tube, sensor response might become a problem. Exposure duration is limited by the attitude drift of the spacecraft. Stray light is another factor to be considered.
- (3) Geometric accuracy: attaining an accuracy of two or three picture elements will probably require the use of fiducial marks on the optical image plane to remove the distortions caused by the imaging sensor. Because the field is dark, the fiducial marks must be luminous. White spots can be produced on the silicon target by such means as shorting out diodes. However, if an intensifier tube is used, the white fiducial marks should be placed on the photocathode rather than on the target to remove the distortions of the intensifier stage. This area needs further development.

3. Possible Mechanizations.

a. Vidicon instrument. The vidicon instrument uses science-imaging technology with approach-guidance optics and, possibly, may use special filters. The instrument does not require any separate sensor development. Furthermore, when the vidicon is used, the science instruments do not have to perform approach guidance, and the approach guidance instrument does not have to perform the science. The disadvantage of the vidicon is that, because it is a separate instrument, it increases cost, weight, and power usage. Also, it may be necessary to remove some of the science to accommodate the approach-guidance instrument. The maximum data per frame is six million bits for a TV picture. In fact, there is not that much information in the star scene, so that, to efficiently transmit the television output to Earth, it is necessary to have some kind of very strong compression system.

b. Microchannel plate (MCP) plus vidicon instrument. This instrument is a microchannel plate image intensifier used with the vidicon sensor. The advantages of this device are that it has a tremendous gain, amplifies

the images by as much as 10^4 , and also has unusual saturation properties so that saturation in an image can be restricted to a bright point of a very small region. For example, if a match is struck in a dark room with a low ambient level, instead of the image going white, the only area lost is where the match is struck. The disadvantages are that it has more noise than ordinary image intensifiers, which could seriously affect the detection of weak-threshold stars. Also, there are uncertainties associated with its development, and it is not yet known if it can survive a 10-year mission.

c. Image dissector instrument. The third instrument has a V-slit image dissector that sweeps out over the image slowly, as opposed to the point-by-point reading of a television system. As the instrument passes over a star, two blips are seen for each star and each satellite. The spacing of the blips gives the vertical position in the scan line, and the position of the blips gives the horizontal position. Although the instrument supplies the same kind of information as that obtained by a point-by-point readout, it requires about 10 scan lines only, instead of 800. However, the scan time has to be relatively long compared to the attitude drift motion to get the signal-to-noise ratio. As a result, the gyro information would have to be used to remove the drifts.

The advantages of this system are substantial. Image dissectors tend to be more reliable and stable than television sensors because they do not have a target or a thermionic cathode. The data are highly compressed. The dynamic range is higher because there is no target to integrate the charge. The disadvantages are that a separate sensor must be developed, and there are the concomitant cost, weight, and power penalties. The slit is more sensitive to stray light than a point scanner because the stray light is integrated over the entire aperture of the slit. It may be as much as 100 times more sensitive. Data reduction is likely to be more complex because there is no point-by-point readout.

d. Science imaging subsystem. One or both science television systems can be used for the approach guidance data. The advantage is that no extra weight is added. Weight and power are almost equivalent in the sense that, if more power is needed, more RTG must be added, and more science must be removed. Another advantage of this system is lower cost.

One disadvantage is the limitation on the field of view, as described previously. However, this may change as the science requirements are better defined. If the science requirements call for a less-sensitive system, it may be impossible to detect enough stars. White fiducial marks would be required. Other disadvantages are that there would be no backup from a separate instrument, and a maximum data frame is required.

4. Special Approach Guidance Components. Certain components are peculiar to the approach guidance system and would not be developed for science purposes:

- (1) Luminous fiducial marks.
- (2) A spot filter to solve the dynamic range problem. If a dark filter is placed in the center of the field of view, which will attenuate by a factor of about 100, then the periphery of the field of view can still be used to detect stars. This technique requires pointing the instrument with sufficient accuracy to put the satellite image on the filter.
- (3) Special readout systems. The data available in an approach guidance frame will be much less than the 5 million bits in a television frame. It may be desirable to sweep along and detect just the threshold where there is a star, and to relay that information only. To do this requires the capability for threshold detection and for reading-out the beam position of a few points rather than sending back the entire picture, line-by-line. These special readout procedures should be investigated because they may be significant, depending on the amount of data and the number of pictures needed.

5. Subsystem Status. The preliminary requirements were defined, and their implementation investigated. Viable instrument alternatives have been examined. The thrust of activities has been toward developing an optimum science/guidance capability within the weight and cost constraints. The navigation development team continued to examine the approach guidance and the navigation requirements in detail.

The science requirements were being defined by a special group of scientists and the imaging team. An imaging science development team was considering systems integration and the detail of the science camera design.

Reference 2 is a general review of the navigation section. References 3 and 10 discuss error analysis work, modeling of optical distortions, etc. The use of the MCP plus intensifier is discussed in Ref. 11. Details on some of the subsystem requirements are given in Ref. 12. Reference 4 discusses approach guidance in some detail and gives the results of some of the tradeoffs and studies that have been done to date. The instruments are discussed in Ref. 13.

REFERENCES

1. Kingsland, L., Jr., "Trajectory Analysis for a Grand Tour Mission to the Outer Planets," J. Spacecraft Rockets, Vol. 6, No. 8, pp. 897-902, Aug. 1969.
2. Hamilton, T. W., and Jordan, J. F., "Coursing Accurately to the Giant Outer Planets and their Moons," Astronaut. and Aeronaut., Vol. 8, No. 5, pp. 66-70, May 1970.
3. Ball, J. E., and Duxbury, T. C., "Navigating the Grand Tours," Astronaut. and Aeronaut., Vol. 8, No. 9, pp. 73-76, Sept. 1970.
4. Moore, J. W., et al., Approach Guidance - Science Imaging Tradeoff Study, Internal Report 900-458, Jet Propulsion Laboratory, Pasadena, Calif., July 15, 1971.
5. Duxbury, T. C., and Acton, C. H., Programmers' Reference Manual for MM'71 Optical Navigation Demonstration, Volume I, Overview, Internal Report 700-112, Jet Propulsion Laboratory, Pasadena, Calif., July 13, 1971.
6. Duxbury, T. C., and Acton, C. H., Programmers' Reference Manuals for MM'71 Optical Navigation Demonstration, Volume II, Objectives, Internal Report 700-113, Jet Propulsion Laboratory, Pasadena, Calif., July 13, 1971.
7. Ondrasik, V. J., and Rourke, K. H., "Applications of Quasi-VLBI Tracking Data Types to the Zero Declination and Process Noise Problems," presented at the AAS/AIAA Astrodynamics Specialists Conference, Fort Lauderdale, Florida, Aug. 17-19, 1971, Preprint AAS No. 71-399.

8. Curkendall, D. W., and McDanell, J. P., "An Investigation of the Effects of Major Earth-Based Navigation Error Sources for an Outer Planet Mission," presented at AAS Annual Meeting, "The Outer Solar System," Seattle, Wash., June 28-30, 1971, Preprint AAS No. 71-118.
9. Friedman, L. D., Hamilton, T. W., and Stanton, R. H., "Estimating Trajectory Correction Requirements for the Outer Planet Grand Tour Missions," presented at AIAA Tenth Aerospace Sciences Meeting, San Diego, Calif., Jan. 17-19, 1972.
10. Duxbury, T. C., "A Spacecraft-Based Navigation Instrument for Outer Planet Missions," J. Spacecraft Rockets, Vol. 7, No. 8, pp. 928-933, Aug. 1970.
11. Stanton, R. H., "Approach Guidance Subsystem Development," in The Deep Space Network, Space Programs Summary 37-65, Vol. III, pp. 107-111, Jet Propulsion Laboratory, Pasadena, Calif., Aug. - Sept. 1970.
12. Stanton, R. H., "Challenges in Developing an Approach Guidance Instrument for the Outer Planets," AAS Paper 71-119, AAS 17th Annual Meeting, Seattle, Wash., June 1971.
13. Stanton, R. H., "Onboard Optical Guidance Instruments for Outer Planet Spacecraft," AIAA Paper 71-945, AIAA Guidance, Control, and Flight Mechanics Conference, Hempstead, N. Y., Aug. 1971.

XII. SPACECRAFT ATTITUDE CONTROL

A. Attitude and Articulation Control

The attitude control and the articulation control functions are combined in the following discussion because much information pertaining to one pertains to the other. Articulation control comprises those functions that move the articulated members on the spacecraft, such as the medium-gain antenna, the science scan platform, and the three focus actuators that focus the sub-reflector on the high-gain antenna.

1. Objectives. The objectives set at the beginning of the TOPS project were:

- (1) To develop the attitude control functional requirements.
- (2) To develop a baseline design. A block diagram and a baseline description of the subsystem were completed, and the tradeoffs required to verify the feasibility of the baseline were made. The baseline was then analyzed in a depth sufficient to improve it and to verify that it could meet the functional requirements.
- (3) To develop those areas wherein the devices were not at the state of the art needed for TOPS.
- (4) To develop basic control laws for the subsystems and to demonstrate the baseline system feasibility. To do this, breadboards sufficient to make up the pitch axis of the spacecraft were built, assembled on the single axis table, and tested.
- (5) To identify those areas that needed further development.

2. Basic Requirements and Constraints. The basic requirements for the subsystem are derived from five areas.

a. Communications. The spacecraft must be Earth-oriented for the high-gain antenna pointing. In the Mariner missions, the spacecraft pitch and yaw axes were Sun-oriented. When required, the position of the high-gain antenna was changed in an open-loop fashion to improve its pointing. For TOPS, lock on the Earth is maintained throughout the mission by biasing

off the sensors, which use the Sun as a reference, and the antenna points at the Earth at all times. The articulation control subsystem must point the medium-gain antenna about two axes during all maneuvers to improve data rates.

b. Science. Primarily for the encounter science, the spacecraft must have three-axis control. Many of the science experiments, e.g., the television, would not be possible on a spinning spacecraft. The spacecraft must be oriented during cruise to accommodate the cruise science and maneuvered to calibrate the science instruments. For example, a 60-h roll must be performed several times during cruise to calibrate the magnetometer. During encounter, the scan platform pointing, and slew and settling must be performed at the rates and times required by the encounter science.

c. Navigation. Mass expulsion must be minimized. Maneuvers must be performed at several points throughout the mission to change the trajectory in accordance with navigation requirements. Autopilot performance must also meet the navigation requirements. Further, the change in velocity imparted to the spacecraft by the midcourse motor burn must be measured.

d. Mission. The effect of Jovian radiation, magnetic fields, and the extremely low temperatures of the devices at the extremities of the spacecraft affect the requirements placed on the attitude control subsystem. Other mission requirements that affect attitude control are the 10-year life, the multimission capability, and launch dates.

e. Spacecraft. A set of constraints is imposed on the attitude control by the hardware configurations and subsystems interfaces. TOPS has greater structural flexibility than previous spacecraft. The increased flexibility complicates stabilization of the subsystem in cruise, principally during the motor burn. In addition, the spacecraft environment, in particular the RTG radiation levels, affect attitude control.

3. Functional Requirements. Figure 154 is a block diagram of the Attitude Control Subsystem. The heart of the Subsystem is the hybrid processing attitude control electronics (HYPACE), which receives signals from a digital inertial reference unit, the acquisition and cruise Sun sensors, and the digital Canopus tracker. These signals are fed through a series of custom buffers to interface with a processor, which derives its basic control

law from memory. They are then fed through a series of custom output buffers either to drive reaction wheels for three-axis control during cruise or to drive hydrazine thrusters, when the rates get too high. When wheel saturation signals are received, the hydrazine thrusters are pulsed to unload the wheels. During maneuvers, the HYPACE controls the autopilot actuators. The HYPACE also is the principal communication link with the rest of the spacecraft, in particular, with the control computer and the measurement processor.

The functional performance requirements are given in Table 55.

Table 55. Functional performance requirements

Acquisition	
Attitude propulsion	Acceleration $0.01 \pm 0.002^\circ/\text{sec}^2/\text{axis}$ Continuous operation 10 min minimum Duty cycle 0 to 100% Minimum torque pulse results in 40 rpm change in wheel speed
Acquisition rates	$3^\circ/\text{sec}$ any axis
Acquisition time	Sun orientation in 30 min maximum
Cruise	
Systematic pointing error	P/Y $0.1^\circ (3\sigma)$ R $0.3^\circ (3\sigma)$
Digital Sun sensor	Field of view $38^\circ (Y) \times 6^\circ (P)$ Resolution 0.025°
Reaction wheels	Momentum storage 0.5 ft-lb-sec Stall torque 0.02 ft-lb
Dead band	Reaction wheel $\pm 0.05^\circ$ Thrusters $\pm 0.2^\circ$ Limit cycle rates $2^\circ/\text{hr}$ maximum
Maneuver	
Turn error	$0.01T \widehat{\min} (3\sigma)$ T = maneuver time (sec)
Thrust vector parameters	$0.3^\circ (3\sigma)$ preaim pointing error $0.3^\circ (3\sigma)$ transient error
Autopilot steady state error	$0.2^\circ (3\sigma) + \text{gyro drift}$

Table 55 (contd)

Maneuver (contd)	
Inertial reference unit	Turn rate 0.17°/sec/axis Scale factor 0.001°/pulse Accuracy ±0.01%
Accelerometer	Linearity 0.1% Range 0.01 g to 0.025 g Bias uncertainty 100 µg max
Scan platform (requested)	
Pointing	0.05° (1σ)
Drift rate	2°/hr
Slew rate and settling time	40° in 40 sec including settling to within 2°/hr

Table 56 gives the general hardware constraints for the entire subsystem with the exception of volume, which is given for only the elements in the electronics main compartment because the volume constraints on those elements are more critical than those for the elements on the extremities of the spacecraft.

Table 56. General hardware constraints

Power, W	
Cruise	29
Maneuver	72
Articulation control	20
Volume, cm ³ (cu in.)	
Electronics	21,303 (1300)
Wheels	1392.9 (85)
Inertial reference unit	7210.3 (440)
Weight, kg (lb)	48.54 (107)
Reliability	0.95 over 10 ⁵ h

4. Baseline Design. The Baseline Subsystem is primarily all digital. Some elements of the Subsystem, such as the reaction wheels, can not be digitized; and others do not need to be digital, e.g., the acquisition Sun sensors.

The HYPACE is digital for many reasons. However, the principal reason is reliability. After launch, the control law can be reprogrammed to improve performance or to overcome any difficulties encountered during cruise. In addition, a digital system saves hardware. The breadboard presently on the single-axis simulator represents one axis of attitude control. It is not programmable; it is hardwired logic containing about 750 electronic components. The HYPACE, with the three-axis design and using 54L single-gate logic, may also require only 750 components.

The acquisition Sun sensors are analog because the Mariner baseline sensor is adequate for the mission.

Because the spacecraft has to be pointed toward Earth and yet use the Sun as a reference, the field of view of the cruise Sun sensors in yaw is 38 deg, and it is necessary to bias the sensor output. In addition, 0.025-deg resolution is required. Digital cruise Sun sensors have been selected to meet these requirements.

The Canopus tracker used the Mariner approach. However, for TOPS, it has been extensively revised to make it digital to improve its compatibility with the rest of the subsystem. There is a possibility that some of the hardware may be turned into software to be included in the HYPACE, thus further decreasing the components in the subsystem.

The inertial reference unit is digital. There were several tradeoffs on this unit, e.g., a six-gyro skew array is used for reliability reasons. When the gyro axes are properly located off the spacecraft principal axis, a significant improvement in reliability is obtained with the same amount of hardware.

Another tradeoff concerned the use of gas-bearing vs ball-bearing gyros in the inertial reference unit. If the gyros should be required throughout a 10-year mission, the gas-bearing gyro is a better choice. Further, the gas-bearing gyro generates less noise than the ball-bearing gyro at a ratio of about 10 to 1, which is quiet enough to meet the required resolution of 0.001 deg per pulse.

A further question is whether to leave the gas-bearing gyros operating throughout the mission or to turn them on only as required. The tradeoff here concerns power. Although it may be more feasible to leave the gyros on, at present, they are turned on only when needed.

Reaction wheels are used in the baseline design principally to reduce expendables required for a 10-year mission. The baseline reaction wheel control is orthogonal, although a skewed reaction wheel has not been rejected.

With the inclusion of reaction wheels in the Attitude Control Subsystem, an expendable-gas thruster is needed to unload the wheels. The question is whether the gas should be hot, warm, or cold. As discussed in Section VII, the hot-gas system (hydrazine) has the highest I_{sp} and uses the same fuel as the midcourse motor, thus requiring only one set of tankage and plumbing. Any residual fuel from the trajectory corrections would thus be available to the attitude propulsion, thereby greatly extending the lifetime of the Subsystem.

A decision was made to use hydrazine thrusters in place of the reaction wheel to perform the commanded turns because the thrusters effect a significant savings in weight with a negligible increase in fuel.

The autopilot is used to provide thrust vector control for the trajectory correction propulsion engine. Both bipropellant and monopropellant engines have been considered. The major difference between the bipropellant and the monopropellant engines is the temperature of the exhaust gasses. A bipropellant motor produces temperatures too high for the use of jet vanes in the exhaust; therefore, the engine is gimballed. However, with the present engine, the jet-vane array appears to be an improvement. This array is similar to that flown by Mariners 4 through 7. When a jet-vane system is used, the actuators can be redundant. The Mariner spacecraft carried four jet vanes. Only three are required for three-axis control, so that, if one fails, three-axis control is maintained with only a slight penalty in translation. A six-vane array would possibly eliminate much of this translation penalty and greatly extend the lifetime. Although the design and analysis of an autopilot with jet vanes is not completed, it appears to be better than the gimballed engine.

The digital baseline design was selected, then, because:

- (1) It is less susceptible to component drifts and degradation.
- (2) The TOPS vehicle interfaces are almost all digital. Those of the CCS are exclusively digital, and it is preferable to interface with a digital system rather than to perform a series of A to D conversions.
- (3) A digital system provides greater design flexibility. LSI and MSI today are digital devices. With an analog baseline, it would be difficult to develop enough high-reliability components at a weight low enough for flight. Also, a digital system provides broader range of design solutions because modules can be used. For example, if it were decided to use a different type of Sun sensor, only the interface buffers would have to be changed. With the digital baseline design, the subsystem can be reprogrammed to meet many various control requirements without redesign of the hardware. Thus, a multiple-mission design is provided with a minimum design impact.

The disadvantage of a digital subsystem is that no direct rate information is available. The gyro package, which has been the source of rate when the gyros are on, now provides position information. Each pulse out is an increment of position, so that rate must be derived, whether the gyros are on or off.

A simulation and analysis of the Attitude Control Subsystem, using the control laws, disclosed that the damping provided with derived-rate schemes used in the past was marginal, at best. However, when the HYPACE is added to the baseline, another option is available. The HYPACE has a Kalman filter optimal control law designed into the software, so that, in effect, rates are estimated, not derived from spacecraft motions. This estimate improves with time because a running log of information is kept in the processor. Thus, the damping, and, consequently, the subsystem performance is greatly improved. Present simulations indicate that the system is extremely stable.

5. Summary. Early development of the Attitude Control Subsystem was initiated in the following areas:

- (1) Digital control electronics.
- (2) The digital Sun sensor.
- (3) The star tracker, including a program to develop the image dissector device.
- (4) The digital inertial reference unit, including development of digital and gas-bearing gyros.
- (5) Analytical techniques, primarily to accommodate structural flexibility in the spacecraft.
- (6) Environmental effects, primarily, radiation effects on components.
- (7) The systems approach to long life. This analysis is in process, and it is not known yet what level of redundancy is required throughout the subsystem to meet a 10-year life goal. However, it is believed that the system is inherently capable of meeting this goal.

Techniques to extend life used in past missions are used for the TOPS Attitude Control Subsystem; e. g. , high-reliability electronic components with selected redundancy, conservative electrical-mechanical design techniques, extensive functional and qualification test programs, a functional backup command capability, and selected block redundancy. However, for the outer planet missions, it is necessary to go beyond these to meet the 10-year extended life requirement. Consequently, the TOPS Attitude Control Subsystem uses a minimum electronic component count with MSI and LSI, extensive block redundancy, a digital control system, the CCS for fault detection and switching, advanced development of special components, extensive functional redundancy, a flight reprogrammable control law, and computer-controlled testing.

B. Attitude Control Analysis Studies

The two primary areas in the Attitude Control Subsystem analysis are the Cruise Attitude Control Subsystem and thrust vector control, or autopilot. The goal for the Cruise Attitude Control Subsystem was to develop a suitable

control law and to implement it digitally as simply as possible. Performing reaction wheel unloading and commanded turns using the digital control system were studied in less depth than the control law and its implementation.

In the area of thrust vector control, the main effort was expended on the gimballed engine because, as the TOPS configuration developed, a variety of engine sizes were considered. The use of an autopilot with a gimballed engine was studied in depth to determine the stability of this controller in relation to vehicle flexibility. Techniques for modeling the flexibility and for simulating the entire craft were developed.

1. Cruise Attitude Control Subsystem. A block diagram shown in Fig. 155 illustrates the approach that was taken to implement the digital, hardwired control that was demonstrated on a single-axis, gas bearing, spacecraft simulator. A control computer word is added to the Sun sensor digital word, and used as a bias to point the spacecraft toward the Earth. In the inertial mode, the gyro signal, which is also a pulse, is added. The sum of this information gives the position-error signal during cruise.

Figure 156 shows the operation of this design in the phase plane. The reaction wheel is pulsed depending on the size of the position error. However, a variable frequency pulsing sequence, designed to operate in certain regions of the phase plane, is used. In the region next to the deadband, for example, the sequence is at fairly low frequencies to begin with and then diminishes. In region II, the wheels are pulsed at full torque. Then, if region VII, for example, is entered again, the maximum rate is cut off and the wheels are pulsed at a minimal rate, just adequate to cross the deadband in a reasonable amount of time. This provides substantially better damping.

Figure 157 shows the control scheme programmed on the single-axis simulator. As the position error increases to 0.025 deg, the wheel pulsing sequence starts at a high rate, then diminishes with time. When the 0.05-deg line is crossed, the torquing increases and again tails off. The 0.1-deg line is crossed at the maximum torquing rate. At the first bit change, representing a decrease in position error, pulsing is shut off. Now, depending on how big the rate is, pulses may or may not be added. This method gives a good return rate. When the opposite deadband is crossed again at the 0.025-deg point, pulsing is resumed, tails off, resumes at 0.05 deg, etc., until, eventually, a fairly small limit cycle is obtained.

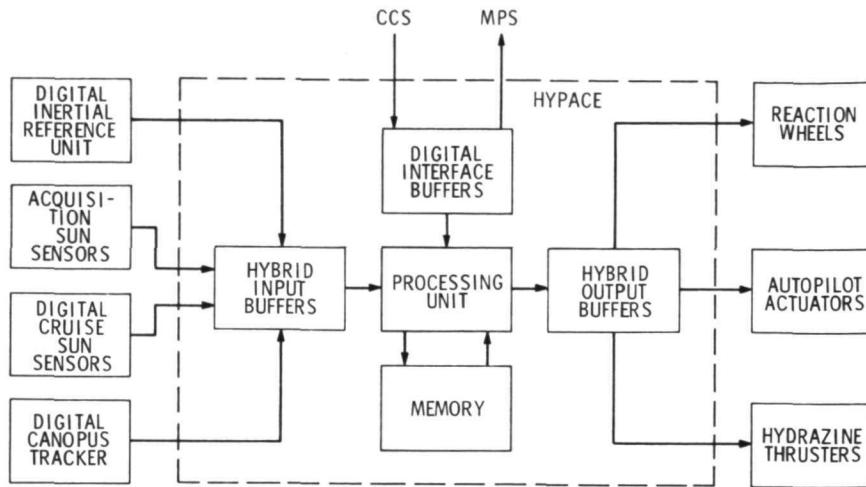


Fig. 154. Attitude Control Subsystem

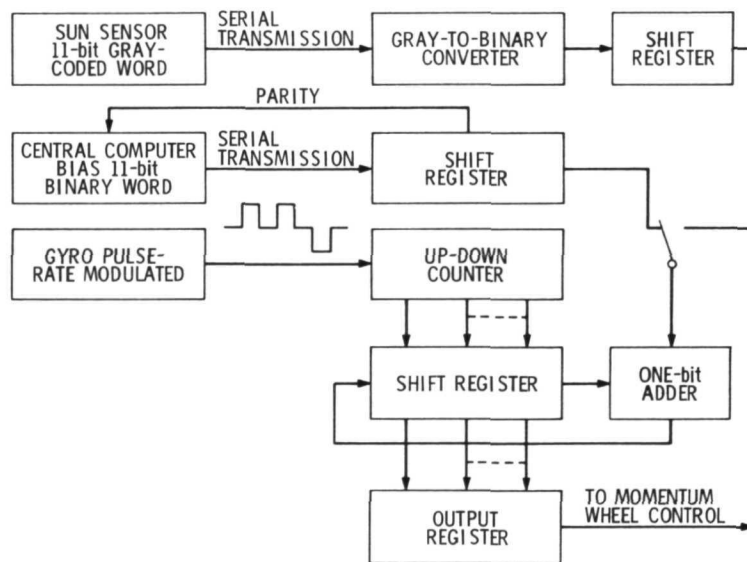


Fig. 155. Digital summing of position signals

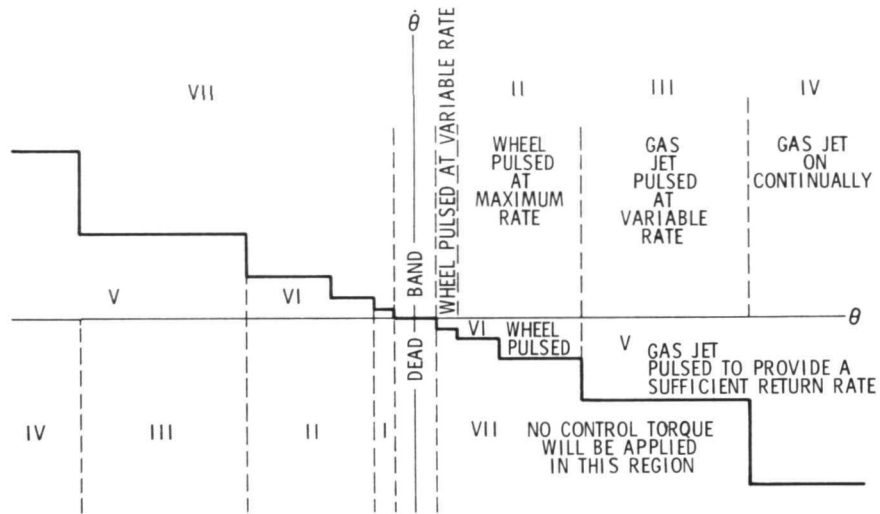


Fig. 156. A digital suboptimal control scheme

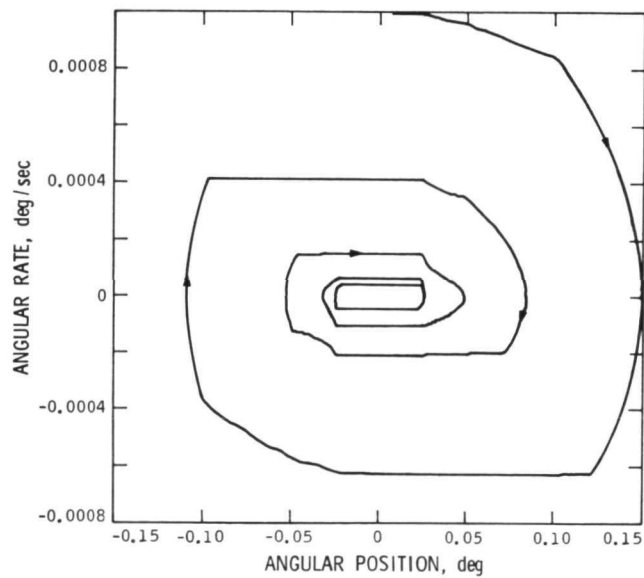


Fig. 157. Suboptimal controller response

2. Thrust Vector Control (Autopilot). As previously mentioned, the gimballed engine was used in these analyses. The primary interest was in the interaction of this controller to vehicle flexibility. Techniques for modeling the flexibility were developed, and the models ranged from very simple to very detailed models. A continuous system simulation language (CSSL3) developed about two or three years ago is an important tool for analyzing nonlinear systems.

a. Vehicle flexibility models. The first approach in analyzing vehicle flexibility was the development of fairly simple, multiple rigid-body models. The Hooker-Margulies formulation of the problem, wherein a system of interconnected rigid bodies is used, was programmed for the digital computer. The spacecraft and two booms were modeled as a three-rigid-body system. With this approach, it was possible to determine that the instruments mounted on the booms are not deflected enough in cruise, or by an 111.2-N (25-lb) thrusting engine, to cause any problems in instrument pointing. Also, no significant interaction effect on the cruise attitude controller would be discernible because the torque pulses of the booms were so small. The application of rigid body techniques to scan slewing dynamics would be valuable; no work has been done on this yet.

The second approach used in analyzing vehicle flexibility was a hybrid-modal-rigid body method wherein some rigid body portion of the vehicle where the gyros and sensors are mounted was contained. This allows the pitch, yaw, and roll angles, and Euler angles to be used. However, the relatively flexible portions of the vehicle can be described with the modal approach. Thus, as much detail as needed can be obtained. The modes can be truncated and the single-axis approximations examined. Root loci are used for stability. The eigenvalues for the 3-axis linear system can be obtained or six-degree-of-freedom simulations using a number of modes can be made to determine the interactions.

The block diagram in Fig. 158 illustrates the linear analysis using hybrid coordinate modal data, with the modes truncated down to about four or five. Figure 159 shows a simplified linear single-axis block diagram of the autopilot controller.

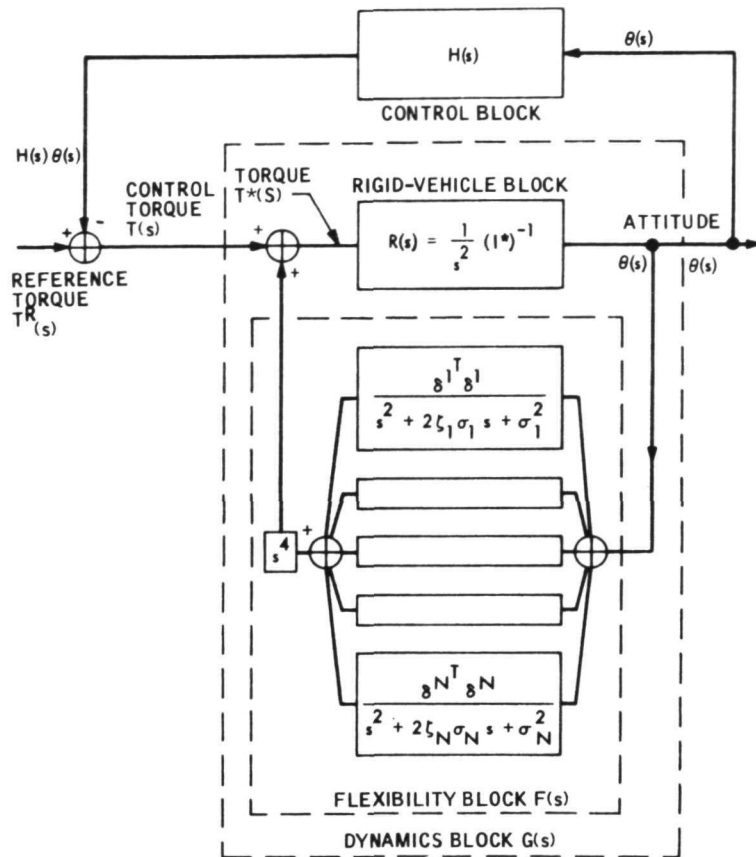


Fig. 158. Linear analysis using hybrid modes

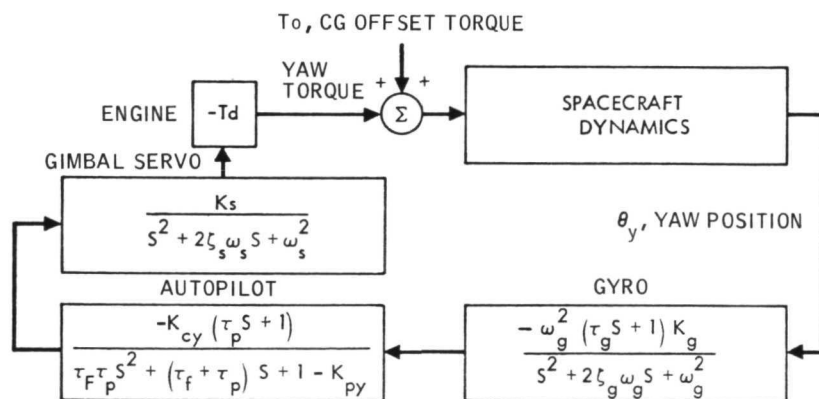


Fig. 159. Yaw axis autopilot block diagram

Figure 160 shows a computer simulation of the yaw response of the spacecraft, assuming that it is an ideal rigid body with a gain in yaw of 2.2. As shown in Fig. 161, if the effect of the booms is added, instability results and saturation occurs as the gimbal angles saturate. However, if the gain is reduced to 1.0, the system can be stabilized, which may or may not be an acceptable solution (Fig. 162), depending upon whether or not other spacecraft subsystems can tolerate the residual oscillation. Figure 163 shows that, with all five modes included, the stability of the gimbal controller for pitch and yaw requires a 1.4-gain limit in yaw, and a 6.3-gain limit in pitch. The Xs on the figure are points that were verified with a six-degree-of-freedom simulation.

C. Attitude Control Electronics

The original concept of the attitude control electronics stemmed from the idea that the digital system should be a controller with a simplicity similar to that of the Mariner device. The Mariners used a single string device with highly reliable components to minimize the component count. However, as the TOPS development progressed, more complex problems became apparent, e. g., flexibility and the complexity of using digital information in conjunction with reaction wheels. A controller, to be used in a single-axis test, was constructed for the yaw axis. Even though the autopilot was not yet incorporated, the coordination of the various factors involved were complex. When the scan platform was moved, the resulting disturbance torque had to be sensed by some methods other than the attitude control sensors, to meet the settling requirements. As a result of the evolutionary process to meet these complexities, the HYPACE was developed.

1. Design. The analytical considerations for the design were that (1) the pointing stability required sophisticated estimation and filtering, and (2) a better damping rate was needed to keep the low-limit cycle rates and to compensate for articulation motion. To attain the latter, it appeared that complicated control laws would have to be used.

In a wired programmer design, like the one used for the single-axis test, more compensation estimation becomes, in a reliability sense, series elements. The signal travels through more things, and when the redundancy necessary to meet the 95% reliability for 12 years is implemented, the series elements compound.

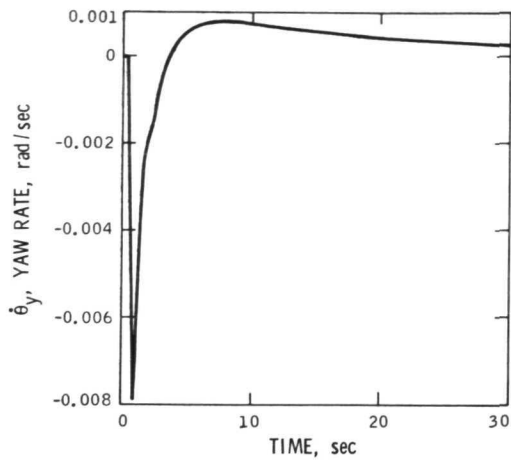


Fig. 160. TOPS yaw axis angular rate vs time (rigid body, $K_y = 2.2$)

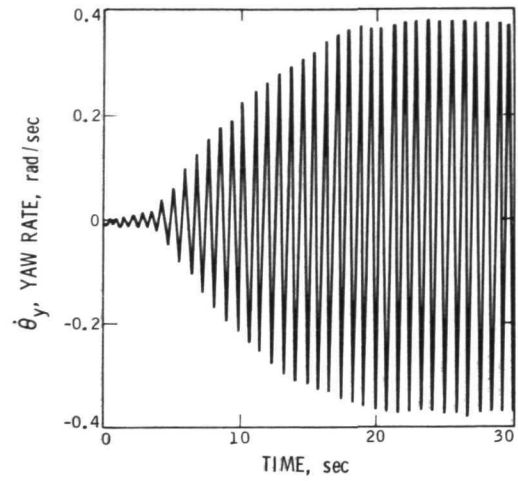


Fig. 161. TOPS yaw axis angular rate vs time (flexible vehicle, $K_y = 2.2$)

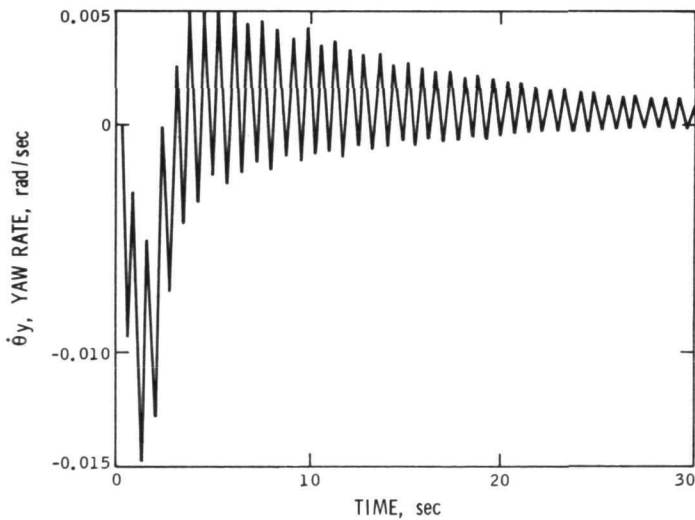


Fig. 162. TOPS yaw axis angular rate vs time (flexible vehicle, $K_y = 1.0$)

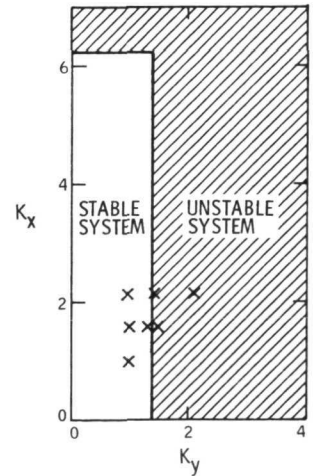


Fig. 163. Autopilot stability in pitch and yaw

The control, during powered flight, requires compensation for spacecraft flexibility. It may be that, by lowering the gain in one case, stable performance can be obtained, but there may not be enough gain in the loop to meet the navigational requirements. In this event, more compensation is needed, which would increase the series elements. The complexity of the single-string design, then, was becoming comparable to that of a fully programmable system with a memory. Therefore, it was decided to develop a programmable system.

Figure 164 shows a block diagram of this system, the HYPACE. Both analog and digital sensors feed into the hybrid input buffers, where some processing on the analog signals takes place, and then they are fed into the processing unit, which is a relatively primitive processor, operating with a memory. The hardware associated with compensation, etc., which would be series elements from a reliability standpoint, are now software. The results are fed from the output buffers into the reaction wheels, autopilot actuators, and thrusters. The result is a sample data system instead of a continuous system, but the analytical tools, such as hybrid coordinates, are still applicable.

To enhance reliability, there is an interface with the measurement processor subsystem (MPS) and the CCS. These subsystems perform reliability maintenance. Malfunctions in flight can be determined by examining the telemetry data going in to the measurement processor. It is difficult in an analog or wired system to pinpoint the trouble so that the appropriate standby program unit can be switched in. However, in the HYPACE system, the primitive instruction set in the processing unit can be checked by the CCS and the MPS. These two share a memory, so that anything available to one is also available to the other to analyze and to send corrective responses. Thus, they can switch in the appropriate redundant units because they can check the individual steps that are going on to make up the complex control law.

2. HYPACE Sizing Study. This programmable system was initiated with a sizing study to determine what would be needed to operate a relatively sophisticated control law. The study included sequential least squares filtering and estimation for the digital sensors, powered flight control with four active actuators and signal mixing, and power sharing between reaction

wheels and thrusters. The CSSL3 was used to determine whether or not the cruise performance was acceptable when the spacecraft was operating in a sampled mode at various cycle times throughout the program.

Results of the study, showed that about 1100 words are needed for a basic loop, and about 950 for the CCS and MPS interfaces plus the ancillary operations. Accuracy and resolution require at least a 16-bit word. An 8- μ s add time is desirable, although a longer add time can be used with a more simple processor. If the direct digital control is limited, an add time of about 18 μ s can be used.

During the CSSL3 simulation, a disturbance was applied, as shown in Fig. 165. The circle indicates the beginning of the simulation, and the disturbance is applied to the spacecraft in the direction of the arrow. The limit-cycle drift rate is 2 deg/h. The X in the figure marks the one-minute point of recovery from the disturbance. The noisy response shown at the end of the curve is caused by a simulation of extreme, unrealistic, sensor noise conditions to determine the estimator performance.

A HYPACE breadboard project was devised to represent the present state of the subsystem. At present, the functional design is complete; the circuit design, 65% complete; the construction, mainly out of 74L components, is 10% complete. The subsystem is designed to mount on an air bearing table for a single-axis test. An 18-bit, 4096-word, plated-wire memory is incorporated. A byte-serial operation is used to minimize power usage and the number of components. The add time is 18 to 19 μ s. The A to D and D to A conversion is being incorporated in the breadboard with the A to D conversion times at about 100 μ s.

Three major elements of the software have been completed: (1) a FORTRAN coded assembler for use with the Univac 1108, (2) a HYPACE simulator for use with the Univac 1108, (3) the HYPACE machine language, which is disassembled by an 1108 symbolic disassembler into a FORTRAN subroutine, which represents the program processor, so that it can be used with the CSSL3 program to obtain interaction with the real dynamics. The disassembled symbolic-to-CSSL interface software is still being written.

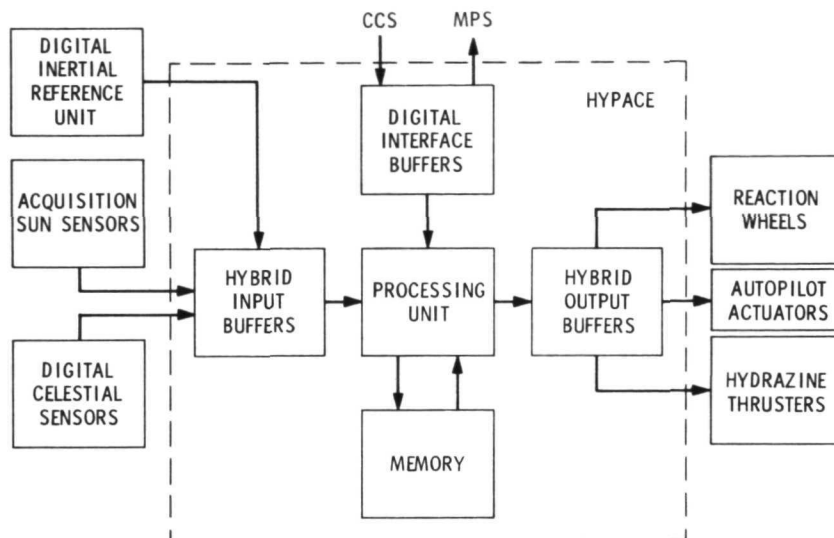


Fig. 164. HYPACE

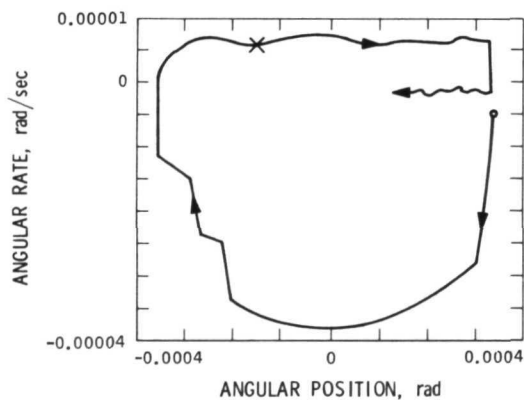


Fig. 165. CSSL3 simulation showing recovery from a disturbance

D. Celestial Sensors

1. Digital Star Tracker. The digital star tracker is similar to the Mariner star trackers in that it uses an image dissector tube in a closed-loop, roll-control system. The major difference is that a digital output is produced to interface with a digital attitude control system.

a. Functional requirements.

- (1) Optical fields of view: the tracking field of view is 6.4 deg in roll \times 40 deg in cone. The 40 deg in cone provides for the apparent motion of Canopus with respect to the spacecraft coordinates. The instantaneous field of view is 0.5 deg in roll \times 4.7 deg in cone.
- (2) Range of trackable stars: the visual magnitude of the range of trackable stars is +3.6 to -2.2. This corresponds to approximately 0.02 to about 4 times Canopus.
- (3) Signal outputs: the roll position error signal is a digital, 11-bit word with a resolution greater than 0.025 deg. The intensity signal is an analog voltage proportional to the logarithm of intensity of the star being viewed. The acquisition signal is a gate change indicating star acquired or star not acquired.
- (4) Logic functions: the logic functions within the tracker are the high- and low-intensity gates. The gates are used to discriminate between stars being viewed or tracked. Sixteen high and sixteen low gates are implemented with an intensity increment of 32% between each gate setting. This allows the gates to be brought in closely to Canopus so that it can be discriminated from other stars to foreign particles, such as dust particles released from the spacecraft. Should the image dissector photocathode degrade over a long lifetime, the gates can be shifted to compensate for the loss of sensitivity, and the same operational characteristics can be maintained.
- (5) Logic commands: on command from HYPACE, the Canopus tracker sweeps across the field of view to search for a star. If some object or star is acquired that is not desired, the star tracker can be commanded to override that star and look for

another source. The gate-position command changes the intensity gates, and the cone-angle position command positions the 4.7-deg cone field of view in any one of 16 positions within the 40-deg cone field of view. This small, 4.7-deg field of view lowers the probability of finding foreign objects or a star that is not wanted, and also reduces the susceptibility of the tracker to stray light.

- (6) Power: the power in the cruise mode is less than 6 W. The sun shutter is a blade that is driven across the face of the image dissector tube to prevent degradation by high intensity sources, such as the Sun. Less than 3 W is required to actuate this shutter. The electrical input to the tracker is 50-V rms at 4800-Hz square wave. All the power processing is done within the tracker.

b. Design. Figure 166 is a simplified block diagram of the Canopus tracker. The image dissector takes the image from the star through the optics of the tracker onto the photocathode tube and produces an output signal, which is amplified through the preamplifier and fed into a phase-sensitive demodulator. The phase-sensitive demodulator produces a dc voltage, plus or minus, depending on the position of the star, and this voltage is fed to a voltage-controlled oscillator. The voltage-controlled oscillator then produces a string of pulses whose frequency is dependent on the demodulator output voltage. The pulse train then goes through a control gate, which is controlled by the acquisition logic. The signal is then fed to an 11-bit, up-down counter, which produces an 11-bit digital word to provide the roll error output to be utilized by the HYPACE. The signal is also fed through a D-to-A converter into the roll deflection amplifier, which closes the loop around the image dissector to keep the tracking field of view centered on the star. This closed-loop operation allows a small instantaneous field of view to provide a large linear scale factor. The roll scan generator produces a sawtooth waveform that sweeps the instantaneous field of view across the electron aperture within the image dissector. The commands from HYPACE come into a command register. The gate commands go into two four-bit D to A converters for high and low gate, and the high- and low-gate outputs go into the acquisition logic. It has not yet been decided whether or not the acquisition logic will be removed and put into the HYPACE. If it should be, it would allow more flexibility within the attitude control system. The signals for the cone-updating go through the D-to-A converter into the deflection amplifiers,

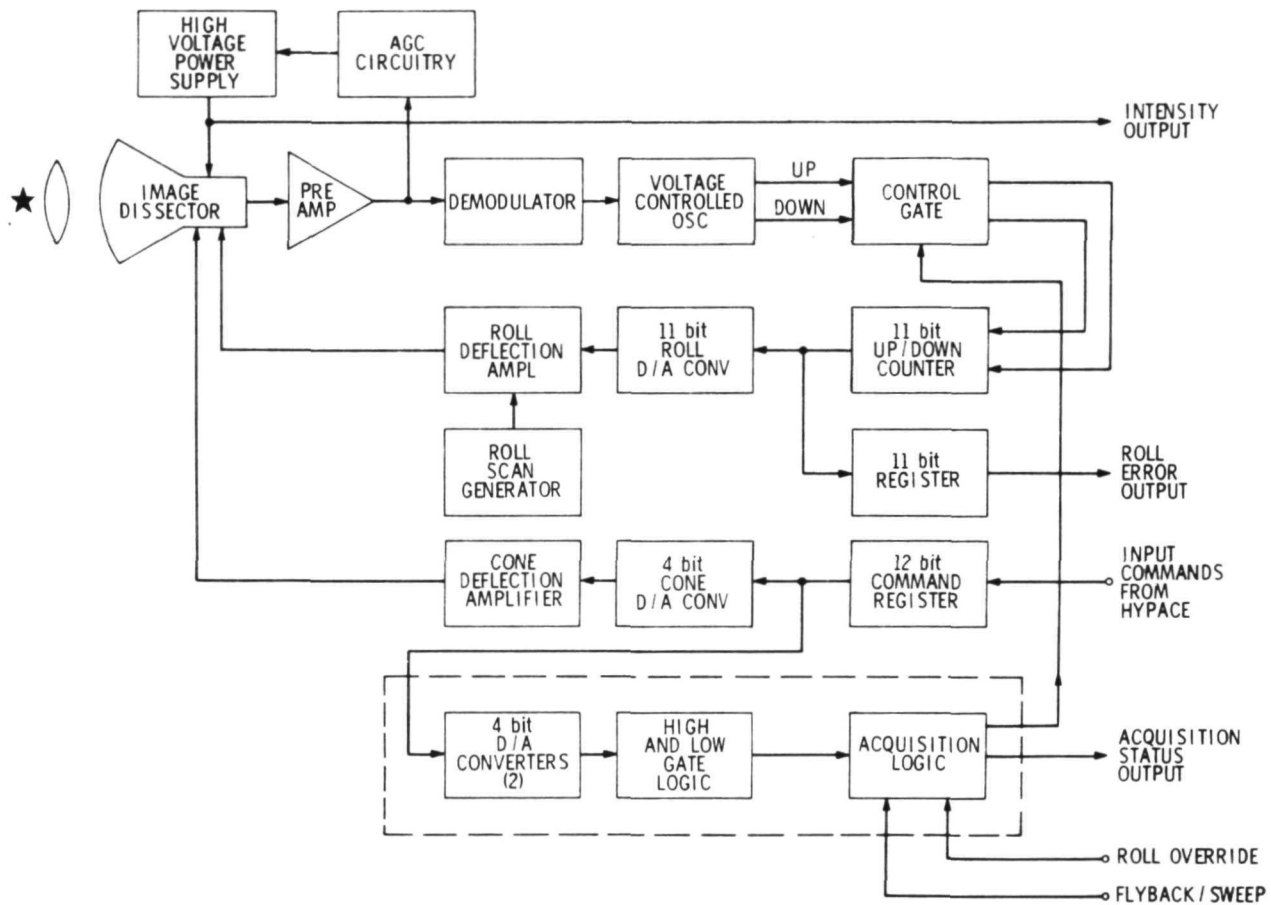


Fig. 166. Digital star tracker

and the dc bias signal is placed on the cone deflection plates of the image dissector to select the field of view desired.

The automatic gain control circuitry takes the signal out of the preamplifier, detects its amplitude, and feeds it back to control the image dissector high voltage to produce a constant amplitude signal independent of the star intensity. This signal, an analog intensity signal output, indicates the intensity of the source.

Figure 167 is a photograph of the digital star tracker breadboard. About one half of the circuitry is analog. The signal loop is analog and digital. The image dissector tube is the type used in the Mariner star trackers. This configuration, which includes all of the acquisition logic, contains about 450 components.

Figure 168 is a schematic diagram of the image dissector tube proposed for flight. The design requirements include long life, low noise, and a low-magnetic signature. The photocathode is deposited on the inside surface of a sapphire face plate. The construction is ceramic/metal. The entire tube preamplifier is then packaged in a magnetic shield.

c. Status. The preliminary electronic design of the star tracker is complete. The electronic breadboard has been fabricated and is being evaluated. The image dissector development is partially complete. After the breadboard evaluation and the image-dissector development are completed, the tracker will be incorporated into the single-axis test program.

2. Digital Sun Sensor. The digital Sun sensor was developed to interface with the Digital Attitude Control Subsystem and to bias the spacecraft off the Sun line.

a. Functional requirements. The functional requirements of the digital Sun sensor are:

- (1) Optical fields of view, 6 deg for pitch and 40 deg for yaw.
- (2) Resolution from 5 to 30 AU, less than 0.025 deg. From 1 to 5 AU, it decreases from 0.2 to 0.025 (limited by detector segment width and the optical characteristics and design constraints).

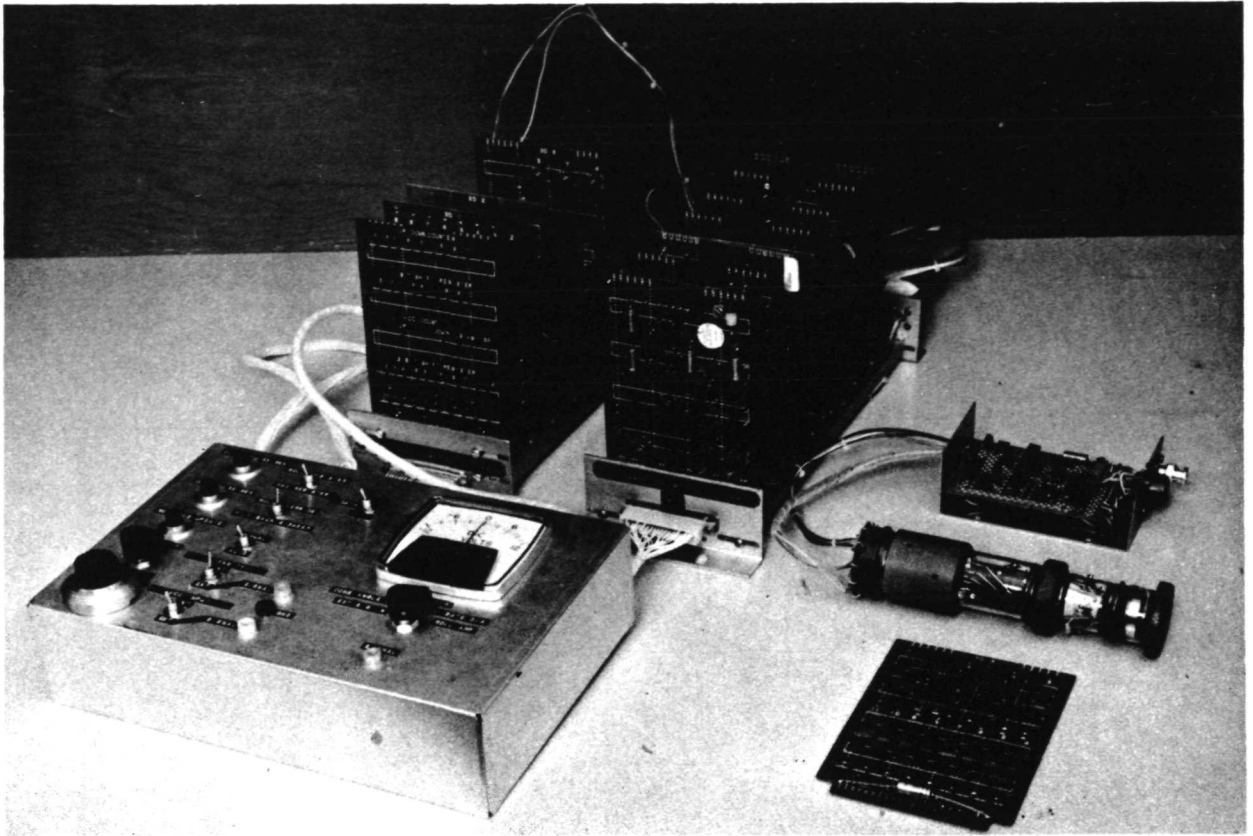


Fig. 167. Digital star tracker breadboard

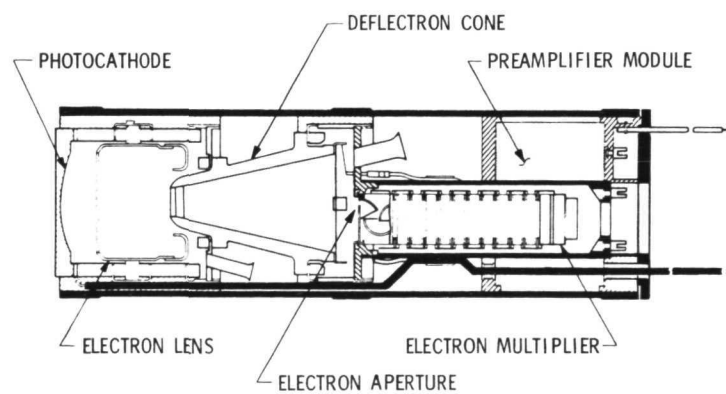


Fig. 168. Image dissector

- (3) Accuracy, 0.05 deg. This is also the system accuracy requirement. The accuracy of the sensor itself or the overall system accuracy must be improved, possibly by means of the HYPACE.
- (4) Operating range in intensity, $135,626 \text{ lm/m}^2$ (12,600 ft-cd) at 1 AU to 150 lm/m^2 (14 ft-cd) at 30 AU. The Sun diameter over that dynamic range goes from 32 to 1 arc-min.
- (5) Power of the cruise sensors (pitch and yaw), 2.45 W.
- (6) Weight of the two cruise sensors, 2.72 kg (6 lb).
- (7) An analog acquisition Sun sensor. The acquisition Sun sensor is an analog design because it is believed that the basic Mariner sensors will be adequate for TOPS.

b. Design. Figure 169 shows a conceptual design of the digital Sun sensor. The detector substrate has recrystallized cadmium sulfide deposited on it in the form of a gray code. As the line image formed by the cylindrical lens of the Sun is moved back and forth across this detector, different segments of this gray code are illuminated.

Depending upon which of the segments is illuminated, there will be high or low outputs. The outputs are fed into a series of buffer amplifiers and then into a storage shift register, which produces a gray code word equivalent to the position of the line image across the detector. (Although a 5-bit detector is shown in the figure, there will actually be an 8-bit detector with a 6-deg field of view for pitch, and an 11-bit detector with a 40-deg field of view for yaw.)

Figure 170 shows the 8-bit pitch detector. The gray code mask formed by the sensitive cadmium sulfide on the substrate can be seen, as well as the numerous electrodes necessary to get the voltages in and the signal out. About 9 leads come off the back of this detector. The 11-bit yaw detector will be physically larger than this. It may be possible to use large field-of-view detectors for both pitch and yaw, masking part of the pitch detector, where the large field of view is not needed, so that one type of detector can be used for both channels of the Sun sensor.

c. Status. The pitch sensor optical and electronic breadboard fabrication and preliminary evaluation are complete. Because the data from

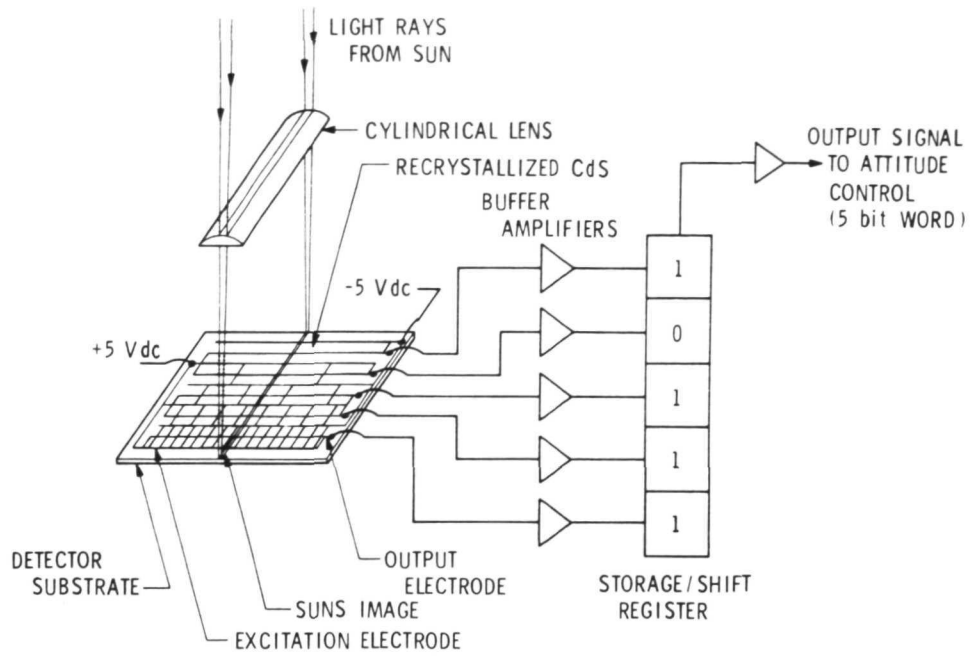


Fig. 169. Digital Sun sensor



Fig. 170. Digital Sun-sensor detector

an 11-bit digital sensor is large, a data acquisition system was designed that utilizes a small computer and an angle generator to compute the transfer characteristics of the device. The first phase of the data-acquisition system development is complete. The yaw sensor detector procurement has been initiated and is under development.

Work to be completed is the yaw sensor breadboard, using the new wide angle detector, and the data acquisition system. Both the pitch and yaw sensors, using the data acquisition system, are yet to be evaluated.

E. Inertial Devices

The inertial devices used on the TOPS are gyros, accelerometers, and bi-directional reaction wheels.

1. Functional Requirements.

a. Gyros. The single-degree-of-freedom gyro is used for the TOPS baseline. A digital pulse-on-demand (ternary mode) is used to interface with the HYPACE and to minimize power usage. The gyro has a scale factor of 0.001 deg/pulse $\pm 0.1\%$, a capture capability of 2 deg/s, and a trimmed drift of 0.2 deg/h.

b. Accelerometer. The accelerometer is also digital pulse on demand with a range of 0.01 to 0.025 g and a bias uncertainty of 100 μg .

Requirements common to both the accelerometer and the gyro are a lifetime of 100,000 h; minimal weight, power, and parts in the electronics; and no single-point failure modes.

2. Environmental Factors. The environmental factors new to the TOPS mission were discussed in Section IV. Tests have been made to determine the effects of radiation in specific areas, one of which is organic fluids. Organic fluids are used both in the gyros and the accelerometers. Changes in viscosity would influence the damping on these instruments, and they could be affected by outgassing effects and any chemical changes caused by the radiation environment.

Organic solids, used in the sensors for encapsulation, adhesives, and seals were tested to determine whether or not any microcreep phenomenon might occur because of the radiation environment. Such an occurrence would affect the long-time stability of the sensors.

In the semiconductor area, the concern is for radiation effects on Hall effect devices, used in the Delco single-degree-of-freedom gyros, and light-emitting diodes, like those used in the Honeywell 134S gyro. A Mariner gyro and accelerometer, and some of the material used in them, were exposed to 2×10^{12} neutrons/cm² and 7,000 rads gamma. It is planned to continue this testing in 1972 using proton and electron exposure. Tests made before and after radiation exposure revealed no degradation in gyro accelerometer performance, and no chemical or physical changes in the materials.

3. Inertial Reference Unit Packaging. The inertial reference unit will have six gyros and two accelerometers. A preliminary study showed that there was no weight or size penalty for using either skewed gyros or orthogonal arrays. The heat loss must be low to conserve power. The sensor alignments must be stable over a long period of time. Weight and volume should be minimized.

Figure 171 is a diagram of the proposed skewing arrangement for the inertial reference unit. The X, Y, and Z axes are the principal spacecraft axes, and they correspond to the principal axes of the unit itself. The circles represent the locations of the input axes of the six gyros. The axis of each gyro is located in a plane determined by the intersection of two axes at 45 deg to one of the two axes. This is called an octahedron-type of configuration.

Figure 172 shows the relative reliability vs time and failure rate plotted for four different configurations of the inertial reference unit. The configuration represented by curve 3 was chosen because the 45-deg angle simplifies the computation, the preparations for testing, and the tests themselves.

A single-axis inertial reference unit (IRU) was tested on the single-axis simulator. The gyro used on the unit was a Honeywell GG334S. The performance achieved in the first digital loop was 0.001 deg/pulse, a capture capability of 1.2 deg/s and a drift stability of 0.02 deg/h. The value for the stability is a trimmed drift value that can be achieved in an 8-h running of the simulator. About 1500 h have been accumulated on this inertial reference unit to date. Because of improvements in the electronics, the capture capability is now 1.6 deg/s. The number of parts have been reduced 35%. Power, exclusive of spin motor or heater power, has been reduced 20%, with

about 1.6 W for the loop and the precision regulators. Testing revealed no degradation in accuracy.

Three different gyros were evaluated during the TOPS project. All were gas-bearing. The tests were not comparative; they were different tests for different purposes. The Honeywell GG334S gyro was tested extensively in a previous sterilization program. Most of this testing was in the analog mode, and the gyro was exposed to severe environments of 275° F, 200 g shock, and 15 g rms vibration. A Honeywell GG134S, was tested for about 3000 h. About one half of the testing was digital and the other half analog. Environmental tests were limited to hot and cold soaks at +30 and +150° F. A fast warm-up test was performed in 12 min. from +30° F.

A Northrop gyro, the GI-K7G, was tested. This gyro, similar to the gyro used in the C5 inertial navigator, is a platform gyro, not a strap-down gyro, as the first two gyros are. Fifteen hundred test hours were put on this gyro: again, about one-half digital and one-half analog. The environmental tests were limited to hot and cold soaks at 0 and 195° F. The normal gain for this platform gyro is 9, but, because it was desirable to have a lower gain for this test and increased damping for compatibility with the digital loop, the gain was dropped to 1.3 by lowering the temperature. The normal motor excitation on the gyro is 3.6 kHz, but this was dropped to 1.2 kHz to achieve a greater torquer scale factor for compatibility with the loop.

Table 57 lists the selection criteria for the single-degree-of-freedom gyros.

4. Reaction Wheels. The TOPS baseline requires that each reaction wheel have an angular momentum capability of 0.678 N-m-s (0.5 ft-lb-s), a maximum torque of 0.027 N-m (0.02 ft-lb), 1,000,000 h of life, and a standby redundant configuration of two wheels per axis (orthogonal).

Some reaction wheel testing in support of the TOPS project is completed. An air bearing torque tester, with a sensitivity of less than 50 dyne-cm was assembled. This tester was used to run torque-speed curves in conjunction with a two-axis recorder, and to determine run-down torques.

Table 57. Selection criteria for single-degree-of-freedom

Requirement	Design features
Long life	Gas bearing motor Long term stability Motor running detector
Digital application	Gas bearing motor Low gyro gain High torquer scale factor High pickoff frequency
Low power	Efficient spin motor Efficient torquer and pickoff Low heat loss design
Size and weight	Size 18 or smaller

A computer analysis for correlating motor run-down speed vs time as an indication of bearing condition was initiated. A simple model of the parameters of the wheel was developed, and no further work is required in this area.

Two Nimbus wheels are in test. One has about 4000 h in the single-axis simulator, and one has about 12,000 h accumulated on a life test.

An AC ball-bearing motor has been tentatively selected as being more practical than the DC brushless motors. However, neither the materials nor the lubrication scheme have been selected. Quality control techniques are needed to assure that the wheel will have a 100,000-h or a 10-year lifetime. Mechanical design modifications are needed to increase the momentum-to-weight ratio of the wheels. Radiated magnetic fields must be reduced, probably by a factor of 100. Further, the tachometer resolution of the wheels must be improved.

5. TOPS Closing Status

a. Completed work. Tasks accomplished during the TOPS project are:

- (1) The breadboard and tests for the digital gyro control electronics. The results are directly applicable to accelerometer control.
- (2) The evaluation of three different gyros in digital control loops.
- (3) Performance of limited radiation testing.
- (4) Studies of skewed vs orthogonal gyros.
- (5) Completion of a preliminary layout of the inertial reference unit.
- (6) Testing of reaction wheels.
- (7) Delivery of both a single-axis inertial reference unit and a reaction wheel for use on the single-axis simulator.

b. Work not completed. The following tasks were not completed in the TOPS project:

- (1) A demonstration of 100,000-h life capability for the sensors and the reaction wheels.
- (2) A demonstration of capability to survive the environment.
- (3) The selection and qualification of the specific sensors, the gyro, the accelerometer, and the reaction wheel.
- (4) The design and qualification of the inertial reference unit itself.

F. Single-Axis Simulator

The single-axis simulator includes a single-axis table, which has about 2400-lb suspended weight and can accommodate up to about 600 lb of electronics and components. At the present time, it has about 200 lb on it and provides a 1-to-1 weight and inertia simulation of the spacecraft yaw axis. Weight would have to be added to the table for a 1-to-1 simulation of the pitch- or roll-axis inertia. The table provides a real simulation without any scaling errors, so that when tests indicate that the design is right, it can be assumed that the design will work on the spacecraft.

The table has an N_2 gas-bearing suspension with hydrostatic thrust and journal bearings. For position readout, there is a 360-deg optical encoder with a resolution of about 0.01 deg.

The command and data line to and from the table goes through a simple device, two pieces of conductive tape, one on the suspended side and one on the fixed side. Coupling is capacitive so that a serial data line can be placed across it. Because the data are all digital, there is no degradation of the signal. A multiplex serial mode must be used, however, which necessitates the use of a series of lights on the table to indicate the state of various elements within the subsystem. A closed-circuit television in a remote control room is used to continuously display the status of the subsystem. The television eliminates the need for a complex multiplexer or a radio transmission from the table.

The simulator itself is located in an optical sensor laboratory and system test area at JPL, which provides the required optical isolation. Optical isolation is particularly important for testing the roll axis, which is especially sensitive because it involves the Canopus tracker. In addition, the ambient environment within the room is fairly well controlled and can be remotely operated so that all motion can be removed from the room during operations to minimize disturbance torques caused by thermal gradients and air currents.

Figure 173 is a block diagram of the single-axis simulator. The simulator shown is that of a pitch axis, involving Sun sensors rather than the Canopus tracker. The nitrogen supply is external to the table through the gas bearing. The attitude control electronics are the hardwired version for interface with the external command console. For reactors, a Nimbus wheel is used and a hydrazine thruster, which has been sized down slightly because it is operating in one atmosphere rather than in a vacuum.

Figure 174 shows a photograph of the suspended table with balance weights around it. The vertical axis of the table can be tilted to take advantage of the gravity vector. When the table is tipped down a few degrees, it seeks a null point, indicating a balance problem. Then, it can be balanced up. A 2-deg tilt is adequate to supply the balance required. The solar simulator is mounted on the support arm. The construction of the table is such that the critical alignments between the solar simulator and the Sun sensor

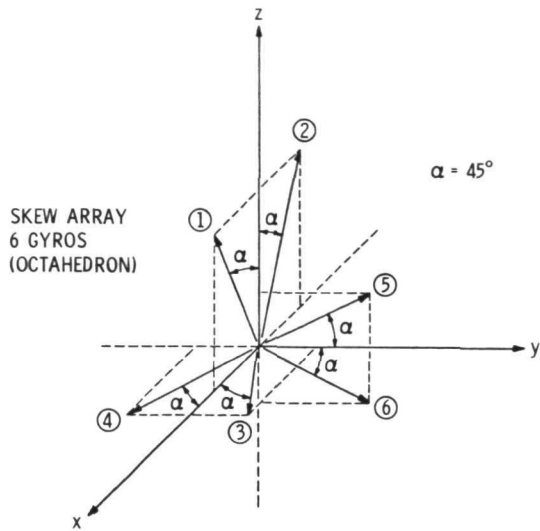
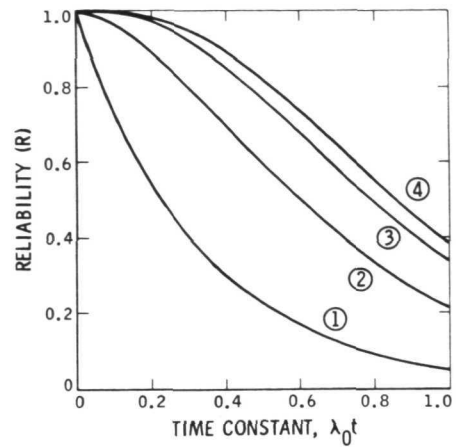


Fig. 171. Inertial reference unit



- ① NON-REDUNDANT IRU
- ② ORTHOGONAL EMPLACEMENT OF TWO GYROS ON EACH AXIS
- ③ OCTAHEDRON (SKEW) CONFIGURATION OF SIX GYROS
- ④ OPTIMUM (SKEW) CONFIGURATION OF SIX GYROS

Fig. 172. Reliability vs time and failure rate

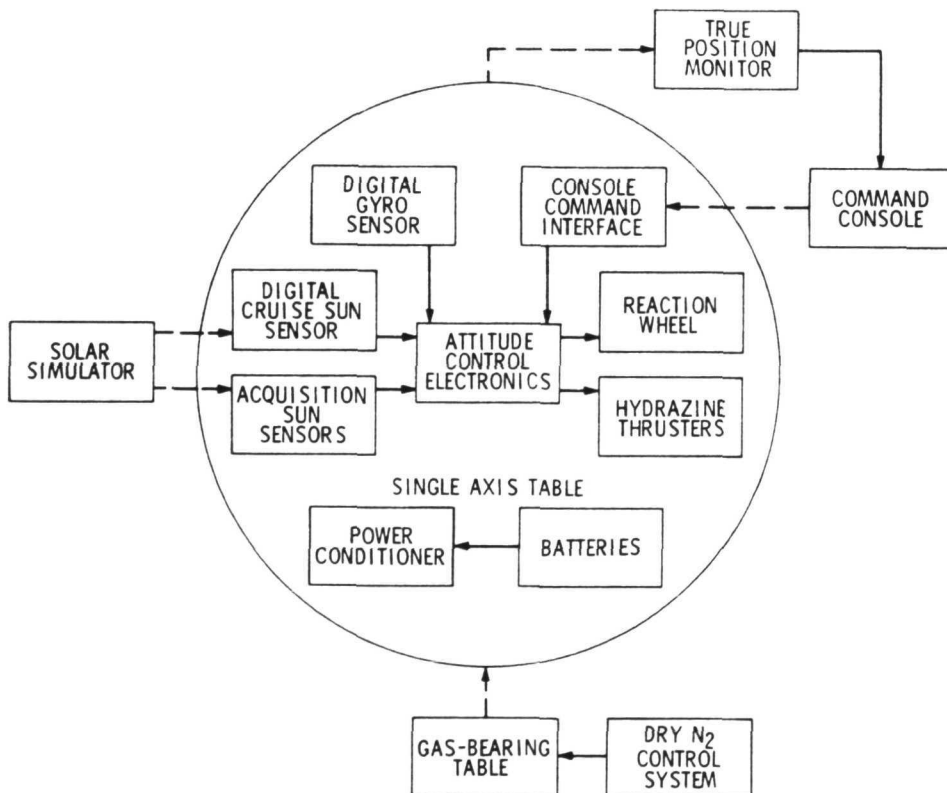


Fig. 173. Single-axis simulator

on the table are maintained. The sensor is mounted on the center of the table so that the radiation pressures from the light source will not unbalance the table.

Figure 175 shows some data from a pitch cruise simulation. This test was run before the parameters of the subsystem were tuned. At the start of the curve, the table was braked and motionless. The curve then shows the motion that resulted when the -0.05 -deg bias shift was changed to $+0.25$ deg. The plot shown is for the optical encoder output and represents the table motion, over-shoot, settling, and return. The shift is greater than would occur at one step in space, but it illustrates the system performance.

The reaction wheel was unloaded at 1200 rpm, which is significantly above any speed that would be attained in space, where the wheel would probably be unloaded at 600 rpm. The 1200 rpm is included only to show the effect of a large external disturbance such as might occur in space during flight through the asteroid belt. In a later simulation for the pitch cruise, the wheels were unloaded at 600 rpm. The disturbance did not cause the system to exceed the position deadband.

G. Summary

For additional information on the attitude control, the reader is directed to the Bibliography at the end of this Section.

Attitude control areas that need further development are:

- (1) The 10-year lifetime technology: several analyses have been made to determine the areas that should be redundant. However, no breadboard has been constructed, nor has the reliability of the subsystem been fully analyzed to determine whether or not the redundancy is optimum. Test technique development is insufficient at present to verify 10-year subsystem life.
- (2) Environmental capability: some sensitive elements within the subsystem, other than gyros, have not yet been fully qualified environmentally.
- (3) Subsystem configuration: the baseline subsystem configuration has been completed and verified. However, the articulation control function needs further development. Articulation control requirements are sensitive to the science requirements, which

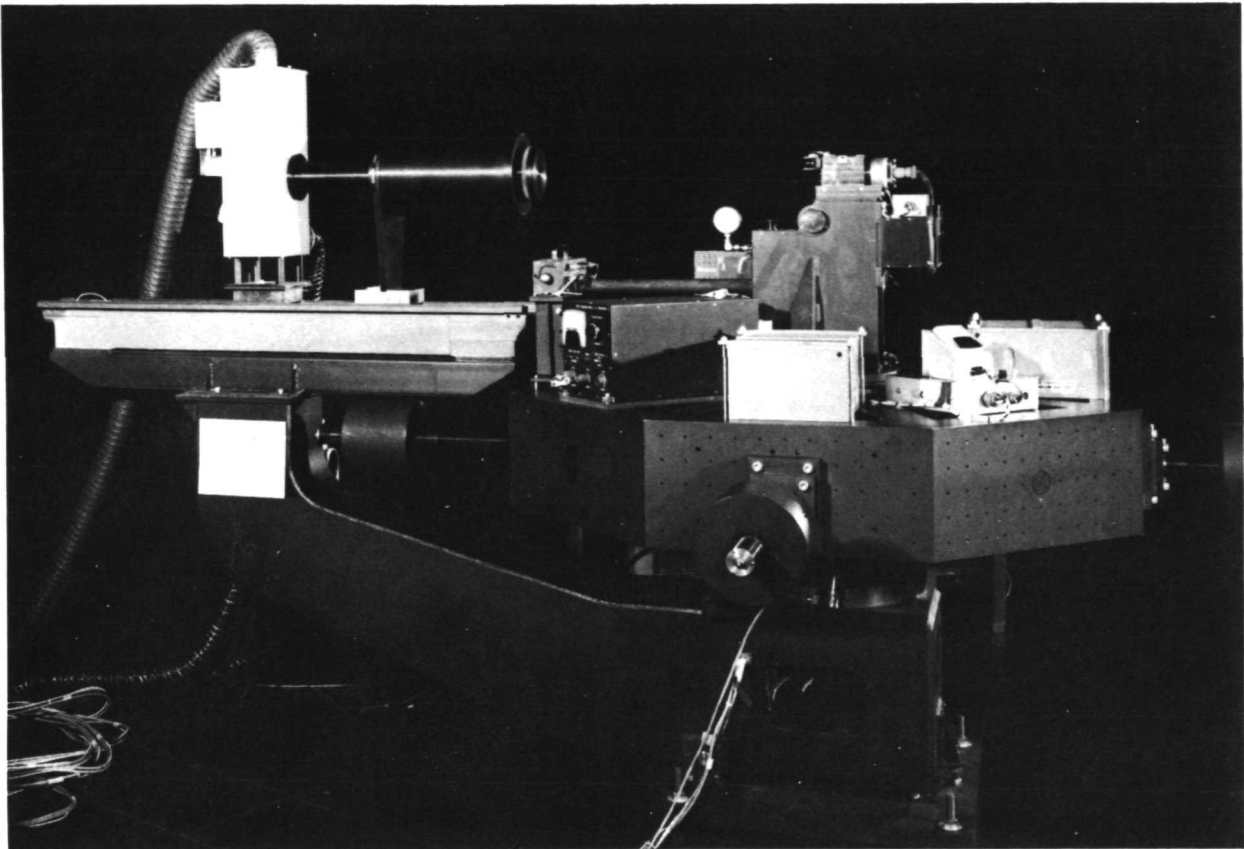


Fig. 174. Single-axis table, pitch-axis simulation

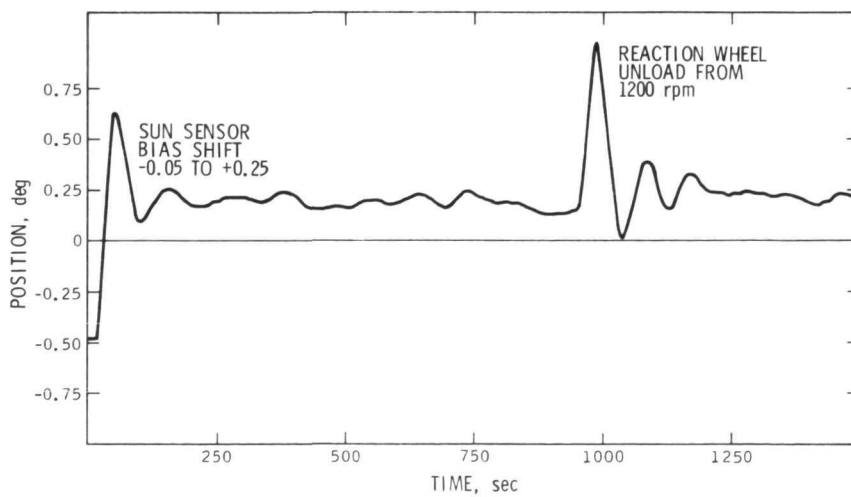


Fig. 175. Single-axis simulator, pitch cruise data

are always defined later in a mission than the engineering requirements. The baseline, which has been developed, is a multiplex scheme wherein the central articulation control electronics can drive any one of several actuators simultaneously or at any point in time. Many tradeoffs were made in the development of the configuration. However, alternative tradeoffs should be investigated.

- (4) Control law algorithms: the algorithms required for implementing the control law in the HYPACE are not complete. The cruise performance algorithms are under development, but none have been worked out in conjunction with the HYPACE to perform the autopilot function with the jet-vane array. The failure detection and switching has not been implemented to verify transient responses caused by switchovers to standby hardware, nor has the breadboard been made.
- (5) The HYPACE: the HYPACE hardware development is incomplete. Although the basic package of the support software is almost complete, reliability and ease of handling can be refined and improved.
- (6) Celestial sensors: the electronics breadboard is operating, but no redundancy is included. The image dissector tube development is not complete. The Sun sensor resolution needs further study.
- (7) Inertial devices: the gyroscope has not been selected nor fully qualified. It may be that the stability and power consumption in the inertial reference unit could be improved by taking advantage of wheel power to heat the package. The breadboard for this package remains to be completed and tested. The reaction wheel has not been developed.
- (8) Actuators: Actuators are required in both attitude and articulation control. The 10-year life must be verified, and actuator bearings, motors, and pick offs require further study.

BIBLIOGRAPHY

- Bouvier, H. K., and P. W. Likins, "Attitude Control of Nonrigid Space Vehicles, " Astronautics and Aeronautics, May 1971.
- Dorroh, W. E., "An Attitude Control Subsystem for a Thermoelectric Outer-Planet Spacecraft, " Astronautics and Aeronautics, September 1970.
- Dorroh, W. E., "Attitude Control of a Tops Based Outer Planet Orbiter Spacecraft, " JPL Space Program Summary, SPS 37-63, Vol. III, June 30, 1970.
- Dorroh, W. E., and T. H. Thornton, Jr., "Stratagies and Systems for Navigation Corrections, " Astronautics and Aeronautics, May 1970.
- Fleischer, G. E., "Applications of the Hybrid-Coordinate Method to the Tops Autopilot, " Proceedings of the Fourth NASA Intercenter Control Systems Conference, November 4-5, 1969.
- Fleischer, G. E., "Spacecraft Antenna Pointing for a Multi-Planet Mission, " JPL Space Program Summary, SPS 37-51, Vol. III, June 30, 1968.
- Fleischer, G. E., Spacecraft Antenna Pointing with a Single Degree of Freedom, JPL Report TR 32-1255, March 15, 1968.
- Horiuchi, H. H., "All-Digital Articulation Control System Development, " JPL Space Program Summary, SPS 37-50, Vol. III, April 30, 1968.
- Hand, P. J., "Digital Gyro System - Phase I, " JPL Space Program Summary, SPS 37-66, Vol. III, December 31, 1970.
- Hand, P. J., "Tops Inertial Reference Unit, " JPL Space Program Summary, SPS 37-63, Vol. III, June 30, 1970.
- Likins, P. W., Dynamics and Control of Flexible Space Vehicles, JPL Report TR 32-1329, January 15, 1970.
- Likins, P. W., Finite Element Appendage Equations for Hybrid Coordinate Dynamic Analysis, JPL Report TR 32-1525, October 12, 1971.
- Likins, P. W., and G. E. Fleischer, "Results of Flexible Spacecraft Attitude Control Studies Utilizing Hybrid Coordinates, " Proceedings of AIAA 8th Aerospace Sciences Meeting, January 19-20-21, 1970.
- Lin, H. S., "Tops Attitude Control Reliability Study, " JPL Space Program Summary, SPS 37-63, Vol. III, June 30, 1970.
- Marsh, E. L., "Analysis of Flexible Structure Effects on Attitude Control Sensors, " JPL Space Program Summary, SPS 37-61, Vol. III, February 28, 1970.

- Marsh, E. L., and P. W. Likins, "Finite Element Modeling for Appendage Interaction with Spacecraft Control, " JPL Space Program Summary, SPS 37-66, Vol. III, December 13, 1970.
- McGlinchey, L. F., "Effects of Inertial Cross-Products on Tops Attitude Control, " JPL Space Program Summary, SPS 37-58, Vol. III, August 31, 1969.
- McGlinchey, L. F., "Extended Mission Control Systems Development, " JPL Space Program Summary, SPS 37-51, Vol. III, June 30, 1968.
- Schmidt, L. F., "Digital Sun Sensor, " JPL Space Program Summary, SPS 37-57, 37-60 and 37-64, Vol. III, June 30, 1969, and August 31, 1970.
- Schumacher, L. L., "An Analysis of Tops Science Package Pointing Errors Due to Structural Vibration of the Supporting Booms, " JPL Space Program Summary, SPS 37-62, Vol. III, April 30, 1970.
- Smith, L. S., "Tops Attitude Control Single Axis Simulator Momentum Wheel Tachometer Circuit, " JPL Space Program Summary, SPS 37-63, Vol. III, June 30, 1970.

XIII. SPACECRAFT POWER

A. Power Subsystem

Functional requirements of the power subsystem, other than the requirement for the solar-independent power, were an RTG power source capability of 440 W at 12 yrs, a subsystem reliability of 0.95 at 10^5 hr, 12-yr lifetime, a weight allocation of 397 lb, load fault tolerance, and load switching flexibility. The last two requirements are peculiar to TOPS and reflect the vigorous environmental and functional requirements of an outer planet mission. It is expected that the power subsystem will experience many load faults in its lifetime. The adaptive nature of the spacecraft and uncertainties in the RTG system require a load switching capability sufficient to accommodate changing demands as the extensive mission progresses.

The functional block diagram of the power subsystem is given in Figure 176. Four RTGs supply 140 to 150 W each at the beginning of life, degrading to about 110 W each at end of mission. Three busses are contained in the subsystem: an AC protected bus, an AC main bus, and a DC regulated bus. The protected bus supplies power to three key fault detection and correction subsystems aboard the spacecraft: the control computer subsystem (CCS), the measurement processor subsystem (MPS), and the timing synchronizer subsystem (TSS). The protected bus maintains power to these vital corrective subsystems in event of faults on other busses within the electrical subsystem. DC power from the RTGs is applied to a protected bus inverter that inverts to 50 V square-wave, single-phase 4.8 kHz power. The DC protected bus is regulated through a current throttle which senses the voltage of the DC protected bus and holds that voltage within a narrow range. In event of a major fault downstream of the current throttle, the throttle reduces the current passing to the AC main bus in such a manner as to maintain the voltage regulation of the protected bus and ensure that sufficient power is available for use by the CCS, MPS, and TSS.

Additional backup power to the CCS, MPS, and TSS has been provided through the main AC bus. The availability of a second source of AC power for these loads makes possible the use of a single standby inverter for the protected bus. In the event of failure involving both the protected bus inverter and its standby, the computer will transfer power to the CCS, MPS, and TSS through the AC main bus.

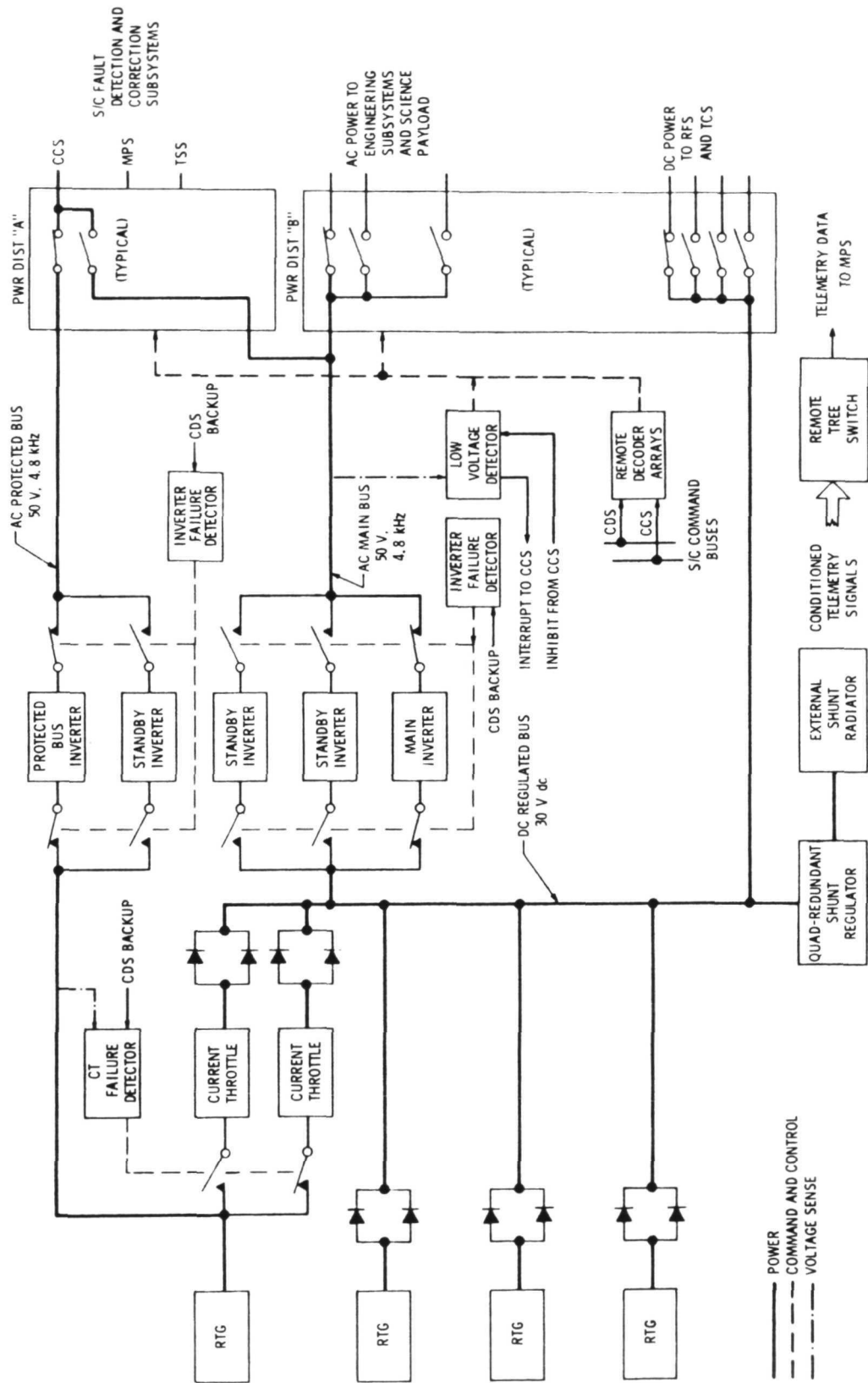


Fig. 176. Power subsystem functional block diagram

Major engineering and science subsystems derive their power from the AC main bus. Where the protected bus has one standby inverter, the AC main bus has two. The DC regulated bus is common to the other busses in the power subsystems. A quad-redundant shunt regulator shunts the excess RTG power to hold the DC regulated bus within a 1% voltage range. The RF subsystem TWTs and certain onboard heaters are the only users of DC power.

Load faults aboard the spacecraft are detected primarily by the control computer subsystem through telemetry data from the shared memory of the measurement processor subsystem. The computer determines the subsystem in which the fault has occurred and commands the power subsystem to remove the faulted load. A backup to this function is provided by the low voltage detector, a device designed to detect an under voltage situation, and to send an interrupt to the computer. The interrupt advises the CCS that in approximately 100 milliseconds, if the computer has still failed to detect and remedy the fault, the low voltage detector will command the turn-off of power to the noncritical spacecraft loads. In event the CCS has detected the fault and is attempting repair, the computer sends an inhibit to the low voltage detector, thereby stopping all action within the power subsystem. When the problem has been solved and voltage restored the low voltage detector automatically resets itself.

Commands to the power subsystem from the CCS and from the earth are processed through remote decoder arrays. These units receive the commands, decode them, and apply the proper logic to steer the commands to appropriate power distribution switches.

Telemetry data enroute to the measurement processor are conditioned within the power subsystem, then routed to a remote tree switch, where they are time multiplexed and ultimately delivered to MPS.

A review of the characteristics of the power subsystem identifies the shunt regulator as a 1 percent 30 V device with a 600 W capability which is quad-redundant in design. The main inverters have a synchronized frequency of 4.8 kHz and an efficiency of 92% at rated power. The output voltage is 50 Vrms, square-wave, single-phase. Power output is rated at 315 W for the main inverter and 90 W for the protected bus inverter. The inverters are short-circuit proof and standby redundant.

To provide adaptability to the various subsystems of the spacecraft, every load has been provided with its own individual power switch. This baseline decision is, of course, changeable should some subsequent development, such as a weight factor, prove it undesirable. The baseline switch design provides redundant "break" capability. Magnetic latching relays are used with redundant relay drivers.

The commands which control the power subsystem originate from two command sources - the control computer subsystem (CCS) and command decoder subsystem (CDS). Either source is capable of changing the state of power switches. Commands are remotely decoded and distributed to the appropriate switch.

A further, more definitive description of the RTG power source identifies the raw power requirement as about 410 W while the spacecraft is on-pad prior to launch. The RTG at this point is sealed, cooled, and filled with an inert gas, probably Xenon. Following launch, the gas is vented and the RTG, stabilized in the vacuum environment of space, is expected to deliver approximately 550 W. Twelve years later, the RTG power source will predictably generate 440 W.

Output voltage of the four RTGs at maximum power is 30 Vdc. The fuel is Plutonium 238. Reliability allocation per RTG is 0.99 at 10^5 hr; the weight of each generator is 80 lb; approximate envelope per RTG; 21.5-in. length, 12-in. diameter.

A spacecraft launch power profile as related to RTG power capability is given in Fig. 177. The transient loads are identified. The power curve depicted is representative and illustrates an approximate margin of available power.

Four major tradeoffs performed for TOPS were power distribution, launch power alternatives, shunt regulator design, and inverter failure detection. A description of each follows.

- (1) The key questions in power distribution were whether to incorporate centralized or distributed power processing and whether to distribute AC power as in the past, or DC power (with each subsystem performing its own conditioning). Parameters of interest were reliability, weight, efficiency, voltage regulation, EMI, producibility, and switching requirements. The baseline

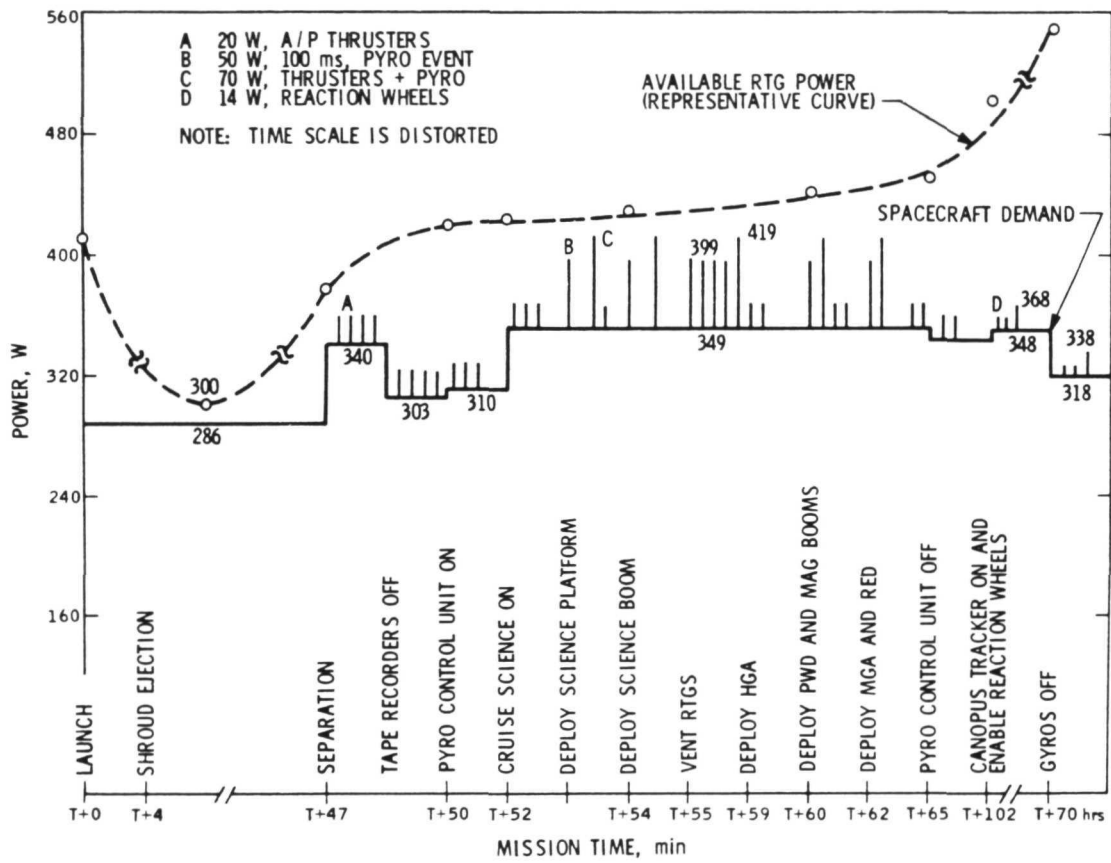


Fig. 177. Spacecraft launch power profile

finally selected was a centralized AC system. Centralized DC power was unacceptable because it failed to provide sufficient load isolation, and switching requirements were excessive. Decentralized DC was comparable in performance to AC, but the latter was adopted as baseline because of long JPL experience with AC power.

- (2) The launch power tradeoff related to power requirements of the spacecraft during launch and the period thereafter, until the vehicle entered the vacuum environment of time space. Battery power was a logical candidate and an intensive study was undertaken to determine the advantages and penalties associated with this source of power. The disadvantages of battery power were soon apparent: a weight increase of 25 lb; increased volume and complexity of power conditioning equipment; the possibility of battery electrolyte leakage. The battery problem was eliminated through intensive development of the RTG. From the activity it was determined that a sealed, inert gas filled, RTG would provide sufficient power to support launch and subsequent power requirements. As noted previously, the gas would be vented upon entry into a vacuum environment. The development of the RTG capability to operate in an air environment led to elimination of the battery in the spacecraft design.
- (3) The baseline selection for the shunt regulator was a sequenced, linear-dissipative device with external power resistors. Low thermal dissipation in the electronics compartment, low bus impedance, good regulation, and minimum variations of RTG hot junction temperature constituted the rationale for selection of this regulator. Alternate shunt regulator designs investigated were 1) linear-dissipative, 2) partial-linear dissipative, 3) switching (shunt switching with duty cycle control), 4) linear-dissipative with auxiliary resistive loads - a scheme whereby the spacecraft houses a relatively small linear dissipative shunt regulator and most excess power is consumed in power resistors - and 5) a sequenced, linear-dissipative regulator employing multiple stages. In this last device, each stage progressively turns on and dissipates excess electrical power.

A common problem to each of the above designs was excessive thermal dissipation. Inasmuch as the regulator is mounted, or confined, in the electronics compartment aboard the spacecraft the problem of heat dissipation becomes a real one. One hundred watts dissipation or more within the shunt regulator was expected. The shunt regulator design finally adopted utilizes external resistors and overcomes the problem of excessive heat in the electronics compartment.

Characteristics of the shunt regulator include: input/output voltage: 30 Vdc; power regulation: ± 1 percent; maximum power: 600 W; dynamic impedance: 0.1 ohm; control module dissipation maximum: 50 W; reliability allocation, 10^5 hr: 0.99 percent; standby power, maximum: 2 W; and transient response: recovery to 30 Vdc ± 1 percent within 0.1 microsecond of a 100 W step load change.

Power reaches the sequence shunt regulator through a +30 Vdc regulated bus. A common comparator provides a sequence logic function that controls the four dissipative stages. As the power transistors of each shunt stage progressively become saturated the next stage is turned on. At no point does the power dissipated within the control module exceed 50 W (Fig. 178).

- (4) The fourth area of tradeoff - the inverter failure detection methodology - determined the means of failure detection for the main and protected bus inverters. Two approaches were studied: software, and hardware. Software failure detection methodology employed the control computer subsystem and the capability of the measurement processor subsystem. The more common hardware approach senses failures by means of sensors located within the power subsystem. Corrective action is then directed to switches within that system.

Parameters of interest included reliability, weight, power consumption, response time, interface complexity, operational complexity, failure modes and effects.

The failure detection method adopted for the TOPS baseline was the hardware approach. With most parameters of interest for each system

being roughly equivalent, the deciding factor became that of elapsed time between the occurrence of failure and a corrective switching action to a redundant circuit. The hardware approach was shown to require but slightly more than one half the time required by the software method to sense and replace a failed inverter.

To summarize this discussion of the TOPS power subsystem, the accomplishments for the project were: 1) major functional elements designed, 2) all major elements breadboarded and tested, 3) configuration trade studies performed, and 4) spacecraft electrical interfaces were defined. Additional activities planned were to conduct further in-depth analysis of the centralized failure detection and correction system, to complete failure detection and software tradeoffs, to complete subsystem integration testing, and to refine design of major functional elements.

B. RTG Power Source

The TOPS electrical power source is four radioisotope thermoelectric generators (RTGs). The generators - developed by the Atomic Energy Commission (AEC) in cooperation with JPL - constitute advance design and performance concepts over extant AEC devices such as Snap 19 and Snap 27.

Requirements and constraints of the four RTGs in the final period of the TOPS project are listed below:

Power (End of Mission)	440 W	(total)
Voltage	30 V	(each)
Life	12 yr	
Weight	320 lb	(total)
Magnetic field	5.0 γ at 3 ft	(total)
Reliability	0.98	
Envelope	21.5 \times 12 in.	(each)

In addition to the above requirements for vacuum operation, air operation is required to provide power while the spacecraft is on the launch pad, and a radiated heat concept would cool the generators in flight.

Major significant components of the RTG (Fig. 179) include 312 silicon germanium thermocouples, each with a silicon moly hot shoe to accept

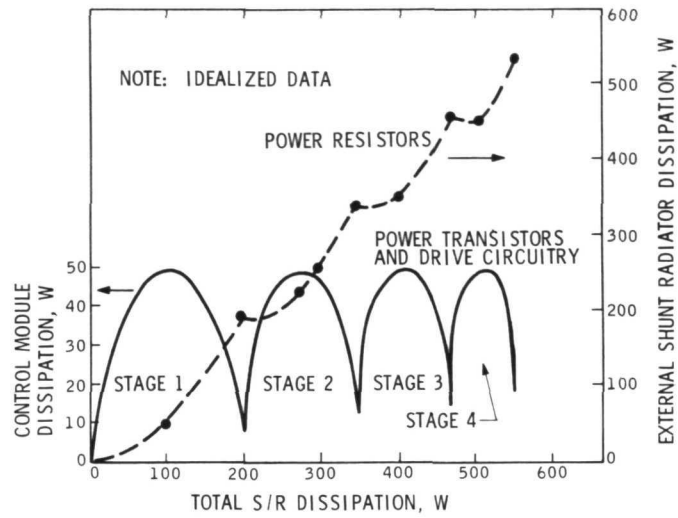


Fig. 178. Sequence shunt regulator thermal characteristics

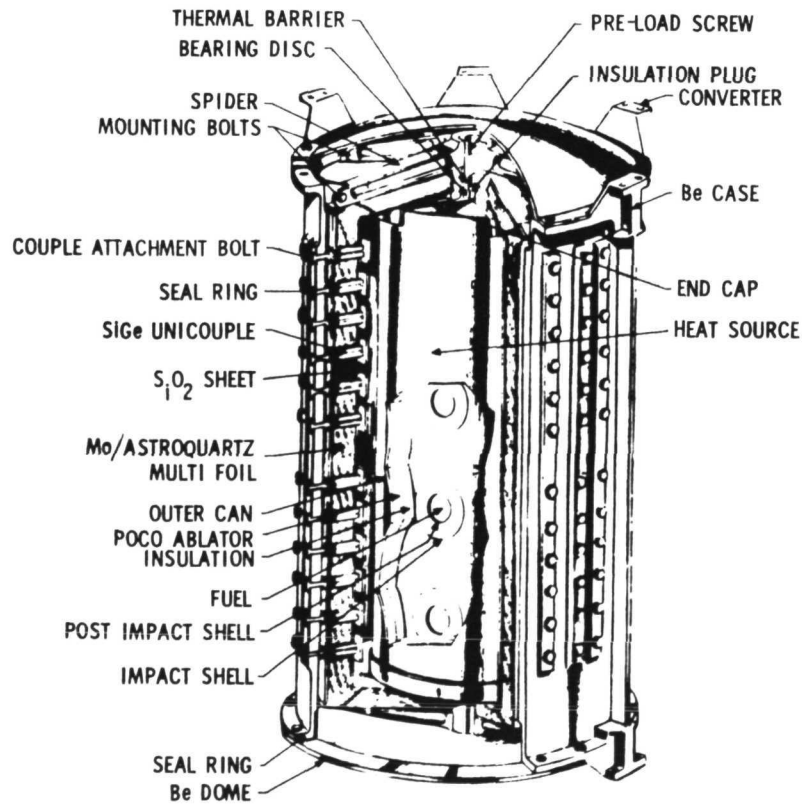


Fig. 179. MHW-RTG

heat from the heat source; silicon dioxide astroquartz and molybdenum multifoil insulation separating the thermocouples; a dome seal at each end of the generator to maintain an internal pressure within the unit, and three ball joints at one end for attachment to the supporting structure. The thermocouples are tied in a series of parallel strings to provide required reliability for the RTG.

Integration of a nuclear power source into the spacecraft called for controls and system requirements to ensure minimum impact on both the RTG and the spacecraft. First, nuclear radiation must be minimized so as not to damage the hardware components nor interfere with the science instrumentation aboard the craft.

Passive temperature control of the spacecraft must allow for radiated coupling of the generator. Other requirements were ease of test and assembly, a minimum magnetic field, minimal operation and handling (as a safety feature), and finally provision for power during prelaunch operations.

To reduce the effects of radiation upon science instrumentation, the four generators were attached to the end of a boom extending 8 ft from the side of the spacecraft bus opposite the scientific payload. Moreover, the positioning of the RTGs in this extended position provided ease of handling, concentrated flow of air around the RTG during prelaunch air conditioning, and facilitated integration of a fluid heat-transfer loop into the system.

To insure ease of handling and quick connect/disconnect of the RTG, the generator utilizes a pin and clevis, ball joint arrangement for attaching the unit to the support structure. Three ball joints with self-aligning bearings are structured into the base of the generator at 120-degree angles. The clevis is attached to the support structure (boom) and easy attachment is performed by aligning the bearing with the clevis and inserting the pin. To prevent this design from causing undue dynamic stress, a reinforcement ring was built into the base of the RTG, while reinforcement ribs approximately 2 in. long were positioned above each bearing.

In a study using a sealed generator filled with Xenon gas, a load voltage of 30 V, and 1100°C temperature on the hot side of the thermocouples the RTG output is down to 410 W at launch and following launch drops to

300 W before rising to its full capability. This phenomenon is explained as follows: Upon removal of the coolant flow to the RTGs prior to launch, the cold junction temperature of the generators rises much more rapidly than the hot junction temperature, thereby decreasing the delta T across the thermocouple and reducing the total power output. Following launch and ejection of the shroud, the RTGs now radiate heat to space and the delta T is reestablished. The temperature ultimately stabilizes, and full power is provided in the vacuum condition.

The magnetic field created by the flow of current in the four RTGs must be minimal in order not to interfere with the magnetometer measurements of planetary and interplanetary magnetic fields. A magnetic field restraint of 5 gamma at a 3-ft distance from the RTG array was a design goal. Subsequent analysis of the field created by four RTG's arranged in a configuration to achieve maximum field cancellation disclosed a value of 35Y at 3 ft, or a factor of 7 over the restraint specification. Since this value produced a magnetic field less than 0.1 percent of the total allowable at the magnetometer, positioned 27 ft from the RTGs, it is thought the 5γ at the 3-ft restriction is too severe. If the specification cannot be changed, degaussing loops probably will be required in each RTG to reduce its magnetic field by at least one order of magnitude.

Although the silicon germanium thermocouples used in the RTG are operable in air, other materials used in the generator are not. The moly foil insulation layers separating the thermocouples, for example, are subject to oxidation, and would degrade the RTG were the generator to be operated in an air environment. The AEC suggested that this problem could be eliminated by not utilizing the RTG until the spacecraft were in the vacuum of space. This solution would not satisfy the TOPS requirements, however, and JPL engineers requested that an inert gas be sealed in the generator and the unit used until the spacecraft had departed the atmosphere, whereupon the gas would be ejected.

Analyses were performed on various inert gases to determine their suitability for the generators. As illustrated in Fig. 180, candidate gases were tested for power capability as a function of their thermal conductivity. Xenon appeared to be the most suitable, not only because it supplies 74 percent of the generator's maximum power capability in a vacuum environment -

the highest conductivity of any gas tested - but because the molecular size of Xenon, with a built-up pressure, prevents incursion of air into the generator. Gas was also being evaluated as a tool to reduce power output at the beginning of a mission, and to provide a lower degradation characteristic of the generator as a function of time.

The need for better understanding of the long term behavior of the RTG in respect to changes in materials led to development of a materials analysis program. Three basic studies were made: (1) the bulk properties of thermoelectric materials, (2) the compatibility of thermoelectric with insulation materials, and (3) the sublimation characteristics of the thermoelectric materials. These efforts were still in progress at the end of the TOPS project.

To summarize the results of the development effort on the RTG, engineers (1) identified and provided solutions to specific integration problems, (2) provided the AEC with information affecting design in such areas as air operation and utilization of an inert gas, (3) developed confidence in hardware based on design test data, (4) provided direction to technology goals, and (5) identified mission and spacecraft effects on the RTG and transmitted such information to the AEC. It should be pointed out that the analysis described in this summary would necessarily be redone as the evolution of the generator, in a dynamic sense, unfolds. Modification of the initial and subsequent designs would result from further analytical studies.

The AEC design effort on the multihundred watt RTG was initiated October, 1969 under Contract Number AT (29-2) 2831. The prime contractor was the General Electric Company, Space Division, located in Philadelphia, Pa. A subcontract was awarded to the Radio Corporation of America (RCA) for development of the silicon germanium thermocouples used in the generators and for certain insulating materials.

The status of the AEC effort at the close of the RTG project revealed the generator design definition to be complete and development work to have been in progress since July, 1971. At that date the program was reclassified from a technology program to a flight support program. The development work had produced, at the project's end, a prototype converter designated as TBC-1, a test bed converter. Some tests had been performed on the device.

The heat source concept employed in the development of the multi-hundred watt generator (Fig. 181) utilizes a fuel consisting of solid ceramic spheres of pure plutonium dioxide (PPO). The PPO spheres are encased in outer shells of refractory oxide, iridium, and graphite. Each sphere is 1.6 inches in diameter and generates approximately 122 watts thermal power. The spheres, weighing about 1.2 pounds each, operate at a temperature of 2500°F (in a room environment). For ease in handling and to facilitate changes in design the spheres have been modularized in groups of three. The modules, or rings, are then inserted into the cylindrical container, which makes up the heat source, and inserted in the RTG.

Safeguarding against nuclear contamination in case of a TOPS mission abort is a prime concern in the design of the RTG. In addition to the impact capability of the solid spheres of PPO fuel the containers incorporate other safety features. Crush-up graphite material absorbs some of the initial shock of impact. Compliance pads separate the spheres and provide an absorption factor. An outer clad, probably composed of iridium, serves as a compliance member. Provision is made, too, against disintegration of the RTG from atmospheric friction by including a space graphite ablator beneath the outer clad. In total, these design features provide for safety during reentry, upon impact, and in a post impact period.

A performance summary of the RTG is given in Table 58. The extant design, Test Bed Converter -1, is compared on the one hand to design goals and on the other to a third design in the making at the close of the TOPS project - a converter designated TBC-3, under development for Lincoln Laboratories for an Air Force spacecraft, the LES 8&9. The apparent failure of the power output to meet the design requirement of 143 W was traced to internal vaporization which deposited graphitic and sodium material on the thermocouples and decreased performance. Vaporization resulted from failure to outgas the electric heat source and to outgas the sodium salt used as a ballast material in the heat source to simulate the heat source dynamic weight. More significantly, the test data demonstrated that only 2236 thermal watts were required to provide the designed temperature of 1000°C, while the actual weight of the converter proved to be 47.3 lb against a designed 32 lb.

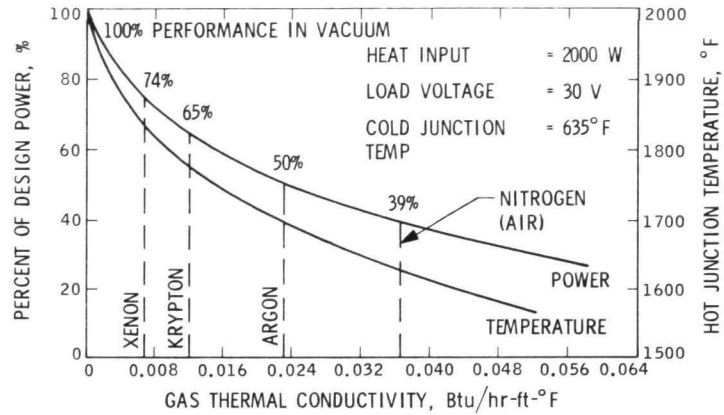


Fig. 180. Effect of gas conductivity on sealed MHW-RTG performance

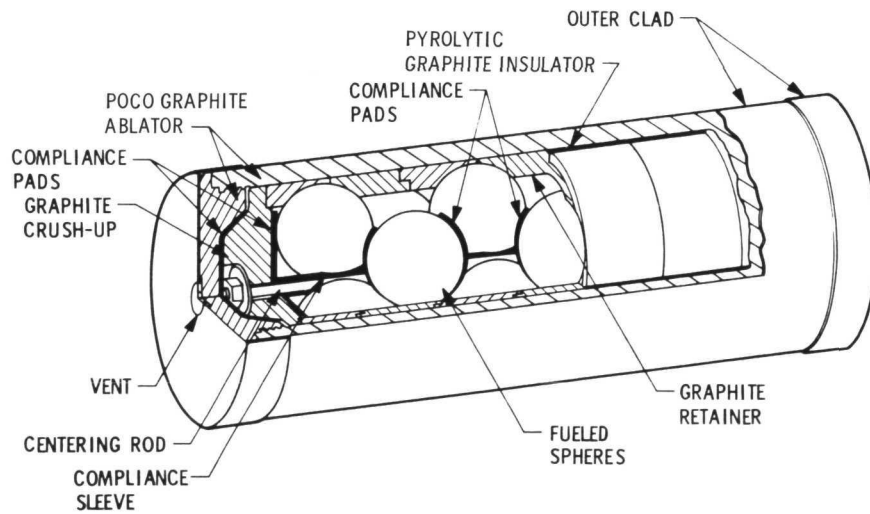


Fig. 181. MHW-RTG reference heat source concept

Because JPL engineers are interested in the development aspects of the TBC-3, key performance characteristics are included in this report. The estimated current-voltage characteristics of the generator as a function of time show that when operating at 30 V an output of 150 W may be expected at the beginning of mission (BOM), 125 W five years later, and 110 W at mission end in the 12th year. The operating temperature of 1000°C at BOM falls only to 980°C in the fifth year and to 960°C at 12 years. Power output approximates 150 W at BOM, 128 W at the 5-yr mark, and 111 W at end of mission, a degradation of 26 percent. Since no provision has been made for premission degradation in the TBC-3 calculations, JPL engineers are concerned that the initial 150 W power output does not meet mission requirements and believe further work in this area is justified.

Table 58. MHW-RTG converter performance status

TBC-1 Design	TBC-1 RCA Test Data	TBC-3 Design		
143	126	145	P_0	W
1000	1000	1000	\bar{T}_H	°C
327	338	318	\bar{T}_C	°C
2350	2236	2400	Q_1	W
27.6	24.6	30.2	V_L	V
5.2	5.1	4.8	I_L	A
6.1	5.6	6.1	η	%
288	288	312	T/E	
12.2	12.2	14.5	Diam	in.
21.5	21.5	20.3	L	in.
32	47.3	38	W	lb